TECHNISCHE UNIVERSITÄT MÜNCHEN

FAKULTÄT FÜR CHEMIE

Biomimetic Proton- and Halonium-Induced Cyclization Reactions

Andreas Michael Arnold

Vollständiger Abdruck der von der Fakultät für Chemie der Technischen Universität München zur Erlangung des akademischen Grades eines

Doktors der Naturwissenschaften

genehmigten Dissertation.

Vorsitzender:	Prof. Dr. Shigeyoshi Inoue
Prüfer der Dissertation:	1. Prof. Dr. Tanja Gulder
	2. apl. Prof. Dr. Wolfgang Eisenreich
	3. Prof. Dr. Alexander Breder

Die Dissertation wurde am 14. April 2021 bei der Technischen Universität München eingereicht und durch die Fakultät für Chemie am 01. Juni 2021 angenommen.

List of Publications

This thesis was produced from February 2016 until December 2019 at the Technical University of Munich and from January 2020 until February 2021 at the University of Leipzig in the group of Biomimetic Catalysis under the supervision of Prof. Dr. Tanja Gulder.

Parts of this thesis have already been published:

Peer-reviewed journals

- **A. M. Arnold**, A. Pöthig, M. Drees, T. Gulder; NXS, Morpholine, and HFIP: The Ideal Combination for Biomimetic Haliranium-induced Polyene Cyclizations; *J. Am. Chem. Soc.* **2018**, *140*, 4344–4353.
  With cover picture: https://pubs.acs.org/toc/jacsat/140/12
  Highlighted as a JACS Spotlight: *J. Am. Chem. Soc.* **2018**, *140*, 4468.

- **A. M. Arnold**, A. Ulmer, T. Gulder; Advances in Iodine(III)-Mediated Halogenations: A Versatile Tool to Explore new Reactivities and Selectivities; *Chem. Eur. J.* **2016**, *22*, 8728–8739. (Hot Paper with cover picture)
  Highlighted in Chem. Views: https://www.chemistryviews.org/details/ezine/8882381/Metal-Free_Fluoro-Benzoxazepine_Synthesis.html

- A. Ulmer, C. Brunner, **A. M. Arnold**, A. Pöthig, T. Gulder; A Fluorination/Aryl Migration/Cyclization Cascade for the Metal-free Synthesis of Fluoro Benzoxazepines; *Chem. Eur. J.* **2016**, *22*, 3660–3664. (Hot Paper)

Conference talks:

- GDCh Wissenschaftsforum, September 15th-18th 2019, Aachen, Germany
- 54. Doktorandenworkshop Naturstoffe: Chemie, Biologie und Ökologie, Oktober 13th 2017, Jena, Germany
- Hochschule trifft Industrie, October 4th 2017, Feldberg-Falkenau, Germany

Poster Presentations:

- GDCh Wissenschaftsforum, September 15th-18th 2019, Aachen, Germany
- Gordon's Research Conference, July 21st-26th 2019, Boston, United States of America
- EuChemS, August 26th-30th 2018, Liverpool, United Kingdom
- American Chemical Society National Meeting, March 17th-22nd 2018, New Orleans, USA

In this work, the convention was used to represent the relative configuration of racemates by bold and hashed bold bonds, and enantiomerically enriched material by wedged and hashed wedged bonds.

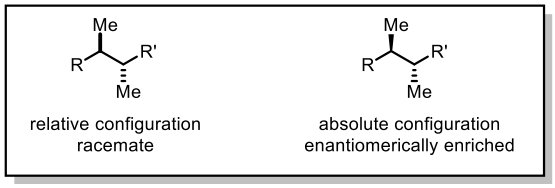

Danksagung

Ich danke Frau Prof. Dr. Tanja Gulder für die Möglichkeit, in ihrem Arbeitskreis und Lehrstuhl meine Dissertation anfertigen zu dürfen. Neben der ausgezeichneten fachlichen Betreuung bei meinen Forschungsthemen ermöglichte sie es mir mehrere nationale und internationale Konferenzen zu besuchen, um so interessanten Diskussionen und Vorträgen folgen zu dürfen.

Des Weiteren gilt mein Dank allen aktiven und ehemaligen Mitgliedern des AK Gulders, die zu mich zu Beginn herzlich aufgenommen haben und von denen ich viel lernen konnte. Qingqi, Gabriel, Christoph, Simon und Steffi sowie besonders meinen langjährigen Laborkollegen Jarek möchte ich danken, denn ihr habt die Stimmung im Labor und bei dem einem oder anderen Feierabendbieren im Kaffeeraum stets hochhalten können. Nach dem Laborumzug Anfang 2020 wurde ich in Leipzig von vielen neuen Kollegen wärmstens empfangen, wobei ich mich besonders bei Fabi, Martin, Caro und Cornelius bedanken möchte sowie beim gesamten AK Schneider. Besonders für die großartige Harmonie im und außerhalb des Labors möchte ich mich bei Julia bedanken, ohne dich wäre die Arbeit in der Tat nicht mal halb so lustig gewesen :-) Trotz der Pandemie habt ihr mir alle ein unvergessliches Jahr in Leipzig beschert!

Ohne die Korrekturleser Julia, Fabi, Simon, Martin und Rita hätte ich sicherlich nicht alle Fehler gefunden, vielen Dank für eure Mühen.

Abschließend möchte ich mich bei meinen Eltern bedanken, die mich auf meinem bisherigen Lebensweg stets tatkräftig unterstützt haben und mir das Studium erst ermöglicht haben. Ebenso danke ich meinem Bruder Max und meiner Oma Maria, auf die man sich stets verlassen kann.

Euch allen vielen, vielen Dank!

„In the end…
We only regret the chances we did not take,
the relationships we were afraid to have,
and the decisions we waited too long to make.”

– Lewis Carroll (1832-1898)

Table of Contents

Abstract

Polyene cyclizations in nature are powerful reactions used to construct complex, cyclic secondary metabolites from linear precursors. The beginnings of their mechanistic understanding date back to 1955 when Eschenmoser and Stork postulated their rationale of the origin of their stereoselectivity.[1] However, mimicking this highly selective reactivity in the lab has been a long-lasting endeavor, which may primarily be achieved by epoxide opening, halonium-induced cyclization, or proton-induced cyclization.[2] Many available methods suffer drawbacks such as inconvenient reaction conditions, toxic or metal-containing reagents, or give poor results regarding yield and/or selectivity of the cyclized material. We envisioned that using fluorinated alcohols as a solvent for these challenging transformations can be beneficial, as the solvent forms tight hydrogen-bonding networks and assists in the prearrangement of the linear polyene through hydrophobic interactions, similar to substrate folding within the enzymatic pocket during biosynthesis.[3]

N-halo imides were found to be suitable halogen sources, albeit in situ halogen transfer giving *N*-halomorpholine as the actual halogen donor greatly improved the selectivity and yield in this transformation. With the presented method a wide range of structurally and electronically diverse linear polyenes was transformed into the corresponding bromo- or iodocyclized material by simply exchanging the halogen source. Chlorocyclized material was obtained by slight adjustment of the reaction conditions. Mechanistic investigations showed that the individual roles of NXS, morpholine, and the fluorinated alcohol solvent are essential in this transformation.

Proton-induced cyclizations were achieved with excellent stereocontrol and likewise good or better yields as for the halocyclization by applying weakly acidic protonated amine salts. A wide range of prenyl-, geranyl- and farnesyl substrates was suitable for these mild cyclization conditions and a high functional group tolerance was observed. Extensive NMR studies and calculations revealed that perfluoro-*tert*-butanol plays an important role as the solvent, as it prearranges the hydrophobic starting material thus easing the cyclization reaction and enhancing the selectivity. Both stronger activation of the desired terminal double bond paired with activation of the Lewis base by the fluoroalcohol were decisive for the success. In contrast to the direct halonium-induced cyclizations, kinetic data and deuteration experiments showed a stepwise process with dynamic protonation and elimination of a proton in α-position to the formed carbocation.

Deutsche Zusammenfassung

Polyenzyklisierungen sind Reaktionen in der Natur, mit der komplexe zyklische Sekundärmetaboliten aus linearen Edukten aufgebaut werden können. Die Anfänge des mechanistischen Verständnisses reichen bis ins Jahr 1955 zurück, als Eschenmoser und Stork ihre Theorie über den Ursprung der Stereoselektivität dieser Transformationen postulierten.[1] Die Nachahmung dieser hochselektiven Reaktivität im Labor ist jedoch ein herausforderndes Unterfangen, das hauptsächlich durch Epoxidöffnung, Haliranium- oder Protonen-induzierte Zyklisierung erreicht werden kann.[2] Viele der verfügbaren Verfahren weisen Nachteile auf, wie ungünstige Reaktionsbedingungen und Verwendung von toxischen oder metallhaltigen Reagenzien, oder liefern schlechte Ergebnisse hinsichtlich der Ausbeute und/oder Selektivität des zyklisierten Materials. Es stellte sich heraus, dass die Verwendung von fluorierten Alkoholen als Lösungsmittel für diese herausfordernden Umwandlungen vorteilhaft ist, da sie ausgedehnte Wasserstoffbrückenbindungsnetzwerke bilden und durch hydrophobe Wechselwirkungen die Knäulung des linearen Polyens unterstützt, ähnlich der Substratfaltung in der enzymatischen Tasche während der Biosynthese.[3]

N-Haloimide erwiesen sich als geeignete Halogenquellen, wobei ein in situ Halogentransfer zu *N*-Halomorpholin als aktiver Halogendonor die Selektivität und Ausbeute bei dieser Umwandlung stark verbesserte. Mit der vorgestellten Methode wurde ein breites Spektrum strukturell und elektronisch unterschiedlicher linearer Polyene durch einfaches Austauschen der Halogenquelle in die entsprechenden Bromo- und Iodozyklen, und bei milderen Bedingungen sogar in chlorozyklisierte Materialien umgewandelt. Mechanistische Untersuchungen zeigten, dass die individuellen Rollen von NXS, Morpholin und dem Lösungsmittel für diese Transformation essenziell sind.

Protoneninduzierte Zyklisierungen wurden, durch den Einsatz schwach saurer protonierter Aminsalze, mit ausgezeichneter Stereokontrolle und ebenfalls guten oder sogar besseren Ausbeuten im Vergleich zur Halozyklisierung ermöglicht. Dank dieser milden Zyklisierungsbedingungen konnte ein breites Spektrum an Prenyl-, Geranyl- und Farnesylsubstraten erfolgreich umgesetzt werden. Es wurde eine hohe Toleranz gegenüber funktionellen Gruppen beobachtet. Umfangreiche NMR-Studien und Berechnungen zeigten, dass Perfluor-*tert*-butanol eine wichtige Rolle als Lösungsmittel spielt, da es das hydrophobe Edukt in Lösung faltet, wodurch die Zyklisierungsreaktion erleichtert und die Selektivität erhöht wird. Eine ausgeprägtere Aktivierung der gewünschten terminalen Doppelbindung, zusammen mit der Aktivierung der Lewis-Base durch den Fluoralkohol, waren hier entscheidend. Im Gegensatz zu den direkten Halonium-induzierten Zyklisierungen zeigten kinetische Daten und Deuterierungsexperimente einen schrittweisen Prozess mit dynamischen Protonierungen und Eliminierungen am jeweiligen Kation.

I. Theoretical Background

1. Terpenes – Occurrence and Biosynthesis

Organisms produce primary metabolites, which are essential for nutrient assimilation, energy production, and growth. Examples are the so-called building blocks of life, such as fatty acids, carbohydrates, amino acids, and nucleobases.[4] In contrast, secondary metabolites have more specialized functions. Examples are pheromones used to communicate with other organisms, (toxic) alkaloids needed to e.g. fight off predators, highly specialized polyketides with e.g. antibiotic activities, and the group with the most representatives, the terpenoids, which for example give flowers and fruits their distinct bouquet of flavor and odor.[5] Since the invention of processes for the extraction of organic compounds in Mesopotamia over 3000 years ago terpenes have been widely used in the preparation of perfumes and fragrances.[6] Table 1 shows selected terpenoids and their characteristic odor. For example, cyclic monoterpenes **1**-**6** have a distinctly different odor depending on their chemical structure. α-Pinene (**1**), exhibits a distinct woody and piney odor, carene (**2**) can be found in cedar trees or rosemary, giving it citrus and terpenic herbal scent and taste similar to limonene (**3**). The linear monoterpene myrcene (**4**) is described as herbaceous and is a main component in the bouquet of myrtle or cannabis, whereas geraniol (**5**), likewise a linear monoterpene, is rather fruity and flowery.[7] Tricyclic ambroxide (**6**) is an important ingredient in upmarket perfumes and lotions. It is traditionally harvested from the ambergris of slain whales, making it a costly resource and – on the other hand – endangering the sperm whales through excessive hunting.[8]

Table 1. Selected examples of naturally occurring terpenes and their distinct odor.

terpenoid	structure	odor	natural occurrence
α-pinene	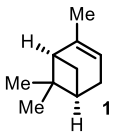	pines	 [9]
carene	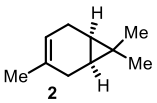	cedar, rosemary	 [10]
limonene	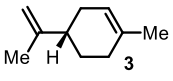	citrus lemon	 [11]

myrcene	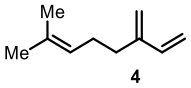 4	myrtle, cannabis	 [12]
geraniol	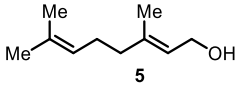 5	roses, cranesbills	 [13]
ambroxide	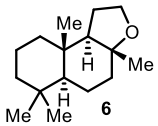 6	ambergris	 [14]

Terpenes, with more than 80.000 distinct representatives characterized to date,[15] are biosynthetically derived from the 5-carbon monomer isoprene pyrophosphate (IPP, **7**, Scheme 1) in a series of chain-elongations, cyclization reactions, and oxidations.[16] The important intermediate **7** is accessible via either the methylerythritol-4-phosphate (MEP, **8**, Scheme 1, top) generally used by bacteria, yeast, and lower eukaryotes, or the mevalonate-dependent (MVA, **9**, Scheme 1, bottom) pathway, which in term is found in higher eukaryotes and some bacteria.[17] The MEP pathway commences by the addition of pyruvate (**10**) to glyceraldehyde-3-phosphate (GAP, **11**) giving 1-deoxyxylulose-5-phosphate (DXP, **12**), which, after skeletal rearrangement and reduction yields MEP (**8**). Formal reductive dehydroxylation via a cyclic phosphoranhydride produces 4-hydroxy-3-methyl-but-2-enyl pyrophosphate (**13**), which is then further converted into either IPP (**7**) or dimethylallylpyrophosphate (DMAPP, **14**), where both of them are interconvertible within the organism. Alternatively, IPP (**7**) is accessible via the MEP pathway starting from two acetyl-CoA (**15**) building blocks to give acetoacetyl-CoA (**16**). Stereoselective aldol addition of a third acetyl-CoA (**15**) and reduction yields mevalonic acid (MVA, **9**). Decarboxylation of mevalonic acid pyrophosphate (MVAPP, **17**) finally gives one equivalent of IPP (**7**). Dimerization of **7** or **14** gives geranyl pyrophosphate (GPP, **18**), the direct precursor for further chain elongations. Another pathway is that GPP (**18**) is converted into linear monoterpenes such as geraniol (**5**), linalool (**19**), or myrcene (**4**). Again, those terpenes can be further functionalized, e.g., through proton-induced cyclization in a so-called "head-to-tail" cyclization. Contrary to the "tail-to-head"-cyclization,[18] the "head" olefin is functionalized first, with the subsequent addition of an internal nucleophile. In this manner, α-cyclogeraniol (**20**), a component isolated from orchard plants,[19] is formed in nature. Similarly, **19** may thus undergo cyclization to geranic oxide (**21**), a component of the volatile bouquet of sour cherries.[20]

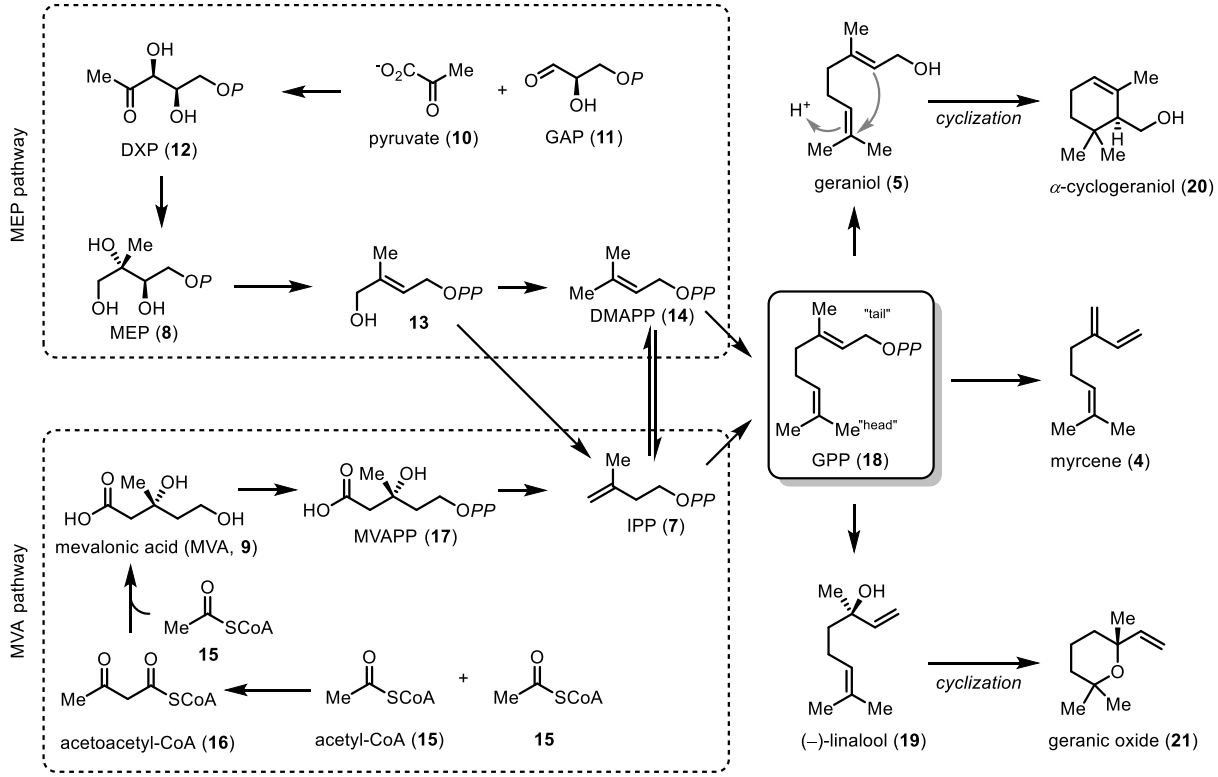

Scheme 1. Biosynthesis of GPP (**18**) and linear monoterpenes via the MEP pathway (top) and MVA pathway (bottom).[21] *P* = phosphate, *PP* = pyrophosphate.

Nature is not only able to produce cyclic monoterpenes such as **20** and **21**, but also more sophisticated polycyclic metabolites. Bark extracts of the *Drymis winteri* tree have been used for generations in the Andean mountains to treat stomach ache and dermatitis.[22] These beneficial effects soon prompted more detailed investigations on the nature of the active ingredients, which led to the isolation of (–)-drimenol (**22**) in 1948 and its structure elucidation in 1956.[23] Its antifungal activity was soon after discovered.[24] As **22** was one of the first of many representatives of structurally similar natural products, this *trans*-decaline skeleton became known as the drimane core (Figure 1). In the following years a plethora of biologically interesting natural products were added to this list, for example (+)-sclareolide **23**,[25] antibacterial (–)-warburganal (**24**)[26] and (+)-totarol (**25**)[27] and the polycyclic anti-tumoral triterpene (+)-hopene (**26**).[28] Their interesting biological activities have sparked tremendous synthetic efforts in preparing those sophisticated structural motifs.[29]

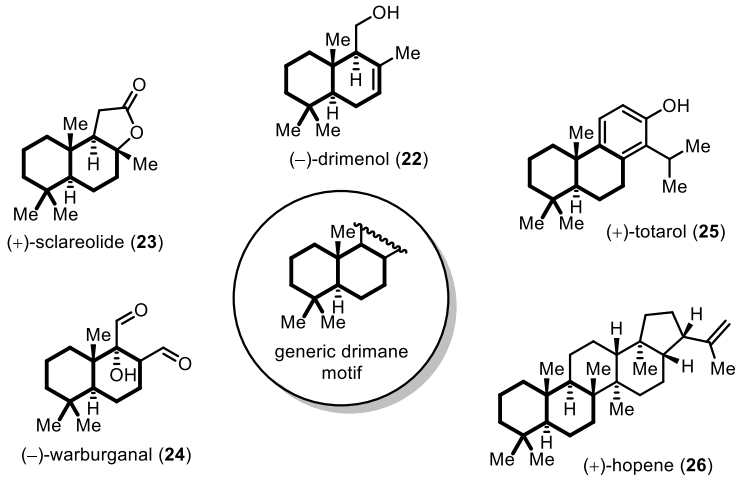

Figure 1. Examples of natural products **22**-**26** bearing the drimane motif.

Polyene cyclization reactions are very powerful synthetic transformations, as a high level of complexity is introduced in a single cascade reaction, creating multiple *C*-*C*-bonds and stereocenters from linear precursors. Nature completes this task by employing highly specialized enzymes, that manage to fold the polyene chain inside the active cavity and guide the cyclization to the desired product.[30] A prime example for this highly selective cyclization is the squalene-hopene cyclase (SHC) enzyme in *Alicyclobacillus acidocaldarius*. It was possible to obtain a cocrystal structure of the enzyme using 2-azasqualene (**27**) as an inhibitor (Figure 2, left).[3] This nicely shows how the linear squalene (**28**) assumes a folded position in the active site. Upon protonation of the head prenyl unit a cyclization and rearrangement cascade takes place, producing pentacyclic (+)-hopene (**26**) in a highly selective manner (Figure 2, right).

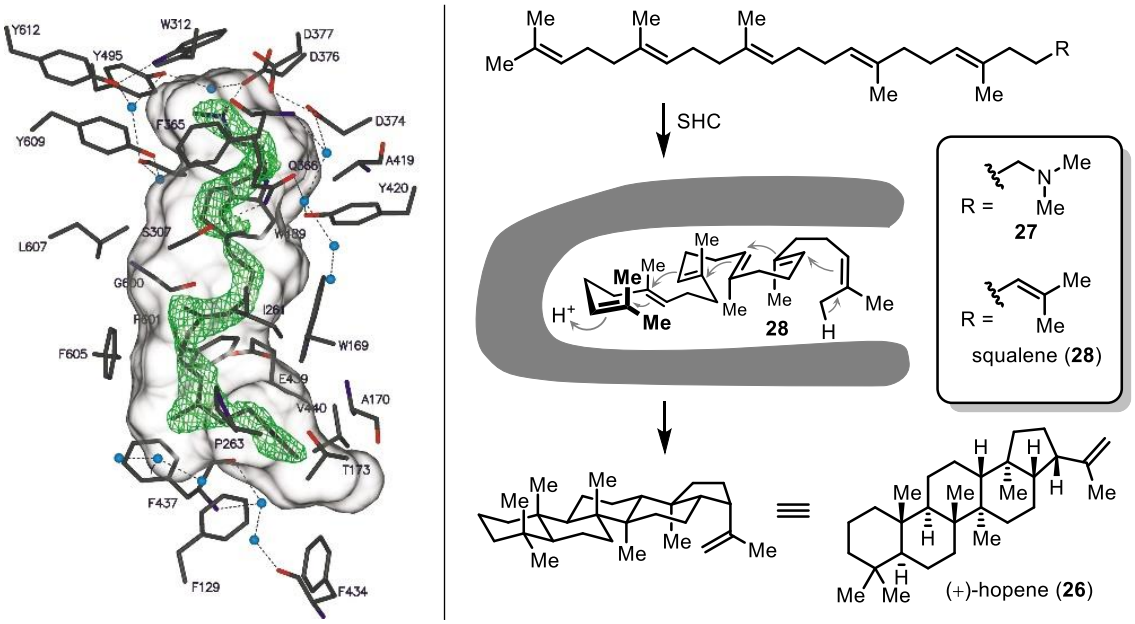

Figure 2. Squalene-hopene cyclase from *Alicyclobacillus acidocaldarius* bound with 2-azasqualene (**27**) as SHC inhibitor (left, reproduced from reference 3 with permission from Elsevier) and schematic enzymatic cyclization process (right).

The importance of substrate folding can be well illustrated for the divergent cyclization of the linear diterpene geranylgeraniol pyrophosphate (**29**, Figure 3).[21] Depending on the layout of the enzymatic pocket a "head-to-tail" (HTT) cyclization may take place, similarly to the hopene cyclase, and furnish the drimane primaradiene (**30**), which is then further oxidized in the oxidation phase to diaporthein B (**31**).[31] The second mode of cyclization is the "tail-to-head" (TTH) cyclization, which mechanistically proceeds via cleavage of the pyrophosphate and subsequent attack of internal alkenes at the terminally formed carbocation. Completion of the cyclization cascade and subsequent oxidation yields taxol (**32**) via taxadiene (**33**)[16] or japodagrin (**34**) via casbene (**35**, Figure 3).[32]

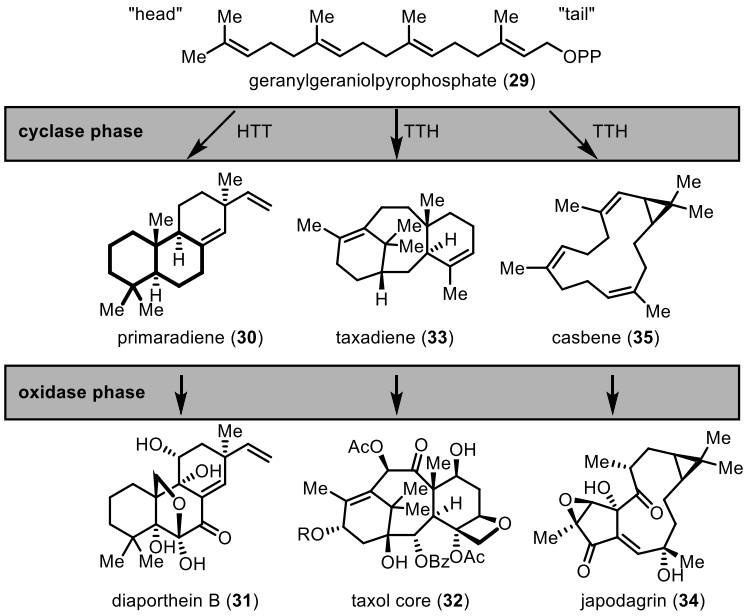

Figure 3. Cyclase phase and oxidase phase in the biosynthesis of **30**-**35**.

A long-standing dream of chemists is mimicking the highly specialized enzymes in the laboratory, thus gaining access to complex products without the need for enzymatic transformations.[33] As shown above, a key element in these highly selective conversions is the control of the conformation of the starting material prior to the reaction. Therefore, our group made cutting-edge efforts to control the conformation of linear polyenes in solution, thus mimicking nature. The presented work focuses on biomimetic strategies to achieve these highly desirable polyene cyclizations.

2. The Endeavour of Mimicking Polyene Cyclization Reactions

2.1. Stereochemical Considerations

It has remained unclear for a long time how highly selective transformations like polyene cyclizations could take place in nature with such precision until the first enzyme was successfully crystallized and its structure elucidated in 1997.[18] In general, the structure of enzymes showed that they form tertiary and quaternary structures with hydrophobic pockets. These reactive sites specifically complement the structure of the substrate, bringing the reaction partners (or for intramolecular reactions the reactive parts of the molecule) into close proximity and, more importantly, pre-arranging the linear substrate into a conformation similar to the product, allowing for a highly selective reaction. Moreover, shielding the substrate from the reaction medium, like e.g. water, solvent, or salts, enables the transformation to proceed without any undesired side reactions. During this process, flexible hydrogen bonds within the enzyme are continuously formed and reshaped to allow the substrate to enter the reactive site and subsequently leave the enzymatic pocket.[34] This is important in the biosynthesis of both small and more complex terpenes from linear precursors, as from one intermediate (geraniol geranyl pyrophosphate, GGPP **29**, *vide supra*) a wide range of structurally unique molecules may be produced.

How these complex structures are produced in the biosynthetic pathway in organisms was disputed for multiple decades.[35] Systematic investigations by Ružićka *et al*. started already in the 1920's[36] and together with Eschenmoser he elaborated three main observations within the following 30 years.

- **The "biogenetic isoprene rule"**

This rule states that naturally occurring linear terpenes, like e.g. squalene (**28**), are built up by isoprene units (**36**, Figure 4). In a series of chain elongations, the linear triterpene squalene (**28**), for example, is produced by three "head-to-tail" chain elongations furnishing the distinct *trans*-1,4 oligoisoprene units and one final "tail-to-tail" connection in the central part of the terpene.[37] Furthermore, Ružićka *et al*. recognized that (poly)cyclic terpenes such as lanosterol (**37**) are likewise forged together from these C_5-isoprene monomers. This hypothesis was strengthened by work from Woodward published in the same year, who postulated the "head-to-tail" cyclization mechanism in the squalene-lanosterol cyclization by ^{14}C-labeling experiments.[38]

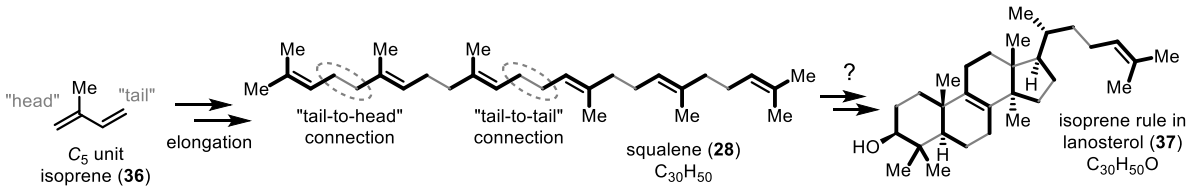

Figure 4. Ružićkas and Eschenmosers "biogenetic isoprene rule" in squalene (**28**) and lanosterol (**37**).

- **Configurational relationships**

The second important finding of the Zurich school was the similarity in stereo information present in triterpenes lupeol (**38**), lanosterol (**37**), and steroid cholesterol (**39**, Figure 5). The absolute and relative configurations were previously established through decomposition experiments, but the question remained how steroids could have the same configuration as cyclic triterpenes. Their rationale was that cholesterol is formed from cyclic terpenes such as lanosterol (**37**), which in turn is produced from **28** during a "head-to-tail" cyclization cascade.

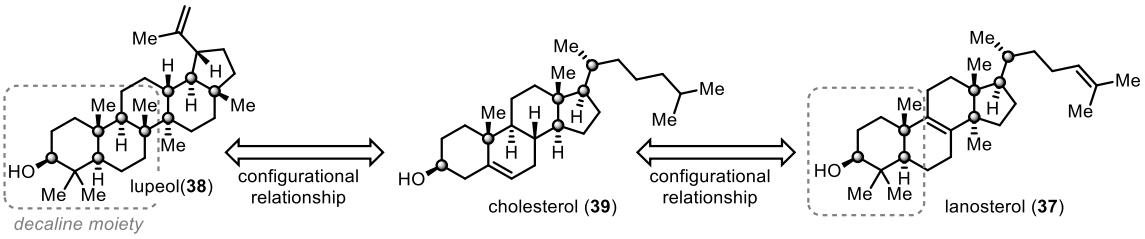

Figure 5. Configurational relationship of triterpenes lupeol (**38**), lanosterol (**37**) and steroid cholesterol (**39**).

- **The origin of stereoselectivity in polyene cyclizations**

Among others, Stork and Eschenmoser, the latter a student of Ružićka, independently investigated the cyclization of farnesoic acid (**40**) with strong acids and investigated the stereochemical outcome of the reaction (Scheme 2). While both groups obtained bicyclic **41** as the main reaction product, Stork initially assumed a stepwise reaction mechanism and thus concluded that the product must have a *cis* decalin scaffold **42**.[1b] Eschenmoser correctly assigned the *trans* structure **41** to the product, and confirmed his findings by extensive derivatizations and *de novo* syntheses,[1a,39] and finally by comparison of a derivative **41** to a natural isolate.[40] Eschenmoser then formulated a hypothesis (named after both Stork and Eschenmoser in recognition of their independent work on polyene cyclizations), that "*the obtained steric result is exactly what would be anticipated if the cyclizations occur according to the chair-like folding* [see **43**] *and proceed throughout an antiplanar addition.*"[41] Scheme 2 illustrates that the other conceivable transition state **44** would yield the wrong isomer **42**, thus confirming the chair-like transition state in the cyclization of polyenes such as **40**. The conformational integrity of the alkene geometry in polyene cyclization could soon be translated to drimanes and other cyclic terpenes that were produced by "head-to-tail" cyclizations.[42]

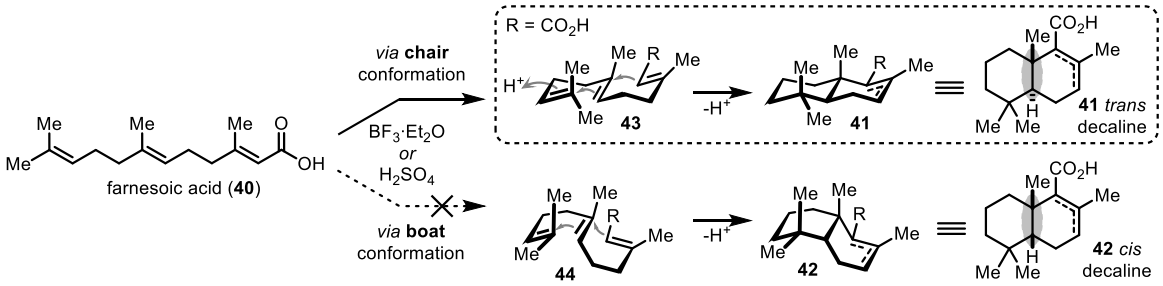

Scheme 2. Chair and boat transition state giving *trans* (**41**) and *cis* (**42**) decalin bicycles.

2.2. Proton Cyclization Reactions

A major challenge of mimicking proton-induced polyene cyclizations in the laboratory is the selective protonation of the "head" prenyl unit in the presence of one or more double bonds with similar electrophilic properties.[43] Protonation of the terminal olefin of **45** and subsequent nucleophilic attack of the internal double bond results in the formation of tertiary carbocation **I** (Scheme 3). Then, regioisomeric proton eliminations may take place (→**Ia**), as well as inter- and intramolecular nucleophilic addition of the carbocation giving **Ib**. The latter is decisive for the diastereoselectivity of the product, as trapping may occur from the top or bottom of the planar cation **I**, giving two possible diastereoisomers **Ib** in respect to the tertiary carbon. However, if the internal olefin of **45** is protonated first (→**II**) two regiodivergent cyclizations may occur depending on the structural nature of the residue R to yield **IIa** or **IIb**. They may then react further through rearrangement reactions, hydride shifts, or eliminations giving rise to a plethora of complex products.[44]

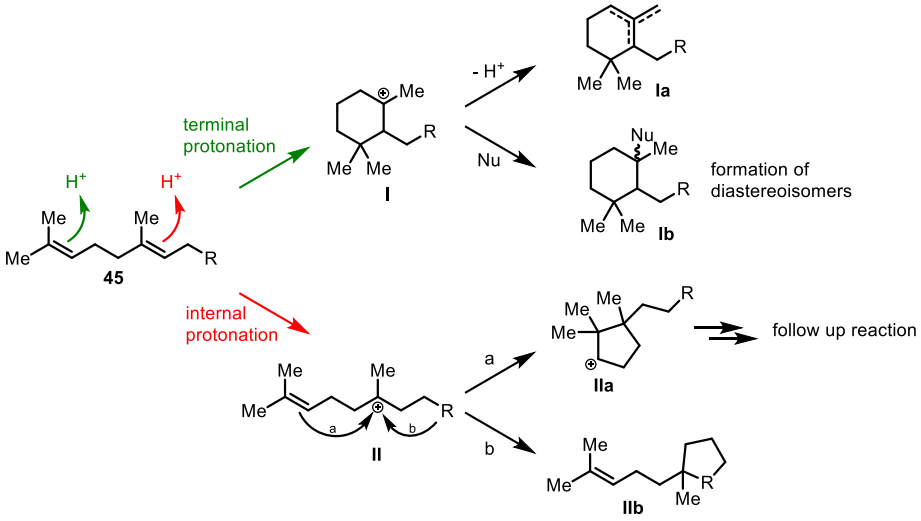

Scheme 3. Selection of possible reactions when linear polyene **45** is protonated.

As demonstrated in the biochemical pathway for proton cyclization different products can be obtained from the same linear starting material (c.f. Scheme 1). Naturally, chemists have since been attempting to copy the reactivity of enzymes and produce the (poly)cyclic products. Since the first attempts over 70 years ago using strong mineral acids, such as sulfuric acid,[45] multiple publications appeared, offering access to complex proton-cyclized products. Generally, linear polyenes, mainly derived from geraniol (**5**) or farnesol (**46**, not shown), were converted with strong organic or inorganic Brønsted or Lewis acids such as trifluoroacetic acid,[8,46] fluorosulfuric acid,[47] $SnCl_4$,[48] $BF_3{\cdot}OEt_2$,[49] $ZnCl_2$,[50] $RuCl_3$[51] and Indium(III) salts.[51b,52] Proton-induced polyene cyclizations have been comprehensively reviewed in the literature as well.[2a,53] Table 2 shows selected examples of the necessary reaction conditions relying on strong acids to promote the cyclization reaction in standard organic solvents to promote the cyclization of substrates **47**-**51** to cyclic **23**, **6**, and **52**-**55**. A diastereomeric ratio was only reported for entry 2.

Table 2. Selected examples for racemic proton-induced polyene cyclization conditions.

entry	starting polyene	conditions	product	yield
1[46]	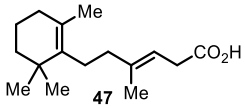 **47**	TFA CH_2Cl_2, 0 °C	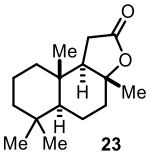 **23**	64%
2[54]	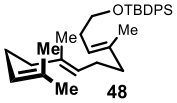 **48**	$ClSO_3H$ $EtNO_2$, -78 °C	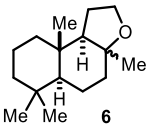 **6**	91% (d.r. = 59:41)
3[51c]	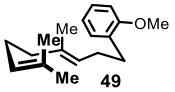 **49**	$RuCl_3$, AgOTf DCE, 60 °C	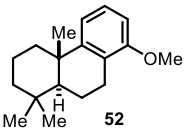 **52**	76%
4[48d]	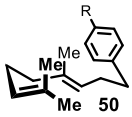 **50**	$SnCl_4$ THF, -78 °C	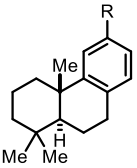	45%, R = H (**53**) 35%, R = Me (**54**)
5[50]	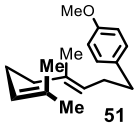 **51**	ZnI_2, $TosOH \cdot H_2O$ CH_2Cl_2, rt	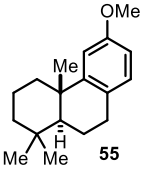 **55**	99%

One more recent approach by Luo *et al.* is the photocatalytic cyclization of geranyl phenols (**56**) with eosin Y (**57**) in 1,1,1,3,3,3-hexafluoroisopropanol (HFIP) producing chromanes **58**-**61** in good yields of up to 93% and diastereoselectivities of > 95:5 (Scheme 4).[55] The mode of activation of the head olefin is, in this case, not the direct protonation. This was shown by control experiments with strong organic acids, which yielded complex product mixtures. The postulated mode of action here is a single electron transfer onto the arene, subsequently forming a radical cation, which then undergoes cyclization. HFIP as the solvent was postulated to assist the hydrogen shift in the final step. The method also tolerated geranyl malonates (→**62-64**). However, the postulated radical cationic activation of the alkene with eosin Y (**57**) was to date only observed for α-hydrogen abstractions of amines and not unactivated alkenes.[56] Similar photochemical cyclizations have used light in a much shorter wavelength, as high energy and highly active catalysts were necessary to activate the weakly absorbing isolated alkene.[57]

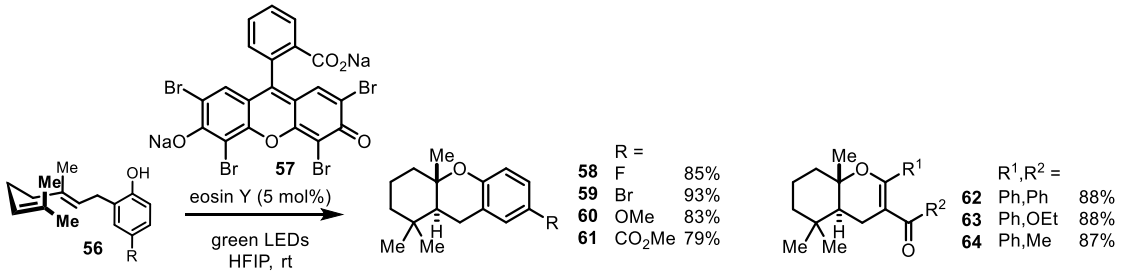

Scheme 4. Photocyclization of geranyl derivatives **56** with eosin Y (**57**) by Luo *et al.*[55]

In the last yearss groundbreaking methods were developed for the enantioselective cyclization of polyenes by employing structurally defined catalysts, thus mimicking the confined space within an enzyme. The first example for an enantioselective version of this reaction was reported in 1999 by Ishihara *et al.* and allowed for the cyclization of geranyl phenol **65** or **66** with good yields of up to 92% and moderate enantioselectivities of up to 69%.[58] The employed stoichiometric reagent was a 1:1 mixture of benzoylated 1,1'-bi-2-naphthol (BINOL) and tin(IV)chloride (**68**, Scheme 5). The Lewis acid was complexed, and attack of the terminal olefin was favored from one side, thus inducing enantioselectivity.

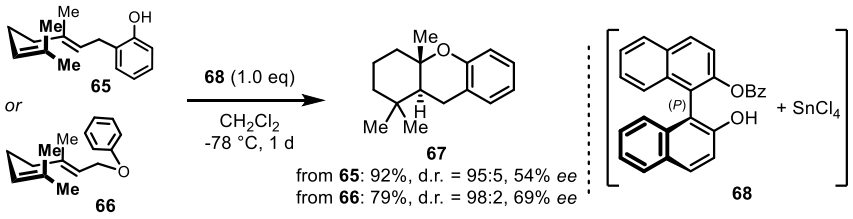

Scheme 5. First enantioselective proton-induced cyclization of geranyl substrates **65** and **66** by Ishihara *et al.*[58]

Corey *et al.* found that by substituting $SnCl_4$ with the bulkier Lewis acid $SbCl_5$ and fine-tuning the BINOL ligand to the 3,3'-dichloro derivative **69** converted linear **70** into the product **53** in excellent diastereomeric ratios, up to 92% *ee* and 80% chemical yield, albeit 50 to 100 mol% of the Lewis acid was necessary to achieve this outcome (Scheme 6).[59] This methodology is currently the benchmark reaction when arene-terminated proton-cyclization products are targeted from linear precursors.[60]

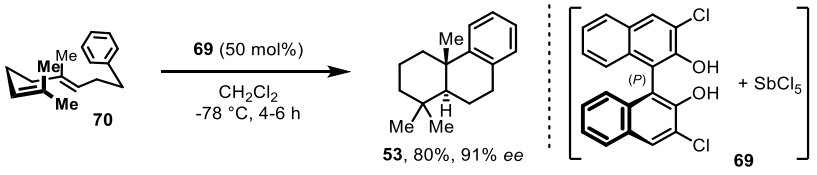

Scheme 6. Corey's BINOL-based cyclization of **70** with antimony(V)pentachloride.[59]

With more complex and sterically demanding BINOL-derived phosphoric triflimide **71**, Zhao *et al.* were able to facilitate the in situ formation of imines from terminal aldehydes (e.g. **72**) and *p*-toluenesulfonamide (**73**) and subsequently cyclizing the intermediate to the product **74** in good yields and *ee*s up to 92% at -60 °C with magnesium thiosulfate as an additive (Scheme 7).[61] A 12-step total

synthesis of the natural product (–)-ferruginol (**75**) was achieved with the shown cyclization being the key step, demonstrating the synthetic utility of this method to access drimanes.

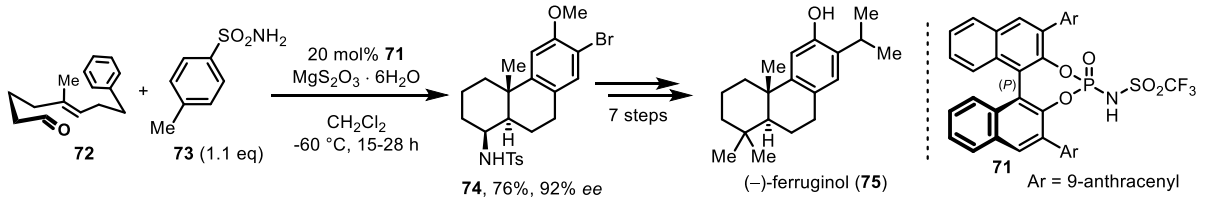

Scheme 7. Zhao's imine activation strategy.[61]

In the same year, the group of List *et al.* developed an even more sterically restricted highly acidic imidodiphosphorimidate (IDPI) catalyst **76** for the cyclization of secondary alkenes with primary alcohols as the terminating nucleophile (**77**→**78**, Scheme 8, right).[62] Compared to BINOL-based phosphoric acid **79** the enantioselectivity in this reaction increased from 40 to 92%. The success of this dimeric catalyst class lies in the tight confinement of the 3,3'-substituents which creates a tighter pocket around the acidic proton in the active site thus allowing for a high enantioselection (Scheme 8, bottom).[63] Albeit this is not a polyene cyclization reaction, the increase in catalyst complexity and the beneficial effect of confinement giving the starting material a defined environment to react in is striking.

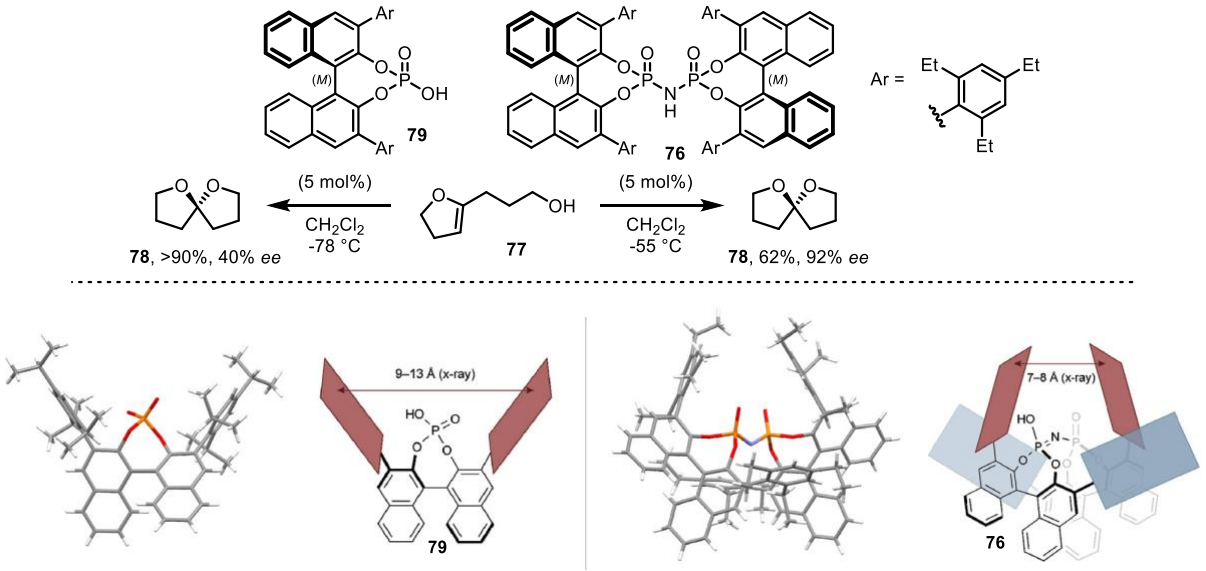

Scheme 8. List's application of IDPI catalyst **76** for the cycloetherification of primary alcohol **77** (top) [62] and comparison of the crystal structures of the catalysts **76** and **79** (bottom, reproduced from reference 63a with permission from Elsevier).

In summary, chemists have been developing a wide range of harsh and mild methods for the diastereo- and enantioselective protoncyclization of alkenes. Most recent developments show that catalysis becomes more selective if the reactive site is heavily confined, allowing only for the desired reactivity initiated by the reactive site.

2.3. Halonium-Induced Polyene Cyclizations

In analogy to proton-induced cyclized polyenes the reaction may also be initiated by an electrophilic haliranium ion such as **II** (Figure 6). Similar to the proton cyclization reactions mentioned before, many undesired side reactions can take place with the first challenge being the addition to the head olefin of **I** thus forming cyclic haliranium ion **II**. Haliranium ions, especially the chlorine derivatives (*vide infra*) tend to form the open, planar carbocation **III**, which is prone to undergo elimination or nucleophilic addition giving **IV** and **V**, respectively. If the desired cyclization to the 6-membered **VI** proceeds, again, elimination may take place (→**VII**), and the final nucleophilic addition may proceed either from the top- or bottom side of the intermediate affording two potential diastereoisomers with **VIII** being the desired reaction product.

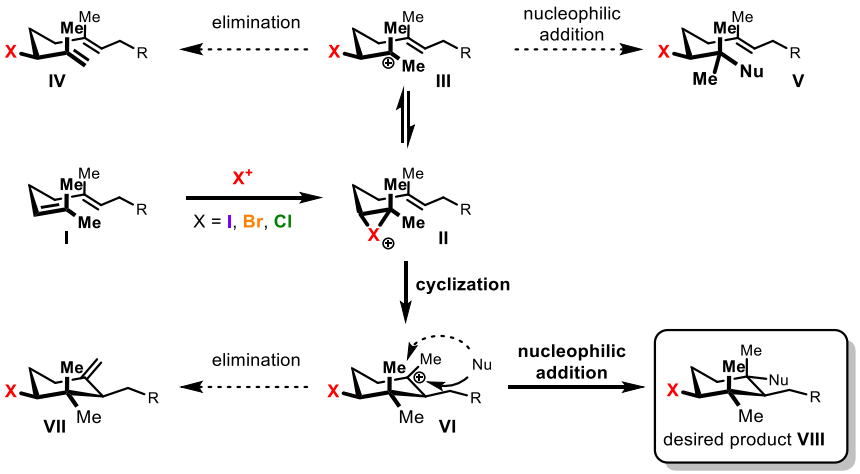

Figure 6. Mechanism of the halonium-induced polyene cyclization with possible undesired side reactions (dashed arrows).[64]

The earliest report of a successful halonium-induced polyene cyclization reactions dates back to 1966 when van Tamelen disclosed that treating farnesoic acid methyl ester **80** with NBS in THF yielded bromohydrine **81** as the major fraction with monocyclic **82** and bicyclic alkene-containing **83** in minor quantities (Scheme 9).[65] Regrettably, no diastereomeric ratio was reported for **83**.

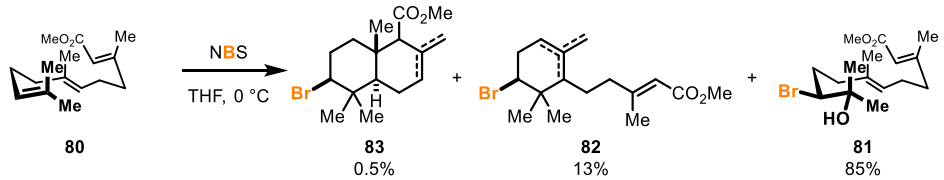

Scheme 9. First reported halonium-induced polyene cyclization by van Tamelen in 1966.[65]

This was the first example of a direct bicyclization of linear polyenes and sparked further exploration of this reaction pathway culminating in numerous methods for the halonium-induced cyclization thereof, which has recently been comprehensively reviewed in the literature.[2b,66] For example, it was found that treating homogeranoic acid (**84**) with bromine and silver tetrafluoroborate resulted in bicyclic **85** in 15% yield (Table 3, entry 1).[67] 2,4,4,6-Tetrabromocyclohena-2,5-dienone (TBCO, **86**) gave a mixture of

mono- and bicyclic products (**87** and **88**) when **89** is treated with the bromination reagent **86** (entry 2)[68] and failed to cyclize electron-poor geranyl cyanide (**90**). Here, solely the dibrominated product **91** was isolated in 98% yield (entry 3).[69] Hennecke and coworkers utilized the stable bromiranium salt **92** to trigger polyene cyclization of **50** furnishing tricycles **93-95** in low to moderate yields (entry 4).[70] Umpolung reaction of bromides with hypervalent iodine reagent $PhI(OPiv)_2$ resulted either in dehalogenation, haloesterification, or bromocyclization of linear homogeranyl benzenes **50** (entry 5).[71] Ishihara disclosed that treating **96** with NBS and PPh_3 as Lewis basic activator yielded tricyclic **97** in 50% yield, and, at lower temperatures, NIS and PBu_3 gave iodinated **98** but only after treatment of the crude mixture with chlorosulfonic acid (entry 6 and 7).[72] Barluenga's reagent Py_2IBF_4 afforded chromane **99** in good yields through rearrangement of the geranyl phenyl ether **66** at cryogenic reaction conditions (entry 8).[73] Further information regarding diastereomeric ratios were not reported in these cases.

Table 3. Examples of direct halocyclization reactions with racemic reagents.

entry	starting polyene	conditions/reagent	product	yield
1[67]	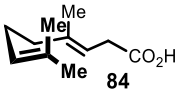 **84**	Br_2 $AgBF_4$	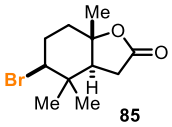 **85**	15%
2[68]	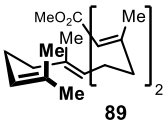 **89**	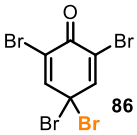 **86**	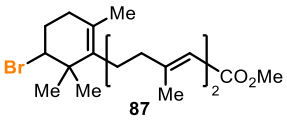 **87** + 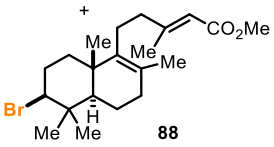 **88**	49% + 25%
3[69]	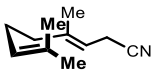 **90**	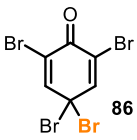 **86**	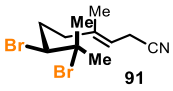 **91**	98%
4[70]	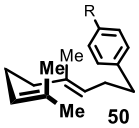 **50**	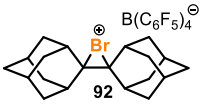 **92**	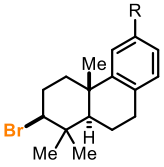	**93**, R = H, 64% **94**, R = *i*Pr, 29% **95**, R = OMe, 50 %
5[71]	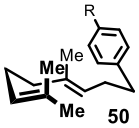 **50**	$PhI(OPiv)_2$ Et_3SiBr	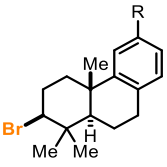	**93**, R = H, 67% **95**, R = OMe, 40%

6[72]	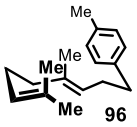 **96**	NBS PPh_3	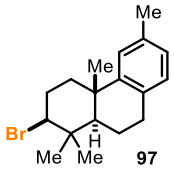 **97**	50%
7[72]	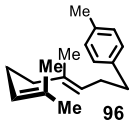 **96**	PBu_3, NIS -78 °C *then* $ClSO_3H$	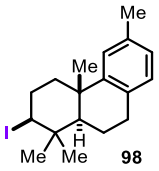 **98**	99%
8[73]	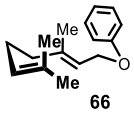 **66**	IPy_2BF_4 HBF_4, -85 °C	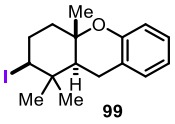 **99**	86%

Despite these efforts, a truly versatile and broadly applicable methodology has not been disclosed until the Snyder group introduced bromodiethylsulfide bromopentachloroantimonate(v) (BDSB, **100**) in 2009, a reactive electrophilic bromonium donor.[74] Treating several geranyl- and farnesyl derived substrates **45** with BDSB (**100**) in nitromethane at low temperatures afforded the cyclized material **85, 93** and **101** in good yields of up to 80% and with good stereocontrol (Scheme 10). Analogous iodination and chlorination reagents IDSI (**102**) and CDSC (**103**), respectively, were reported shortly after giving likewise access to the iodinated **104**-**106** and, to a significantly lower extend, chlorinated derivatives **107**-**109**.[75] Besides being considered as the "gold-standard" for those kinds of halocyclization reactions the drawbacks of this system include the utilization of a specialized, not commercially available and heavy-metal based halogenating agent with limited group tolerance, and examples for the challenging yet highly interesting chlorocyclization are limited.

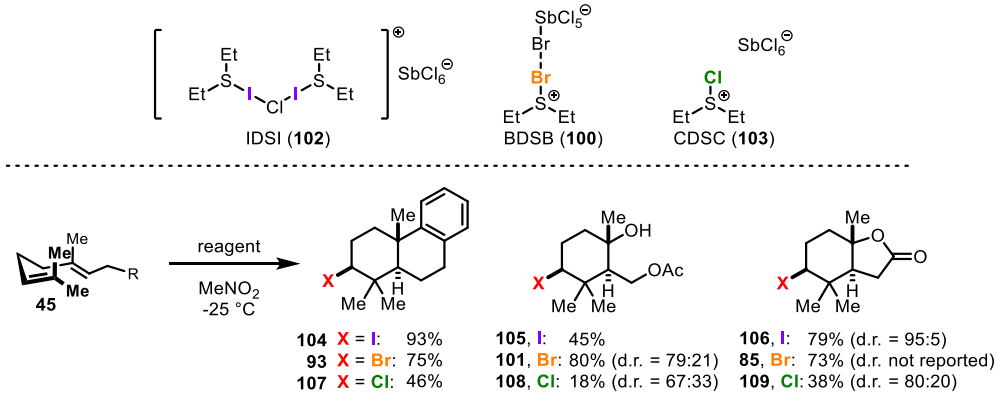

Scheme 10. Snyder's halogenation reagents **100**, **102** and **103** and their applications in polyene cyclization reactions.[75-76]

Since Ishihara's publication in 2007 on the enantioselective iodocyclization of homogeranyl- and homofarnesylbenzene derivatives (e.g. **96**) it became feasible to render the halocyclization enantioselective with promotor **110** (Scheme 11). However, in most cases, the reaction was terminated after the first enantiodetermining cyclization step, thus giving a mixture of monocyclic material **111** and

98, which was then treated with chlorosulfonic acid at low temperatures in 2-nitropropane furnishing the completely cyclized product **98** in good yields of 57% and enantioselectivities of up to 95% *ee*. However, if NIS was exchanged by NBS the enantioselectivity dropped drastically.[72] Switching to promotor **112**, however, produced **97** in 36% *ee* and 75% yield. Moreover, phosphines **110** and **112** were added in stoichiometric amounts in order to ensure high enantioselectivity. Geranylphenols were likewise successfully converted by the Ishihara group with adjusted catalysts and reaction conditions in the following years (not shown).[77]

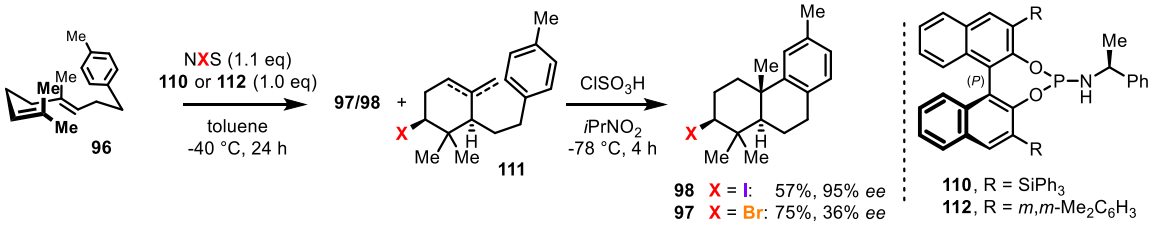

Scheme 11. First enantioselective halocyclization of polyene **96** reported by the Ishihara group.[72]

Following this pioneering work, Yamamoto *et al.* developed a bromocyclization reaction of **113** capable of producing the bromocyclized materials **93**, **95**, **97** and **114-119** with enantioselectivities of up to 87% (Scheme 12).[78] The temperature of the reaction had to be lowered to -90 °C and a highly coordinating phosphorthioamidate catalyst **120** with sterically demanding substituents had to be employed. Complete cyclization was again only achieved through treatment of the crude product with chlorosulfonic acid in 2-nitropropane. This work showed that a catalytic enantioselective bromonium-induced cyclization is feasible and was demonstrated for a range of homogeranyl arenes **50** and geranyl phenols **56**. The noteworthy trend is that compared to Ishihara's method an increase in spatial confinement was necessary to achieve sufficient enantioselectivity.

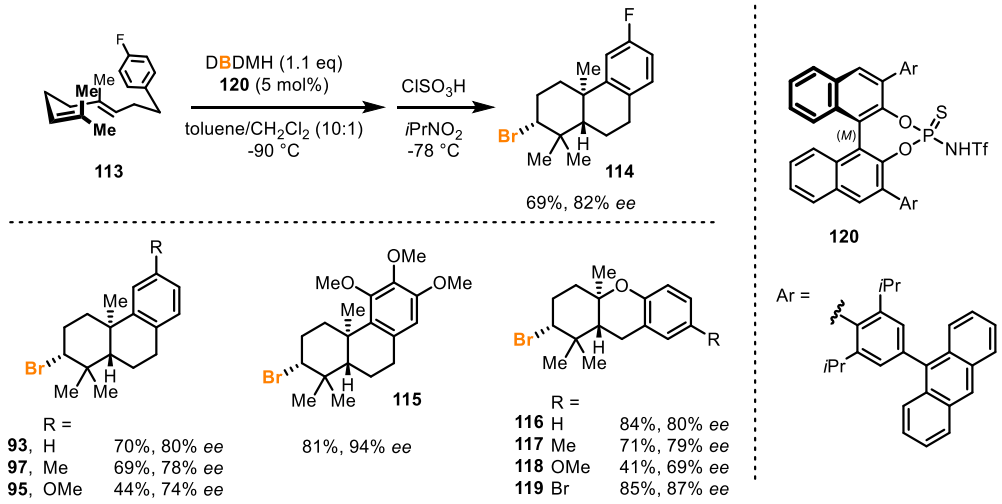

Scheme 12. Enantioselective bromocyclization by Yamamoto *et al.*[78]

There are, on the other hand, only few reports for the direct chloronium-induced cyclizations compared to bromiranium- and iodiranium-induced cyclizations mentioned above. in 2010 Snyder's CDSC (**103**)

was, for the first time, able to perform this reaction (Scheme 10), however, with low yields and poor diastereoselectivites compared to BDSB (**100**) and IDSI (**102**).[75] Shortly thereafter the same group disclosed a two-step mimic using mercury(II) salts in stoichiometric quantities together with the chiral BOX-ligand **121** to induce cyclization (Scheme 13).[79] The enantiomerically enriched organomercurate intermediate **122** was isolated, purified and subsequently treated with the corresponding elemental halogen and halide salt to afford the desired cyclized products **93**, **101**, **104**, **107** and **124** in good yields of up to 72% and enantioselectivities of up to 81% *ee*. However, this cyclization reaction does not proceed via a haliranium ion but a mercuronium ion, but as similar structures are accessed here it should be briefly mentioned.

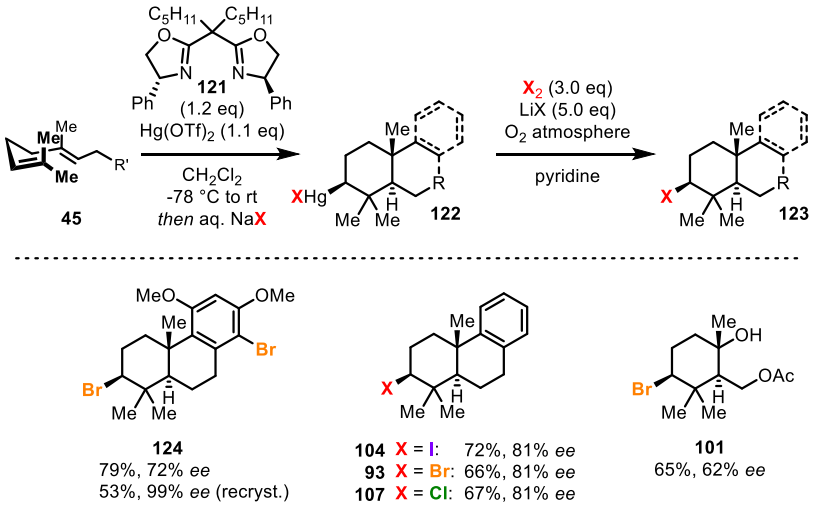

Scheme 13. Enantioselective mercury(II)-induced polyene cyclization with displacement by halides published by Snyder *et al.*[79]

Enantioselective, bromonium initiated cyclizations were also made possible by solvolysis of a chiral halogenated starting material. Braddock *et al.* have reported a 5-step synthesis of chiral bromohydrine **125**, in which the alcohol was activated by converting it into a good leaving group, thus allowing for nucleophilic attack of the bromine and generating the enantioenriched bromiranium ion (not shown Scheme 14a). The cyclization takes place with stereoretention under the reported reaction conditions, albeit the diastereoselectivity is poor (d.r. = 75:25) and the yield low (25-35% from the activated linear precursor). Intramolecular substitution created the enantiopure bromiranium ion, which underwent cyclization to give **95** without observable olefin-to-olefin transfer in cryogenic dichloromethane.[80] Similarly, Burns *et al.* disclosed that treating dihalide **126** with potassium carbonate in HFIP resulted in chloride abstraction and thus formation of the bromiranium ion, which cyclized with 96% enantiospecificity to acetate **101** (Scheme 14b). It is noteworthy that again only minor racemization of the chiral bromiranium ion was observed and the product could be further functionalized to structurally related brominated chamigrenes.[81]

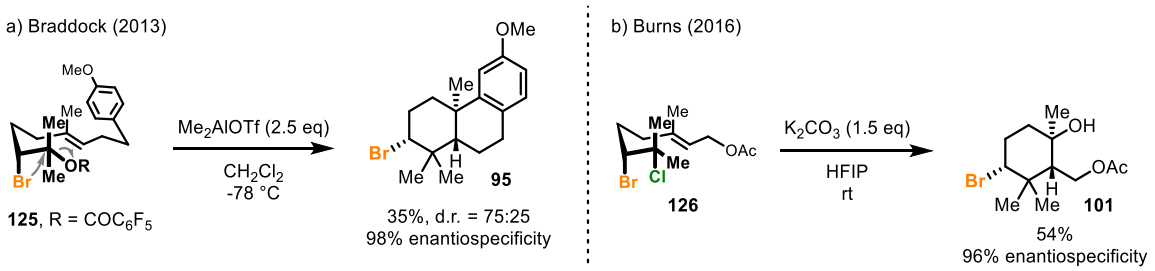

Scheme 14. Braddock's (a)[80] and Burns' approach (b)[81] for the enantiospecific generation of bromiranium ions.

Burns *et al*. also took on the total synthesis of azamerone (**127**), with one key step being the enantioselective chloroetherification of quinone **128** to set the stereocenter in the top part of the structure (**129**, Scheme 15).[82] This method is a substrate-specific further development of their alkene dihalogenation strategy[83] and tailored for the chlorocyclization of **128** by providing a trapping oxygen nucleophile in the substrate (→**129**) with chiral ligand **130**. The lower part of the molecule **127**, consisting of a chlorocyclized geranyl chain was produced from **130** in a racemic fashion with Snyder's mercury(II)-based method without a chiral ligand, and the enantiomers were separated by chiral resolution via esterification with (*S*)-α-methoxyphenylacetic acid and separation of the diastereoisomers to access multi-gram quantities of chiral **108** (not shown).

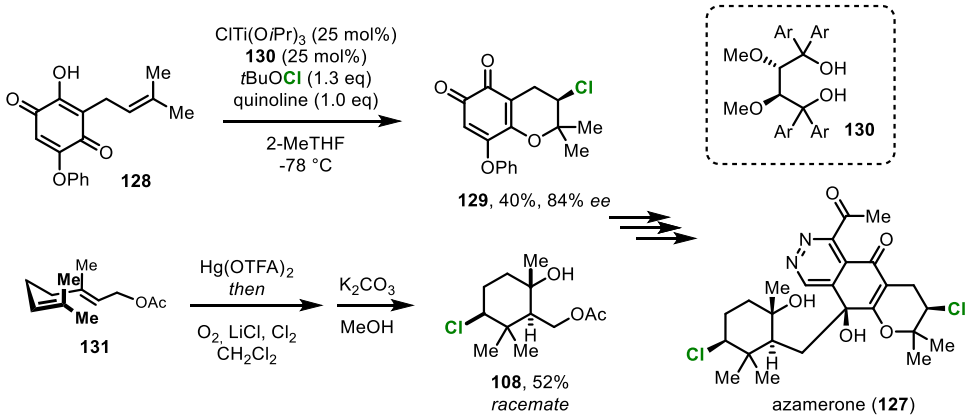

Scheme 15. Burn's enantioselective chlorocyclization and application of racemic mercury(II)-induced cyclization in the total synthesis of azamerone (**127**).[82]

To the best of my knowledge, those reports present the only examples for the direct, chloronium-induced cyclizations of polyenes reported thus far. Considering the large and ever-growing number of halogenated natural products being isolated from natural sources[84] creates the need for novel, direct and selective iodo-, bromo-, and chlorocyclization methods.

2.4. Stability of Haliranium Ions

Compared to bromo- and iodocyclizations, chlorocyclizations are much more challenging to achieve chemically. An explanation for the lack of broadly applicable chlorination methods as compared to bromo- or iodocyclizations is the propensity of chloriranium ions to preferentially form the ring-opened carbocation **141** in contrast to the chloriranium ion (**142**, Scheme 16).[85] In his landmark work, Olah *et al.* studied the formation of haliranium ions **132** at -78 °C in sulfur dioxide by treatment of *β*-fluorohalides **133** with SbF_5. Iodiranium and bromiranium ions were observed for all substitution patterns from tetra- to unsubstituted haliranium ions (**134-139**). For chloriranium ions, only the tetrasubstituted **140** and trisubstituted **142** were detected, albeit the latter was in equilibrium with the planar carbocation **141** allowing for rotation around the sp^3 bond. Chlorinated analogs of **136** resided in the open form **143**, whereas the disubstituted species were constitutionally unstable and underwent rapid rearrangement to **144** and **145**. Mono- or unsubstituted chloriranium ions were not observed, rather the analysis revealed polymerization or decomposition of the starting material.

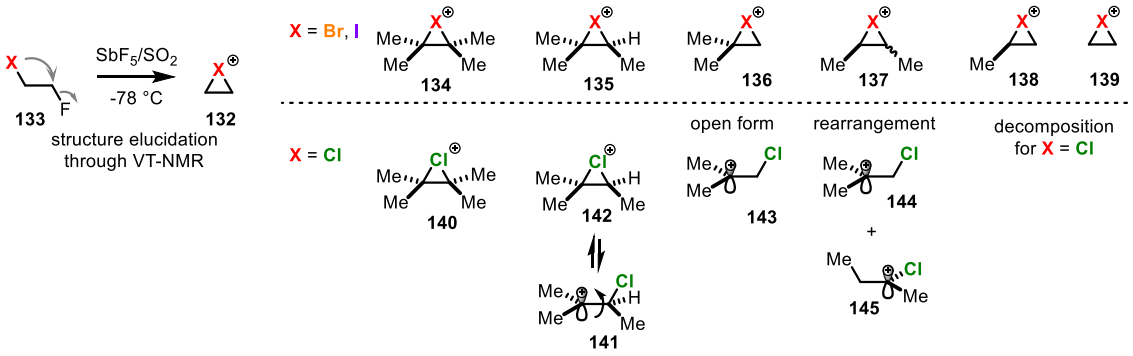

Scheme 16. Generation (left) and observed haliranium ions in SO_2 solution.[85c]

As described, Olah *et al*. investigated the *chemical* stability of haliranium ions. In 2010 Denmark and coworkers conducted detailed studies on the absolute *configurational* stability of haliranium ions **147** (Scheme 17a).[86] Here, they subjected *β*-halo sulfonates **146** to anchimerically assisted solvolysis conditions in HFIP, thus generating enantiomerically pure haliranium ions **147**. Nucleophilic trapping of C_2 symmetric **147** with two equivalents of sodium acetate or tetrabutylammonium acetate gave acetate **148**, of which the enantiomeric purity was determined. The enantiospecificity (e.s.) is calculated by dividing the *ee* of the product by the *ee* of the starting material, thus having a convenient method of describing the conservation of configurational purity in the course of the reaction. An erosion thereof can take place by the addition of (*E*)-oct-4-ene (**149**, Scheme 17b), which adds to the haliranium ion **147** through a low-barrier associative displacement at the halogen via transition state **150**.[87] Subsequently, the free haliranium ion *ent*-**147** forms, thus diminishing any initial enantiopurity of **148** after an analogous nucleophilic attack of the acetate.

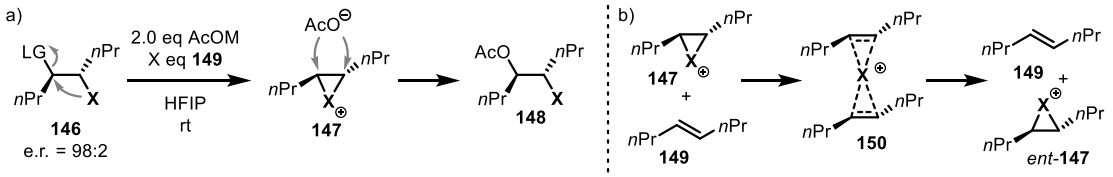

Scheme 17. (a) Denmark's studies on the absolute configurational stability of bromiranium and chloriranium ions. (b) Enantiomeric erosion through olefin-to-olefin transfer.[86]

With sodium acetate as the nucleophile and the halogen being bromine the addition product **148** formed in 79% with 100% e.s. (Table 4, entry 1). Increasing amounts of **149** in the reaction mixture rapidly diminished the e.s. to 46% with 0.5 eq of **149** and 25% with 1.0 eq of **149**, respectively (entries 2 and 3). When the counterion of the acetate nucleophile was exchanged with the less coordinating tetrabutylammonium, thus increasing the nucleophilicity of acetate, the haliranium opening proceeded more rapidly. This reduced the olefin-to-olefin transfer pathway and gave the product **148** in 81% e.s. (entry 4).

As chlorine is more electronegative than bromine, the positive charge of the chloriranium ion thus resides preferably at the carbon and not the halogen.[85a] This results in the propensity of chloriranium ions to undergo processes characteristic for carbocations, such as eliminations and rearrangements.[86] On the other hand, a nucleophilic attack of an olefin on the chlorine is less favored, hence greatly reducing the susceptibility to undergo olefin-to-olefin transfer. Entries 5 and 6 show the results of the solvolysis of **146** with or without alkene **149**, giving the acetolysis product **148** with perfect e.s. in both cases. However, due to the lower chemical stability of the formed chloriranium ion, the yield is reduced to 32 and 44%, respectively. The results by Denmark and Olah et al. illustrate that chloriranium ions have high configurational stability and a low tendency of racemizing, however possess a low chemical stability and are thus prone to carbocationic follow-up reactions. Bromiranium ions, on the other hand, are chemically more stable but may undergo olefin-to-olefin transfer to other alkenes, thus potentially losing their original absolute configuration.

Table 4. Results of Denmark's studies on the configurational stability of bromiranium and chloriranium ions (conditions: see Scheme 17a).[86]

entry	X, LG	cation	eq of 149	yield of 148 [%]	e.s. of 148 [%]
1	Br, OTs	Na^+	–	79	100
2	Br, OTs	Na^+	0.5	71	46
3	Br, OTs	Na^+	1.0	75	25
4	Br, OTs	Bu_4N^+	1.0	73	81
5	Cl, OTf	Bu_4N^+	–	32	100
6	Cl, OTf	Bu_4N^+	1.0	43	100

2.5. Cyclization Reactions in Macromolecular Assemblies

As mentioned in the previous chapters, enantioselective polyene cyclizations proceed best in confined spaces or pockets in order to yield the desired material with high selectivity. Besides phosphoric acid-based organocatalysts (c.f. chapter I.2.2, Scheme 6), confinement could also be achieved by employing structurally defined macromolecular cages. Toste and colleagues applied a polyanionic supramolecular assembly **150** together with aqueous buffer at elevated temperatures in the "tail-to-head" cyclization of citronellal (**151**) which furnished isopulegols **152** as a mixture of diastereoisomers (Scheme 18).[88] In this case, water was successfully hindered from trapping carbocation **153**. Under the same conditions, but lacking assembly **150**, diol **154** is produced as the major product. This work demonstrates that a tailored reaction environment is beneficial in steering the carbocationic follow-up reaction towards the desired chemoselectivity.

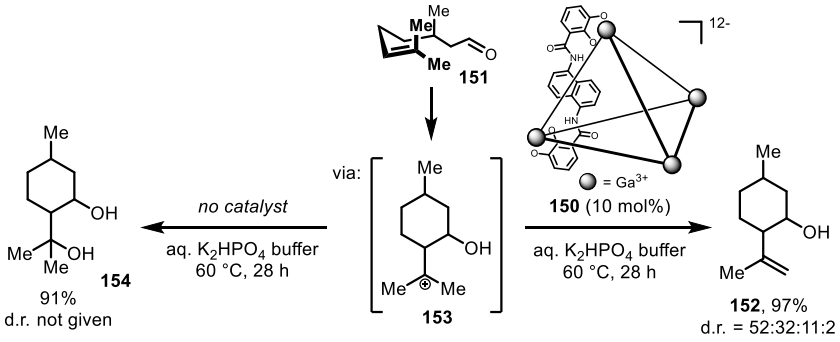

Scheme 18. Cyclization of citronellal (**151**) with and without supramolecular assembly **150**.[88]

The previous example focused on the exclusion of nucleophilic water in proximity to the reactive species during the cyclization process. A few years later the Tiefenbacher group reported the application of self-assembled resorcinol-based hexameric capsules of six units of **155** and eight water molecules for the "tail-to-head" cyclization of simple monoterpenes through activation of the allylic alcohol or acetate.[89] This reactivity was enabled by the ability of **156** to stabilize positive charges, explicitly allylic cations, inside the cavity (Scheme 19a).[90] These properties were needed to effectively catalyze cyclization reactions in an organic capsule for the first time. The key step is the flip from the 2,3-*transoid* carbocation **157** to the 2,3-*cisoid* cation **158**, now prone to cyclization giving α-terpinene (**159**). This flip was only possible through the extraordinary stabilizing effect of the capsule, emphasizing the necessity of cation stabilization during polyene cyclizations.[15] The product selectivity was dependent on the configuration of the starting material, as nerol (**160**) gave α-terpineol (**161**) and subsequently eucalyptol (**162**) in up to 40 % GC yield (Scheme 19b).[91]

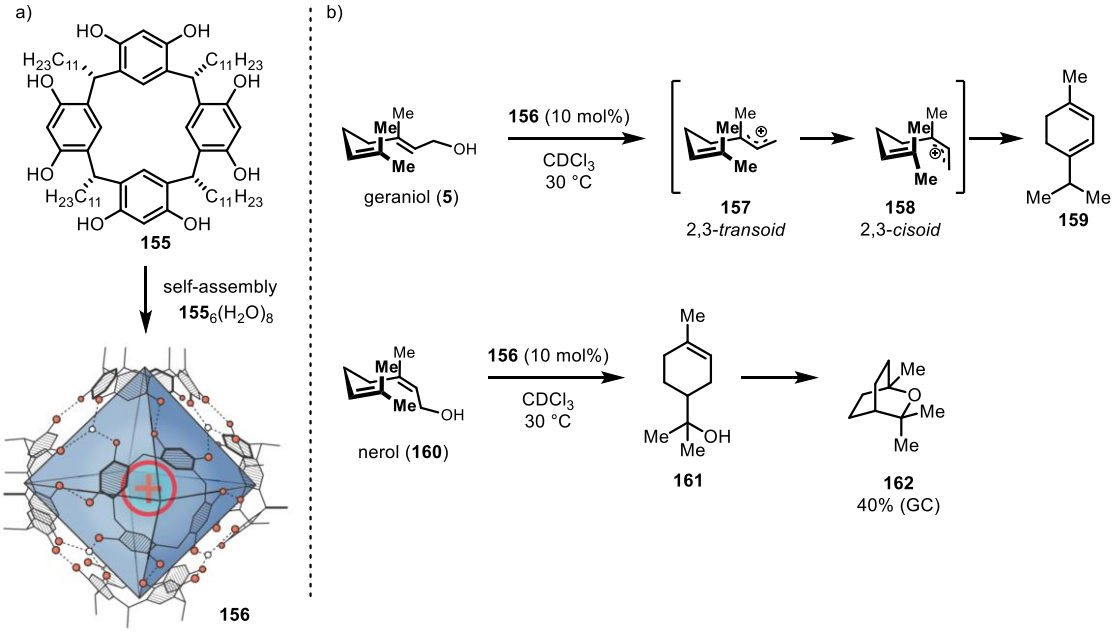

Scheme 19. (a) First generation resorcinol-based capsules **156** and (b) their use in tail-to-head polyene cyclizations by Tiefenbacher *et al*. Reproduced from reference 89 with permission from Springer Nature.

2.6. Self-Assembled Confinement in Solution

Confinement of small molecules either in enzymes or within bulky catalysts is indispensable to stir the reactivity towards the desired product and to significantly enhance the selectivity. That such a compartmented reaction system may be created in solution was under investigation by the Berkessel group since 2001, when they thoroughly examined the beneficial effect of the fluoroalcohol HFIP in the oxidation of alkenes with hydrogen peroxide.[92] To fully understand the uniqueness of HFIP one has to look at its interesting physical properties. For instance, the pK_a value in HFIP is drastically reduced due to the electron-withdrawing fluorine atoms as compared to its non-fluorinated analog isopropanol, being 9.3[93] and 16.5,[94] respectively. Consecutive systematic computational investigations revealed that the fluorinated alcohol also differs immensely from isopropanol on a molecular level.[95] The fluorine groups do not only increase the acidity but also hinder rotation of the C-O bond in the alcohol. The potential energy of rotation of HFIP in the gas phase is about 1 kcal/mol higher than in isopropanol (Figure 7a), as the bulky CF_3 groups hinder the free rotation around the HC_2OH angle to a larger extend than in the non-fluorinated isopropanol (dashed line). The torsion angle in solid-state HFIP was determined to be 22°, which is in close agreement with the calculations (Figure 7b).

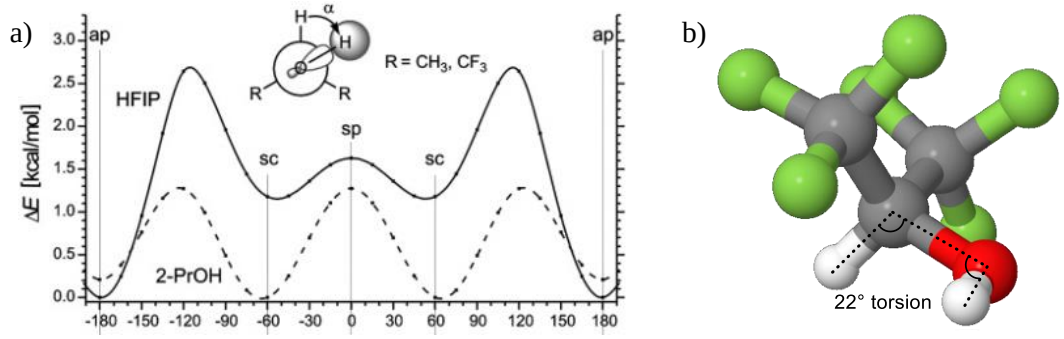

Figure 7. a) Conformational analysis of HFIP in the gas phase: potential energy for HFIP and isopropanol, reproduced with permission from reference 95. Copyright 2006 American Chemical Society. b) Torsion angle in solid state HFIP.[95]

The apolar CF_3 groups and the highly polarized hydroxyl group give HFIP a very high dielectric constant of $\varepsilon = 15.7$,[96] which has repercussions on the macroscopic properties of the solvent. Molecular modeling of the epoxidation of cyclooctene (**163**) with aqueous peroxide in HFIP showed that HFIP forms comparted aggregates around the apolar alkene, with the polar hydroxyl groups facing towards the aqueous phase and the hydrophobic CF_3 moieties towards the alkene (Figure 8a).[97] The high tendency of the OH groups in being both hydrogen bond donors and acceptors results in a dense hydrogen bonding network to other donors and acceptors such as H_2O_2 or HFIP itself, thus forming a chained or helical aggregate of HFIP monomers which overall increases the H-bond donor ability of the terminal HFIP molecule to Lewis bases (Figure 8b).[95]

Due to the bulkiness of the CF_3 groups, HFIP is a notably weak nucleophile, as demonstrated by the methylation of either HFIP or isopropanol with **164** to the methyl ethers **165** and **166**, respectively. The nucleophilicity values (N_{OTs}) are on a logarithmic scale, meaning that HFIP is four orders of magnitude less nucleophilic than isopropanol (Figure 8c). This means HFIP can on occasion act as a nucleophile, but mainly with highly reactive carbocations.[64,98] Taken together, the low nucleophilicity and the high dielectric constant make HFIP a prime solvent for stabilizing carbocationic transition states. The effect was quantified by Pezacki *et al*. by photochemically generating diazo compounds **167** and upon TFA treatment the corresponding aliphatic carbocations **168** formed (Figure 8d). They measured the reactivity of the generated carbocations in the presence of the nucleophile trimethoxybenzene (**169**) in acetonitrile, TFE, and HFIP. The obtained respective lifetimes of **168** were up to two orders of magnitude higher in HFIP for cyclobutyl cation (**171**) and 1-cyclopropylethan-1-ylium cation **172**.[99] This showed that HFIP is indeed able to stabilize transient carbocations and significantly prolong their lifetimes. All the described properties make HFIP a versatile solvent promoting a wide range of reactions,[100] and due to its multi-ton commercial availability has been used in large-scale syntheses.[101]

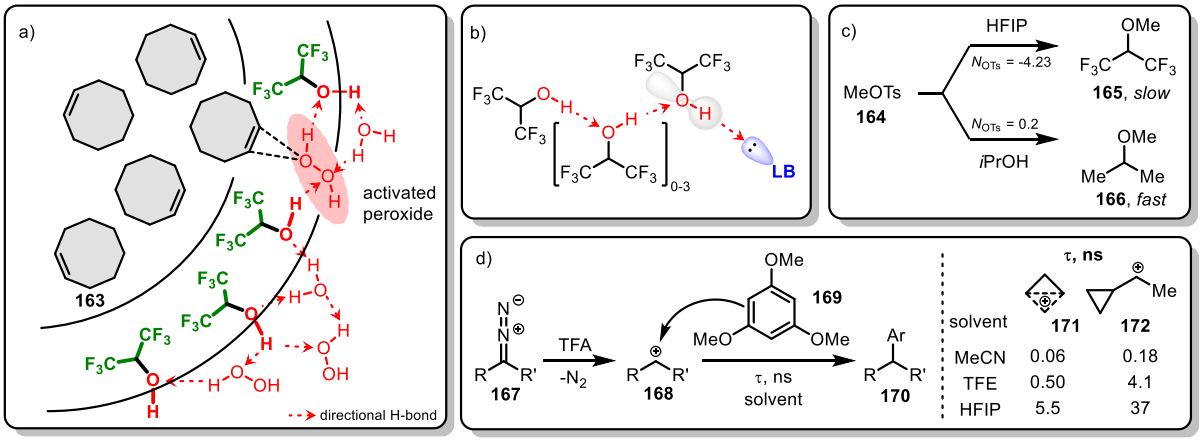

Figure 8. Key properties of HFIP. a) Cluster formation between apolar cyclooctane (**163**), HFIP layer and polar aq. peroxide phase (red).[97] b) Aggregation-induced H-bonding enhancement of HFIP and interaction with Lewis base.[95] c) Nucleophilicity of HFIP compared to isopropanol.[102] d) Lifetimes of carbenium ions **168** in HFIP compared to MeCN and TFE.[99]

The group of Prof. Gulder is developing methods to recreate nature's unique ability to create complex products with ease. We particularly are interested in mimicking the active cavity in enzymes by employing catalytic supramolecular assemblies constructed through Lewis acid/Lewis base interactions.[64] The presented thesis thus focuses on exploiting the unique properties and interactions of fluorinated alcohols and Lewis bases to create triphilic structures as shown in Figure 8a with distinct compartmentalization of apolar starting materials and polar reagents in solution. The reaction medium shall thus be used for the construction of polycyclic terpenes from linear precursors, with a special focus on gaining an in-depth understanding of the distinct interactions between the components in the reaction mixture.

3. Motivation and Goals

While enzymes have the capability of performing halogenation reactions with high selectivity, contemporary synthetic halogenation methods are by far not as sophisticated. In particular, the highly challenging halonium-induced polyene cyclization yields a wide range of biologically active natural products in a single reaction cascade in the organism, which is why this transformation received much attention from synthetic chemists in the last decade.[72,103] Currently available synthetic methods, however, have significant drawbacks regarding yield, selectivity, or convenient reaction execution. Building on the experience in the Gulder group in selective catalytic halogenation methods,[104] we envisioned a biomimetic approach towards halonium-induced polyene cyclizations. This biomimicry shall be achieved by creating a macromolecular assembly in solution. Therefore, the solvent must possess enzyme-like properties, such as the ability to activate the halogenating reagent and/or the substrate, being able to stabilize charged – especially cationic – transition states and ideally control the substrate conformation in solution.

Prime solvent candidates are fluorinated alcohols, such as 1,1,1,3,3,3-hexafluoroisopropanol (HFIP), which have, compared to its non-fluorinated analogs a higher Lewis and Brønsted acidity at the hydroxy function due to the highly electronegative fluorine substituents.[97] Moreover, the hydrogen bond donating ability is vastly increased due to the polarized O-H bond, the nucleophilicity reduced due to steric repulsion of the bulky CF_3 groups, and positive charges stabilized well due to its high dipole moment.[96] HFIP has thus been employed in various reactions with beneficial effects regarding rate and/or selectivity enhancements.[95-97,100,105] As HFIP meets the required criteria for mimicking enzymes in solution exceptionally well, the aim of this thesis is to investigate its ability to promote polyene cyclization reactions. Therefore, the first goal is to employ the work group's expertise in selective halogenation reactions and combine it with the unique solvent properties of HFIP to promote the challenging haliranium-induced polyene cyclization reactions.

Based on the first results obtained during my master's thesis[106] on the bromonium-induced cyclization it became clear that linear polyene substrates with an intramolecular terminating nucleophile are superior substrates for reaction optimization. Hence, model polyene **70** (Scheme 20) should be used to further optimize the reaction conditions with the aim to establish a broadly applicable and easy to carry out reaction providing high yields and diastereoselectivities for product **93**. Once optimal reaction conditions are established the substrate scope should be evaluated for a broad range of electronically diverse polyenes bearing electron-rich and -poor internal alkenes, the latter providing challenges considering the propensity for nucleophilic addition of the internal alkene to the cyclic haliranium ion is lowered. Next, the ability of the established system should be evaluated for iodonium and the even more challenging chloronium-induced cyclization reactions to access a wide range of halogenated,

cyclic products under convenient modular reaction conditions. With the successful completion of these tasks, in-depth mechanistic investigations on the role of both the Lewis and Brønsted acidic solvent, as well as the interplay with Lewis bases as additives should be closely examined. These results will help to gain a deeper understanding of the mode of action during these reactions and the distinct influence between the different components in the reaction.

A plethora of biologically interesting scaffolds bear the drimane skeleton and current methods for their construction mainly rely on harsh Lewis or Brønsted acid-induced proton cyclization of linear polyenes or other inconvenient reaction conditions (see chapter 2.2). Building on findings from the halocyclization project, the concept of Lewis acid/Lewis base interplay should be extended towards the H^+-cyclization of polyenes for model substrate **70** (Scheme 20, X = H). Reaction optimization with a wide range of Lewis and Brønsted acids in fluorinated solvents should be performed, adjusting solvent, catalyst(s), reaction temperature, and concentration. Preparation and testing of various structurally and electronically diverse mono- and sesquiterpene substrates bearing different functional groups and terminating nucleophiles should ensue, followed by extensive mechanistic studies to confirm the mode of action and activation during the reaction. A special focus should lie on the conformational change and activation of polyene **70** from the fluorinated alcohol during the reaction.

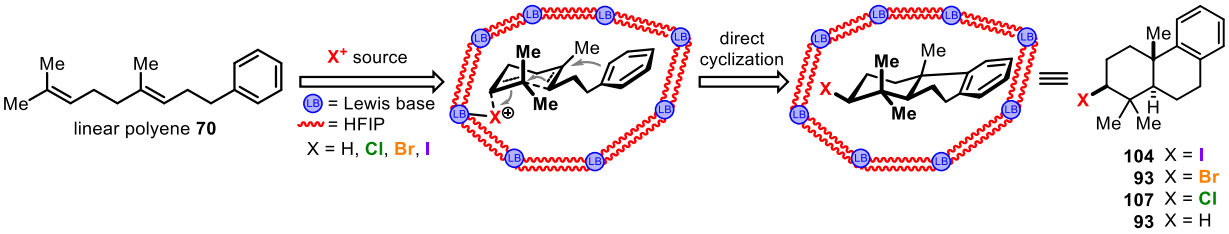

Scheme 20. Concept for the haliranium- and proton induced polyene cyclization in HFIP and Lewis bases to create a reactive supramolecular assembly.

The following goals are emphasized:

- Development of a biomimetic method for the bromonium-induced polyene cyclization reaction.
- Extension of the modular method towards iodonium- and the highly challenging chloronium-induced cyclizations.
- Harnessing the unique properties of the molecular assembly of fluorinated alcohols and Lewis bases towards selective proton-induced cyclizations.
- Uncovering the roles of Lewis bases and the solvent on substrate configuration, reactivity, and selectivity.

II. Results and Discussion

1. NXS, Morpholine and HFIP: The Ideal Combination for Biomimetic Haliranium-Induced Polyene Cyclizations

A. M. Arnold, A. Pöthig, M. Drees, T. Gulder; NXS, Morpholine, and HFIP: The Ideal Combination for Biomimetic Haliranium-induced Polyene Cyclizations; *J. Am. Chem. Soc.* **2018**, *140*, 4344–4353.[64]

Nature generates structurally complex, cyclic secondary metabolites in a direct, highly controlled manner from linear precursors.[30] However, mimicking the corresponding transformations in the laboratory has been a long-lasting endeavor for organic chemists, and are – even to date – still difficult to achieve with high selectivity.[72,78,107]

A breakthrough in this area was reported by Snyder in 2009 with the preparation of the antimonypentachloride-diethylsulfide-bromine complex BDSB, which, for the first time, was capable of cyclizing a wide range of linear 1,5-dienes. However, BDSB does not conform to the requirements of modern halogenating agents, such as sustainability and atom economy. Within our work concerning selective and catalytic halogenation methods of alkenes,[104a,104c,104d,104g] we discovered that standard X^+-sources such as *N*-bromosuccinimide (NBS), *N*-iodosuccinimide (NIS), and 1,3-dichloro-5,5-dimethylhydanthoin (DCDMH) together with an unprecedented Lewis acid/base combination of 1,1,1,3,3,3-hexafluoroisopropanol (HFIP) and morpholine were exceptionally well suited to promote biomimetic halonium-induced polyene cyclization reactions of a wide range of substrates.[64]

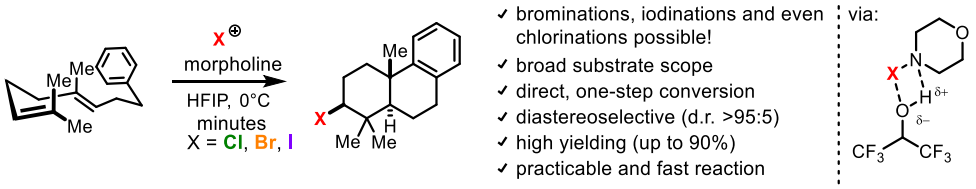

Figure 9. Biomimetic Haliranium-induced Polyene Cyclizations in HFIP.

The method tolerates electron-poor and –rich substrates, aromatic and *O*-nucleophiles as well as intermolecular nucleophilic trapping with water yielding mono, di-, tri-, and tetracyclic products. In-depth mechanistic studies and control experiments with a plethora of fluorinated and standard solvents revealed interesting insights into the mode of action, underlining the unique and indispensable role of NBS, morpholine, and HFIP in the success of these reactions. The solvent plays hereby multiple roles:

- activating NXS and the in situ formed *N*-halomorpholine,
- stabilizing the formed haliranium-ion intermediate,
- prearranging the linear polyene into a chair-like transition state,

- stabilizing the intermittently formed carbocation, thus reducing undesired elimination products to a minimum.

The presented method employs standard bench-stable reagents and is atom economic, scalable, and easily conductible. Paired with high yields of up to 90% and excellent diastereoselectivities of > 95:5 makes this protocol widely applicable to access halonium cyclized polyenes.

JACS JOURNAL OF THE AMERICAN CHEMICAL SOCIETY
Cite This: J. Am. Chem. Soc. 2018, 140, 4344−4353
Article
pubs.acs.org/JACS

NXS, Morpholine, and HFIP: The Ideal Combination for Biomimetic Haliranium-Induced Polyene Cyclizations

Andreas M. Arnold,[†,‡] Alexander Pöthig,[‡] Markus Drees,[‡] and Tanja Gulder*[,†,‡]

[†]Biomimetic Catalysis, Department of Chemistry, Technical University of Munich, Lichtenbergstrasse 4, 85748 Garching, Germany
[‡]Catalysis Research Center, Technical University of Munich, Ernst-Otto-Fischer-Straße 1, 85748 Garching, Germany

Supporting Information

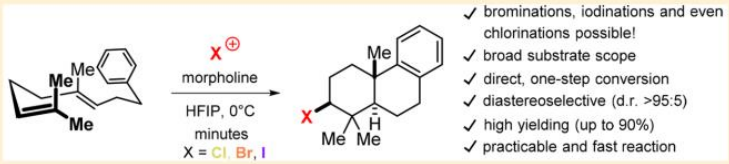

ABSTRACT: In contrast to Nature that accomplishes polyene cyclizations seemingly with ease, such transformations are difficult to conduct in the lab. In our program dealing with the development of selective halogenations of alkenes, we now asserted that standard X^+ reagents are perfectly suited for the biomimetic cation-π cyclization of both electron rich and poor linear polyenes in the presence of the Lewis base morpholine and the Lewis acid HFIP. The method stands out due to its broad substrate scope and practicability together with high chemical yields and excellent selectivities, even for highly challenging chloriranium-induced polyene cyclizations.

INTRODUCTION

The cation-π cyclization is an impressive example for the efficiency and selectivity of biosynthesis. In a single step structurally highly complex carbon scaffolds are built by cyclization of a simple isoprenyl chain in a controlled fashion, thereby creating multiple C,C bonds and stereocenters at once. Mimicking the way Nature beautifully orchestrates these ring-closing events has been a long-lasting dream for synthetic chemists. Since the pioneering work by Stork[1] and Eschenmoser[2] in 1955, numerous catalytic as well as reagent-based methods have been established, triggering polyene cyclizations with excellent yields and stereoselectivities.[3] These procedures, however, are mostly initiated by protonation of the terminal olefin or by epoxide opening mimicking cyclase I enzymes. Establishing the corresponding haliranium-ion induced ring formation has been way less successful, even for racemic products.[3d,4] Having such a polyene cyclization method available would add a valuable tool to organic synthesis as it grants straightforward access to roughly 200 brominated and chlorinated marine terpenes biosynthetically assembled in a halo-polyene cyclization.[5] Intriguing examples of such natural products are the antibiotic napyradiomycin B3 (**1**),[6] the potential HIV inhibitor peyssonol A (**2**),[7] and the antimutagenic 4-isocymobarbatol (**3**,[8] Figure 1).

As the biomimetic halonium-induced polyene cyclization would offer a versatile and efficient pathway to these, mostly brominated metabolites, numerous efforts have been made to establish standard electrophilic bromine sources in such reactions, like, e.g., *N*-bromosuccinimide (NBS),[9] bromine,[10] and 2,4,4,6-tetrabromocyclohexa-2,5-dione (TBCO),[11] with[10,12] or without additives (Figure 2).[13−15]

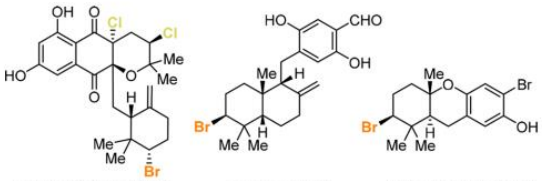

Figure 1. Examples of bioactive, halogen-containing terpenes.

The development of asymmetric haliranium-ion triggered cation-π cyclizations constitutes an even greater challenge. In 2007, Ishihara et al. described the first enantioselective method using stoichiometric amounts of axially chiral phosphoramidites, such as **I** (Figure 2b).[12] While the iodocyclization converted different homogeranyl aryl derivatives with high enantioselectivity (not shown), the corresponding bromiranium-induced reactions have been less successful. A breakthrough in this area was achieved recently by Yamamoto reporting on a catalytic, asymmetric method to furnish tricyclic products with high optical purity.[14] Here, utilizing a dual Lewis base/Brønsted acid activation of the bromenium source dibromo-5,5-dimethyl hydantoin (DBDMH) by the chiral BINOL-derived thiophosphoramide **II** turned out to be decisive. Despite all of these attempts to convert polyene precursors into the (poly)cyclized products, the methods available today still suffer from severe drawbacks with regards to

Received: January 4, 2018
Published: February 7, 2018

DOI: 10.1021/jacs.8b00113
J. Am. Chem. Soc. 2018, 140, 4344−4353

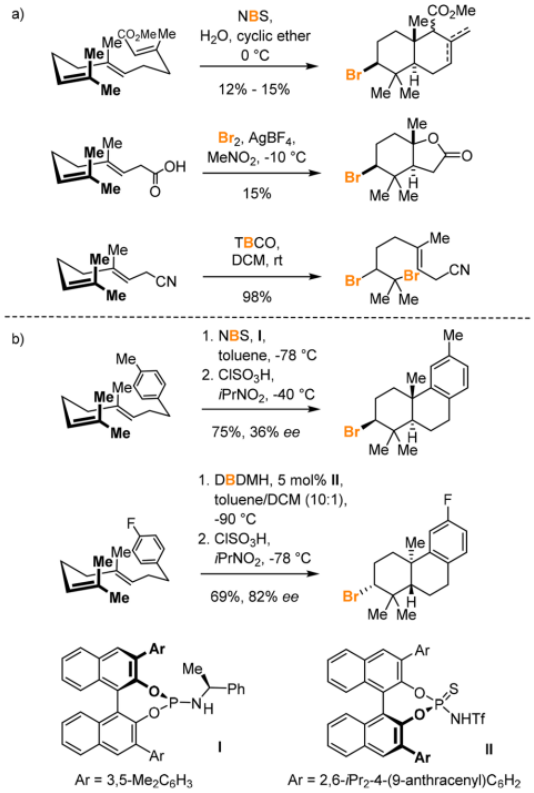

Figure 2. Selected literature examples of (attempted) (a) racemic[9−11] and (b) asymmetric bromiranium-ion cation-π cyclizations.[12,14]

scope, practicability, reactivity, and/or selectivity. The major problem encountered is the low rates of trapping the haliranium intermediate **5** by intramolecular cyclization, leading to the desired products **7** or **8** via the carbocation **6** (Scheme 1). β-H abstraction giving linear olefin **9** or addition of a competing, intermolecular nucleophile to **5**, such as halides or water, resulting in acyclic **10** occurs more rapidly, in particular if R is electron-deficient. Controlling the opening of the three-membered heterocycle in **5** is thus highly challenging and the

Scheme 1. Possible Reaction Pathways in the Haliranium-Triggered Transformation of Polyenes 4

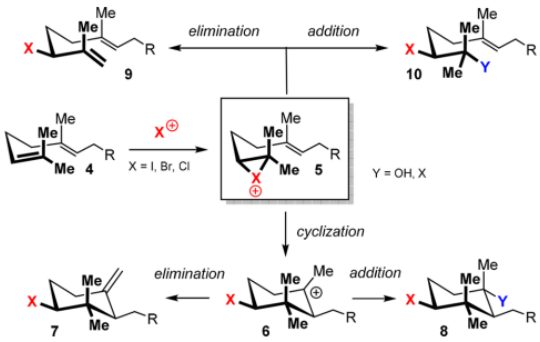

known methods lead mostly to product mixtures with the desired cyclohexyl derivatives **7** and/or **8** being minor components. Only recently, Snyder and co-workers achieved a landmark improvement in this field by introducing the bench-stable, but highly reactive, electrophilic bromenium reagent $Et_2SBr{\cdot}SbCl_5Br$ (**17**, BDSB, cf. Table 1).[16] Employing BDSB (**17**) in nitromethane has become the gold standard over the last years. Various cyclic geraniol-, nerol-, and farnesol-derived terpenoids[17] as well as members of the chamigrene[18] and lauroxocane[19] natural product families were obtained in good yields and diastereoselectivities using **17**. The method was extended also to the corresponding iodination and chlorination reactions.[17] Employing $Et_2SCl{\cdot}SbCl_6$ (CDSC), chlorine-triggered polyene cyclizations have been achieved to the best of our knowledge for the first time, albeit with low diastereoselectivities. Because of our experience in the field of hypervalent iodane triggered halogenations,[20] with special emphasis on selective bromocarbocyclizations[21] and rearrangements,[22] we were encouraged to extend our reaction repertoire and to challenge our catalytic system also in direct bromiranium-ion-induced cation-π cyclizations.

RESULTS AND DISCUSSION

Bromiranium-Induced Polyene Cyclizations. We thus started our investigations by subjecting homogeranyl benzene (**11**) to the conditions optimized for the bromocarbocyclization (Table 1, entry 1, and SI).[21] Unfortunately, only a complex product mixture was obtained, with the tricyclic product **12** detectable only in traces. Switching the solvent from DCM to HFIP (1,1,1,3,3,3-hexafluoroisopropanol, entry 2) afforded for the first time formation of **12** in an encouraging amount (33%) with a diastereomeric ratio of 80:20. Interestingly, it turned out that activation of Br^+ by in situ formation of a hypervalent iodane-bromine species[22a] was not necessary. When **13** was omitted, the amount of product **12** was increased to 42% (entry 3). The use of HFIP, however, proved to be crucial, as other common solvents, such as DCM, MeCN, or isopropanol, produced **12** in very low yields accompanied by various apolar, inseparable byproducts (entries 4−6 and SI).

Thorough analysis of the reaction course revealed to our surprise (for details see SI) that conversion of the geraniol derivative **11** occurred within seconds and longer reaction times (>3 min) resulted in substantial decomposition of **12**. To further improve our protocol, the temperature was lowered to 0 °C, which gave **12** in significantly enhanced 68% if the reaction was terminated after 1 min (entry 7). As HFIP has a melting point of −4 °C,[23] thus preventing the transformation being performed at lower temperatures than 0 °C, and combinations of HFIP with other solvents gave a significantly decreased conversion compared to HFIP alone, other F-containing solvents, like, e.g., 3,3,4,4,4-pentafluor-1-propanol (PFNP), were tested but were not successful (entry 8).[24] Next, a screening of alternative bromine sources was conducted in order to fine-tune the activation and thus the reactivity of the electrophilic bromine equivalent by HFIP (for details see the SI). As strong H-bonds are formed between the succinimide carbonyl groups in NBS and HFIP (see the SI for NMR studies) triggering a rapid conversion, a more tamed reactivity might be achievable by lowering the activation of Br^+ by the fluoro alcohol. Along these lines, the best results were obtained by using *N*-bromo morpholine (**14**, entry 9). With **14**, similar yields as before were obtained (62%), but the reaction time was increased to a more manageable time scale (10 min) and

DOI: 10.1021/jacs.8b00113
J. Am. Chem. Soc. 2018, 140, 4344−4353

Table 1. Optimization of the Reaction Conditions for the Direct Bromiranium-Induced Polyene Cyclization[a,k]

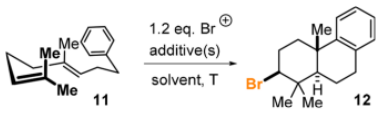

entry	Br^+	solvent	additive	yield	d.r.[b]
1	NBS	DCM	**13**[c]	<5%	n.d.
2	NBS	HFIP	**13**[c]	33%	80:20
3	NBS	HFIP		42%	79:21
4	NBS	DCM		8%	n.d.
5	NBS	MeCN		12%[d]	n.d.
6	NBS	*i*PrOH		<5%[e]	n.d.
7[f,g]	NBS	HFIP		68%	79:21
8[24,g]	NBS	PFNP		17%	n.d.
9[g]	**14**	HFIP		62%	>95:5
10[g]	NBS	HFIP	**15**[h]	78%	>95:5
11[g]	NBS	HFIP	**16**[h]	78% 76%[i]	>95:5
12[16b,j]	**17**	$MeNO_2$		75%	>95:5

[a]21.4 mg of NBS (0.12 mmol, 1.2 equiv) was added to 22.8 mg (0.10 mmol, 1.0 equiv) of substrate **11** in 1.00 mL of solvent at rt. [b]Determined by ^{1}H NMR spectroscopy from the crude mixture. [c]10 mol% used. [d]12% of monocyclic product. [e]Mostly acylic O*i*Pr-addition product. [f]t = 1 min. [g]Reaction performed at 0 °C. [h]1.4 equiv used. [i]Isolated yield. [j]Reaction performed at −25 °C. [k]

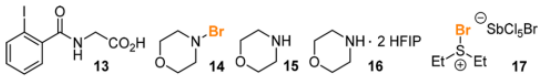

product **12** was isolated as a single diastereomer. In order to provide an easy to conduct method, even applicable on large-scale, an in situ generation of **14** was envisaged, as pure *N*-bromomorpholine (**14**) rapidly decomposes upon isolation at room temperature. Stirring morpholine (**15**) or the more convenient, solid morpholine-HFIP salt (**16**) with NBS in HFIP for 10 min prior to the addition of substrate **11** even enhanced the yield of diastereomerically pure terpenoid **12** to 78% (entries 10 and 11). Comparing the results realized here to those reported by Snyder using BDSB (**17**, entry 12)[16b,25] showed that the outcomes are indeed comparable.

In order to evaluate the scope and thus the generality of our cation-π cyclization method, we subjected several geraniol-derived substrates **18**−**20** equipped with an aromatic portion as the terminating nucleophile to our optimized reaction conditions (Table 2). All compounds smoothly delivered the corresponding tricyclic products with excellent diastereoselectivities (>95:5) and chemical yields (72−88%). The latter exceed even those obtained for the tricyclic products **22**−**24** with the standard reagent BDSB (**17**). For the electron-rich phenol **20** the outcome can be controlled by adjusting the equivalents of NBS applied. 1.1 equiv of NBS solely delivered the cyclic ether **24** with no competitive aromatic substitution observed. Enhancing the amount of electrophilic bromine to 2.2 equiv and of morpholine-HFIP salt (**16**, 2.6 equiv) immediately facilitated an in situ aryl bromination after formation of **24**. The para substituted bromo benzene **25** was isolated in 88% as the final product. It is noteworthy that in all cases no additional acidic treatment of the crude mixture at low temperatures was necessary to achieve complete cyclization.[12,14,26] Our method can likewise be employed for substrates with an extended en-system, such as the homo-

Table 2. Substrate Scope for the Direct, Bromiranium-Induced Polyene Cyclization of Aromatic Mono and Sesquiterpenes

substrate	product	yield (d.r.)[b,c] NBS/**16**[a]	yield (d.r.)[b,c] BDSB (**17**)
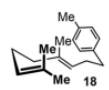	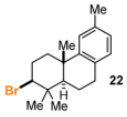	72% (>95:5)	67%[g] (94:6)
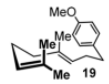		85% (>95:5)	76%[16b] (>95:5)
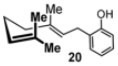	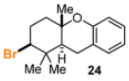	77%[d] (>95:5)	72%[g] (>95:5)
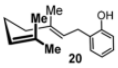	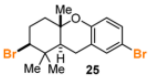	88%[e] (>95:5)	-
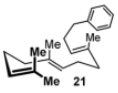	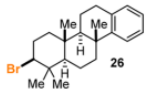	40%[f] (>95:5)	56%[16b] (>95:5)

[a]42.8 mg of NBS (0.24 mmol, 1.2 equiv) was added to 119 mg (0.28 mmol, 1.4 equiv) of morpholine-HFIP salt (**16**) in 2.00 mL of HFIP at 0 °C. After stirring for 10 min at 0 °C, 0.20 mmol of substrate (1.0 equiv) was added. [b]Isolated yield. [c]Determined by ^{1}H NMR spectroscopy from the crude mixture. [d]1.1 equiv NBS were used. [e]2.2 equiv NBS and 2.6 equiv **16** were used. [f]$ClSO_3H$ (10.0 equiv) added in *i*$PrNO_2$ at −25 °C to complete the final cyclization. [g]54.9 mg of BDSB (0.10 mmol, 1.0 equiv) was dissolved in 0.50 mL of abs. $MeNO_2$ and added quickly to a stirring solution of 0.10 mmol of substrate (1.0 equiv) in 1.50 mL of abs. $MeNO_2$ at −25 °C.

farnesyl benzene **21**. The polycyclization was achieved here with 40% isolated yield and complete diastereoselection.

Encouraged by our results obtained with aryl geraniols and farnesols, we next strived to extend the scope to substrates affording mono- and bicyclic products (Table 3). Treatment of prenyl benzene **27** as well as structurally and electronically diverse substituted geranyl compounds **28**−**34** triggered the bromiranium-induced cation-π cyclization again in high yields of up to 83%. Interestingly, treating geraniol (**34**) with morpholine salt **16** and NBS in HFIP resulted in the generation of the HFIP ether in 65% and a d.r. of >95:5. The carbocation here was trapped by the weak HFIP nucleophile. The syn,anti,anti-relative configuration was determined by X-ray crystal analysis of **41** showing that the conformation of the alkene was conserved during the reaction (Figure 3). In order to test the practicability of our bromiranium-induced polyene cyclization method, geraniol (**34**), for example, was converted on a gram scale (10.0 mmol), yielding fluoro ether **41** in similar yields of 58%.

To our surprise, electron deficient esters, exclusively gave cyclohexanols **43** in 51−65% with only traces of elimination or

DOI: 10.1021/jacs.8b00113
J. Am. Chem. Soc. 2018, 140, 4344−4353

Table 3. Scope for the Bromocyclization Yielding Mono- and Bicyclic Products[a,d]

substrate	product	Yield (d.r.)[b,c] NBS/**16**	Yield (d.r.)[b,c] BDSB (**17**)[25]
 **27**	 **35**	83%	79%
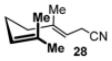 **28**	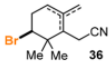 **36**	52%[e,f]	73%[16b,g]
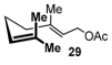 **29**	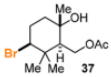 **37**	62%[f] (82:18)	80% (79:21)
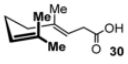 **30**	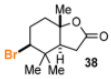 **38**	58% (89:11)	73%[16b] (>95:5)
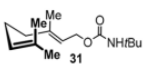 **31**	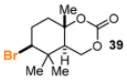 **39**	57% (>95:5)	13%[h] (>95:5)
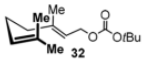 **32**	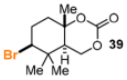 **39**	38% (>95:5)	65% (83:17)
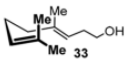 **33**	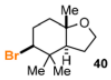 **40**	78% (>95:5)	22%[h]
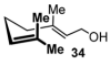 **34**	 **41**	65% (>95:5)	-
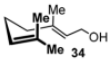 **34**	 **41**	58%[i] (>95:5)	-

[a]42.8 mg of NBS (0.24 mmol, 1.2 equiv) was added to 119 mg (0.28 mmol, 1.4 equiv) of morpholine-HFIP salt (**16**) in 2.00 mL of HFIP at 0 °C. After stirring for 10 min at 0 °C 0.20 mmol of substrate (1.0 equiv) was added. [b]Isolated yield. [c]Determined by ^{1}H NMR spectroscopy from the crude mixture. [d]54.9 mg of BDSB (**17**, 0.10 mmol, 1.0 equiv) was dissolved in 0.50 mL of abs. $MeNO_2$ and added quickly to a stirring solution of 0.10 mmol of substrate (1.0 equiv) in 1.50 mL of abs. $MeNO_2$ at −25 °C. [e]A 12:53:35 ratio of di-, tri-, and tetrasubstituted alkenes was isolated. [f]1.2 equiv **16** together with 0.95 equiv NBS were used. [g]A 10:65:25 ratio of di-, tri-, and tetrasubstituted alkenes was isolated. [h]Several attempts to convert the respective substrate using BDSB (**17**) resulted mainly in decomposition of starting material. [i]Reaction was carried out using 1.54 g (10.0 mmol) of geraniol (**34**).

substitution products detectable in the crude ^{1}H NMR spectrum (Table 4).

For the nitrobenzene derivatives **42a**−**42d** the diastereoselectivity turned out to be highly dependent on the position of the NO_2-substituent. While the 2-NO_2 and 4-NO_2 equipped benzoyl substrates **42a** and **42c** were converted only with

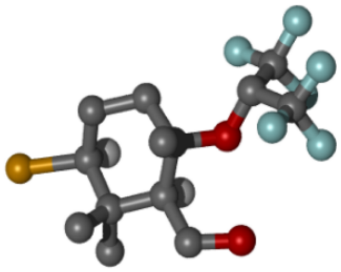

Figure 3. X-ray crystal structure of **41**.

Table 4. Bromocyclization of Geraniol Benzoates 42[a]

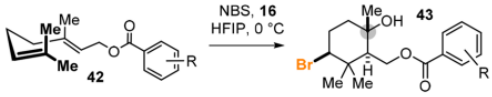

entry	R	yield (d.r.)[b,c]
1	**43a**: 2-NO_2	60% (71:29)[d]
2	**43b**: 3-NO_3	65% (>95:5)
3	**43c**: 4-NO_2	60% (78:22)[e]
4	**43d**: 3,5-di-NO_2	51% (>95:5)
5	**43e**: 3,5-di-F	54% (71:29)[e]

[a]42.8 mg of NBS (0.24 mmol, 1.2 equiv) was added to 119 mg (0.28 mmol, 1.4 equiv) of morpholine-HFIP salt (**16**) in 2.00 mL of HFIP at 0 °C. After stirring for 10 min at 0 °C, 0.20 mmol of substrate **42** (1.0 equiv) was added. [b]Isolated yield. [c]Determined by ^{1}H NMR spectroscopy from the crude mixture. [d]Inseperable mixture of diastereomers differing at the highlighted carbon atom. Main diastereomer drawn. [e]Separable mixture of diastereomers differing at the highlighted carbon atom. Main diastereomer drawn.

moderate diastereocontrol (entries 1 and 3), the 3- and 3,5-substituted derivates **42b** and **42d** afforded products **43b** and **43d**, respectively, as a single diastereomer (entries 2 and 4). Subjecting 3,5-difluoro benzylester **42e** to our standard conditions generated the cyclic product **43e** in a similar diastereomeric ratio (d.r. = 71:29) as with **43a** and **43c**, concluding that this phenomenon most likely originates from the structural properties of the nitro group.

To further shed light on this difference in stereoselection, DFT calculations about the structure of the carbocation **44** and the corresponding transition states **TS** leading to the water addition intermediates **45** have been conducted with particular focus on comparing the effects exhibited by the 4-NO_2 and the 3-NO_2 substitution (Table 5 and for details see the SI). Within this study, it became obvious that the carboxylic ester group plays an important role in stabilizing the cationic intermediate **44** by flipping around to make a C−O contact. This stabilization is almost independent from the phenyl substitution pattern and accounts for a free energy stabilization of −13 kcal/mol for the 4-NO_2-substrate **42c** and −12 kcal/mol for the 3-NO_2-compound **42b**, respectively.

Next, we had a closer look at the directed trapping of **44** by water that occurs from the face opposite to the benzylic ester moiety, preferentially giving the adduct major-**45**. Interestingly, it can clearly be seen that the phenylic ring as a whole gives steric pressure when water adds from the same face as the ester. The barriers are higher than that corresponding to an anti addition (Scheme 2).

DOI: 10.1021/jacs.8b00113
J. Am. Chem. Soc. 2018, 140, 4344−4353

Table 5. Energies (ΔG [kcal/mol]) of Transition States for the Water Addition (TS) and the Corresponding Adducts 45

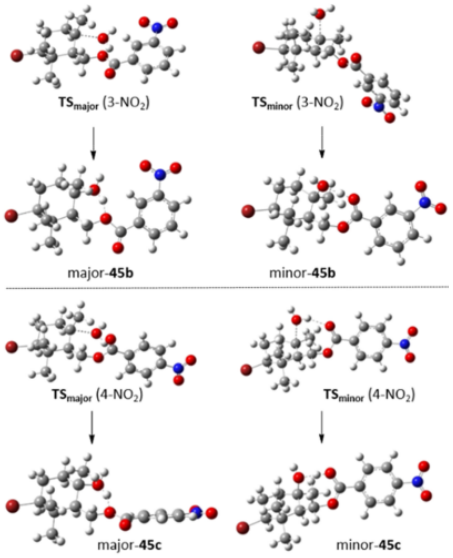

	ΔG (3-NO$_2$) [kcal/mol]	ΔG (4-NO$_2$) [kcal/mol]
TS$_{minor}$	+7.9	+6.5
minor-**45**	−1.1	−3.5
TS$_{major}$	+3.7	+3.5
major-**45**	+2.0	+2.6

The ΔΔG difference of the two barriers for each system might be a hint for the alteration of the d.r. values. In the case of the para nitro group, the ΔΔG is much smaller (3 kcal/mol) than for the meta nitro group (4.2 kcal/mol). This finding nicely explains the altered d.r. values being higher for the formation of the meta nitro product **43b**.

Iodiranium-Induced Polyene Cyclizations. Although no iodine-containing terpenoid natural products have been isolated so far that biosynthetically originate via an iodiranium-induced cyclization, efficient and easy-to-handle iodine triggered polyene cyclizations are of great value. With the installed iodine atom being an ideal functional handle, these compounds can be easily further manipulated to introduce structural complexity into the carbon framework.[17] They thus serve as versatile building blocks that give rise to various natural and artificial terpenoid structures. Only a few electrophilic iodonium reagents have proven capable of inducing polyene cyclizations of linear terpene precursors.[12,17,28] However, these methods are mostly restricted to substrates with electron-rich functional groups. The most powerful electrophilic I$^+$ source in this context is iodosulfonium antimonate IDSI,[17] which was developed by Snyder to complement BDSB (**17**).[29]

Being curious if our concept can also be extended to direct iodiranium-triggered reactions, we simply exchanged the electrophilic halogen reagent NBS by NIS (*N*-iodosuccinimide) and exposed various acyclic substrates to these conditions. The cation-π cyclization proceeded smoothly in all cases and chemoselectively afforded the (poly)cylic products **46**−**56** with excellent diastereomeric ratios of up to >95:5 (Figure 4), regardless whether electron-donating or -withdrawing substituents were attached. Single crystal X-ray analysis of dinitrobenzoic ester **56** confirmed unambiguously the relative configuration of the tertiary alcohol **56**.[40] The obtained isolated yields ranged from 50−90% and were mostly even superior to those achieved in the bromiranium-induced cyclizations.

Chloriranium-Induced Polyene Cyclizations. We next probed our method in chloriranium-induced cation-π cyclizations. Until now, only the chlorosulfonium antimonate CDSC was reported to directly convert acyclic precursors into polycyclic compounds, albeit with lower diastereoselectivities than for the corresponding bromo cyclizations.[16a,17] The latter might be explained by the propensity of the three-membered chloriranium ions **64** to preferentially exist in their acyclic, carbocationic form such as **65** (Scheme 3, bottom).[30] The

Scheme 2. Free Energy Plot [kcal/mol] for the Investigated Water Addition[a]

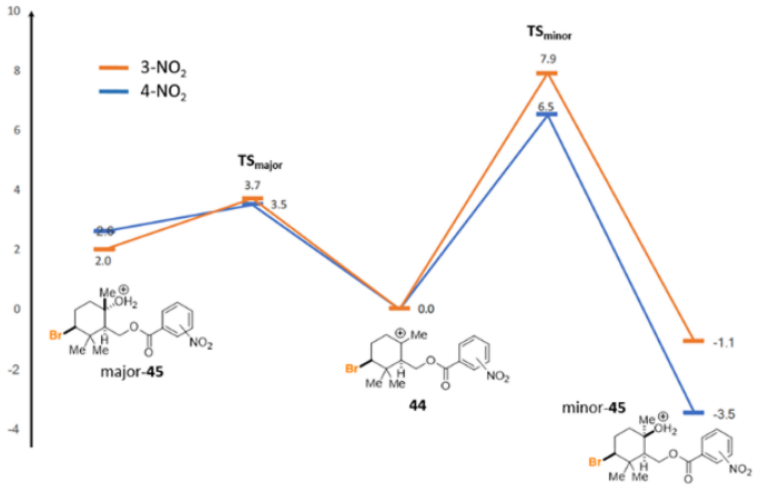

[a]H_2O addition from below (left) and above (right) the cyclohexyl ring plane.

DOI: 10.1021/jacs.8b00113
J. Am. Chem. Soc. 2018, 140, 4344−4353

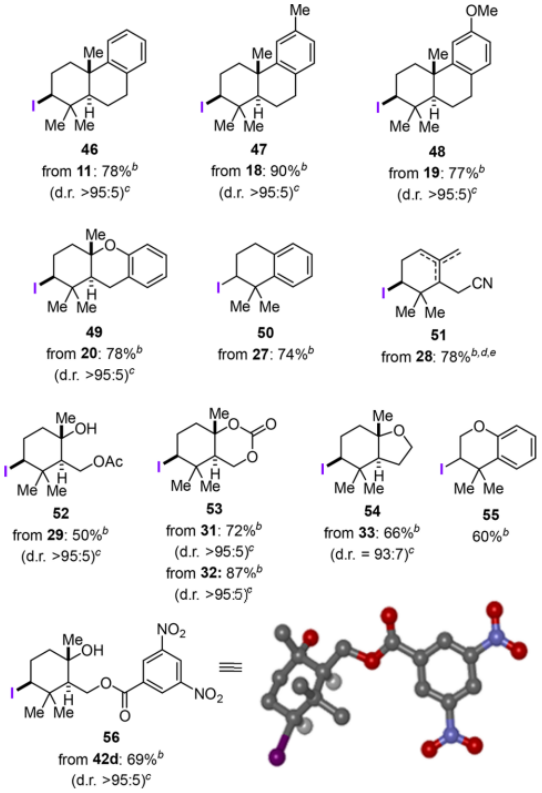

Figure 4. Substrate scope of the direct iodocyclization of polyenes. [a]54.0 mg of NIS (0.24 mmol, 1.2 equiv) was added to 119 mg (0.28 mmol, 1.4 equiv) of morpholine-HFIP salt (**16**) in 2.00 mL of HFIP at 0 °C. After stirring for 10 min at 0 °C, 0.20 mmol of substrate (1.0 equiv) was added. [b]Isolated yield. [c]Determined by ^{1}H NMR spectroscopy from the crude mixture. [d]1.2 equiv **16** together with 0.95 equiv NIS were used. [e]A 51:40:9 ratio of di-, tri-, and tetrasubstituted alkenes was isolated.

Scheme 3. Chlorinative Cyclizations of (Poly)enes

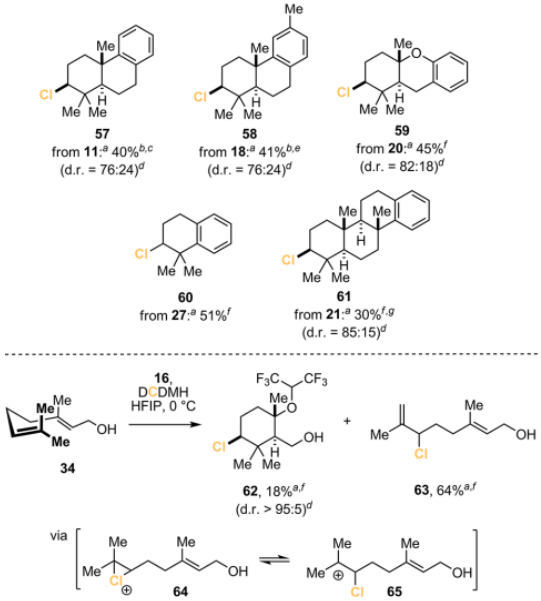

[a]52.8 mg of DCDMH (0.27 mmol, 1.34 equiv) was added to 156 mg (0.37 mmol, 1.70 equiv) of morpholine-HFIP salt (**16**) in 2.00 mL of HFIP at rt. After stirring for 1 h at rt, 0.20 mmol substrate (1.00 equiv) was added. [b]NMR yield. [c]The major diastereomer of **57** was isolated in 32%. [d]Determined by ^{1}H NMR spectroscopy from the crude mixture. [e]The major diastereomer of **58** was isolated in 30%. [f]Isolated yield. [g]$ClSO_3H$ (10.0 equiv) in $iPrNO_2$ was added at −25 °C to complete the final cyclization.

nucleophilic attack of the pendant olefin moiety forming the cyclohexyl chloride occurs then with almost no differentiation of the two diastereomeric faces generating both diastereomers in a similar amount. Using our morpholine/HFIP-reaction conditions it turned out that the best results are achieved by using DCDMH (1,3-dichloro-5,5-dimethylhydantoin) instead of NCS (*N*-chloro succinimide, see the SI).

As expected, the chemical yield for **57** (Scheme 3) was lower than that obtained in the corresponding brominative and iodinative ring closure reactions (40% versus 78%).[31] The diastereomeric ratio, however, was determined to be 76:24 for both **57** and **58** favoring the chlorine atom in an equatorial position. Trapping the cationic intermediate with a more reactive *O*-nucleophile even showed an increased diastereomeric ratio of up 82:18 for **59**. Homoprenylbenzene (**27**) and even the farnesyl derivative **21** were likewise cyclized in 51% and 30% isolated yield, respectively. The latter substrate produced the tetracyclic product **61** with an excellent d.r. of 85:15. Remarkably, treatment of geraniol (**34**) under the presented chlorocyclization conditions gave exclusively one diastereomer of the HFIP-product **62** (d.r. >95:5), which constitutes, to the best of our knowledge, the highest d.r. observed for any chloriranium-induced polyene cyclization. Because of the low nucleophilicity of HFIP, elimination constitutes the major trapping pathway for carbocation **65**, thus delivering the chloro alkene **63** as the major product (64%). Nevertheless, the significant diastereocontrol observed here clearly corroborates our hypothesis of HFIP having a decisive influence on the stereochemical course of these transformations. HFIP forces the cationic intermediate to adopt a highly organized chair conformation that guarantees for the diastereotopos-differentiating attack of the intramolecular nucleophile producing **57**−**62** with excellent diastereomeric excess.

In preliminary investigations on the interesting chlorination ability observed for our system, we determined its halenium affinity (HalA), a parameter introduced by Borhan and co-workers[32] that allows for a better comparison of the reactivity and the chemoselectivity of different halonium reagents. The results of the NMR titrations (for details see the SI) showed the decisive influence of HFIP on the halogenating ability of the in situ formed *N*-chloro morpholine (NCM). In HFIP, NCM is more activated than other commonly used chlorenium sources, and as a consequence, it becomes more productive (selective) as observed in the described chloro cyclization.

Mechanistic Investigations. Within the current work, we further demonstrated that the interplay between the Lewis basic morpholine (**15**) and the Lewis acidic, highly polar, strongly hydrogen-bond donating, but weakly nucleophilic solvent HFIP

DOI: 10.1021/jacs.8b00113
J. Am. Chem. Soc. 2018, 140, 4344−4353

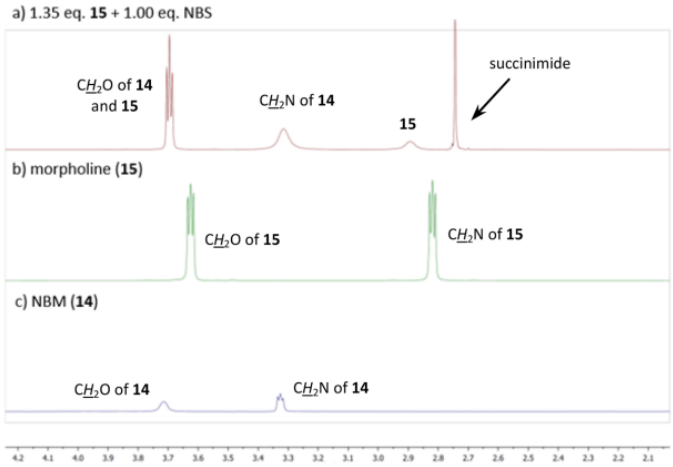

Figure 5. In situ formation of *N*-bromo morpholine (NBM, **14**).

has been proven to be key to successful biomimetic haliranium-ion induced polyene cyclizations described above. NMR studies show that treatment of morpholine (**15**) with NBS indeed produced in situ in a clean reaction the *N*-bromo morpholine (**14**), which constitutes the actual halogenation agent (Figure 5).

When HFIP was added to *N*-bromo morpholine (**14**) the OH group, normally resonating at 3.01 ppm, was immediately shifted to lower fields, proving the complexation of the fluoro alcohol with **14** (Figure 6, top). Independent from the HFIP

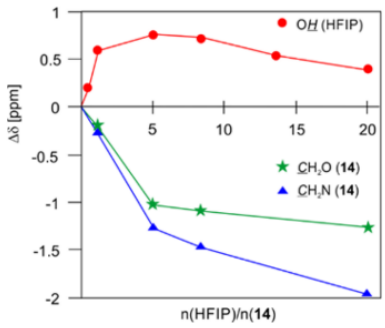

Figure 6. NMR titration curves of *N*-bromo morpholine (**14**) and HFIP at 25 °C.

equivalents, only one signal for the hydroxyl proton was witnessed in all NMR spectra, hinting at a fast equilibrium of coordinated and noncoordinated HFIP on the NMR time scale (for detailed NMR spectra see the SI).

Further evidence for such an adduct formation was obtained by examining the ^{13}C NMR signals of **14** upon titration with HFIP. Here again, distinct hydrogen bonding to the *N*-bromo and, albeit to a smaller extent, to the ether moiety in **14** was visible (Figure 6, bottom).[33] The fast exchange of the HFIP molecules in the HFIP-**14** complex resulted in very broad CH_2 signals, in particular at HFIP/**14**-ratios greater than 8.5 (Figure 7). This effect was more pronounced for the *N*-methylene group. Both noncovalent interactions are crucial for the precise and balanced reactivity of **14**. Employing other nitrogen Lewis bases, such as *N*-methyl morpholine or piperidine, resulted in a more sluggish conversion of our standard substrate homogeranyl benzene (**11**, see the SI).

In contrast to HFIP, almost no interaction of the bromination agent **14** and *O*-methyl HFIP (HFIPMe) was visible. Conducting the polyene cyclization of **11** in HFIPMe resulted in a completely abolished product formation. These results clearly corroborate that the hydrogen bond donor capacity of HFIP is fundamental for the activation of the Br^+ agent[34,35] and thus for the success of the polyene cyclization (see the SI).

In addition to its activating properties via H-bonding, we believe that HFIP is able to prearrange the acyclic polyene in a rigid conformation due to hydrophobic interactions of the apolar hydrocarbon and the hydrogen-bonding networks. This results in a highly organized, tight chair conformation of the starting material and thus facilitates its direct and highly controlled cyclization.[27] In HFIP, the in situ generated haliranium ion **5** (cf. Scheme 1) should be activated toward ring opening, again via hydrogen bonding. The nucleophilic attack to the three-membered heterocycle occurs in an intramolecular fashion, as the HFIP-hydrogen bond cluster acts as a protective shield for the cation by forming a close solvent shell. Such an effect within a supramolecular scaffold was impressively demonstrated recently for proton-induced polyene cyclizations. Because of this stabilization effect,[36] undesired side reactions, such as elimination and/or addition caused by external nucleophiles, are abolished, thus accounting for the excellent chemo- and diastereoselectivity.[37] All these properties make HFIP[38] extremely beneficial in a plethora of other chemical transformations,[39] including the cation-π cyclization presented here.

■ CONCLUSIONS

The method presented in this paper offers a general yet simple solution to some of the existing problems in haliranium-triggered polyene cyclizations by utilizing balanced Lewis base/Lewis acid interactions in order to fine-tune the reactivity and selectivity. Treatment of both electron-rich and -poor linear polyenes in HFIP with an electrophilic halogen source

DOI: 10.1021/jacs.8b00113
J. Am. Chem. Soc. 2018, 140, 4344−4353

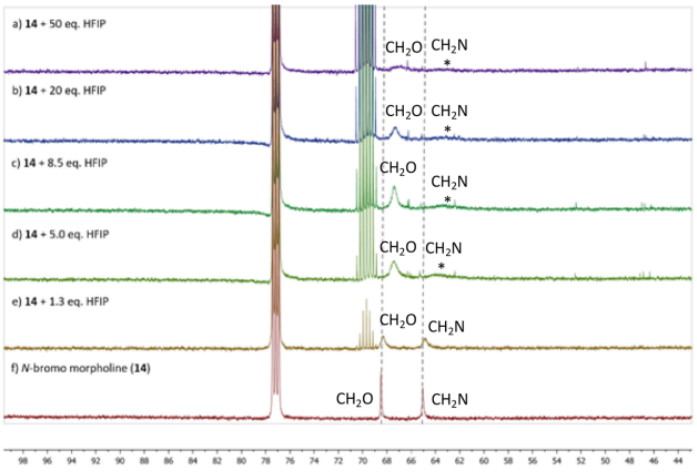

Figure 7. Overlap of the ^{13}C NMR spectra of *N*-bromo morpholine (**14**) and different equivalents HFIP at 25 °C. *the CH_2N-signal, resonating at ~63 ppm significantly broadens using >5.0 equiv HFIP but can still be detected in the ^{13}C spectra upon significant sensitivity enhancement.

delivered upon the addition of morpholine (**15**) the corresponding carbocycles with excellent chemical yields (up to 90%) and diastereoselectivities (>95:5) regardless of the employed halogen. Even for the highly challenging chloro cyclization globally excellent diastereoselectivities of up to >95:5 have been achieved for the first time. The procedure is conducted easily using readily available, cheap, off-the-shelf standard chemicals that allow for the direct, one-step cyclization, even to polycyclic products. Because of its modular design, simply the commercially available X^+ source needs to be exchanged to achieve the reaction for the different halogen congeners. Before this, new and for each halogen atom different reagents needed to be prepared. The presented procedure thus contributes to a significant decrease in the step count usually needed for such transformations and makes the protocol even more convenient. The combination of morpholine (**15**) and the fluoro alcohol HFIP is crucial for a successful transformation. HFIP thereby plays multiple roles by activating the in situ formed bromo morpholine (**14**) and the haliranium-ion intermediate **5**, by prearranging the polyene substrate in a tight, accurate conformation, and by stabilizing the intermediate carbocation. HFIP is responsible for the balanced reactivity as well as the excellent chemo- and diastereoselectivity observed in this biomimetic haliranium-induced cation-π cyclization, again demonstrating its power and unique properties in organic synthesis. Overall, we are convinced that our method contributes to the field of haliranium-induced cation-π cyclizations and will lead to an array of bioactive natural products and their analogs in a more efficient way in the future.

■ ASSOCIATED CONTENT

Supporting Information

The Supporting Information is available free of charge on the ACS Publications website at DOI: 10.1021/jacs.8b00113.

Additional studies, experimental procedures, and compound characterization. (PDF)

Copies of NMR spectra. (PDF)

Data of the X-ray crystal analysis for compound **16**. (CIF)

Data of the X-ray crystal analysis for compound **41**. (CIF)

Data of the X-ray crystal analysis for compound **56**. (CIF)

■ AUTHOR INFORMATION

Corresponding Author

*tanja.gulder@tum.de

ORCID

Alexander Pöthig: 0000-0003-4663-3949

Markus Drees: 0000-0001-6744-2370

Tanja Gulder: 0000-0003-4870-2266

Notes

The authors declare no competing financial interest.

■ ACKNOWLEDGMENTS

This work was funded by the Emmy-Noether (DFG, GU 1134-3) and Heisenberg (DFG, GU 1134-4) program of the German Research Foundation (DFG). A.M.A. thanks the Fonds der Chemischen Industrie for a Ph.D. Fellowship. The authors thank B. Sc. H. Plendl for technical assistance in synthesizing starting material.

■ REFERENCES

(1) Stork, G.; Burgstahler, A. W. *J. Am. Chem. Soc.* **1955**, *77*, 5068−5077.

(2) (a) Eschenmoser, A.; Arigoni, D. *Helv. Chim. Acta* **2005**, *88*, 3011−3050. (b) Eschenmoser, A.; Ruzicka, L.; Jeger, O.; Arigoni, D. *Helv. Chim. Acta* **1955**, *38*, 1890−1904.

(3) (a) Snyder, S. A.; Levinson, A. M. In *Compr. Org. Synth.*, 2nd ed.; Knochel, P., Molander, G. A., Eds.; Elsevier: Amsterdam, 2014; Vol. 3, pp 268−292. (b) Yoder, R. A.; Johnston, J. N. *Chem. Rev.* **2005**, *105*, 4730−4756. (c) Baunach, M.; Franke, J.; Hertweck, C. *Angew. Chem., Int. Ed.* **2015**, *54*, 2604−2626. (d) Ungarean, C. N.; Southgate, E. H.; Sarlah, D. *Org. Biomol. Chem.* **2016**, *14*, 5454−5467.

(4) (a) Snyder, S. A.; Treitler, D. S.; Brucks, A. P. *Aldrichim. Act.* **2011**, *44*, 27−40. (b) Chung, W.-j.; Vanderwal, C. D. *Angew. Chem., Int. Ed.* **2016**, *55*, 4396−4434.

(5) (a) Gribble, G. W. *J. Nat. Prod.* **1992**, *55*, 1353−1395. (b) Gribble, G. W. *Mar. Drugs* **2015**, *13*, 4044−4136. (c) Gribble,

DOI: 10.1021/jacs.8b00113
J. Am. Chem. Soc. 2018, 140, 4344−4353

G. W. *Environ. Chem.* **2015**, *12*, 396−405. (d) Blunt, J. W.; Copp, B. R.; Keyzers, R. A.; Munro, M. H. G.; Prinsep, M. R. *Nat. Prod. Rep.* **2017**, *34*, 235−294.
(6) (a) Shiomi, K.; Iinuma, H.; Hamada, M.; Naganawa, H.; Manabe, M.; Matsuki, C.; Takeuchi, T.; Umezawa, H. *J. Antibiot.* **1986**, *39*, 487−493. (b) Shiomi, K.; Nakamura, H.; Iinuma, H.; Naganawa, H.; Isshiki, K.; Takeuchi, T.; Umezawa, H.; Iitaka, Y. *J. Antibiot.* **1986**, *39*, 494−501.
(7) (a) Talpir, R.; Rudi, A.; Kashman, Y.; Loya, Y.; Hizi, A. *Tetrahedron* **1994**, *50*, 4179−4184. (b) Loya, S.; Bakhanashvili, M.; Kashman, Y.; Hizi, A. *Arch. Biochem. Biophys.* **1995**, *316*, 789−796.
(8) (a) Wall, M. E. *J. Nat. Prod.* **1992**, *55*, 1561−1568. (b) Wall, M. E.; Wani, M. C.; Manikumar, G.; Taylor, H.; Hughes, T. J.; Gaetano, K.; Gerwick, W. H.; McPhail, A. T.; McPhail, D. R. *J. Nat. Prod.* **1989**, *52*, 1092−1099.
(9) Van Tamelen, E. E.; Hessler, E. J. *Chem. Commun.* **1966**, 411−413.
(10) Hoye, T. R.; Kurth, M. J. *J. Org. Chem.* **1978**, *43*, 3693−3697.
(11) Kato, T.; Ichinose, I. *J. Chem. Soc., Perkin Trans. 1* **1980**, 1051−1056.
(12) Sakakura, A.; Ukai, A.; Ishihara, K. *Nature* **2007**, *445*, 900−903.
(13) For examples on racemic polyene cyclizations see refs 9−12 and the following: (a) Wolinsky, L. E.; Faulkner, D. J. *J. Org. Chem.* **1976**, *41*, 597−600. (b) Kato, T.; Ichinose, I.; Kamoshida, A.; Kitahara, Y. *J. Chem. Soc., Chem. Commun.* **1976**, 518−519. (c) Shieh, H. M.; Prestwich, G. D. *Tetrahedron Lett.* **1982**, *23*, 4643−4646. (d) Yamaguchi, Y.; Uyehara, T.; Kato, T. *Tetrahedron Lett.* **1985**, *26*, 343−346. (e) Kato, T.; Mochizuki, M.; Hirano, T.; Fujiwara, S.; Uyehara, T. *J. Chem. Soc., Chem. Commun.* **1984**, 1077−1078. (f) Tanaka, A.; Sato, M.; Yamashita, K. *Agric. Biol. Chem.* **1990**, *54*, 121−123. (g) Tanaka, A.; Oritani, T. *Biosci., Biotechnol., Biochem.* **1995**, *59*, 516−517. (h) Ascheberg, C.; Bock, J.; Buß, F.; Mück-Lichtenfeld, C.; Daniluc, C. G.; Bergander, K.; Dielmann, F.; Hennecke, U. *Chem. - Eur. J.* **2017**, *23*, 11578−11586.
(14) Samanta, R. C.; Yamamoto, H. *J. Am. Chem. Soc.* **2017**, *139*, 1460−1463.
(15) For examples on asymmetric polyene cyclizations see refs 12 and 14 and the following: (a) Sawamura, Y.; Nakatsuji, H.; Sakakura, A.; Ishihara, K. *Chem. Sci.* **2013**, *4*, 4181−4186. (b) Sawamura, Y.; Nakatsuji, H.; Akakura, M.; Sakakura, A.; Ishihara, K. *Chirality* **2014**, *26*, 356−360. (c) Sawamura, Y.; Ogura, Y.; Nakatsuji, H.; Sakakura, A.; Ishihara, K. *Chem. Commun.* **2016**, *52*, 6068−6071.
(16) (a) Snyder, S. A.; Treitler, D. S. *Org. Synth.* **2011**, *88*, 54−69. (b) Snyder, S. A.; Treitler, D. S. *Angew. Chem., Int. Ed.* **2009**, *48*, 7899−7903.
(17) Snyder, S. A.; Treitler, D. S.; Brucks, A. P. *J. Am. Chem. Soc.* **2010**, *132*, 14303−14314.
(18) Shen, M.; Kretschmer, M.; Brill, Z. G.; Snyder, S. A. *Org. Lett.* **2016**, *18*, 5018−5021.
(19) (a) Snyder, S. A.; Brucks, A. P.; Treitler, D. S.; Moga, I. *J. Am. Chem. Soc.* **2012**, *134*, 17714−17721. (b) Snyder, S. A.; Treitler, D. S.; Brucks, A. P.; Sattler, W. *J. Am. Chem. Soc.* **2011**, *133*, 15898−15901.
(20) (a) Arnold, A. M.; Ulmer, A.; Gulder, T. *Chem. - Eur. J.* **2016**, *22*, 8728−8739. (b) Kohlhepp, S. V.; Gulder, T. *Chem. Soc. Rev.* **2016**, *45*, 6270−6288.
(21) Fabry, D. C.; Stodulski, M.; Hoerner, S.; Gulder, T. *Chem. - Eur. J.* **2012**, *18*, 10834−10838.
(22) (a) Ulmer, A.; Stodulski, M.; Kohlhepp, S. V.; Patzelt, C.; Poethig, A.; Bettray, W.; Gulder, T. *Chem. - Eur. J.* **2015**, *21*, 1444−1448. (b) Patzelt, C.; Poethig, A.; Gulder, T. *Org. Lett.* **2016**, *18*, 3466−3469.
(23) Berrien, J. F.; Ourevitch, M.; Morgant, G.; Ghermani, N. E.; Crousse, B.; Bonnet-Delpon, D. *J. Fluorine Chem.* **2007**, *128*, 839−843.
(24) The solubility of NBS in PFNP at −40 °C is very poor thus leading to an unsatisfying conversion.
(25) To verify that our results of converting alternate substrates with BDSB (**17**) are valid and have not been falsified in any way, we treated as a standard reaction homogeranyl benzene (**11**) with **17** using the conditions described by Snyder and co-workers[16b] and obtained **12** in comparable 72% yield (75% yield reported by Snyder).
(26) (a) Ishibashi, H.; Ishihara, K.; Yamamoto, H. *J. Am. Chem. Soc.* **2004**, *126*, 11122−11123. (b) Ishihara, K.; Ishibashi, H.; Yamamoto, H. *J. Am. Chem. Soc.* **2002**, *124*, 3647−3655. (c) Ishihara, K.; Ishibashi, H.; Yamamoto, H. *J. Am. Chem. Soc.* **2001**, *123*, 1505−1506.
(27) Van Tamelen, E. E. *Acc. Chem. Res.* **1968**, *1*, 111−120.
(28) Barluenga, J.; Alvarez-Perez, M.; Rodriguez, F.; Fananas, F. J.; Cuesta, J. A.; Garcia-Granda, S. *J. Org. Chem.* **2003**, *68*, 6583−6586.
(29) Snyder reported that IDSI is stable upon storage at −20 °C but decomposes completely within 30 min at rt.[17]
(30) (a) Olah, G. A.; Bollinger, J. M. *J. Am. Chem. Soc.* **1968**, *90*, 947−953. (b) Olah, G. A.; Westerman, P. W.; Melby, E. G.; Mo, Y. K. *J. Am. Chem. Soc.* **1974**, *96*, 3565−3573. (c) Ohta, B. K.; Hough, R. E.; Schubert, J. W. *Org. Lett.* **2007**, *9*, 2317−2320. (d) Denmark, S. E.; Burk, M. T.; Hoover, A. J. *J. Am. Chem. Soc.* **2010**, *132*, 1232−1233.
(31) The major diastereomer of **57** was isolated in 32%, while the minor isomer appeared only as an inseparable mixture with other unidentified byproducts.
(32) Ashtekar, K. D.; Marijarani, N. S.; Jaganathan, A.; Holmes, D.; Jackson, J. E.; Borhan, B. *J. Am. Chem. Soc.* **2014**, *136*, 13355−13362.
(33) For studies on HFIP-ether and HFIP-amine adduct formation see: (a) Berkessel, A.; Adrio, J. A.; Huettenhain, D.; Neudoerfl, J. M. *J. Am. Chem. Soc.* **2006**, *128*, 8421−8426. (b) Berkessel, A.; Adrio, J. A. *J. Am. Chem. Soc.* **2006**, *128*, 13412−13420. (c) Vuluga, D.; Legros, J.; Crousse, B.; Slawin, A. M. Z.; Laurence, C.; Nicolet, P.; Bonnet-Delpon, D. *J. Org. Chem.* **2011**, *76*, 1126−1133.
(34) For selected examples utilizing Lewis base activation of X^+ in various reaction types see ref 12 and the following: (a) Denmark, S. E.; Burk, M. T. *Proc. Natl. Acad. Sci. U. S. A.* **2010**, *107*, 20655−20660. (b) Chen, F.; Tan, C. K.; Yeung, Y.-Y. *J. Am. Chem. Soc.* **2013**, *135*, 1232−1235. (c) Ke, Z.; Tan, C. K.; Chen, F.; Yeung, Y.-Y. *J. Am. Chem. Soc.* **2014**, *136*, 5627−5630. (d) Kawato, Y.; Kubota, A.; Ono, H.; Egami, H.; Hamashima, Y. *Org. Lett.* **2015**, *17*, 1244−1247. (e) Ke, Z.; Wong, Y.-C.; See, J. Y.; Yeung, Y.-Y. *Adv. Synth. Catal.* **2016**, *358*, 1719−1724.
(35) For a more comprehensive overview on activating electrophilic halonium reagents in transformations even beyond polyene cyclizations see (a) Castellanos, A.; Fletcher, S. P. *Chem. - Eur. J.* **2011**, *17*, 5766−5776. (b) Denmark, S. E.; Kuester, W. E.; Burk, M. T. *Angew. Chem., Int. Ed.* **2012**, *51*, 10938−10953. (c) Hennecke, U. *Chem. - Asian J.* **2012**, *7*, 456−465. (d) Tan, C. K.; Yu, W. Z.; Yeung, Y.-Y. *Chirality* **2014**, *26*, 328−343. (e) Cheng, Y. A.; Yu, W. Z.; Yeung, Y.-Y. *Org. Biomol. Chem.* **2014**, *12*, 2333−2343. (f) Cresswell, A. J.; Eey, S. T. C.; Denmark, S. E. *Angew. Chem., Int. Ed.* **2015**, *54*, 15642−15682. (g) Andries-Ulmer, A.; Gulder, T. *Sci. Synth.* **2017**, 389−428.
(36) (a) Zhang, Q.; Catti, L.; Pleiss, J.; Tiefenbacher, K. *J. Am. Chem. Soc.* **2017**, *139*, 11482−11492. (b) Zhang, Q.; Tiefenbacher, K. *Nat. Chem.* **2015**, *7*, 197−202.
(37) (a) Cozens, F. L.; McClelland, R. A.; Steenken, S. *J. Am. Chem. Soc.* **1993**, *115*, 5050−5055. (b) McClelland, R. A.; Mathivanan, N.; Steenken, S. *J. Am. Chem. Soc.* **1990**, *112*, 4857−4861. (c) Steenken, S.; McClelland, R. A. *J. Am. Chem. Soc.* **1990**, *112*, 9648−9649. (d) Mo, X.; Yakiwchuk, J.; Dansereau, J.; McCubbin, J. A.; Hall, D. G. *J. Am. Chem. Soc.* **2015**, *137*, 9694−9703. (e) Ricardo, C. L.; Mo, X.; McCubbin, J. A.; Hall, D. G. *Chem. - Eur. J.* **2015**, *21*, 4218−4223.
(38) Ammer, J.; Mayr, H. *J. Phys. Org. Chem.* **2013**, *26*, 59−63.
(39) For selected examples of HFIP as solvent playing a crucial role see ref 22a and the following: (a) Tanuwidjaja, J.; Ng, S.-S.; Jamison, T. F. *J. Am. Chem. Soc.* **2009**, *131*, 12084−12085. (b) Dohi, T.; Yamaoka, N.; Kita, Y. *Tetrahedron* **2010**, *66*, 5775−5785. (c) Dohi, T.; Hu, Y.; Kamitanaka, T.; Washimi, N.; Kita, Y. *Org. Lett.* **2011**, *13*, 4814−4817. (d) Yoshimura, A.; Middleton, K. R.; Luedtke, M. W.; Zhu, C.; Zhdankin, V. V. *J. Org. Chem.* **2012**, *77*, 11399−11404. (e) Trillo, P.; Baeza, A.; Najera, C. *J. Org. Chem.* **2012**, *77*, 7344−7354. (f) Motiwala, H. F.; Fehl, C.; Li, S.-W.; Hirt, E.; Porubsky, P.; Aube, J. *J. Am. Chem. Soc.* **2013**, *135*, 9000−9009. (g) Hu, Y.; Kamitanaka, T.; Mishima, Y.; Dohi, T.; Kita, Y. *J. Org. Chem.* **2013**, *78*, 5530−5543. (h) Elsler, B.; Wiebe, A.; Schollmeyer, D.; Dyballa, K. M.; Franke, R.;

DOI: 10.1021/jacs.8b00113
J. Am. Chem. Soc. 2018, 140, 4344−4353

Waldvogel, S. R. *Chem. - Eur. J.* **2015**, *21*, 12321−12325. (i) Lips, S.; Wiebe, A.; Elsler, B.; Schollmeyer, D.; Dyballa, K. M.; Franke, R.; Waldvogel, S. R. *Angew. Chem., Int. Ed.* **2016**, *55*, 10872−10876. (j) Wencel-Delord, J.; Colobert, F. *Org. Chem. Front.* **2016**, *3*, 394−400. (k) Dherbassy, Q.; Schwertz, G.; Chesse, M.; Hazra, C. K.; Wencel-Delord, J.; Colobert, F. *Chem. - Eur. J.* **2016**, *22*, 1735−1743. (l) Colomer, I.; Batchelor-McAuley, C.; Odell, B.; Donohoe, T. J.; Compton, R. G. *J. Am. Chem. Soc.* **2016**, *138*, 8855−8861. (m) Tian, Y.; Xu, X.; Zhang, L.; Qu, J. *Org. Lett.* **2016**, *18*, 268−271. (n) Burckle, A. J.; Vasilev, V. H.; Burns, N. Z. *Angew. Chem., Int. Ed.* **2016**, *55*, 11476−11479. (o) Burckle, A. J.; Gal, B.; Seidl, F. J.; Vasilev, V. H.; Burns, N. Z. *J. Am. Chem. Soc.* **2017**, *139*, 13562−13569. (p) Colomer, I.; Chamberlain, A. E. R.; Haughey, M. B.; Donohoe, T. J. *Nat. Rev. Chem.* **2017**, *1*, 0088.

(40) The data of the X-ray crystal analysis for compounds **16**, **41**, and **56** were deposited at Cambridge Crystallogaphic Data Center (CCDC 1584440, CCDC 1571223, and CCDC 1584439).

DOI: 10.1021/jacs.8b00113
J. Am. Chem. Soc. 2018, 140, 4344−4353

2. Controlling Conformation in Solution: Mild Biomimetic Proton-Induced Polyene Cyclizations through Fluorinated Alcohol Solvent Cluster Arrays

During screening efforts to optimize the haliranium-induced polyene cyclization reaction presented in chapter II.1 close attention was paid on what side products were formed, as this helped the efforts to increase the yield and diastereoselectivity. Aside from partially cyclized halogenated products (not shown) some amounts of proton-cyclized product **53** were detected when homogeranyl benzene **70** was converted (Scheme 21). Namely, pyrrole (**173**), *N*,*O*-dimethylhydroxylamine hydrochloride (**174**), and sulfamic acid (**175**) as Lewis basic additives gave proton cyclized **53** in 69%, 32%, and 12%, respectively.

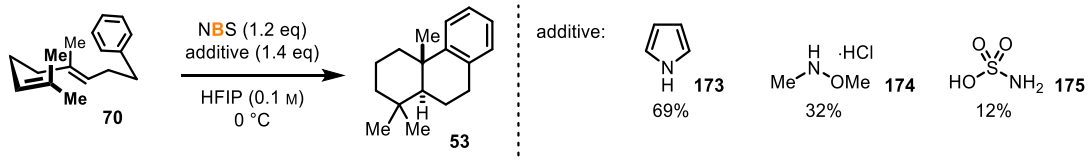

Scheme 21. Formation of **53** during the screening of Lewis base additives.

This sparked our synthetic interest, as a plethora of natural products possesses “head-to-tail” cyclized moieties (*vide supra*), and present methods do have drawbacks concerning functional group tolerance, yield, and selectivity. Moreover, we hoped to utilize the unique properties of HFIP towards the proton cyclization of linear polyenes **70**. Especially intrigued by the ability of the weakly acidic *N*,*O*-dimethylhydroxylamine hydrochloride (**174**) to induce proton cyclization we set out to explore this reactivity further. The first step was to omit the halogen source NBS in order to see the full potential of the reaction in the proton-induced cyclization of **70**. Screening of different strong acids showed good results in respect to yields of **53**. It is notable that in all cases presented in this chapter **70** was formed with excellent diastereoselectivity of > 95:5. This was ensured by comparison of the ^{1}H-NMR spectra to literature known *p*-tolyl cyclization product **54**, where a close analog of the *cis*-decalin framework shows a distinct upfield shifted methyl singlet at 0.37 ppm.[108] As in the previous halocyclization project, the model substrate to optimize the reaction was homogeranyl benzene (**70**) in 0.1 M distilled HFIP with 20 mol% of acid (Table 5). The aim was to find a mild and simple method at ambient conditions and no need for the exclusion of air or moisture, which was the reason why the reaction was conducted without a protective atmosphere at room temperature from the beginning. However, the quality of HFIP was decisive. When HFIP was used as received, there was a strong background reaction without any additive or catalyst, and full conversion of **70** was observed after one day of reaction time, but with the formation of ample side products. Desired **53** was, on the other hand, only produced in 61% yield (entry 1). This was avoided by distilling the solvent from molecular sieve and KOH prior to use in order to remove trace amounts of residual acid. Putatively, residual amounts of hexafluoroacetone (HFA, **176**) from the

industrial production process of HFIP[101] may be responsible for the increased acidity of the solvent, as the ketone is prone to form a geminal diol **177** with water. This highly electron-deficient diol has a high pH value in water ranging between 1 and 2.[109] Gratifyingly, with this purification, no background reaction was observed without the addition of external acid (entry 2). Then, a wide range of strong and weak acids such as TFA, *p*-toluenesulfonic acid, sulfuric acid, and **178**-**181** were tested (entries 3 to 9), with the most promising one being the super acidic BINOL-derived bisthiophosphoric acid **180** (entry 8).

Table 5. Acid screening for the conversion of **70** to **53**.

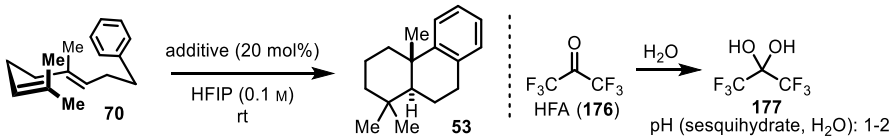

entry	acid	pK_a (H_2O)	reaction time	conversion[a]	yield 53[a]
1[b]	-	-	1 d	> 95%	61%
2	-	-	7 d	< 5%	< 5%
3	TFA	0.23[110]	15 min	> 95%	56%
4	$TosOH \cdot H_2O$	-2.8[111]	15 min	> 95%	62%
5	H_2SO_4	-3.0, 2.0[110]	15 min	> 95%	59%
6	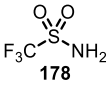 178	6.3[110]	2 d	> 95%	64%
7	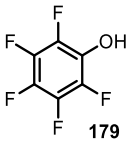 179	5.5[112]	7 d	89%	62%
8	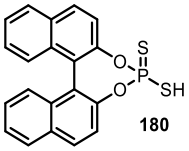 180	**-4.21[113]**	**5 h**	**> 95%**	**76%**
9	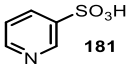 181	2.9[114]	1 h	> 95%	61%

22.8 mg **70** (100 µmol, 1.0 eq) were mixed with 20 mol% acid in 1.0 mL HFIP (0.1 M) at rt under air in a closed vessel. HFIP was distilled under argon from a mixture of activated 3 Å and 4 Å molecular sieve and KOH (250 mg per 100 mL of solvent). The reaction time indicates the first time at which either full conversion was observed (which could be prior to that time) or the time the last data point collected. [a]Conversion and yield determined through GC-FID using an internal standard. [b]HFIP was used as received.

No direct correlation between reaction time, yield, and pK_a value of the employed acid could be observed at first sight. It is, however, notable that the cyclization occurs even with weak acids such as **178** (entry 6). A mild methodology to achieve this cyclization is highly desirable because previous literature reports usually rely on strong Brønsted or Lewis acids (*vide supra*), which severely hamper the

functional group tolerance and require a more effortful reaction setup. As the results in Scheme 21 show even amine hydrochloric salts may facilitate the conversion and based on the knowledge of the beneficial effects of morpholine in the haliranium-induced polyene cyclizations,[64] we next tried various morpholinium salts as additives (Table 6). Weakly acidic salts such as morpholinium acetate (**182a**, entry 1) gave no conversion of the starting material. TFA (**182b**) and tosylate (**182c**) salts showed very slow conversion and poor selectivity, as a major fraction of the product was determined not to be the desired product as judged by GC-FID (entries 2 and 3). Of the strong acid salts hemisulfate **182d**, chloride **182e**, and bromide **182f** the latter gave the fastest conversion within only 5 hours, whereas the hydrochloride **182e** gave with 74% the best yield of **53** (entries 4-6). Switching to pyridine (**183**) as a weaker base and employing pyridinium salts **183a-f** in the reaction turned out to be advantageous in regard to conversion and reaction time (entries 7-12). In all cases, full conversion of **70** was observed in less than 24 h. Again, no direct correlation between reaction rate, yield, and pK_a value of the corresponding acid could be doubtlessly established. However, within these results commercially available pyridinium bromide **183d** gave 74% yield after 13 h of reaction time (entry 10), which is why this was the catalyst of choice for further investigations.

Table 6. Screening of morpholinium (**182a-f**) and pyridinium salts (**183a-f**) as additives.

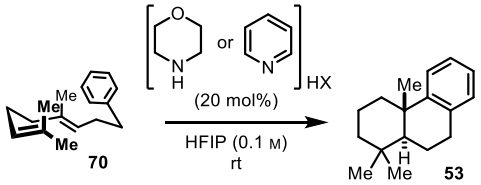

entry	amine	HX		pK_a (acid)	time	conversion of 70[a]	yield of 53[a]
1		AcOH	**182a**	4.76[110]	20 d	< 5%	< 5%
2		CF_3CO_2H	**182b**	0.23[110]	3 d	> 95%	66%
3		TosOH	**182c**	-2.8[111]	20 d	56%	38%
4	182	H_2SO_4	**182d**	-3.0, 2.0[110]	1 d	95%	65%
5		HCl	**182e**	-8.0[110]	1 d	> 95%	74%
6		HBr	**182f**	-9.0[110]	5 h	> 95%	71%
7		HBF_4	**183a**	-0.44[115]	12 h	> 95%	55%
8		TosOH	**183b**	-2.8[111]	13 h	> 95%	67%
9		HCl	**183c**	-8.0[110]	1 d	> 95%	66%
10	183	**HBr**	**183d**	**-9.0[110]**	**13 h**	**> 95%**	**74%**
11		HI	**183e**	-9.5[116]	15 h	> 95%	63%
12		TfOH	**183f**	-20[116]	3 h	> 95%	64%

22.8 mg **70** (100 µmol, 1.0 eq) were mixed with 20 mol% catalyst **182a-f** or **183a-f** in 1.0 mL HFIP (0.1 M) at rt under air in a closed vessel. HFIP was distilled under argon from a mixture of activated 3 Å and 4 Å molecular sieve and KOH (250 mg per 100 mL of solvent). [a]Conversion and yield were determined by GC-FID using an internal standard.

It was previously postulated that HFIP has a distinct effect on apolar, linear polyenes and their conformation in solution, namely that the linear polyene **70** is thought to assume a chair-like conformation to reduce the overall surface area through hydrophobic interactions of the solvent.[64,117] The next step before optimizing the reaction conditions was hence to conduct a solvent screening of standard laboratory solvents as well as a selection of other fluorinated alcohols to confirm the unique role of HFIP in the desired transformation. The best conditions from Table 6 are shown in Table 7, entry 1. Standard laboratory solvents such as DCM, toluene, and diethyl ether gave neither conversion nor product formation after 5 days (entries 2-4). 2-Nitropropane or 2-propanol gave no conversion either (entries 5 and 6). Of the other fluorinated solvents such as 1,1,1-trifluoroethanol (TFE, **184**), 1,1,1-trifluoro-2-propanol (**185**) or 2,2,3,3,3-pentafluoro-1-propanol (**186**) only **185** showed conversion, albeit only 44% and 28% yield of **53** after 5 days. Surprisingly, perfluoro-*tert*-butanol (PFTB, **187**) furnished desired **53** after one day in 96% chemical yield (entry 10).

Table 7. Solvent screening with best catalyst **183d**.

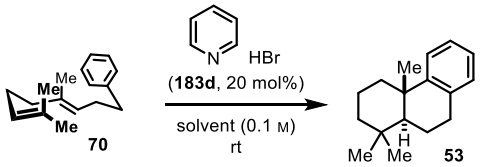

entry	solvent	reaction time	conversion of 70[a]	yield of 53[a]
1	HFIP	13 h	> 95%	74%
2	CH_2Cl_2	5 d	< 5%	< 5%
3	toluene	5 d	< 5%	< 5%
4	Et_2O	5 d	< 5%	< 5%
5	*i*PrNO$_2$	5 d	< 5%	< 5%
6	*i*PrOH	5 d	< 5%	< 5%
7	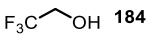 **184**	5 d	< 5%	< 5%
8	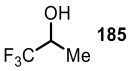 **185**	5 d	44%	28%
9	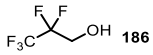 **186**	5 d	< 5%	< 5%
10	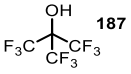 **187**	**1 d**	**> 95%**	**96%**

22.8 mg **70** (100 µmol, 1.0 eq) were mixed with 20 mol% py-HBr (**183d**) in 1.0 mL solvent (0.1 M) at rt under air in a closed vessel.

To visually demonstrate the course of optimization Figure 10 displays experimental GC traces of selected transformations after the reaction has been completed. In a) starting material **70** is displayed, b) shows the reaction of **70** with the strong acid TFA in HFIP, where many undesired products have been formed, most likely stemming from internal protonation. In c) the increase in selectivity when employing

the mildly acidic py-HBr salt **183d** can be seen, and in d) presents the chromatogram of the final optimized reaction conditions with product **53** being almost the sole signal.

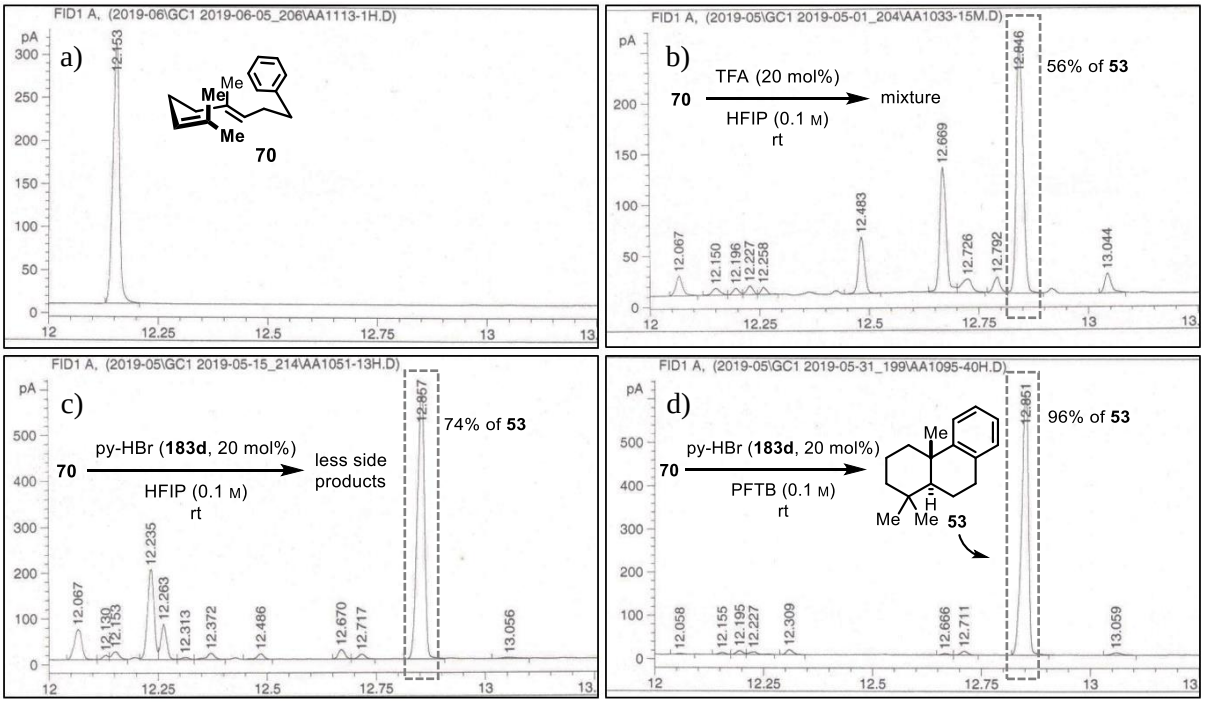

Figure 10. Experimental GC traces: a) Starting material **70**. b) Reaction Table 5, entry 3. c) Reaction Table 5, entry 1. d) Optimized reaction conditions from Table 5, entry 10.

As PFTB proved to be the optimal solvent to promote the desired proton-induced cyclization reaction it was worthwhile to compare some physical properties of HFIP and PFTB (Table 8). PFTB has a lower boiling and melting point of 45 °C and -20 °C, respectively, as compared to HFIP. Due to the higher content of fluoride atoms in the molecule its density is slightly higher (1.6 compared to 1.7 g/mL), and, most noteworthy, the pK_a value is significantly lower and with 5.4 almost in the range of some carboxylic acids, such as acetic acid with 4.8.[110] The even more polarized OH bond of PFTB could be the reason why the cyclization of **70** proceeds so exceedingly smooth. PFTB is commercially available, yet its contemporary use is limited to the formation of the currently least-coordinating aluminate counterion $Al(PFTB)_4^-$[118] or for the introduction of highly hydrophobic ether groups to enhance material properties.[119] To the best of my knowledge, it was not used as a solvent in chemical transformations to date.

Table 8. Selected properties of the fluorinated alcohol solvents HFIP and PFTB.

physical property	HFIP[96]	PFTB[120]
m.p.	-4 °C	-20 °C
b.p.	59 °C	45 °C
Density	1.6 g/mL	1.7 g/mL
pK_a	9.3	5.4
price[a]	0.17 €/mL	2.25 €/mL

[a]from Fluorochem online shop, 20.03.2021

Next, various mechanistic investigations were conducted to gain a deeper understanding of the interactions between PFTB and the model substrate **70**. Figure 11 shows the titration of **70** with different solvents analyzed by ^{13}C NMR spectroscopy, whereas the shifts of **70** in $CDCl_3$ are set as the zero points. Increasing amounts of PFTB (red) resulted in significant shifts, which is most pronounced for the sp^2 carbons *C*2 and *C*6. Even more intriguingly, the "head" alkene group (*C*2 and *C*3) shifts stronger than the internal alkene (*C*6 and *C*7), hinting towards a stronger activation of the terminal alkene due to electronic interactions of the more exposed alkene. In apolar toluene (green) or in non-fluorinated *t*BuOH (purple) only negligible shifts or upfield shifts were observed, underlining the unique properties of PFTB.

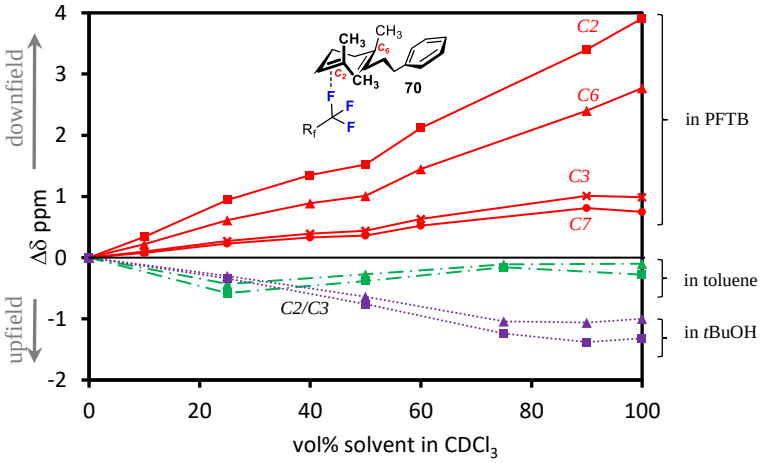

Figure 11. Titration of **70** in $CDCl_3$ with increasing vol% of co-solvent PFTB (red), toluene (green) and *t*BuOH (purple) analyzed by ^{13}C NMR spectroscopy. 12.7 mg **70** was dissolved in 0.5 mL solvent with the shown composition (0.1 M).

Next, a reaction profile was recorded. Continuous reaction monitoring via GC-FID and GC-MS for fragment identification resulted in the reaction kinetic shown in Figure 12a. Starting material **70** (black) is converted either directly into the tricyclic product **53** (blue), into the three regioisomeric monocyclic elimination products **188**-**190** (grey, red and purple, respectively), or the alkene isomerization product **191**. The *exo*-elimination product **190** was formed with the lowest quantity, followed by the *endo*-product **189**. The thermodynamically most stable tetrasubstituted **188** was produced slowest and is

consumed at the lowest rate, yet holds the highest percentile share during the reaction. However, all shown side products eventually yield desired **53** after 17 hours. The yellow graph depicts not identified side products, which are consumed during the reaction and do not give any significant additional signals in the GC.

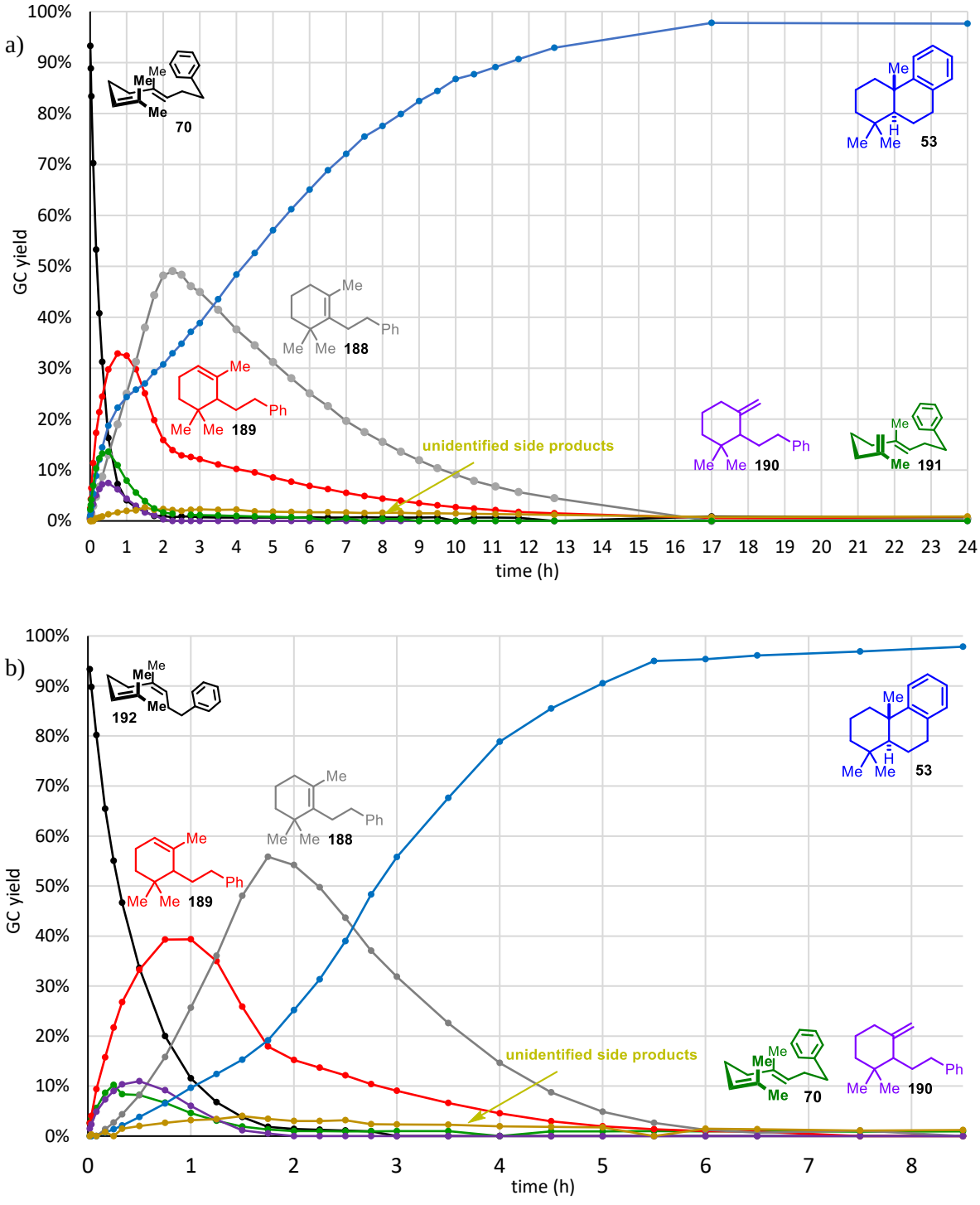

Figure 12. Product **53** and intermediate formation of **188-190** over time. 22.8 mg **70** (a) or **192** (b) (100 µmol, 1.0 eq) were mixed with 3.2 mg py-HBr (**183d**, 20.0 µmol, 20 mol%) in 1.0 mL PFTB.

On the other hand, if the (*Z*)-configured homoneryl benzene (**192**) is used as the starting material the reaction profile is that of a consecutive reaction (Figure 12b).[121] In this case, formation of **53** is not observed in the initial few minutes and just then slowly proceeds to form. This is in contrast to the transformation of (*E*)-homogeranyl benzene (**70**), where product formation was observable within the first few seconds. Analysis of the final reaction product revealed unambiguously that only the major *trans*-decalin product is produced in likewise good yield as for **70**. This means that either isomerization occurs from **192** to **70**, which was observed in this reaction mixture (green), or first a monocyclization, followed by a second protonation of the alkene and cyclization. The reaction time is also shorter in the neryl case, and the reaction is terminated after only 6 hours.

The GC data showed a stepwise process. It is, however, possible that the monocyclic intermediates **188**-**190** are interconvertible by protonation and elimination. To test this hypothesis, the reaction was run with deuterated pyridinium bromide in deuterated PFTB. To have a clean and reproducible method for preparation of PFTB-OD the acidic alcohol was converted into its sodium salt, dried, acidified with D_2SO_4 (isotopic purity > 99.5%), and distilled twice (Scheme 22a). Applying the deuterated solvent in the proton-induced cyclization showed that at all expected sites in allylic positions or on the intermediate sp^2 carbons deuterium incorporation was detectable (Scheme 22b). This result further confirms the formation of intermediate products, which in turn are deuterated, forming a carbocation, and ensue in cyclization reactions.

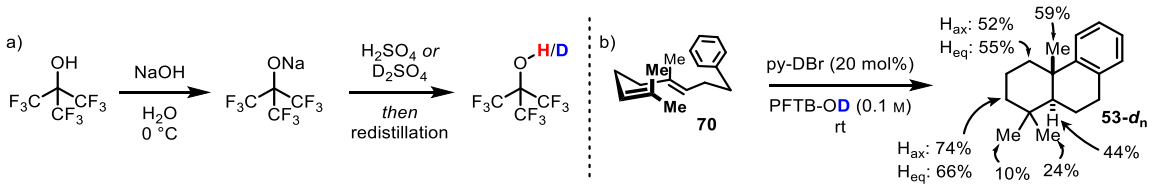

Scheme 22. a) Preparation of PFTB-OD and purification of PFTB-OH for kinetic studies. b) Conversion of **70** with pyridine deuterobromide. Percentages refer to the degree of deuteration at the specified site. All unlabeled sites show <5% incorporation.

Next, the effect of the catalyst was investigated. Again using **70** as model substrate, four salts, namely morpholine-HBr (**182f**), pyridinium bromide (**183d**), DABCO bishydrobromide (**193**), and DABCO bistriflate (**194**) were tested. Without catalyst, there is also a conversion of **70** in PFTB, albeit really slow with a reaction time of over 14 days until the starting material was fully consumed giving a complex mixture (Figure 13, purple). Morpholine derivative **182f** gave a faster conversion (blue), and with **183d** the reaction was already completed within 1 day (orange). Using the weaker base DABCO as its HBr salt (**193**) increased the reaction rate even further (grey), and with bistriflate **194** the reaction was completed after only 2 hours (red), increasing the relative rate compared to the background reaction by a factor of 205. Notably, in all cases the yield of 96% and diastereoselectivity was unchanged with > 95:5, it was just the reaction rate that drastically increased.

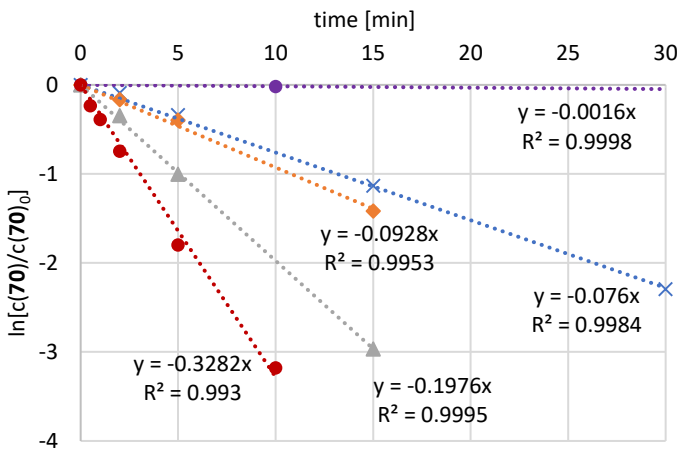

catalyst		k_{rel}
none	●	1
HBr **182f**	×	48
HBr **183d**	◆	58
2 HBr **193**	▲	124
2 TfOH **194**	●	205

Figure 13. Comparison of the rate of consumption of **70** with different amine salts (conditions from Figure 12).

We utilized the synergistic Lewis acid/Lewis base approach in our reaction,[64] with the base being the amine salt and the acid originating from the H-bonding network of the fluorinated alcohol solvent. To see and quantify the Lewis acidity strength we conducted a Gutmann-Beckett experiment,[122] which is used to quantify the Lewis acidity of various solvents and other Lewis acids in relation to one another. A 0.1 M solution of triethylphosphine oxide (**195**) is dissolved in different solvents and the ^{31}P-NMR shift recorded in relation to $(MeO)_3PO$ (2.0 M in $CDCl_3$, δ = 2.2 ppm)[123] as an internal reference. In *t*BuOH (Figure 14a) the shift of **195** resides at 54.5 ppm. A visible downfield shift is observed in TFE (b) and HFIP to 64.5 and 69.7 ppm, respectively (b,c), whereas in PFTB the shift moves downfield to 65.3 ppm (d). This could be due to the steric hindrance of the fluorine groups, limiting the access of the proton to the phosphine oxide. Thus, PFTB may be sorted around water and acetic acid (Figure 14, right) on the Lewis acidity scale. Adding py-HBr (**183d**, 20 mol%, d) slightly increases the shift to 65.4 ppm, and with 20 mol% of DABCO bistriflate (**194**, e) the ^{31}P-NMR shift is now moved significantly to 68.0 ppm. Interestingly, the signal with **195** is not a sharp but rather broad singlet, hinting towards a dynamic activation of the phosphine oxide similarly observed with strong acids.[122a] To also compare Lewis acids that are not liquid, e.g. metal chlorides or boron halides Beckett introduced the acceptor number (AN), which can also be extrapolated for non-liquid Lewis acids and are calculated according to equation 1. This sets the AN of **195** in hexanes as the zero value and a 1:1 complex of **195** and $SbCl_5$ in DCE to 100.[124]

$$AN = (\delta_{sample} - 41.0) \times \left(\frac{100}{86.14 - 41.0}\right) \quad (1)$$

It is noteworthy that pure PFTB shows a higher AN than acetic acid, albeit its pK_a is lower by about one order of magnitude. This means that the NMR shift does not correlate directly with the pK_a value of the solvent, but rather with the Lewis acidity and the ability to coordinate a Lewis base, in this case, the phosphine oxide **195**. Upon activation with catalyst **194**, the AN even surpasses the Lewis acidity of $SnCl_4$.

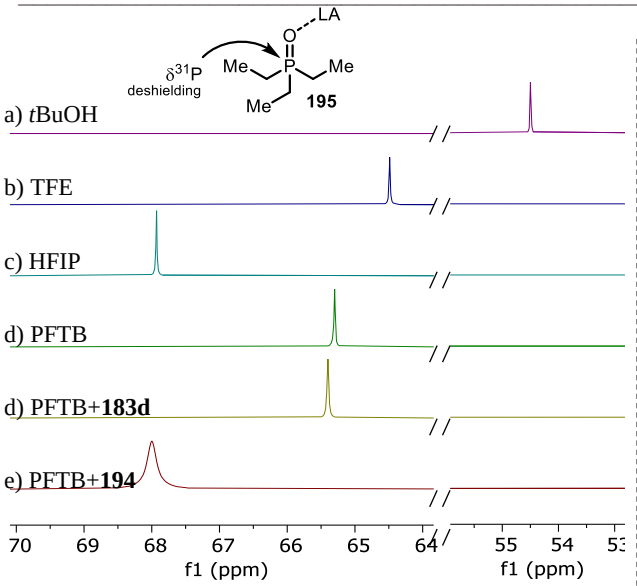

solvent/LA	δ (^{31}P, ppm)	AN
n-hexane[122a]	41.0	0.0
CH_2Cl_2[122a]	50.2	20.4
*t*BuOH	54.5	29.9
EtOH[122a]	58.7	37.1
TFE	64.5	52.1
AcOH[122a]	64.9	52.9
PFTB	**65.3**	**53.8**
PFTB+183d	**65.4**	**54.1**
$SnCl_4$[124]	–	59.0
HFIP	67.9	59.6
PFTB+194	**68.0**	**59.8**
$TiCl_4$[124]	–	70.0
$SbCl_5$ (DCE)[122a]	86.1	100.0
TFA[122a]	88.5	105.3
TfOH[122a]	99.3	129.1

increasing Lewis acidity

Figure 14. Gutmann-Beckett experiment of **195** in different solvents (left) and ^{31}P shifts and acceptor number AN (right). **183b** and **194** were added in 20 mol% in respect to **195**.

Since the solvent PFTB is postulated to play a decisive role in this transformation we wanted to see how important the H-bonding network is in this reaction. With both deuterated and non-deuterated PFTB having the same purity in hand (c.f. Scheme 22), we subjected **70** to the more active catalyst DABCO bistriflate (**194**) and measured the rate of starting material (**70**) consumption (Figure 15a). Linearization of the results (Figure 15b) gave the slope of the logarithmic plot with good determination coefficients R^2 of 0.997 for PFTB-OD and 0.993 for PFTB-OH, respectively. Setting the slope of PFTB-OH in relation to PFTB-OD then gave a significant KIE value of k_{OH}/k_{OD} of 2.83, showing that the H-bonding network is an important factor in the rate-determining step of the reaction. The intrinsically stronger O-D bond would not influence the reaction rate to that extent if not a significant influence of the H-bonding network was present.[125]

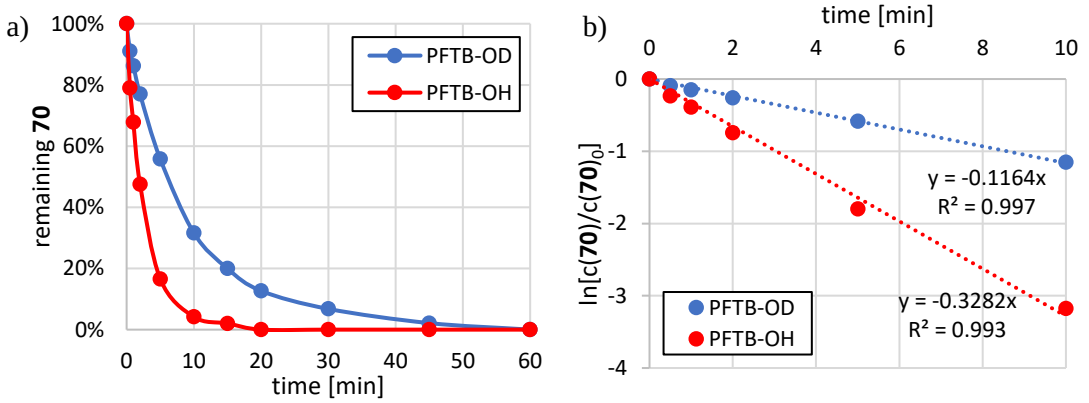

Figure 15. Decrease of starting material **70** over time in PFTB-O**H** (red) and PFTB-O**D** (blue) with 20 mol% **194**.

The reaction has been optimized, the mode of activation investigated, and the stepwise mechanism has been confirmed. To shed more light on the special and unique properties of fluorinated alcohol solvents on the conformation in solution and thus the diastereoselectivity of this conversion, 1D-^{1}H-NOESY

spectra of substrate **70** in various solvents were recorded. The aim of this experiment was to determine if any changes in the average distance between protons would be measurable on the NMR timescale. To reproduce the reaction conditions as closely as possible the concentration was chosen to be 0.1 M for all solvents investigated. To selectively excite a proton in NMR measurements its signal should be as isolated from other signals as possible to avoid minor excitation of protons in close frequency proximity. Therefore, the aromatic protons were collectively and selectively excited in a 100 MHz window and the corresponding NOESY correlation spectra were recorded. As shown in Figure 16 only in PFTB clear correlations were detectable between the aromatic protons and methyl groups **A** and **B** that are furthest away from the arene ring. In all other standard solvents tested such as $CDCl_3$, methanol-d_4, or cyclohexane-d_{12} only the carbon of the closest methyl group **C** showed an interaction through space (Figure 16).[126] This result confirmed that **70** assumes a more coiled form compared to other solvents, bringing the reactive alkene sites in closer proximity and thus enabling a selective protonation and cyclization only possible in PFTB under the presented reaction conditions.

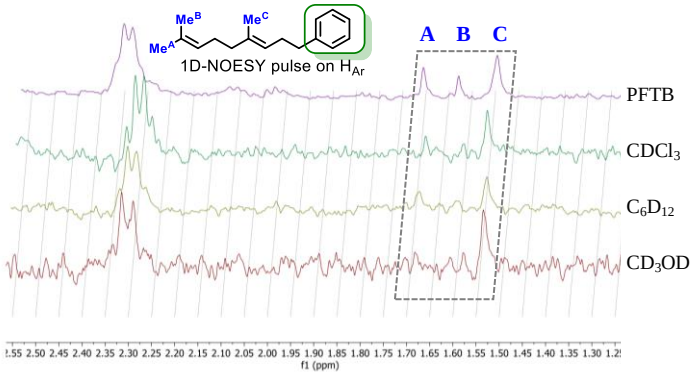

Figure 16. 1D-^{1}H-NOESY correlation of the aromatic protons of **70** with the three methyl groups. In all experiments the same concentration and pulse sequence are used.[127]

After the first mechanistic details were investigated, we set out to see what substrates were tolerated with this novel proton cyclization method. Therefore, different geraniol derivatives were prepared and submitted to the optimized conditions (Figure 17). Model product **53** was isolated in 94% yield, *p*-methoxy substituted product **55** in 88%, and cyclohexyl derivative **196** in 91% yield with perfect diastereoselectivity, the latter showing that not only dimethyl substituents were tolerated. Oxygen nucleophiles gave phenol ethers **60** and **67** with a diastereomeric ratio of > 95:5 and 93:7, respectively, and **197** in a regioisomeric ratio of 64:36. Homogeranoic acid **84** gave (±)-tetrahydroactinidiolide (**198**) upon cyclization with a diastereomeric ratio of 76:24 in 98% chemical yield.

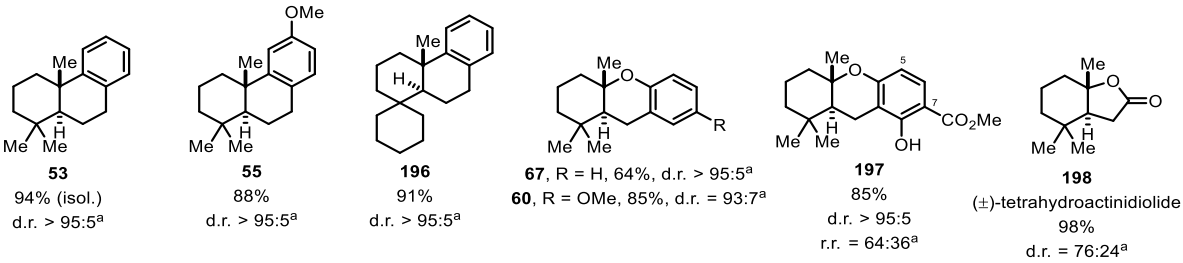

Figure 17. Substrate scope with internal *C* and *O* nucleophiles. [a]Determined by ^{1}H-NMR analysis of the crude mixture.

Next, we set out to see how well the method tolerates functional groups. Various geranyl esters and ethers were prepared and subjected to the cyclization conditions (Figure 18). Since an internal nucleophile is absent, a regioisomeric mixture of elimination products (*endo*/*exo* material) was obtained in those cases with varying selectivities. Geranyl benzoic acid derivatives gave the products **199**-**202** in good chemical yields of 73-85% and selectivity, albeit the latter showed no clear correlation between electron-donating or -withdrawing substituents at the arene ring. Isoxazole, thiophene, and acetic esters **203**-**205** were likewise tolerated as well as the organometallic ferrocene ester **206** with good to excellent regioselectivities of > 95:5.

Next, cyclogeranyl benzyl ether **207** was obtained in quantitative yield without any evidence of the formation of a 7-membered ring under these conditions. Alkyne **208** was isolated in a similar excellent yield. Intriguingly, both epoxide (→**209**) and MOM-protected geraniol (→**210**) were likewise tolerated, where both functional groups are generally decomposing under acidic conditions.[128] This nicely shows how mild and selective the method is even for acid-labile substrates. To test the stability of substituted alkenes, allyl (→**211**) and but-2-ene ethers (→**212**) were prepared and cyclized. The disubstituted alkene retained the original E/Z selectivity in product **212**, which means that no isomerization took place at the alkene. This shows that the conditions selectively protonate only trisubstituted alkenes, and preferably the ones in closest proximity to the solvent. Only prenyl ether (→**213**) gave a complex mixture of products, as the residual alkene is even more electron-rich than the desired site of protonation in the geranyl chain. Interestingly, all ethers **207**-**212**, unlike esters **199**-**203**, were isolated in excellent regioselectivity favoring the $\Delta_{2,3}$-elimination product.

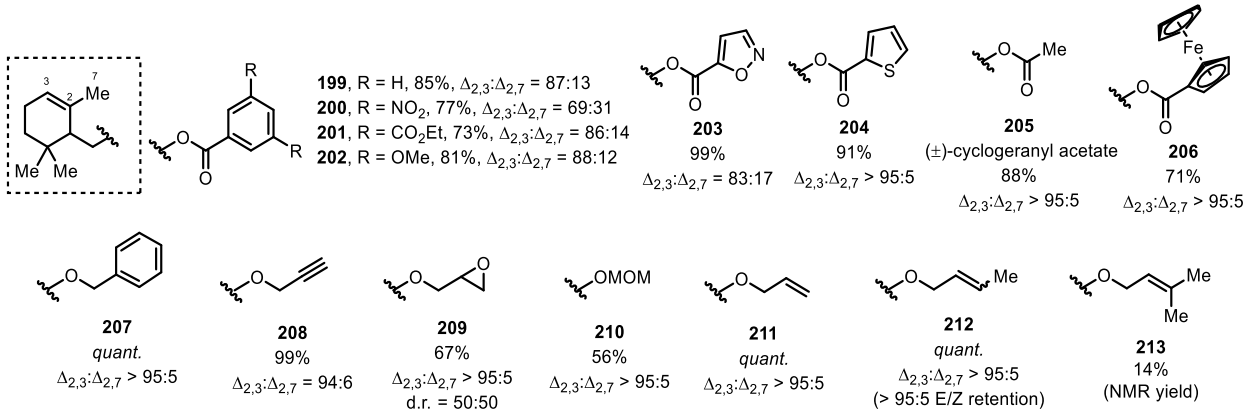

Figure 18. Substrate scope of geranyl esters and ethers.

The proton cyclization can be extended to more complex and chiral structures as showcased by biotin ester (→**214**) and santonic acid (→**215**, Figure 19). The latter is interesting as the two carbonyl groups are known for their strong hydrogen-bond accepting properties, which could explain the slightly lower yield of 66% compared to esters (Figure 18).[129] Fmoc-protected proline (→**216**) and Boc-protected lysine ester (→**217**) were furnished in 59% and 77% yield, respectively, with no significant diastereoselection on the tertiary carbon in the cyclic geranyl structure.

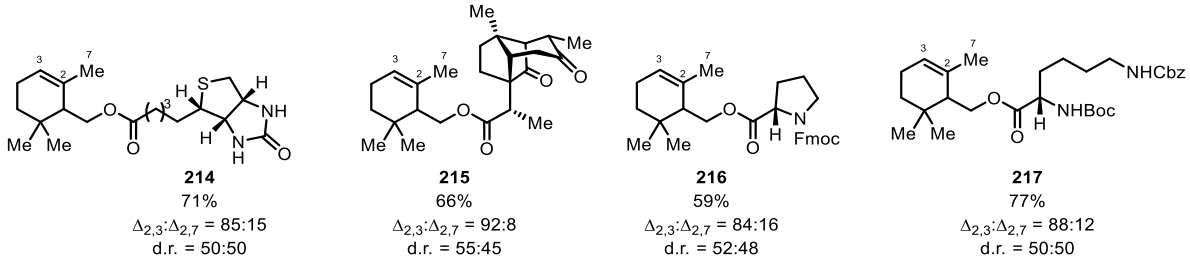

Figure 19. Geranyl esters linked to natural products and protected amino acids.

Figure 20 shows some examples for products with electron-withdrawing substituents. Cyanide **218**, malonate **219** and phthalimide **220** derivatives were isolated in good yields of 72-90%. Interestingly, *exo*-elimination was only a minor side product, with the tetrasubstituted olefin being the main product in **220**. Eucalyptol (**162**) was obtained from *α*-terpineol in 77% yield, and cyclization of lapachol gave the kinetic product *β*-lapachone (**221**) in 87% yield.[130]

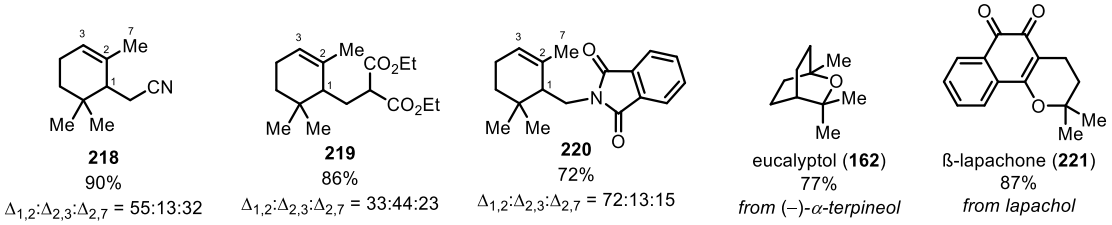

Figure 20. Cyclization of electron deficient geranyl substrates and non-geranyl substrates.

To further extend the substrate scope some neryl derivatives were subjected to the reaction conditions as well (Scheme 23). It seemed that there is no obvious difference in reactivity (except the rate enhanced as shown in Figure 10) or selectivity. **53** was produced in 90% yield with perfect diastereoselectivity, benzyl ether **207** in 94% and – like for the corresponding geranyl ether – perfect regioselection in the elimination step. The same is true for dinitrobenzoic ester **200**, which was produced with 68:32 r.r. as compared to 69:31 for the corresponding geranyl ester (c.f. Figure 18).

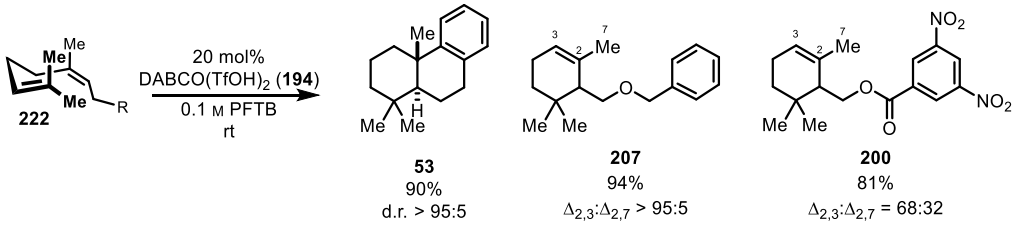

Scheme 23. Cyclization scope of neryl derivatives.

Since for all substrates with no internal terminating nucleophile the elimination product formed, we then investigated if a change in the workup procedure would allow to selectively give the *exo*-elimination product from the potentially long-lived carbocation **I** (Scheme 3). Therefore, the well-working allyl substrate **223** (Table 9, entry 1) was cyclized with the help of the DABCO bistriflate catalyst **194** and after 10 minutes subjected to crude solid KOH, basic aluminum oxide, neat NEt_3 or bulky KO*t*Bu (entries 2-5). In all cases, the $\Delta_{2,3}$ selectivity remained unchanged, hinting that proton elimination does not take place upon workup, but already during the reaction process.

Table 9. Studies on reaction termination and workup.

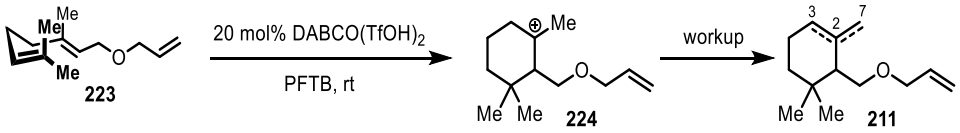

entry	workup	$\Delta_{2,3}$:$\Delta_{2,7}$[a]
1	standard[b]	> 99:1
2	addition of the crude solution to 2.0 g solid KOH pellets[c]	> 99:1
3	addition of the crude solution to basic aluminium oxide[c]	> 99:1
4	addition of the crude solution to 2.0 mL neat NEt_3	> 99:1
5	addition of the crude solution to 2.0 g solid *t*BuOK	> 99:1

[a]Ratio determined by GC-FID from the crude mixture. [b]Aqueous workup. [c]The solids were filtered off and the filtrate was partitioned between water and CH_2Cl_2.

As mentioned above, drimanes constitute an interesting structural motif in natural products and originate from protoncyclization of (*E*,*E*)-farnesyl derivatives. We were pleased to see that tetracyclic **225** was

obtained in 69% yield and with excellent diastereoselectivity (Figure 21). Farnesyl acetate (→**226**) and dimethoxybenzoate (→**227**) cyclized as well in 66% and 62% yield, respectively, with excellent elimination selectivity, albeit with a lower diastereomeric ratio of 65:35 in each case. Sclareolide (**23**) was prepared from homofarnesoic acid in 57% and a diastereomeric ratio of 75:25.

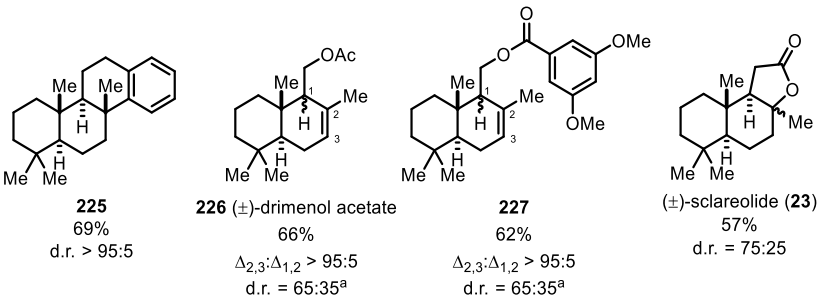

Figure 21. Substrate scope of farnesyl derivatives. [a]Determined from the crude ^{1}H-NMR spectra.

In conclusion, the presented method for the proton-induced cyclization of geranyl- and farnesyl derivatives was thoroughly investigated. A delicate interplay between the Lewis acidic properties of the fluorinated alcohol solvent PFTB and the employed Lewis base is decisive for the success of this extraordinarily mild transformation. Preliminary experiments confirm that linear polyenes adopt a more coiled form than in other solvents thus selectively protonating the more exposed terminal alkene. A wide substrate scope showed the broad applicability of this method, even tolerating acid labile groups such as *N*-Boc protected amino acids, MOM groups, epoxides, and complex natural product analogs.

3. Summary and Perspectives

Polyene cyclization reactions are one of the most complex reactions in nature, enabling the organisms to form (poly)cyclic secondary metabolites from linear polyene precursors in a complex reaction cascade.[42,52-53] Challenges include the regioselectivity of initial electrophilic attack, the diastereoselective formation of multiple stereocenters, and the controlled nucleophilic attack, all while conserving the stereochemistry of the linear alkene. This is achieved by pre-arranging the substrate inside the enzymatic pocket, thus allowing for selective reactions to occur. The basis of understanding the stereopreservation in these cyclization reactions was laid by Eschenmoser and Stork over 50 years ago in their infamous hypothesis.[1b] Therein, they rationalized the stereospecific outcome of the protoncyclization of (*trans*,*trans*)-farnesoic acid (**40**) by postulating a chair-like transition state over a boat-like transition state during the reaction.[40-41] In the following years, many chemists attempted to reproduce this biomimetic reaction by treating linear polyenes with a range of electrophiles such as proton- or halonium-sources, but often obtained only minor yields or inferior diastereoselectivities. In particular, the more challenging halonium-induced polyene cyclization has fascinated chemists for a long time, however, only just recently sufficient methods have become available to trigger this reaction in good yields and selectivities. These methods generally rely on specialized halogenating reagents or employ complex catalysts under often inconvenient reaction conditions. This is why the first goal of this thesis was to develop a biomimetic haliranium-induced polyene cyclization methodology by harnessing the unique properties of fluorinated alcohol solvents, which differ significantly from their non-fluorinated analogs. They are capable of forming distinct H-bonding networks thus generating supramolecular structures and stabilizing carbocations through their high dielectric constant.[96] Thus, they are putatively able to alter the folding of linear polyenes in solution through hydrophobic interactions.[117] We wanted to utilize the special properties of 1,1,1,3,3,3-hexafluoro-*iso*-propanol (HFIP) to mimic the enzymatic pocket in which substrate prearrangement, selective halogenation, and transition state stabilization are the key to successful and selective halocyclization reactions. The goal was to facilitate the halonium-induced polyene cyclization with standard halogen sources such as *N*-halosuccinimides in fluoroalcohols and thus mimic the way nature performs these reactions.

Starting with polyene **70** as model substrate extensive reaction optimizations were performed in the first stage of this PhD thesis to induce the desired halocyclization. Key findings were that HFIP is activating NBS via H-bonding towards the carbonyl groups, thus drastically increasing the reactivity thereby and reducing the selectivity and yield of the reaction. Employing *N*-bromomorpholine instead, and finally in situ generating this highly unstable reagent via transhalogenation of NBS to morpholine proved to be optimal and furnished tricycle **93** in 76% isolated yield and perfect diastereoselectivity (Scheme 24). To our delight, a broad substrate scope was tolerated, allowing for the halocyclization of various

electronically rich- and poor prenyl, geranyl, and even farnesyl derivatives forming two, three, and four new bonds in the reaction course. Through the modular approach of pre-mixing NBS with morpholine in HFIP simple substitution with the iodonium source NIS furnished the corresponding iodocyclized products in likewise good or even better chemical yields of up to 90% with mostly excellent diastereoselectivities of > 95:5. Even the far more challenging chlorocyclization was possible for electron-rich polyenes by adjusting the Cl^+ source to 1,3-dichloro-5,5-dimethylhydanthoin (DCDMH). Besides a broad substrate scope being evaluated, several mechanistic studies were performed in order to get a deeper understanding of the role of each component in the reaction. It was proven that NBS transfers the bromonium ion onto morpholine, and the resulting *N*-bromomorpholine is indeed deactivated by HFIP through hydrogen bonding, thus reducing the reactivity and enabling the selective formation of the desired product.

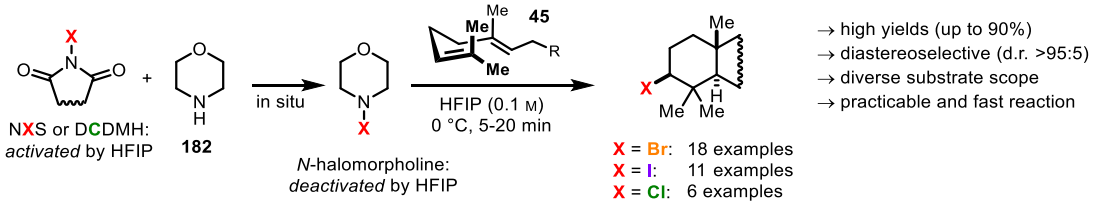

Scheme 24. Summary of the biomimetic halocyclization of polyenes.[64]

As a plethora of naturally occurring bioactive terpenoids possess the drimane core (Scheme 25) built up through proton-induced head-to-tail cyclization of farnesyl-derivatives, many efforts have been made to mimic nature's strategy in the laboratory.[2a] The simplest form to achieve the proton-induced polyene cyclization is treating the polyene with strong mineral acids, but neither yields were good due to uncontrolled side reactions, nor does this method tolerate many functional groups. Building on our previous findings for the biomimetic haliranium-induced polyene cyclization reaction in HFIP,[64] we set out to extend the concept of biomimicry towards the proton-induced cyclization. Again, we strived to harness the unique properties of fluorinated alcohol solvents to stabilize cationic intermediates, putatively pre-arrange the substrate through hydrophobic interactions, and activate the electrophile via H-bonding.

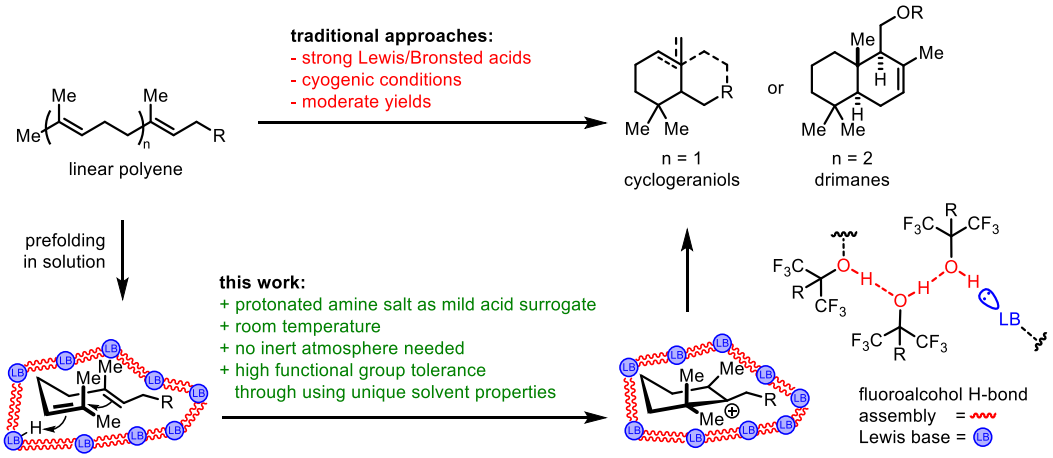

Scheme 25. Concept for the proton-induced cyclization of geranyl- and farnesyl derivatives using macromolecular H-bonding properties of fluorinated alcohol solvents.

Initial attempts with model substrate homogeranyl benzene (**70**) and strong acids, e.g. sulfuric or triflic acid in HFIP showed full conversion of the starting material, albeit with the simultaneous formation of apolar side products resulting from undesired protonation of the internal olefin. Using the weakly acidic pyridinium bromide salt **183d** as proton source increased the chemical yield to 74%, and finally switching the solvent to the more fluorinated and thus stronger acidic perfluoro-*tert*-butanol (PFTB) gave full conversion and a very clean formation of desired **53** in 96% yield without any trace of the minor diastereomer being produced. If a weaker amine base and thus stronger corresponding acid 1,4-diazabicyclo[2.2.2]octane bistriflate (DABCO(TfOH)$_2$, **194**) is used as the catalyst the yield of **53** remained unaltered at 96%, but the reaction time was reduced from one day to only 2 hours. The presented protocol convinces not only through simple experimental implementation at room temperature and without the need for an inert atmosphere, but also through successful conversion of electronically diverse substrates and an extensive functional group tolerance. Unprecedented so far, *N*-Boc-, Cbz- and Fmoc-protected amino acids with geranyl residues, as well as a geranyl functionalized epoxide and even the highly acid labile MOM-group were tolerated under these reaction conditions.

As it is postulated that the surface area of polyenes decreases due to hydrophobic interactions with the fluorinated solvents[64,117] we finally set out to experimentally investigate this claim. 1D-^{1}H-NOESY studies revealed that a visible spatial correlation between the arene protons in **70** and all methyl groups is indeed only visible in PFTB, whereas in other standard solvents this interaction is absent. This strongly hints towards a more coiled structure in solution as compared to other solvents, such as MeOH, $CHCl_3$, or cyclohexane. The preferential activation of the terminal alkene was likewise demonstrated through titration experiments, again showing the superiority of PFTB as compared to other solvents in this reaction.

Experimenting with different protonated Lewis bases revealed that morpholinium, pyridinium, and protonated DABCO are able to yield the desired model product **53** in excellent yield and diastereoselectivity. The rate, however, increased with rising acid strength of the protonated counterion and decreased basicity of the Lewis base catalyst. Compared to the very slow cyclization of **70** in pure PFTB, DABCO bistriflate (**194**) accelerated the conversion of **70** by a factor of 205. This highly efficient ensemble of Lewis acid/Lewis base made even the efficient proton cyclization of electron-poor substrates possible. In total 37 substrates were successfully converted to a total of 34 unique products bearing cyclogeranyl, drimane, or cycloprenyl motifs. It was found during the course of this work that not only the (*E*)-configured alkene of the geranyl motif was able to smoothly undergo this cyclization, but in likewise good yields and selectivities also the (*Z*)-configured neryl moiety yielded the same *trans* products in unaltered selectivity and yield. These results are in line with the recorded kinetic measurements of the conversion of either homogeranyl benzene (**70**) and homonerylbenzene (**192**), indicating a stepwise process with the intermediate formation of the three monocyclic elimination products, which are then selectively further converted into the desired *trans*-decalin polycyclic product **53**. This observation was further supported by deuteration experiments, which show multiple protonation and elimination steps during the reaction.

In both presented biomimetic methods for the halonium- and proton-induced polyene cyclizations the roles of the fluoroalcohols HFIP and PFTB, respectively, have been thoroughly investigated. Not only help they pre-arrange the substrate into a more reactive chair-like transition state, but they also interact very distinctly with the added Lewis base, creating a precise balance between enhanced reactivity and selectivity necessary to allow for polyene cyclizations to occur under these conditions.

Besides the undeniable synthetic benefit of the presented method enantioselective version thereof would be of great interest. Established methods rely on a chiral catalyst – in the case of proton- or haliranium-induced cyclizations a substituted SPINOL motif – for enantioinduction.[59,72,78] The generic approach in these methods is the synthesis and examination of more and more confined catalysts specifically tailed to the desired reaction. Nature utilizes chiral amino acid building blocks to achieve cyclization reactions highly selectively. It would be desirable to achieve asymmetric transformations with the help of an enantioselective environment induced by the solvent, thus exponentially extending the possible applications to a plethora of reactions. First attempts to utilize chiral solvents by Seebach and Oei in 1975 with *ee*s of up to 24%[131] remained unmatched for decades, resulting in the general conception, that "*asymmetric induction caused by chiral solvents is usually rather small*".[132] However, widely accepted paradigms in the chemical community often stand strong – until proven wrong. Striking examples thereof are the asymmetric Baylis-Hillman reactions of **227** with methacrylate (**228**) in ionic liquid (**229**, IL) giving alcohol **230** in up to 44% *ee* (Scheme 26a)[133] and the aza-Baylis-Hillman

reaction of imino tosylate **231** with methyl vinyl ketone (**232**) and IL **233** furnishing the addition product **234** in up to 39% yield and up to 84% *ee* (Scheme 26b).[134] The sole source of chiral induction in both cases stemmed from the ionic liquids used as the solvent, wherein **229** the cation is the chiral inducer and in **233** the anion.

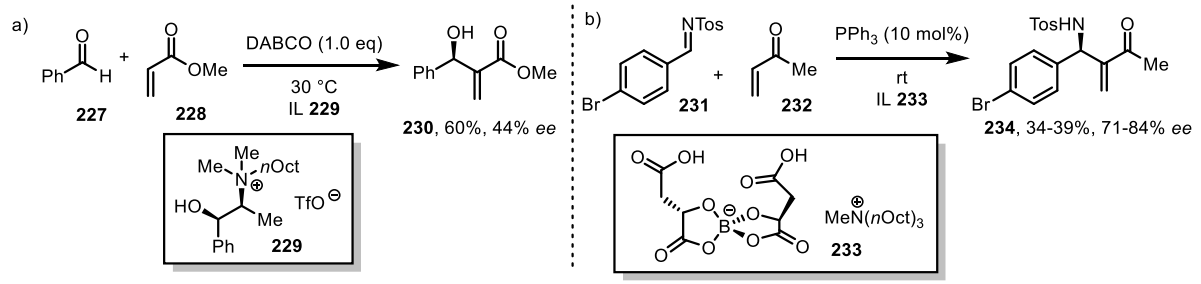

Scheme 26. (a) Asymmetric Baylis-Hillman reaction[133] and (b) aza-Baylis-Hillman reaction[134] through induction by chiral ionic liquid **229** and **233**.

This leads to the question if other known reactions could be rendered enantioselectively when a chiral solvent is used. Combining the unique properties of fluorinated alcohol solvents with chiral induction through the solvent itself may have a staggering influence on the conformation and aggregation of the hydrogen network. Possible targets for a "chiral HFIP" **235** and **236**, which may be able to introduce asymmetry during the reaction are shown in Figure 22 with the former even being commercially available.[135] On the other hand, chiral Lewis bases may be utilized to introduce enantioselectivity. Literature known C_2 symmetric morpholine **237**[136] or pyBOX ligands **238**[137] are readily available, and a chiral version of Selectfluor (**239**-F) bearing a DABCO scaffold was successfully used in enantioselective fluorinations by the Gouverneur group.[138] Those could then replace the achiral Lewis bases described in this thesis and act as a chiral catalyst or reagent. Either approach could result in novel strategies for enantioselective transformations presented herein.

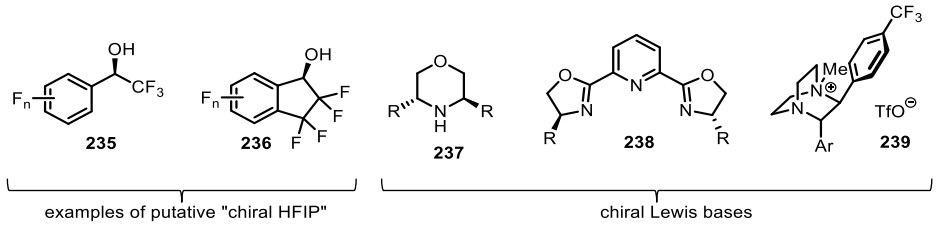

Figure 22. Chiral fluoro alcohols **235** and **236** and chiral Lewis bases **237**-**239**.

Even though methods for selective halo- or protoncyclization are available, none of them conceptually mimic nature's unmatched selectivity. With this work valuable novel insights were collected into the mode of action and activation for the cyclization of (poly)isoprene substrates in highly fluorinated alcohol solvents, resulting in highly selective and broad methodologies to access cyclic terpene substrates and building blocks. Further developments into chiral amplification using defined Lewis acid/Lewis base synergies could lead to unprecedented possibilities in organic synthesis.

4. Zusammenfassung und Ausblick

Polyenzyklisierungsreaktionen sind eine der komplexesten Reaktionen in der Natur und ermöglichen es den Organismen, aus linearen Polyenen zyklische Sekundärmetaboliten in einer komplexen Reaktionskaskade zu bilden.[42,52-53] Zu den Herausforderungen gehört die Regioselektivität des anfänglichen elektrophilen Angriffs, diastereoselektive Bildung mehrerer Stereozentren und kontrollierter nukleophiler Angriff unter Beibehaltung der Stereochemie des linearen Alkens. Dies wird erreicht, indem das Substrat in der Enzymtasche vorab angeordnet wird, wodurch selektive Reaktionen stattfinden können. Die Grundlage für das Verständnis der Stereokonservierung in diesen Zyklisierungsreaktionen wurde vor über 50 Jahren von Eschenmoser und Stork in ihrer Hypothese gelegt.[1b] Darin klärten sie das stereospezifische Ergebnis der Protonenzyklisierung von (*trans*,*trans*)-Farnesolsäure (**40**) auf. In den folgenden Jahren versuchten viele Chemiker, diese biomimetische Reaktion durch Behandlung linearer Polyene mit einer Reihe von Elektrophilen, wie Protonen oder Haloniumquellen, zu reproduzieren, erhielten aber oft nur geringe Ausbeuten oder schlechte Diastereoselektivitäten. Insbesondere die schwierigere Halonium-induzierte Polyenzyklisierung hat Chemiker schon lange fasziniert, doch erst seit kurzem stehen ausreichende Methoden zur Verfügung, um diese Reaktion in guten Ausbeuten und Selektivitäten durchzuführen. Diese Verfahren beruhen im Allgemeinen auf speziellen Halogenierungsreagenzien oder verwenden komplexe Katalysatoren unter oft umständlichen Reaktionsbedingungen. Aus diesem Grund bestand das erste Ziel dieser Arbeit darin, eine biomimetische Haliranium-induzierte Polyenzyklisierungsmethode zu entwickeln, indem die einzigartigen Eigenschaften fluorierter Alkohollösungsmittel genutzt werden, die sich erheblich von ihren nicht fluorierten Analoga unterscheiden. Sie sind in der Lage, unterschiedliche H-Brückennetzwerke zu bilden, wodurch supramolekulare Strukturen gebildet werden, welche wiederum durch ihre hohe Dielektrizitätskonstante Carbokationen stabilisieren können.[96] Sie sind daher vermutlich in der Lage, lineare Polyene in Lösung durch hydrophobe Wechselwirkungen in eine Sesselkonformation vorzufalten.[117] Wir wollten die besonderen Eigenschaften von 1,1,1,3,3,3-Hexafluorisopropanol (HFIP) nutzen, um die enzymatische Tasche nachzuahmen, in der Substratfaltung, selektive Halogenierung und Stabilisierung des Übergangszustands der Schlüssel zum Erfolg von selektiven Halogenzyklisierungsreaktionen sind. Ziel war es, die Halonium-induzierte Polyenzyklisierung mit Standardhalogenquellen, wie *N*-Halosuccinimiden in Fluoralkoholen, zu optimieren, und so die Art nachzuahmen, mit der die Natur diese Reaktionen durchführt.

Beginnend mit Polyen **70** als Modellsubstrat wurden in der ersten Stufe dieser Dissertation eine umfangreiche Reaktionsoptimierung durchgeführt, um das gewünschte Halozyklisierungsprodukt zu erhalten. Die wichtigsten Ergebnisse waren, dass HFIP das NBS über H-Brücken zu den Carbonylgruppen aktiviert, wodurch die Reaktivität drastisch erhöht, und die Selektivität und Ausbeute

der Reaktion verringert wird. Die Verwendung von *N*-Brommorpholin und schließlich die in-situ-Erzeugung dieses hochinstabilen Reagenzes durch Transhalogenierung von NBS zu Morpholin erwies sich als optimal und lieferte den Trizyklus **93** in 76% isolierter Ausbeute und perfekter Diastereoselektivität (Schema 1). Es wurde ein breites Substratspektrum toleriert, das die Halozyklisierung verschiedener elektronenreicher und -armer Prenyl-, Geranyl- und sogar Farnesylderivate ermöglichte, wobei im Reaktionsverlauf entsprechend zwei, drei oder vier neue Bindungen gebildet wurden.

Ersetzt man in dem modularen Ansatz das NBS durch die Iodoniumquelle NIS, so erhält man die entsprechenden iodozyklisierten Produkte in ebenfalls guten oder sogar besseren Ausbeuten von bis zu 90% mit meist hervorragenden Diastereoselektivitäten von > 95:5. Sogar die weitaus schwierigere Chlorzyklisierung war für elektronenreiche Polyene möglich, indem die Cl^+-Quelle auf 1,3-Dichlor-5,5-dimethylhydanthoin (DCDMH) geändert wurde. Neben der Erweiterung des breiten Substratspektrums wurden mehrere mechanistische Studien durchgeführt, um ein tieferes Verständnis der Rolle jeglicher Komponente in der Reaktion zu erhalten. Es wurde nachgewiesen, dass NBS das Bromiumion auf Morpholin überträgt, und das resultierende *N*-Bromomorpholin tatsächlich von HFIP durch Wasserstoffbrückenbindung deaktiviert wird, wodurch die Reaktivität verringert, und so die selektive Bildung des gewünschten Produkts ermöglicht wird.

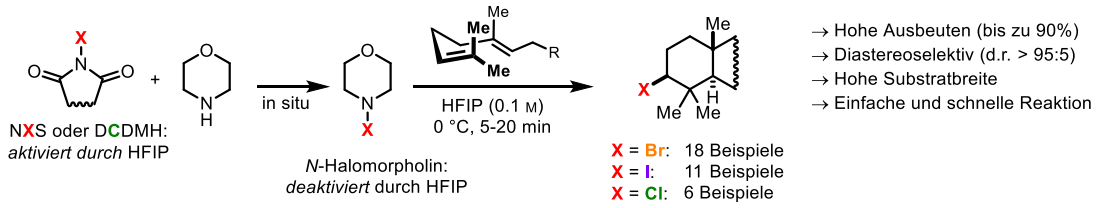

Schema 1. Zusammenfassung der biomimetischen Halozyklisierung von Polyenen.[64]

Da eine Vielzahl natürlich vorkommender bioaktiver Terpenoide das Drimanmotiv (Schema 2) besitzt, welches durch protoneninduzierte Kopf-zu-Schwanz-Zyklisierung von Farnesyl-Derivaten aufgebaut wird, wurden bereits viele Anstrengungen unternommen, um die Strategie der Natur im Labor nachzuahmen.[2a] Die einfachste Form, um protoneninduzierte Polyenzyklisierungen zu ermöglichen, ist die Behandlung des Polyens mit starken anorganischen Säuren. Jedoch waren weder die Ausbeuten aufgrund unkontrollierter Nebenreaktionen gut, noch toleriert diese Methode viele funktionelle Gruppen. Aufbauend auf unseren früheren Erkenntnissen zur biomimetischen Haliranium-induzierten Polyenzyklisierungsreaktion in HFIP[64] haben wir es uns zum Ziel gesetzt, das Konzept der Biomimetik auf die protoneninduzierte Zyklisierung auszudehnen. Wir haben uns erneut bemüht, die einzigartigen Eigenschaften fluorierter Alkohollösungsmittel zu nutzen, um kationische Zwischenprodukte zu stabilisieren, das Substrat durch hydrophobe Wechselwirkungen vorzufalten und das Elektrophil über H-Brücken zu aktivieren.

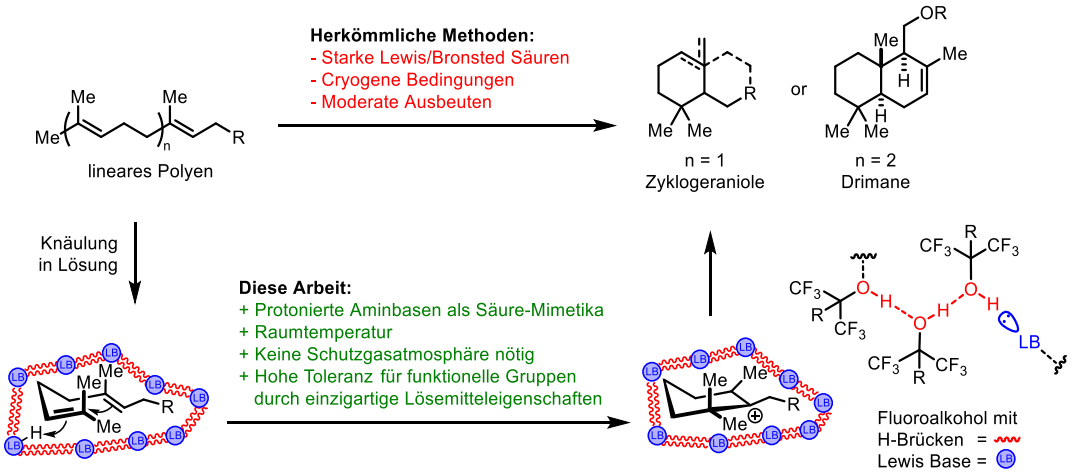

Schema 2. Konzept für die Protonen-induzierte Zyklisierung von Geranyl- und Farnesylderivaten mithilfe von Fluoralkoholen aufgespannten makromolekularen Wasserstoffbrückenbindungsnetzwerken.

Erste Versuche mit Modellsubstrat Homogeranylbenzol (**70**) und starken Säuren, z.B Schwefel- oder Trifluoromethansulfonsäure, in HFIP zeigten eine vollständige Umsetzung des Startmaterials, jedoch bildeten sich eine Vielzahl an unpolaren Nebenprodukten durch die Protonierung des internen Alkens. Die Verwendung des schwach sauren Pyridiniumbromidsalzes **183d** als Protonenquelle erhöhte die Ausbeute auf 74%, und schließlich führte die Umstellung des Lösungsmittels auf das höher fluorierte und damit stärker saure Perfluor-*tert*-butanol (PFTB) zu vollständigem Umsatz und einer sehr sauberen Bildung des gewünschten Produktes **53** in 96% Ausbeute, ohne Spuren des entsprechenden Diastereomers. Wenn eine schwächere Aminbase und damit eine stärkere korrespondierende Säure 1,4-Diazabicyclo[2.2.2] oktan bistriflat (DABCO(TfOH)$_2$, **194**) als Katalysator verwendet wird, bleibt die Ausbeute unverändert bei 96%, aber die Reaktionszeit wurde von einem Tag auf nur 2 Stunden verringert. Das vorgestellte Protokoll überzeugt nicht nur durch einfache experimentelle Durchführung bei Raumtemperatur und ohne die Notwendigkeit einer Schutzgasatmosphäre, sondern auch durch die erfolgreiche Umwandlung elektronisch diverser Substrate und eine umfassende Toleranz gegenüber funktionellen Gruppen. Bisher beispiellos konnten so *N*-Boc-, Cbz- und Fmoc-geschützte Aminosäuren mit Geranylresten sowie ein geranyl-funktionalisiertes Epoxid und sogar die säurelabile MOM-Gruppe unter diesen Reaktionsbedingungen toleriert werden.

Da postuliert wird, dass die Oberfläche von Polyenen aufgrund hydrophober Wechselwirkungen mit den fluorierten Lösungsmitteln verringert wird,[64,117] haben wir uns schließlich vorgenommen, diese Behauptung experimentell zu untersuchen. 1D-^{1}H-NOESY-Studien zeigten, dass eine sichtbare räumliche Korrelation zwischen den aromatischen Protonen in **70** und allen Methylgruppen tatsächlich nur in PFTB sichtbar ist, während in anderen Standardlösungsmitteln diese Wechselwirkung fehlt. Dies deutet stark auf eine stärker gefaltete Struktur in PFTB Lösung im Vergleich zu anderen Lösungsmitteln, wie MeOH, $CHCl_3$ oder Cyclohexan, hin. Die bevorzugte Aktivierung des terminalen Alkens wurde

ebenfalls durch Titrationsexperimente bewiesen, was wiederum die Überlegenheit von PFTB im Vergleich zu anderen Lösungsmitteln in dieser Reaktion zeigte.

Experimente mit verschiedenen protonierten Lewis-Basen zeigten, dass Morpholinium, Pyridinium und protoniertes DABCO das gewünschte Modellsubstrat in ausgezeichneter Ausbeute und Diastereoselektivität liefern können. Die Geschwindigkeit nahm jedoch mit zunehmender Säurestärke des protonierten Gegenions und abnehmender Basizität des Lewis-Base-Katalysators zu. Im Vergleich zur sehr langsamen Zyklisierung von **70** in reinem PFTB, beschleunigte DABCO-Bistriflat (**194**) die Umwandlung von **70** um den Faktor 205. Dieses hocheffiziente Ensemble aus Lewis-Säure/Lewis-Base ermöglichte sogar die effiziente Protonenzyklisierung elektronenarmer Substrate. Insgesamt 37 Substrate wurden erfolgreich in insgesamt 34 Produkte mit Cyclogeranyl-, Driman- oder Cycloprenylmotiven umgewandelt. Im Verlauf dieser Arbeit wurde festgestellt, dass nicht nur das (*E*)-konfigurierte Alken des Geranylmotivs diese Zyklisierung reibungslos durchlaufen konnte, sondern in ebenfalls guten Ausbeuten und Selektivitäten auch die (*Z*)-konfigurierte Neryleinheit das gleiche *trans*-Produkt **53** in unverändert hoher Selektivität und Ausbeute ergab. Diese Ergebnisse stimmten mit den aufgezeichneten kinetischen Messungen der Umwandlung von Homogeranylbenzol (**70**) und Homonerylbenzol (**192**) überein, was auf einen schrittweisen Prozess mit der Bildung der drei monocyclischen Eliminierungsprodukte hinweist, die dann selektiv weiter in das gewünschte *trans*-Decalin-Produkt **53** umgewandelt werden. Diese Beobachtung wurde weiter durch Deuterierungs-experimente gestützt, die mehrere Protonierungs- und Eliminierungsschritte während der Reaktion zeigten.

In beiden vorgestellten biomimetischen Methoden für die Halonium- und Protonen-induzierten Polyenzyklisierungen wurden die Rolle der Fluoralkohole HFIP bzw. PFTB gründlich untersucht. Die Lösemittel helfen nicht nur dabei, das Substrat in einen reaktiveren sesselartigen Übergangszustand zu bringen, sondern interagieren auch sehr deutlich mit der zugesetzten Lewis-Base, wodurch ein präzises Gleichgewicht zwischen erhöhter Reaktivität und Selektivität eingestellt wird, das erforderlich ist, um Polyenzyklisierungen unter diesen überaus milden Bedingungen zu ermöglichen.

Neben dem unbestreitbaren synthetischen Nutzen der vorgestellten Methode wäre eine enantioselektive Version davon von großem Interesse. Etablierte Methoden beruhen auf einem chiralen Katalysator – bei Protonen- oder Halonium-induzierten Cyclisierungen ein substituiertes SPINOL-Motiv – für die Enantioinduktion.[59,72,78] Der generische Ansatz bei diesen Methoden ist die Synthese und Untersuchung von Katalysatoren mit erhöhter struktureller Komplexität, die speziell auf die gewünschte Reaktion abgestimmt sind. Die Natur nutzt chirale Aminosäurebausteine, um hochselektiv Zyklisierungsreaktionen zu ermöglichen. Es wäre wünschenswert, asymmetrische Transformationen mit Hilfe einer durch das Lösungsmittel induzierten enantioselektiven Umgebung zu erreichen, wodurch

die möglichen Anwendungen auf eine Vielzahl von Reaktionen ausgedehnt werden könnten. Die ersten Versuche von Seebach und Oei im Jahr 1975, chirale Lösungsmittel für die Enantioinduktion zu verwenden, lieferten Produkte mit einem *ee* von bis zu 24%.[131] Diese Ergebnisse blieben jahrzehntelang unerreicht, was zu der allgemeinen Auffassung führte, dass „die durch chirale Lösungsmittel verursachte asymmetrische Induktion normalerweise eher gering ist“.[132] Weithin akzeptierte Paradigmen in der chemischen Gemeinschaft halten sich jedoch oft hartnäckig – bis sich schließlich herausstellt, dass sie falsch sind. Markante Beispiele hierfür sind die asymmetrischen Baylis-Hillman-Reaktionen von **227** mit Methacrylat (**228**) in der ionischer Flüssigkeit (IL) **229**, die Alkohol **230** in bis zu 44% *ee* lieferten (Schema 3a),[133] und die Aza-Baylis-Hillman-Reaktion von Imino-Tosylat **231** mit Methylvinylketon (**232**) und IL **233** liefert das Additionsprodukt **234** in bis zu 39% Ausbeute und bis zu 84% *ee* (Schema 3b).[134] Die einzige Quelle der chiralen Induktion waren in beiden Fällen die als Lösungsmittel verwendeten ionischen Flüssigkeiten, wobei in **229** das Kation und in **233** das Anion der chirale Induktor ist.

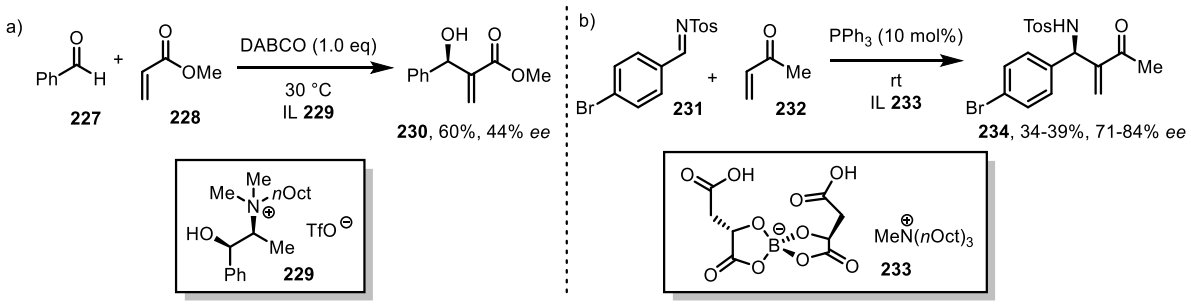

Schema 3. (a) Asymmetrische Baylis-Hillman Reaktion[133] und (b) aza-Baylis-Hillman Reaktion[134] ermöglicht durch IL basierte asymmetrische Induktion von **229** und **233**.

Dies führt zu der Frage, ob andere bekannte Reaktionen bei Verwendung eines chiralen Lösungsmittels enantioselektiv ablaufen könnten. Die Kombination der einzigartigen Eigenschaften fluorierter Alkohollösungsmittel mit der chiralen Induktion durch das Lösungsmittel selbst kann einen erstaunlichen Einfluss auf die Konformation und Aggregation des Wasserstoffnetzwerks haben. Mögliche Strukturen für ein „chirales HFIP“ **235** und **236**, die möglicherweise während der Reaktion Asymmetrie induzieren können, sind in Abbildung 1 dargestellt, wobei ersteres sogar kommerziell erhältlich ist.[135] Andererseits können chirale Lewis-Basen verwendet werden, um Enantioselektivität einzuführen. Das literaturbekannte C_2-symmetrische Morpholin **237**[136] oder pyBOX-Liganden **238**[137] sind leicht zugänglich, und eine chirale Version von Selectfluor (**239**-F) mit einem DABCO-Gerüst wurde von der Gouverneur-Gruppe erfolgreich bei enantioselektiven Fluorierungen eingesetzt.[138] Diese könnten dann die in dieser Arbeit beschriebenen achiralen Lewis-Basen ersetzen, und als chiraler Katalysator oder Reagenz wirken. Jeder Ansatz könnte zu neuen Strategien für enantioselektive Transformationen führen, die hier vorgestellt werden.

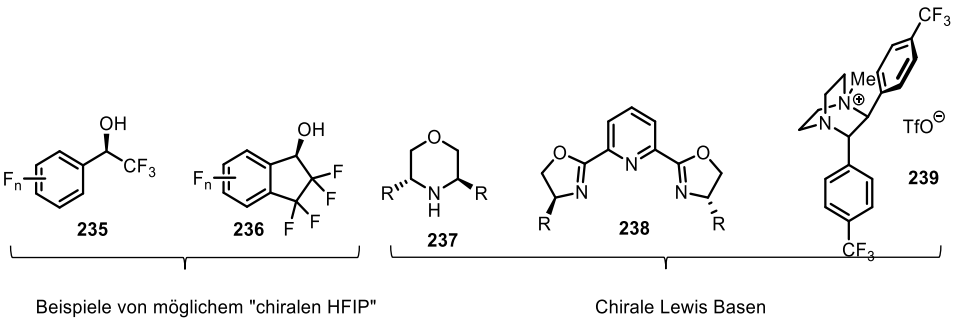

Abbildung 1. Mögliche chirale Fluoralkohole **235** und **236** und chirale Lewis Basen **237**-**239**.

Obwohl Methoden zur selektiven Halo- oder Protoncyclisierung verfügbar sind, ahmt keine von ihnen konzeptionell die unübertroffene Selektivität der Natur nach. Mit dieser Arbeit wurden wertvolle neue Erkenntnisse über die Wirkungsweise und Aktivierung der Zyklisierung von (Poly)isoprensubstraten in fluorierten Alkohollösungsmitteln gewonnen, was zu hochselektiven Methoden für den Zugang zu cyclischen Terpensubstraten und Bausteinen führte. Weitere Entwicklungen in der chiralen Amplifikation unter Verwendung definierter Lewis-Säure/Lewis-Base-Synergien könnten zu beispiellosen neuen Möglichkeiten in der organischen Synthese führen.

III. Experimental Section

1. General Information

Solvents used in reactions were p.A. grade. Solvents for chromatography were technical grade and distilled prior to use. Anhydrous dichloromethane, diethylether, and THF were obtained from a MBraun MB-SPS 800 solvent purification system. Other dry solvents were obtained from Fluka and Acros in the highest purity available and used without further purification. 1,1,1,3,3,3-hexafluoroisopropanol (HFIP) and nonafluro-*tert*-butanol (PFTB) were purchased from Fluorochem with a purity >99%. Reagents were purchased at the highest commercial quality and used without further purification. Yields refer to chromatographically and spectroscopically (^{1}H NMR) homogeneous material unless otherwise stated. Reactions were monitored by thin-layer chromatography (TLC) carried out on Merck silica gel aluminum plates with F-254 indicator using UV light as the visualizing agent (UV), basic potassium permanganate solution ($KMnO_4$), ceric ammonium molybdate (CAM), and heat as developing agents, or by GC-FID or GC-MS where applicable. Silica gel Merck 60 (particle size 40 – 60 µm) was used for flash column chromatography. n-Hexane refers to HPLC grade solvent (Fischer), whereas hexanes refer to distilled technical hexane fractions. Solvent mixtures are understood as volume/volume. NMR spectra were recorded on Bruker AV300, Bruker AV400, Bruker AV500, or Bruker AV500-cryo spectrometers. The spectra were calibrated using signals of residual undeuterated solvent as an internal reference ($CDCl_3$ @ 7.26 ppm, $CDCl_3$ @ 77.16 ppm ^{13}C NMR). The following abbreviations (or combinations thereof) were used to explain the multiplicities: s = singlet, d = doublet, dd = doublet of doublets, t = triplet, dt = doublet of triplets, q = quartet, p = pentet, quint = quintet (with 1:2:3:2:1 intensity), hept = heptet, m = multiplet, br = broad. Melting points were measured on a Büchi 510 and are not calibrated. IR spectra were recorded on a JASCO FT-IR-4100 (ATR) and are reported in terms of frequency of absorption (cm^{-1}). Mass spectra were conducted on a Finnigan MAT SSQ 7000 (MS-EI, 70 eV; CI, 100 eV), or a Thermo Scientific LTQ-FT ultra and ThermoFisher Scientific LTQ Orbitrap XL spectrometer (ESI HRMS). The following method was used for GC separation: 60 °C 3 min, 15 °C/min → 250 °C, 250 °C 5 min.

2. Preparation of Deuterated PFTB and py-DBr (183d-d_1)

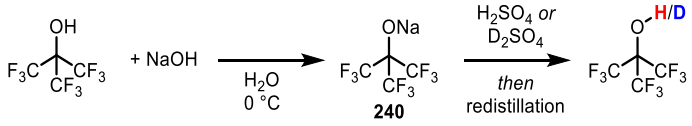

11.2 g PFTB (47.7 mmol, 1.25 eq) were carefully added to a flask submerged in an ice bath containing 15 mL H_2O and 1.52 g NaOH (38.1 mmol, 1.0 eq) while stirring. Upon complete dissolution, the volatiles were removed under high vacuum, 500 µL PFTB added, stirred for 1 minute and the volatiles again removed under high vacuum to dryness affording 9.31 g (24.0 mmol, 63%) of a white, subliming powder of PFTB sodium salt **240**.

2.50 g PFTB sodium salt (**240**, 9.69 mmol, 1.0 eq) were slowly added to 1.5 mL of either concentrated sulfuric acid or D_2SO_4 (1.86 g, 29.1 mmol, 3.0 eq) at rt. Reduced pressure was applied via a neoprene tubing leading to a –78 °C cooled flask collecting the volatiles. Redistillation from rt to –78 °C afforded 1.2 mL of PFTB-OH and 1.1 mL PFTB-OD, respectively. These solvents were applied in the KIE determination.

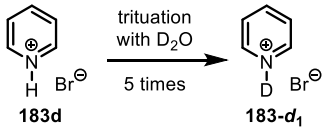

500 mg Pyridinium bromide (**183d**, 313 µmol) were dissolved in 2 mL of D_2O, stirred for 1 minute and the solvent was removed under reduced pressure with gentle heating. This procedure was repeated 5 times to afford 502 mg pyridine deuterobromide **183d**-d_1 (312 µmol, 99%) as a colorless solid.

IR (neat) $\tilde{\nu}_{max}$ = 2135, 1477, 1304, 1188, 1151, 1053, 989, 925, 799, 756, 684 cm^{-1}.

The spectroscopic data are in accordance to those reported in the literature.[139]

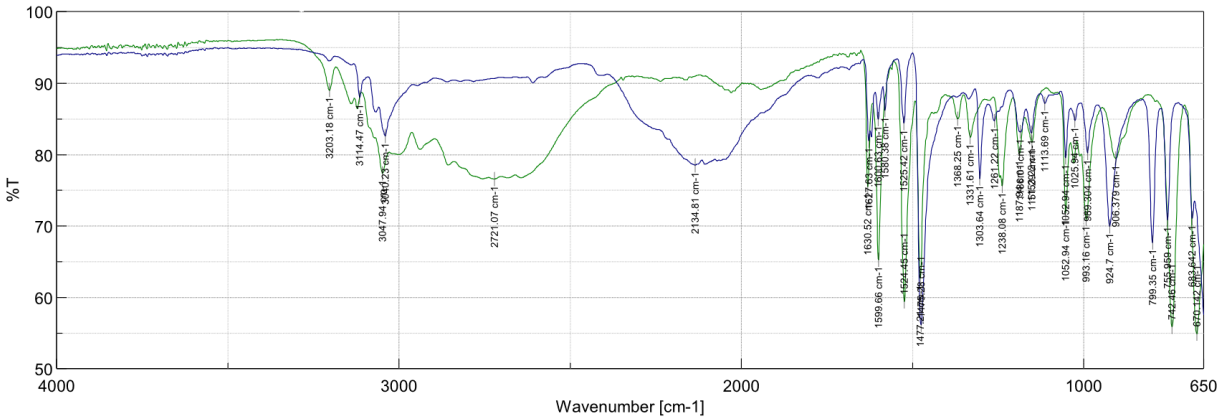

Figure 23. Overlaid IR spectra (neat) of py-HBr (**183d**, green) and py-DBr (**183d**-d_1, blue).

3. 1D-^{1}H-NOESY Measurements of 70

12.5 mg homogeranyl benzene (**70**, 55.0 µmol) were dissolved in 0.55 mL (0.1 M) solvent and directly subjected to 1D-^{1}H-NOESY measurements. The aromatic protons were selectively excited with 100 ± 10 Hz. Interactions with Me_a and Me_b were only observed on the NMR timescale in PFTB or $CDCl_3$/PFTB (1:1).

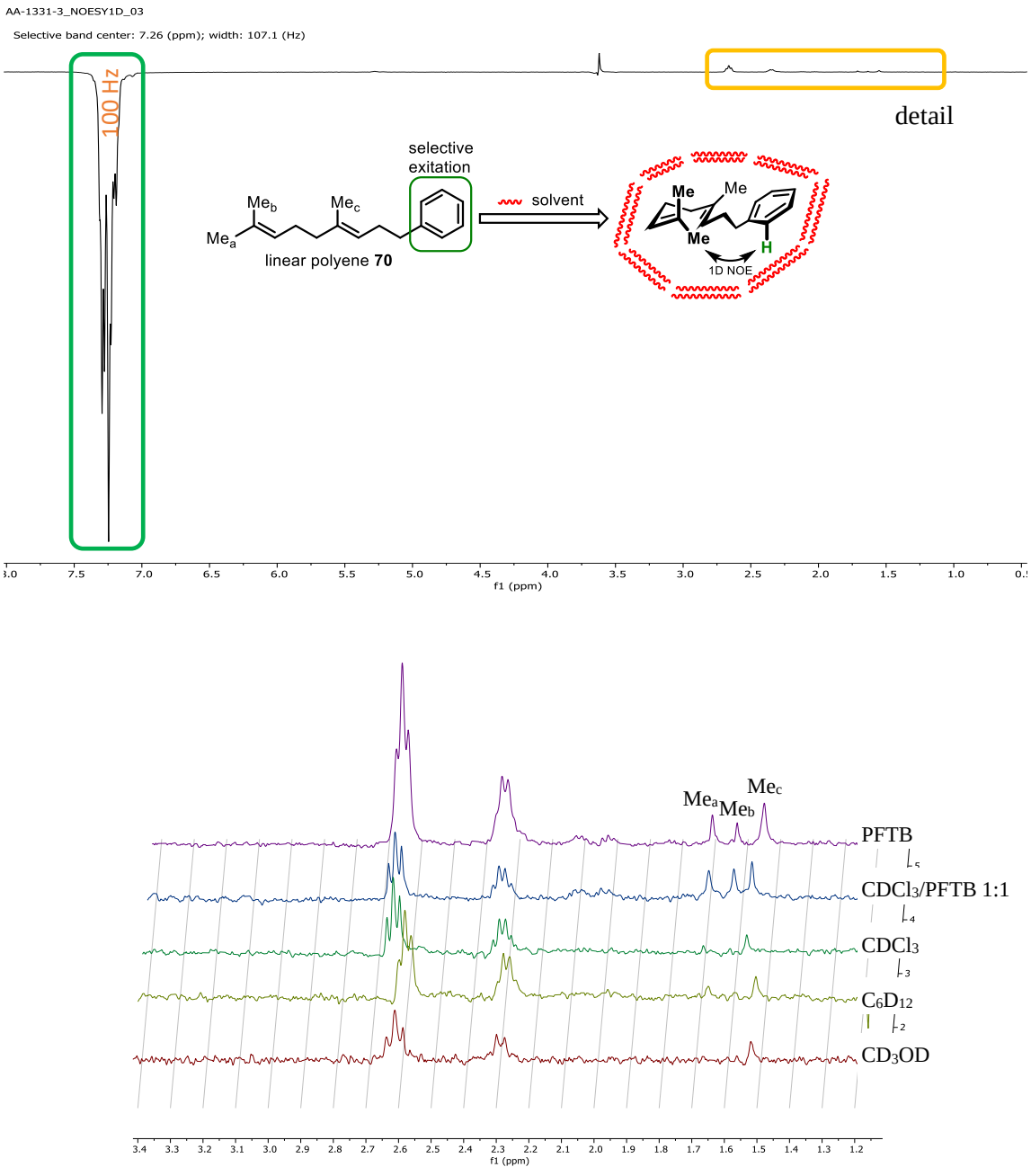

Figure 24. Top: 1D-^{1}H-NOESY of **70** in PFTB. Positive signals show interactions of the protons through space. Bottom: Stacked 1D-^{1}H-NOESY of 0.1 M **70** in (1) CD_3OD, (2) C_6D_{12}, (3) $CDCl_3$, (4) $CDCl_3$/PFTB 1:1, (5) PFTB. Where PFTB is used as a solvent a more rigid conformation of the linear polyene is assumed, making the adjacent methylene groups more visible on the NMR timescale. Coupling of the arene protons with the terminal methyl groups is indicative for folding in fluorinated alcohol solvent.

4. NMR Titration of 70 in Different Solvents

12.6 mg **70** (55.0 µmol) was dissolved in 550 µL (0.1 M) of the corresponding solvent or solvent mixture with $CDCl_3$ and a ^{13}C-NMR was spectrum recorded. In the *tert*-butanol/$CDCl_3$ and toluene/$CDCl_3$ titrations all signals, especially the ones of the olefin at *C*2 and *C*6, shifted upfield, and with $CDCl_3$/PFTB all shifts except the methyl groups moved downfield. The highest change in shifts was observed at *C*2, suggesting that this position is the most activated and hence most reactive in PFTB.

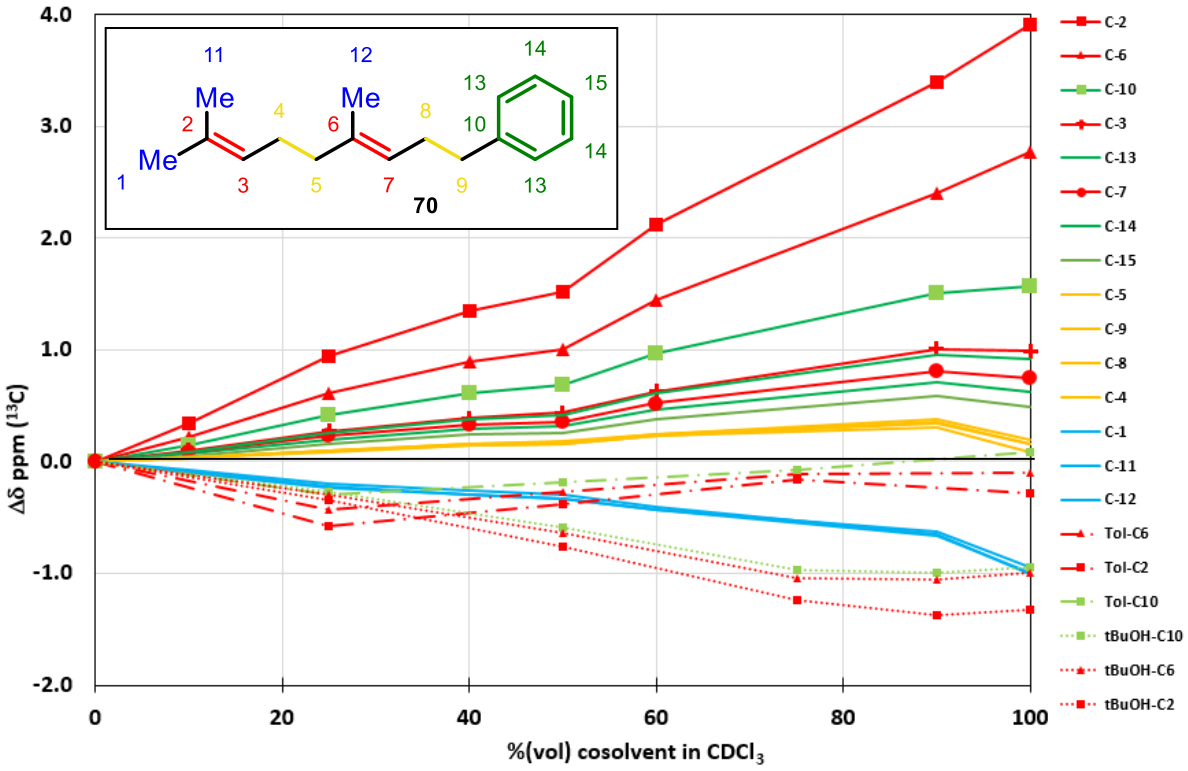

Figure 25. Chemical shift dependence of **70** (^{13}C NMR) in different solvents as mixtures with $CDCl_3$.

5. Preparation of DABCO(TfOH)$_2$ (194)

2.00 g 1,4-diazabicyclo[2.2.2]octane (DABCO, 17.8 mmol, 1.0 eq) were dissolved in 40 mL abs. CH_2Cl_2. At 0 °C, 3.31 mL trifluoromethanesulfonic acid (5.61 mL, 37.4 mmol, 2.1 eq) were added dropwise. The mixture was allowed to stir for 30 min at rt and then the volatiles removed under reduced pressure. The crude product was triturated with abs. isopropanol twice and dried under high vacuum to give 6.06 g **194** (14.7 mmol, 83%) as a colorless solid.

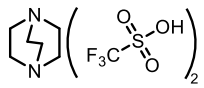

194

m.p. 320 °C (dec., *i*PrOH); **^{1}H NMR** (400 MHz, DMSO-d_6) δ 3.54 (s, 12H); **^{13}C NMR** (101 MHz, DMSO-d_6) δ 120.7 (q, J = 322.2 Hz, 2C), 42.95 (6C); **^{19}F NMR** (377 MHz, DMSO-d_6) δ -77.75 ppm; **IR** (KBr) $\tilde{\nu}_{max}$ = 3450, 1266, 1178, 1038, 648, 521cm^{-1}.

6. General Cyclization Procedure

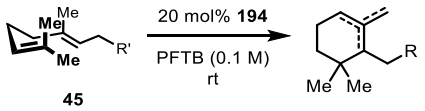

45

The corresponding starting material was dissolved in 0.1 M PFTB at rt under air in a 4 mL screw cap vial with a magnetic stir bar. 20 mol% of DABCO(TfOH)$_2$ **194** were added and the mixture stirred until completion (GC or TLC). Then, 2 mL chloroform were added to terminate the reaction and the solvent was removed under reduced pressure. The crude mixture was purified by column chromatography on silica gel to obtain the products.

7. Physical and Spectroscopic Data of Prepared Compounds

1,1,4a-Trimethyl-1,2,3,4,4a,9,10,10a-octahydrophenanthrene (**53**), prepared from **70** (22.8 mg, 100 µmol): 21.4 mg, 93.8 µmol, 94% and from **192** (22.8 mg, 100 µmol): 20.5 mg, 89.9 µmol, 90%; colorless oil.

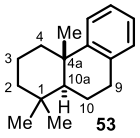

TLC: R_f = 0.60 (silica gel, hexanes) [CAM]; **^{1}H NMR** (400 MHz, $CDCl_3$) δ 7.29 – 7.26 (m, 1H), 7.16 – 7.02 (m, 3H), 3.00 – 2.81 (m, 2H), 2.30 (dtd, *J* = 12.9, 3.5, 1.6 Hz, 1H), 1.94 – 1.86 (m, 1H), 1.81 – 1.68 (m, 2H), 1.62 (dt, *J* = 14.0, 3.6 Hz, 1H), 1.50 (ddt, *J* = 13.3, 3.6, 1.9 Hz, 1H), 1.46 – 1.32 (m, 2H), 1.25 (dd, *J* = 13.5, 4.2 Hz, 1H), 1.20 (s, 3H), 0.97 (s, 3H), 0.95 (s, 3H) ppm; **^{13}C NMR** (101 MHz, $CDCl_3$) δ 150.3, 135.4, 129.1, 125.7, 125.3, 124.5, 50.44, 41.84, 38.95, 37.95, 33.62, 33.45, 30.54, 25.01, 21.79, 19.45, 19.17 ppm.

The spectroscopic data are in accordance to those reported in the literature.[59]

6-Methoxy-1,1,4a-trimethyl-1,2,3,4,4a,9,10,10a-octahydrophenanthrene (**55**), prepared from **51** (34.2 mg, 132 µmol); colorless oil (30.0 mg, 116 µmol, 88%).

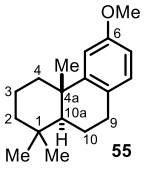

TLC: R_f = 0.43 (silica gel, hexanes/EtOAc; 95:5) [CAM]; **^{1}H NMR** (300 MHz, $CDCl_3$) δ 6.96 (dt, *J* = 8.4, 1.0 Hz, 1H), 6.82 (d, *J* = 2.8 Hz, 1H), 6.67 (dd, *J* = 8.4, 2.7 Hz, 1H), 3.78 (s, 3H), 2.94 – 2.84 (m, 1H), 2.85 – 2.75 (m, 1H), 2.30 – 2.19 (m, 1H), 1.93 – 1.82 (m, 1H), 1.81 – 1.71 (m, 2H), 1.71 – 1.58 (m, 1H), 1.53 – 1.40 (m, 2H), 1.33 (dd, *J* = 12.3, 2.4 Hz, 1H), 1.28 – 1.21 (m, 1H), 1.20 (d, *J* = 0.8 Hz, 3H), 0.96 (s, 3H), 0.94 (s, 3H) ppm; **^{13}C NMR** (75 MHz, $CDCl_3$) δ 157.8, 151.6, 130.0, 127.6, 110.9, 110.3, 55.40, 50.47, 41.83, 38.99, 38.17, 33.64, 33.46, 29.71, 24.89, 21.81, 19.47, 19.30 ppm.

The spectroscopic data are in accordance to those reported in the literature.[50]

4a'-Methyl-3',4',4a',9',10',10a'-hexahydro-2'H-spiro[cyclohexane-1,1'-phenanthrene] (**196**), prepared from (*E*)-(7-cyclohexylidene-4-methylhept-3-en-1-yl)benzene (35.2 mg, 131 µmol); colorless oil (32.0 mg, 119 µmol, 91%).

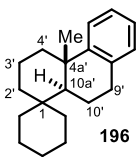

TLC: R_f = 0.78 (silica gel, hexanes) [CAM]; **^{1}H NMR** (300 MHz, $CDCl_3$) δ 7.30 – 7.23 (m, 1H), 7.17 – 7.08 (m, 1H), 7.08 – 6.99 (m, 2H), 3.01 – 2.75 (m, 2H), 2.29 (td, *J* = 12.0, 11.4, 5.3 Hz, 2H), 1.99 (ddt, *J* = 13.6, 7.1, 2.1 Hz, 1H), 1.85 – 1.73 (m, 2H), 1.66 (ddd, *J* = 15.2, 7.9, 5.0 Hz, 4H), 1.45 (ddt, *J* = 16.1, 9.2, 3.9 Hz, 4H), 1.33 – 1.24 (m, 2H), 1.21 (s, 3H), 0.98 – 0.73 (m, 4H) ppm; **^{13}C NMR** (76 MHz, $CDCl_3$) δ 150.7, 135.4, 129.1, 125.7, 125.3,

124.5, 51.42, 39.41, 39.20, 38.27, 36.45, 33.62, 31.15, 28.12, 26.72, 26.24, 21.96, 21.92, 18.75, 18.70 ppm; **IR** (KBr) $\tilde{\nu}_{max}$ = 2935, 1683, 1449, 1217, 1044, 759 cm^{-1}; **HRMS** (EI) calcd. for $C_{20}H_{28}$ $[M]^+$ 268.2184, found 268.2194.

1,1,4a-Trimethyl-2,3,4,4a,9,9a-hexahydro-1*H*-xanthene (**67**), prepared from **65** (39.1 mg, 170 µmol); colorless solid (25.0 mg, 109 µmol, 64%).

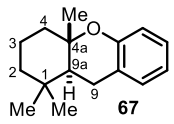

67

TLC: R_f = 0.19 (silica gel, *n*-hexane) [CAM]; **^{1}H NMR** (500 MHz, $CDCl_3$) δ 7.11 – 7.03 (m, 2H), 6.82 (t, *J* = 7.3 Hz, 1H), 6.76 (d, *J* = 8.0 Hz, 1H), 2.71 (dd, *J* = 16.3, 5.0 Hz, 1H), 2.61 (dd, *J* = 16.4, 13.1 Hz, 1H), 2.00 – 1.94 (m, 1H), 1.71 (dd, *J* = 13.2, 5.1 Hz, 1H), 1.69 – 1.63 (m, 1H), 1.61 (d, *J* = 4.2 Hz, 1H), 1.55 (dt, *J* = 11.7, 3.0 Hz, 1H), 1.52 – 1.46 (m, 1H), 1.37 – 1.29 (m, 1H), 1.22 (s, 3H), 1.01 (s, 3H), 0.91 (s, 3H); **^{13}C NMR** (75 MHz, $CDCl_3$) δ 153.4, 129.8, 127.3, 122.8, 119.8, 117.2, 77.36, 48.25, 41.68, 40.17, 33.54, 32.25, 23.41, 20.83, 20.00, 19.95 ppm.

The spectroscopic data are in accordance to those reported in the literature.[140]

7-Methoxy-1,1,4a-trimethyl-2,3,4,4a,9,9a-hexahydro-1*H*-xanthene (**60**), prepared from 2-geranyl-4-methoxyphenol (28.1 mg, 108 µmol); produced as a 93:7 mixture of inseparable diastereoisomers; clear oil (24.0 mg, 92.2 µmol, 85%).

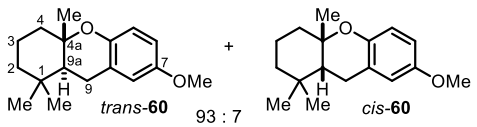

trans-**60** 93 : 7 *cis*-**60**

TLC: R_f = 0.61 (silica gel, hexanes/EtOAc; 90:10) [CAM]; *trans isomer*: **^{1}H NMR** (300 MHz, $CDCl_3$) δ 6.71 – 6.64 (m, 2H), 6.64 – 6.61 (m, 1H), 3.75 (s, 3H), 2.69 (dd, *J* = 16.5, 5.5 Hz, 1H), 2.58 (dd, *J* = 16.5, 12.7 Hz, 1H), 1.99 – 1.91 (m, 1H), 1.70 (dd, *J* = 12.6, 5.5 Hz, 1H), 1.64 – 1.55 (m, 2H), 1.54 – 1.45 (m, 1H), 1.41 – 1.26 (m, 2H), 1.20 (s, 3H), 1.00 (s, 3H), 0.90 (s, 3H) ppm; **^{13}C NMR** (75 MHz, $CDCl_3$) δ 153.1, 147.4, 123.3, 117.6, 114.4, 113.3, 77.00, 55.84, 48.27, 41.68, 40.13, 33.49, 32.23, 23.78, 20.78, 19.94, 19.84 ppm; *characteristic signals for cis isomer*: **^{1}H NMR** (300 MHz, $CDCl_3$) δ 3.01 (dd, *J* = 17.6, 8.1 Hz, 1H), 1.18 (s, 3H), 0.96 (s, 3H), 0.67 (s, 3H) ppm.

The spectroscopic data are in accordance to those reported in the literature.[140]

Methyl-8-hydroxy-1,1,4a-trimethyl-2,3,4,4a,9,9a-hexahydro-1*H*-xanthene-7-carboxylate (**197**), prepared from methyl geranyl-2,4-dihydroxybenzoate (23.6 mg, 77.5 µmol); produced as a 64:36 mixture of inseparable *C*-5/*C*-7 regioisomers; clear oil (20.1 mg, 66.0 µmol, 85%).

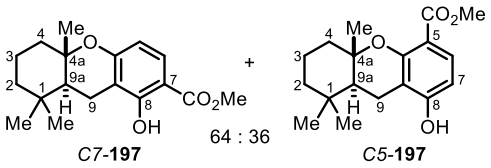

TLC: R_f = 0.35-0.42 (silica gel, hexanes/EtOAc; 95:5) [CAM]; *C7-isomer*: **^{1}H NMR** (400 MHz, $CDCl_3$) δ 11.28 (s, 1H), 7.60 – 7.53 (m, 1H), 6.31 (d, *J* = 8.8 Hz, 1H), 3.90 (s, 3H), 2.81 (dd, *J* = 16.9, 4.8 Hz, 1H), 2.32 (ddd, *J* = 16.9, 13.3, 0.9 Hz, 1H), 2.01 – 1.94 (m, 1H), 1.75 – 1.54 (m, 4H), 1.52 – 1.39 (m, 2H), 1.38 – 1.27 (m, 2H), 1.22 (s, 3H), 1.04 (s, 3H), 0.94 (s, 3H) ppm; *C5-isomer*: **^{1}H NMR** (400 MHz, $CDCl_3$) δ 10.60 (s, 1H), 7.62 – 7.52 (m, 1H), 6.31 (d, *J* = 8.8 Hz, 1H), 3.89 (s, 3H), 2.73 – 2.60 (m, 1H), 2.52 (ddd, *J* = 15.9, 13.3, 1.3 Hz, 1H), 2.01 – 1.94 (m, 1H), 1.71 – 1.55 (m, 4H), 1.53 – 1.39 (m, 2H), 1.34 – 1.29 (m, 2H), 1.22 (s, 3H), 0.99 (s, 3H), 0.89 (s, 3H) ppm; *mixture*: **^{13}C NMR** (101 MHz, $CDCl_3$) δ 171.0, 170.4, 161.4, 161.1, 160.0, 159.4, 131.2, 128.3, 124.0, 114.7, 110.4, 109.1, 105.1, 104.2, 104.0, 51.86, 51.84, 48.09, 47.39, 41.49, 41.34, 39.78, 39.74, 33.56, 33.48, 32.11, 32.02, 22.42, 20.68, 20.62, 20.06, 19.76, 19.72, 17.56 ppm; **IR** (KBr) $\tilde{\nu}_{max}$ = 2951, 2866, 1667, 1492, 1439, 1346, 1264, 1164, 987, 758 cm^{-1}; **HRMS** (ESI+) calcd. for $C_{18}H_{25}O_4^+$ $[M+H]^+$ 305.1747, found 305.1726.

4,4,7a-Trimethylhexahydrobenzofuran-2(3*H*)-one (**198**), prepared from **84** (32.3 mg, 177 µmol); produced as a 76:24 mixture of separable diastereoisomers; 31.6 mg (173 µmol, 98% combined).

trans-isomer: colourless semisolid (24.0 mg, 132 µmol, 74%); **TLC:** R_f = 0.45 (silica gel, hexanes/EtOAc; 50:50) [CAM]; **^{1}H NMR** (300 MHz, $CDCl_3$) δ 2.42 (dd, *J* = 16.3, 14.6 Hz, 1H), 2.29 (ddd, *J* = 16.3, 6.8, 0.6 Hz, 1H), 2.03 – 1.94 (m, 2H), 1.83 – 1.72 (m, 1H), 1.69 – 1.49 (m, 3H), 1.34 (d, *J* = 0.7 Hz, 3H), 1.32 – 1.21 (m, 1H), 0.96 (s, 3H), 0.93 (s, 3H) ppm; **^{13}C NMR** (75 MHz, $CDCl_3$) δ 176.6, 86.63, 55.73, 40.24, 37.34, 32.86, 32.40, 29.35, 20.86, 20.61, 19.95 ppm.

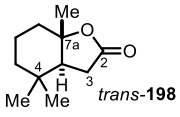

cis-isomer: colourless semisolid (7.6 mg, 41.7 µmol, 24%); **TLC:** R_f = 0.33 (silica gel, hexanes/EtOAc; 50:50) [CAM]; **^{1}H NMR** (500 MHz, $CDCl_3$) δ 2.51 (dd, *J* = 17.3, 12.7 Hz, 1H), 2.43 (dd, *J* = 17.4, 8.2 Hz, 1H), 2.06 (dd, *J* = 12.8, 8.2 Hz, 1H), 1.89 – 1.83 (m, 1H), 1.64 – 1.59 (m, 2H), 1.53 (s, 3H), 1.51 – 1.35 (m, 2H), 1.33 – 1.27 (m, 1H), 1.05 (s, 3H), 0.91 (s, 3H) ppm; **^{13}C NMR** (126 MHz, $CDCl_3$) δ 175.9, 86.25, 52.09, 34.85, 33.70, 33.41, 32.34, 30.28, 28.55, 27.08, 19.10 ppm.

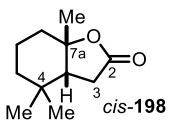

The spectroscopic data for the *trans*[141] and *cis*[142] isomer are in accordance to those reported in the literature.

(2,6,6-Trimethylcyclohex-2-en-1-yl)methyl benzoate (**199**), prepared from geranyl benzoate (32.3 mg, 125 µmol); produced as a 87:13 mixture of inseparable regioisomers ($\Delta_{2,3}$-**199** and $\Delta_{2,7}$-**199**:); clear oil (27.4 mg, 106 µmol, 85%).

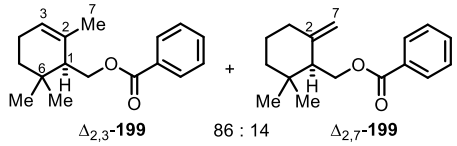

$\Delta_{2,3}$-**199** $\Delta_{2,7}$-**199**

TLC: R_f = 0.50 (silica gel, hexanes/EtOAc; 95:5) [$KMnO_4$]; $\Delta_{2,3}$-**199**: **^{1}H NMR** (300 MHz, $CDCl_3$) δ 8.06 – 7.99 (m, 2H), 7.58 – 7.52 (m, 1H), 7.48 – 7.40 (m, 2H), 5.50 (s, 1H), 4.38 (d, *J* = 4.6 Hz, 2H), 2.03 (ddt, *J* = 7.4, 3.9, 2.1 Hz, 2H), 1.95 (q, *J* = 3.9, 3.4 Hz, 1H), 1.80 (d, *J* = 1.9 Hz, 3H), 1.64 – 1.49 (m, 1H), 1.26 (dtd, *J* = 13.2, 5.0, 1.2 Hz, 1H), 1.03 (s, 3H), 0.97 (s, 3H) ppm; **^{13}C NMR** (75 MHz, $CDCl_3$) δ 166.7, 132.9, 132.3, 130.7, 129.7, 128.5, 123.5, 64.69, 49.16, 32.32, 31.95, 27.57, 27.40, 23.11, 23.06 ppm; $\Delta_{2,7}$-**199**: **^{1}H NMR** (300 MHz, $CDCl_3$) δ 4.85 (s, 1H), 4.71 (s, 1H), 4.54 (dd, *J* = 11.1, 4.9 Hz, 1H), 4.11 (d, *J* = 2.4 Hz, 1H), 2.33 (dd, *J* = 9.4, 4.9 Hz, 1H), 0.95 (s, 3H) and further signals could not be discerned; **^{13}C NMR** (75 MHz, $CDCl_3$) δ 132. 9, 129.7, 128.4, 63.51, 52.47, 36.81, 35.28, 33.47, 28.44, 25.50, 24.00 ppm and further signals could not be discerned; *mixture*: **IR** (film) $\tilde{\nu}_{max}$ = 1718, 1451, 1275, 1114, 712 cm^{-1}; **HRMS** (EI) calcd. for $C_{17}H_{22}O_2^+$ $[M]^+$ 258.1614, found 258.1629.

(2,6,6-Trimethylcyclohex-2-en-1-yl)methyl 3,5-dinitrobenzoate (**200**), prepared from geranyl 3,5-dinitrobenzoate (38.3 mg, 110 µmol): 29.5 mg, 84.6 µmol, 77%, produced as a 69:31 mixture of inseparable regioisomers ($\Delta_{2,3}$-**200** and $\Delta_{2,7}$-**200**); yellow oil and from neryl 3,5-dinitrobenzoate (50.3 mg, 144 µmol): 40.6 mg, 117 µmol, 81%, produced as a 68:32 mixture of inseparable regioisomers ($\Delta_{2,3}$-**200** and $\Delta_{2,7}$-**200**); yellow oil.

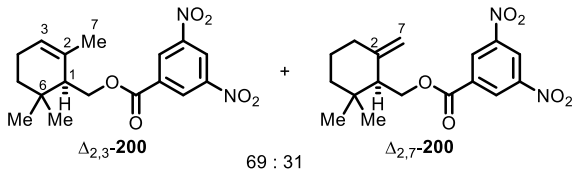

$\Delta_{2,3}$-**200** $\Delta_{2,7}$-**200**

TLC: R_f = 0.84 (silica gel, hexanes/EtOAc; 80:20) [UV]; $\Delta_{2,3}$-**200**: **^{1}H NMR** (500 MHz, $CDCl_3$) δ 9.23 (t, *J* = 2.1 Hz, 1H), 9.13 (d, *J* = 2.1 Hz, 2H), 5.56 (s, 1H), 4.53 (dd, *J* = 11.7, 5.7 Hz, 1H), 4.48 (dd, *J* = 11.7, 3.1 Hz, 1H), 2.09 – 2.05 (m, 2H), 1.97 (br s, 1H), 1.79 (q, *J* = 1.9 Hz, 3H), 1.66 – 1.48 (m, 2H), 1.31 (dt, *J* = 13.8, 4.6 Hz, 1H), 1.04 (s, 3H), 0.98 (s, 3H) ppm; **^{13}C NMR** (126 MHz, $CDCl_3$) δ 162.6, 148.8, 134.3, 131.3, 129.5, 124.2, 122.4, 66.35, 49.02, 32.09, 31.98, 27.71, 27.38, 23.08, 22.97 ppm; $\Delta_{2,7}$-**200**: **^{1}H NMR** (500 MHz, $CDCl_3$) δ 9.21 (t, *J* = 2.2 Hz, 1H), 9.12 (d, *J* = 2.2 Hz, 2H), 4.87 (s, 1H), 4.69 (s, 1H), 4.61 (d, *J* = 0.9 Hz, 1H), 4.60 (s, 1H), 2.39 (t, *J* = 7.6 Hz, 1H), 2.25 – 2.18 (m, 1H), 2.13 (dt, *J* = 13.5, 5.3 Hz, 2H), 1.04 (s, 3H), 0.97 (s, 3H) ppm and further signals could not be discerned; **^{13}C NMR** (126 MHz, $CDCl_3$) δ 162.6, 148.8, 146.8, 134.3, 129.6, 122.4, 110.8, 65.17, 52.46, 37.33, 34.49, 32.86, 28.70, 25.93, 23.34 ppm; *mixture*: **IR** (neat) $\tilde{\nu}_{max}$ = 2959, 2924, 1733, 1629, 1548, 1458, 1344, 1261, 1165, 1075, 800 cm^{-1}; **HRMS** (EI) calcd. for $C_{17}H_{20}N_2O_6^+$ $[M]^+$ 348.1316, found 348.1318.

1,3-Diethyl 5-((2,6,6-trimethylcyclohex-2-en-1-yl)methyl) benzene-1,3,5-tricarboxylate (**201**), prepared from 1-geranyl 3,5-diethylbenzene tricarboxylate (28.1 mg, 69.9 µmol); produced as a 86:14 mixture of inseparable regioisomers ($\Delta_{2,7}$-**201** and $\Delta_{2,7}$-**201**); clear oil (20.4 mg, 50.7 µmol, 73%).

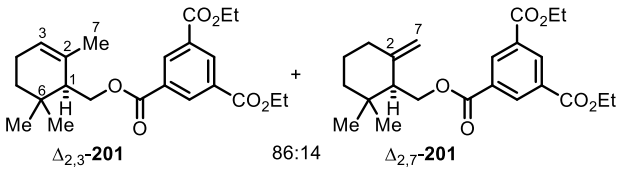

$\Delta_{2,3}$-**201** 86:14 $\Delta_{2,7}$-**201**

TLC: R_f = 0.24 (silica gel, hexanes/EtOAc; 95:5) [CAM]; $\Delta_{2,3}$-**201**: **^{1}H NMR** (300 MHz, $CDCl_3$) δ 8.89 – 8.81 (m, 1H), 8.84 – 8.81 (m, 2H), 5.53 (s, 1H), 4.45 (d, *J* = 5.3 Hz, 2H), 4.43 (q, *J* = 7.1 Hz, 4H), 2.11 – 2.01 (m, 2H), 1.95 (t, *J* = 4.0 Hz, 1H), 1.79 (q, *J* = 1.6 Hz, 3H), 1.65 – 1.54 (m, 1H), 1.43 (t, *J* = 7.2, Hz, 6H), 1.28 (dt, *J* = 13.3, 4.6 Hz, 1H), 1.04 (s, 3H), 0.97 (s, 3H) ppm; **^{13}C NMR** (75 MHz, $CDCl_3$) δ 165.2, 165.2, 134.6, 134.6, 131.9, 131.7, 131.6, 123.8, 65.20, 61.82, 49.12, 32.22, 31.98, 27.59, 27.54, 23.11, 23.05, 14.43 ppm; $\Delta_{2,7}$-**201**: **^{1}H NMR** (300 MHz, $CDCl_3$) δ 4.86 (s, 1H), 4.71 (s, 1H), 2.37 (dd, *J* = 8.1, 6.5 Hz, 1H), 2.28 – 2.14 (m, 2H), 1.04 (s, 3H), 0.96 (s, 3H) and further signals overlapped with the other isomer; *mixture*: **IR** (KBr) $\tilde{\nu}_{max}$ = 2964, 1728, 1241, 1026, 741 cm^{-1}; **HRMS** (ESI+) calcd. for $C_{23}H_{30}NaO_6^+$ $[M+Na]^+$ 425.1935, found 425.1903.

(2,6,6-Trimethylcyclohex-2-en-1-yl)methyl 3,5-dimethoxybenzoate (**202**), prepared from geranyl 3,5-dimethoxybenzoate (41.0 mg, 129 µmol); produced as a 88:12 mixture of inseparable regioisomers ($\Delta_{2,3}$-**202** and $\Delta_{2,7}$-**202**); clear oil (33.2 mg, 104 µmol, 81%).

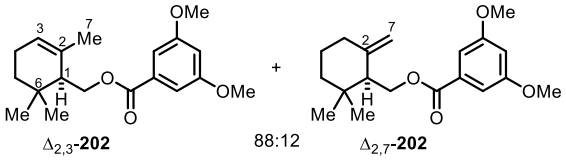

$\Delta_{2,3}$-**202** 88:12 $\Delta_{2,7}$-**202**

TLC: R_f = 0.36 (silica gel, hexanes/EtOAc; 95:5) [CAM]; $\Delta_{2,3}$-**202**: **^{1}H NMR** (300 MHz, $CDCl_3$) δ 7.18 (d, *J* = 2.4 Hz, 2H), 6.64 (t, *J* = 2.4 Hz, 1H), 5.50 (s, 1H), 4.36 (d, *J* = 4.6 Hz, 2H), 3.82 (s, 6H), 2.06 – 1.98 (m, 2H), 1.92 (t, *J* = 4.7 Hz, 1H), 1.79 (q, *J* = 1.4 Hz, 3H), 1.57 (dt, *J* = 16.2, 6.5 Hz, 1H), 1.30 – 1.20 (m, 1H), 1.03 (s, 3H), 0.96 (s, 3H) ppm; **^{13}C NMR** (75 MHz, $CDCl_3$) δ 166.4, 160.8, 132.6, 132.2, 123.5, 107.3, 107.3, 105.7, 64.79, 55.64, 49.14, 32.27, 31.94, 27.55, 27.46, 23.09 ppm; $\Delta_{2,7}$-**202**: **^{1}H NMR** (300 MHz, $CDCl_3$) δ 7.17 (d, *J* = 2.4 Hz, 2H), 6.63 (t, *J* = 2.4 Hz, 1H), 4.85 (br s, 1H), 4.70 (dt, *J* = 1.9, 0.9 Hz, 1H), 4.51 (dd, *J* = 11.1, 5.1 Hz, 1H), 4.42 (dd, *J* = 11.0, 9.4 Hz, 1H), 3.81 (s, 6H), 2.32 (dd, *J* = 9.6, 5.3 Hz, 1H), 2.27 – 2.07 (m, 2H), 1.40 – 1.30 (m, 4H), 1.03 (s, 3H), 0.94 (s, 3H) ppm; **^{13}C NMR** (75 MHz, $CDCl_3$) δ 160.7, 147.3, 110.2, 107.3, 105.7, 63.68, 52.49, 37.74, 34.46, 33.31, 28.84, 25.68, 23.50 ppm and further signals overlapped with the other isomer; *mixture*: **IR** (KBr) $\tilde{\nu}_{max}$ = 1718, 1598, 1463, 1302, 1206, 1157, 1050, 767 cm^{-1}; **HRMS** (ESI+) calcd. for $C_{19}H_{26}NaO_4^+$ $[M+Na]^+$ 341.1723, found 341.1723.

(2,6,6-Trimethylcyclohex-2-en-1-yl)methyl isoxazole-5-carboxylate (**203**), prepared from geranyl isoxazole-5-carboxylate (39.9 mg, 160 µmol); produced as a 83:17 mixture of inseparable regioisomers ($\Delta_{2,7}$-**203** and $\Delta_{2,7}$-**203**); clear oil (39.7 mg, 159 µmol, 99%).

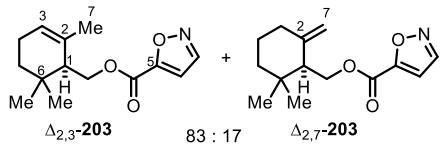

$\Delta_{2,3}$-**203** 83 : 17 $\Delta_{2,7}$-**203**

TLC: R_f = 0.35 (silica gel, hexanes/EtOAc; 95:5); $\Delta_{2,3}$-**203**: **^{1}H NMR** (300 MHz, $CDCl_3$) δ 8.36 (d, *J* = 1.8 Hz, 1H), 6.91 (d, *J* = 1.8 Hz, 1H), 5.53 – 5.46 (m, 1H), 4.47 (dd, *J* = 11.6, 5.8 Hz, 1H), 4.36 (dd, *J* = 11.7, 3.5 Hz, 1H), 2.03 – 1.96 (m, 2H), 1.93 – 1.88 (m, 1H), 1.77 (q, *J* = 1.7 Hz, 3H), 1.58 – 1.49 (m, 1H), 1.30 – 1.20 (m, 1H), 1.00 (s, 3H), 0.94 (s, 3H) ppm; **^{13}C NMR** (75 MHz, $CDCl_3$) δ 160.3, 156.7, 150.7, 131.5, 124.1, 108.7, 65.88, 48.96, 31.99, 31.89, 27.39, 27.37, 23.05, 22.97 ppm; $\Delta_{2,7}$-**203**: **^{1}H NMR** (300 MHz, $CDCl_3$) δ 8.34 (d, *J* = 1.8 Hz, 1H), 6.89 (d, *J* = 1.8 Hz, 1H), 4.82 (d, *J* = 1.6 Hz, 1H), 4.64 (br s, 1H), 4.54 (d, *J* = 3.3 Hz, 1H), 4.52 (d, *J* = 0.7 Hz, 1H), 2.31 (dd, *J* = 8.6, 5.9 Hz, 1H), 1.01 (s, 3H), 0.92 (s, 3H) and further signals could not be discerned; **^{13}C NMR** (75 MHz, $CDCl_3$) δ 160.2, 158.3, 150.9, 146.5, 110.6, 109.7, 64.78, 52.28, 37.69, 34.47, 33.20, 28.76, 25.54, 23.36 ppm; *mixture*: **IR** (neat) $\tilde{\nu}_{max}$ = 2962, 1736, 1280, 1204, 1143, 769 cm^{-1}; **HRMS** (ESI+) calcd. for $C_{14}H_{19}NNaO_3^+$ $[M+Na]^+$ 272.1257, found 272.1255.

(2,6,6-trimethylcyclohex-2-en-1-yl)methyl thiophene-2-carboxylate (**204**), prepared from geranyl thiophene-2-carboxylate (34.6 mg, 131 µmol); slightly yellow oil (31.6 mg, 120 µmol, 91%).

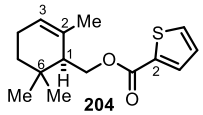

204

TLC: R_f = 0.60 (silica gel, hexanes/EtOAc; 95:5); **^{1}H NMR** (400 MHz, $CDCl_3$) δ 7.78 (dd, *J* = 3.7, 1.3 Hz, 1H), 7.54 (dd, *J* = 5.0, 1.3 Hz, 1H), 7.09 (dd, *J* = 5.0, 3.7 Hz, 1H), 5.49 (tt, *J* = 3.7, 1.6 Hz, 1H), 4.41 – 4.29 (m, 2H), 2.07 – 1.96 (m, 2H), 1.90 (t, *J* = 4.5 Hz, 1H), 1.78 (q, *J* = 1.9 Hz, 3H), 1.70 – 1.50 (m, 2H), 1.29 – 1.17 (m, 1H), 1.02 (s, 3H), 0.95 (s, 3H) ppm; **^{13}C NMR** (101 MHz, $CDCl_3$) δ 162.3, 134.4, 133.3, 132.3, 132.1, 127.9, 123.6, 64.81, 49.11, 32.22, 31.91, 27.55, 27.44, 23.12, 23.06 ppm; **IR** (neat) $\tilde{\nu}_{max}$ = 2963, 1710, 1419, 1258, 1096, 751, 718 cm^{-1}; **HRMS** (ESI+) calcd. for $C_{15}H_{20}NaO_2S^+$ $[M+Na]^+$ 287.1076, found 287.1072.

(2,6,6-Trimethylcyclohex-2-en-1-yl)methyl acetate (**205**), prepared from geranyl acetate (18.9 mg, 96.3 µmol); clear oil (16.6 mg, 84.6 µmol, 88%).

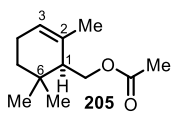

205

TLC: R_f = 0.51 (silica gel, hexanes/EtOAc; 95:5); **^{1}H NMR** (300 MHz, $CDCl_3$) δ 5.44 (tt, *J* = 3.5, 1.6 Hz, 1H), 4.16 (dd, *J* = 11.7, 5.8 Hz, 1H), 4.05 (dd, *J* = 11.7, 3.7 Hz, 1H), 2.02 (s, 3H), 1.96 (dtq, *J* = 7.2, 3.7, 1.5 Hz, 2H), 1.83 – 1.74 (m, 1H), 1.72 (q, *J* = 1.9 Hz, 3H), 1.46 (dt, *J* = 13.3, 8.1 Hz, 1H), 1.23 – 1.17 (m, 1H), 0.93 (s, 3H), 0.90 (s, 3H) ppm;

^{13}C NMR (75 MHz, $CDCl_3$) δ 171.3, 132.4, 123.3, 64.44, 48.90, 32.14, 31.87, 27.46, 27.13, 23.08, 23.01, 21.26 ppm.

The spectroscopic data are in accordance to those reported in the literature.[143]

(2,6,6-Trimethylcyclohex-2-en-1-yl)methyl ferrocene-1-carboxylate (**206**), prepared from geranyl ferrocene-1-carboxylate (25.1 mg, 68.5 µmol); deep orange oil (17.8 mg, 48.6 µmol, 71%).

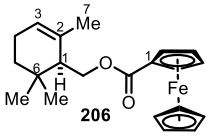

206

TLC: R_f = 0.53 (silica gel, hexanes/EtOAc, 90:10); **^{1}H NMR** (400 MHz, $CDCl_3$) δ 5.52 (s, 1H), 4.77 (dt, *J* = 3.4, 1.8 Hz, 2H), 4.38 (t, *J* = 2.0 Hz, 2H), 4.31 (dd, *J* = 11.7, 5.4 Hz, 1H), 4.23 (dd, *J* = 11.7, 3.3 Hz, 1H), 4.19 (s, 5H), 2.08 – 2.03 (m, 2H), 1.86 (s, 1H), 1.80 (d, *J* = 1.9 Hz, 3H), 1.63 (dt, *J* = 13.3, 8.3 Hz, 1H), 1.27 (dt, *J* = 12.5, 4.3 Hz, 1H), 1.06 (s, 3H), 0.97 (s, 3H) ppm; **^{13}C NMR (**101 MHz, $CDCl_3$) δ 171.9, 132.3, 123.4, 71.77, 71.29, 71.27, 70.24, 70.18, 69.82, 63.84, 49.22, 32.50, 31.96, 27.73, 27.55, 23.15, 23.11 ppm; **IR** (neat) $\tilde{\nu}_{max}$ = 2958, 1711, 1460, 1380, 1273, 1135, 821 cm^{-1}; **Anal. Calcd.** for $C_{21}H_{26}FeO_2$: C: 68.86, H: 7.16, Fe: 15.25; found: C: 68.92, H: 7.47, Fe: 15.6.

(((2,6,6-Trimethylcyclohex-2-en-1-yl)methoxy)methyl)benzene (**207**), prepared from geranyl benzyl ether (35.2 mg, 144 µmol); colorless oil (35.2 mg, 144 µmol, *quant*.).

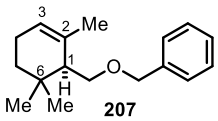

207

TLC: R_f = 0.33 (silica gel, hexanes/EtOAc; 95:5); **^{1}H NMR** (300 MHz, $CDCl_3$) δ 7.41 – 7.25 (m, 5H), 5.43 (dt, *J* = 3.6, 2.0 Hz, 1H), 4.48 (s, 2H), 3.52 (dd, *J* = 9.9, 5.4 Hz, 1H), 3.44 (dd, *J* = 9.9, 3.5 Hz, 1H), 1.97 (dddq, *J* = 9.3, 5.7, 3.9, 2.0 Hz, 2H), 1.74 (q, *J* = 1.9 Hz, 3H), 1.64 (m, 1H), 1.53 – 1.43 (dt, *J* =13.1, 7.4 Hz, 1H), 1.19 (dtd, *J* = 13.2, 5.4, 1.5 Hz, 1H), 0.97 (s, 3H), 0.91 (s, 3H) ppm; **^{13}C NMR** (75 MHz, $CDCl_3$) δ 138.9, 133.7, 128.4, 127.7, 127.5, 122.4, 73.10, 70.93, 50.17, 32.58, 31.93, 27.63, 27.23, 23.28, 23.15 ppm; **IR** (neat) $\tilde{\nu}_{max}$ = 2955, 2868, 1454, 1363, 1101, 733, 697 cm^{-1}; **HRMS** (EI) calcd. for $C_{17}H_{24}O^+$ $[M]^+$ 244.1822, found 24.1815.

1,5,5-Trimethyl-6-((prop-2-yn-1-yloxy)methyl)cyclohex-1-ene (**208**), prepared from geranyl propargyl ether (20.5 mg, 107 µmol); produced as a 94:6 mixture of inseparable regioisomers ($\Delta_{2,3}$-**208** and $\Delta_{2,7}$-**208**); colorless oil (20.3 mg, 106 µmol, 99%).

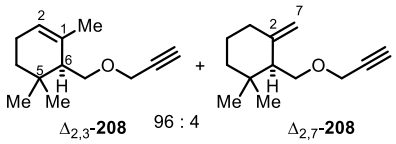

TLC: R_f = 0.63 (silica gel, hexanes/EtOAc; 95:5); $\Delta_{2,3}$-**208**: **^{1}H NMR** (400 MHz, $CDCl_3$) δ 5.44 (s, 1H), 4.12 – 4.10 (m, 2H), 3.58 (dd, *J* = 9.8, 5.3 Hz, 1H), 3.50 (dd, *J* = 9.8, 3.2 Hz, 1H), 2.40 (t, *J* = 2.4 Hz, 1H), 1.97 (dtdd, *J* = 7.3, 5.3, 3.1, 2.0 Hz, 2H), 1.74 (q, *J* = 1.9 Hz, 3H), 1.48 (dt, *J* = 13.1, 8.0 Hz, 1H), 1.18 (dtd, *J* = 13.0, 5.0, 1.2 Hz, 1H), 0.96 (s, 3H), 0.90 (s, 3H) ppm; **^{13}C NMR** (75 MHz, $CDCl_3$) δ 133.4, 122.7, 80.19, 74.23, 70.29, 58.08, 49.94, 32.70, 31.96, 27.69, 27.12, 23.14, 23.10 ppm; $\Delta_{2,7}$-**208**: **^{1}H NMR** (400 MHz, $CDCl_3$) δ 4.85 (dq, *J* = 1.9, 1.0 Hz, 1H), 4.69 (br s, 1H), 0.99 (s, 3H), 0.84 (s, 3H) and further signals could not be discerned; *mixture*: **IR** (neat) $\tilde{\nu}_{max}$ = 2956, 2914, 1452, 1364, 1096, 663 cm^{-1}; **HRMS** (EI) calcd. for $C_{13}H_{20}O^+$ $[M]^+$ 192.1509, found 192.1511.

2-(((2,6,6-Trimethylcyclohex-2-en-1-yl)methoxy)methyl)oxirane (**209**), prepared from 2-geranyl methyloxirane ether (29.9 mg, 142 µmol); produced as a 50:50 mixture of inseparable diastereoisomers; clear oil (20.0 mg, 95.1 µmol, 67%).

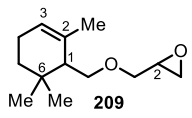

TLC: R_f = 0.29 (silica gel, hexanes/EtOAc 90:10); *diastereoisomer 1*: **^{1}H NMR** (400 MHz, $CDCl_3$) δ 5.42 (tt, *J* = 3.5, 1.5 Hz, 1H), 3.68 (ddd, *J* = 11.5, 6.3, 3.1 Hz, 2H), 3.36 (ddd, *J* = 11.5, 5.7, 3.1 Hz, 2H), 3.17 – 3.11 (m, 1H), 2.78 (ddd, *J* = 5.1, 4.1, 1.7 Hz, 1H), 2.60 (ddd, *J* = 5.2, 4.3, 2.7 Hz, 1H), 1.96 (dddq, *J* = 8.8, 5.7, 3.9, 2.0 Hz, 2H), 1.74 (q, *J* = 1.9 Hz, 3H), 1.47 (dtd, *J* = 13.2, 8.1, 2.3 Hz, 1H), 1.18 (dt, *J* = 13.1, 4.6 Hz, 1H), 1.02 – 0.96 (m, 1H), 0.95 (d, *J* = 1.1 Hz, 3H), 0.90 (s, 3H) ppm; *diastereoisomer 2*: **^{1}H NMR** (400 MHz, $CDCl_3$) δ 5.42 (tt, *J* = 3.5, 1.5 Hz, 1H), 3.57 (dd, *J* = 10.0, 5.5 Hz, 1H), 3.50 (dd, *J* = 4.5, 1.6 Hz, 2H), 3.42 (dd, *J* = 10.0, 3.4 Hz, 1H), 3.17 – 3.11 (m, 1H), 2.78 (ddd, *J* = 5.1, 4.1, 1.7 Hz, 1H), 2.60 (ddd, *J* = 5.2, 4.3, 2.7 Hz, 1H), 1.96 (dddq, *J* = 8.8, 5.7, 3.9, 2.0 Hz, 2H), 1.74 (q, *J* = 1.9 Hz, 3H), 1.47 (dtd, *J* = 13.2, 8.1, 2.3 Hz, 1H), 1.18 (dt, *J* = 13.1, 4.6 Hz, 1H), 1.02 – 0.96 (m, 1H), 0.95 (d, *J* = 1.1 Hz, 3H), 0.90 (s, 3H) ppm; m*ixture of diastereoisomers*: **^{13}C NMR** (101 MHz, $CDCl_3$) δ 133.5, 122.6, 71.98, 71.93, 71.68, 71.46, 51.05, 50.07, 44.51, 44.45, 32.54, 31.87, 27.61, 27.20, 27.14, 23.26, 23.12 ppm; **IR** (KBr) $\tilde{\nu}_{max}$ = 2923, 1716, 1455, 1109, 759 cm^{-1}; **HRMS** (EI) calcd. for $C_{13}H_{22}O_2^+$ $[M]^+$ 210.1614, found 210.1633.

6-((Methoxymethoxy)methyl)-1,5,5-trimethylcyclohex-1-ene (**210**), prepared from geranyl methoxymethyl ether (18.9 mg, 95.3 µmol); colorless oil (10.6 mg, 53.5 µmol, 56%).

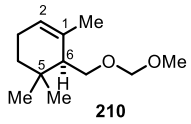

210

TLC: R_f = 0.53 (silica gel, hexanes/EtOAc; 95:5); **^{1}H NMR** (500 MHz, $CDCl_3$) δ 5.44 (s, 1H), 4.60 (q, *J* = 6.6 Hz, 2H), 3.59 (dd, *J* = 10.2, 5.2 Hz, 1H), 3.53 (dd, *J* = 10.3, 3.4 Hz, 1H), 3.37 (s, 3H), 1.97 (dtt, *J* = 7.8, 4.3, 2.2 Hz, 2H), 1.74 (q, *J* = 1.9 Hz, 3H), 1.73 – 1.68 (m, 1H), 1.56 – 1.45 (m, 1H), 1.18 (dtd, *J* = 13.3, 5.0, 1.2 Hz, 1H), 0.97 (s, 3H), 0.91 (s, 3H) ppm; **^{13}C NMR** (126 MHz, $CDCl_3$) δ 133.4, 122.6, 96.74, 68.08, 55.53, 49.96, 32.59, 31.89, 27.70, 27.20, 23.16, 23.10 ppm; **IR** (KBr) $\tilde{\nu}_{max}$ = 2927, 1715, 1457, 1378, 1037, 756 cm^{-1}; **HRMS** (EI) calcd. for $C_{12}H_{22}O_2^+$ $[M]^+$ 198.1614, found 198.1626.

6-((Allyloxy)methyl)-1,5,5-trimethylcyclohex-1-ene (**211**), prepared from geranyl allyl ether (17.5 mg, 90.1 µmol); colorless oil (17.5 mg, 90.1 µmol, *quant*.).

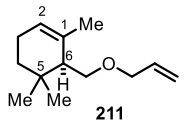

211

TLC: R_f = 0.58 (silica gel, hexanes); **^{1}H NMR** (500 MHz, $CDCl_3$) δ 5.91 (ddt, *J* = 17.2, 10.8, 5.5 Hz, 1H), 5.42 (dt, *J* = 3.9, 2.2 Hz, 1H), 5.26 (dq, *J* = 17.2, 1.8 Hz, 1H), 5.16 (dq, *J* = 10.4, 1.5 Hz, 1H), 3.94 (dd, *J* = 5.5, 1.5 Hz, 2H), 3.47 (dd, *J* = 9.9, 5.5 Hz, 1H), 3.38 (dd, *J* = 10.0, 3.6 Hz, 1H), 1.96 (tdt, *J* = 7.0, 3.8, 2.0 Hz, 2H), 1.74 (d, *J* = 2.0 Hz, 3H), 1.70 – 1.62 (m, 1H), 1.49 (dt, *J* = 13.1, 8.1 Hz, 1H), 1.17 (dt, *J* = 13.2, 4.7 Hz, 1H), 0.95 (s, 3H), 0.90 (s, 3H) ppm; **^{13}C NMR** (75 MHz, $CDCl_3$) δ 135.3, 133.8, 122.4, 116.7, 71.94, 70.79, 50.10, 32.56, 31.89, 27.63, 27.18, 23.29, 23.14 ppm; **IR** (neat) $\tilde{\nu}_{max}$ = 2959, 2925, 1453, 1383, 1102, 921 cm^{-1}; **HRMS** (EI) calcd. for $C_{13}H_{22}O^+$ $[M]^+$ 194.1665, found 194.1664.

6-((But-2-en-1-yloxy)methyl)-1,5,5-trimethylcyclohex-1-ene (**212**), prepared from geranyl but-2-en ether (31.5 mg, 151 µmol, *E*/*Z* = 87:13); produced as a 86:14 inseparable mixture of configurational isomers (*E*/*Z*); colorless oil (31.5 mg, 151 µmol, *quant*.).

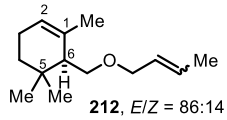

212, *E*/*Z* = 86:14

TLC: R_f = 0.38 (silica gel, hexanes/EtOAc; 95:5); *E-isomer*: **^{1}H NMR** (300 MHz, $CDCl_3$) δ 5.77 – 5.63 (m, 1H), 5.63 – 5.51 (m, 1H), 5.40 (tt, *J* = 3.5, 1.6 Hz, 1H), 3.88 – 3.84 (m, 2H), 3.43 (dd, *J* = 10.0, 5.6 Hz, 1H), 3.34 (dd, *J* = 10.0, 3.6 Hz, 1H), 1.96 (dddd, *J* = 8.6, 5.3, 3.8, 2.0 Hz, 2H), 1.74 – 1.72 (m, 3H), 1.71 (q, *J* = 1.2 Hz, 2H), 1.69 (q, *J* = 1.3 Hz, 2H), 1.58 – 1.42 (m, 1H), 1.21 – 1.11 (m, 1H), 1.08 – 0.99 (m, 1H), 0.94 (s, 3H), 0.90 (s, 3H) ppm; **^{13}C NMR** (75 MHz, $CDCl_3$) δ 133.9, 129.0, 128.1, 122.2, 71.61, 70.58, 50.11, 32.56, 31.90, 27.60, 27.15, 23.29, 23.15, 17.91 ppm; *Z-isomer*: **^{1}H NMR** (300 MHz, $CDCl_3$) δ 4.00 (dt, *J* = 6.2, 1.0 Hz, 2H) ppm and further signals could not be discerned; *mixture*: **IR** (neat) $\tilde{\nu}_{max}$ = 2957, 1452, 1365, 1102, 966 cm^{-1}; **HRMS** (EI) calcd. for $C_{14}H_{24}O^+$ $[M]^+$ 208.1822, found 208.1811.

(2,6,6-trimethylcyclohex-2-en-1-yl)methyl 5-((3a*S*,4*S*,6a*R*)-2-oxohexahydro-1*H*-thieno[3,4-d]imidazol-4-yl)pentanoate (**214**), prepared from geranyl biotinate (39.4 mg, 104 µmol); produced as a 85:15 mixture of inseparable regioisomers ($\Delta_{2,3}$-**214** and $\Delta_{2,7}$-**214**); colorless semisolid (28.1 mg, 73.8 µmol, 71%).

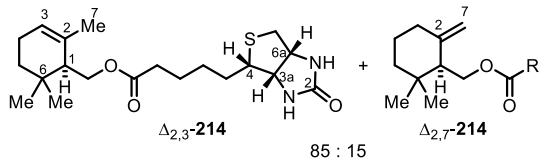

TLC: R_f = 0.36 (silica gel, EtOAc/MeOH; 90:10); $\Delta_{2,3}$-**214**: **^{1}H NMR** (400 MHz, $CDCl_3$) δ 5.67 (s, 1H), 5.44 (s, 1H), 5.36 (s, 1H), 4.51 (dd, *J* = 7.8, 5.0 Hz, 1H), 4.31 (ddd, *J* = 7.8, 4.5, 1.6 Hz, 1H), 4.17 (ddd, *J* = 11.7, 5.8, 3.1 Hz, 1H), 4.05 (dd, *J* = 11.7, 3.5 Hz, 1H), 3.15 (ddt, *J* = 8.4, 6.1, 4.5 Hz, 1H), 2.91 (dd, *J* = 12.9, 5.0 Hz, 1H), 2.74 (d, *J* = 12.8 Hz, 1H), 2.31 (t, *J* = 7.5 Hz, 2H), 2.00 – 1.93 (m, 2H), 1.79 – 1.76 (m, 1H), 1.72 (q, *J* = 1.9 Hz, 3H), 1.70 – 1.59 (m, 4H), 1.48 – 1.40 (m, 3H), 1.19 (dt, *J* = 12.9, 4.9 Hz, 1H), 0.93 (s, 3H), 0.91 (s, 3H) ppm; **^{13}C NMR** (101 MHz, $CDCl_3$) δ 173.7, 163.7, 132.3 (d, *J* = 1.8 Hz), 123.4 (d, *J* = 2.5 Hz), 64.26 (d, *J* = 3.4 Hz), 62.12, 60.30, 55.55, 48.97, 40.70, 34.28, 32.19, 31.89, 28.54 (d, *J* = 3.5 Hz), 27.51, 27.28, 27.26, 24.87, 23.12, 23.04 ppm; $\Delta_{2,7}$-**214**: **^{1}H NMR** (400 MHz, $CDCl_3$) δ 4.81 (s, 1H), 4.58 (d, *J* = 2.0 Hz, 1H), 4.25 – 4.21 (m, 1H), 2.15 (dt, *J* = 8.9, 4.8 Hz, 2H), 0.98 (s, 3H), 0.86 (s, 3H) ppm and further signals could not be discerned; *mixture*: **IR** (neat) $\tilde{\nu}_{max}$ = 3215, 2921, 1733, 1698, 1472, 1168, 731 cm^{-1}; **HRMS** (ESI+) calcd. for $C_{20}H_{33}N_2O_3S^+$ $[M+H]^+$ 381.2206, found 381.2210.

(2,6,6-Trimethylcyclohex-2-en-1-yl)methyl 2-(-3a,5-dimethyl-6,8-dioxooctahydro-1*H*-1,4-methanoinden-1-yl)propanoate (**215**), prepared from geranyl santonate (41.4 mg, 103 µmol); produced as a 55:45 mixture of separable diastereoisomers; colorless oil (combined yield: 27.3 mg, 68.0 µmol, 66%); *major diastereoisomer*, produced as a 92:8 mixture of inseparable regioisomers ($\Delta_{2,3}$-**215** and $\Delta_{2,7}$-**215**).

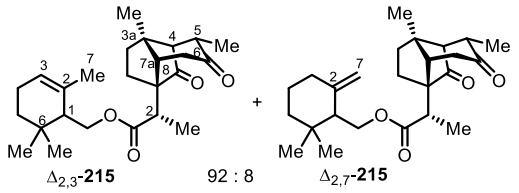

major diastereomer: **TLC:** R_f = 0.26 (silica gel, hexanes/EtOAc; 80:20); ($\Delta_{2,3}$-*isomer*: **^{1}H NMR** (400 MHz, $CDCl_3$) δ 5.45 (s, 1H), 4.23 (dd, *J* = 11.8, 5.7 Hz, 1H), 3.96 (dd, *J* = 11.7, 2.9 Hz, 1H), 2.78 (q, *J* = 7.2 Hz, 1H), 2.71 – 2.57 (m, 2H), 2.48 (dd, *J* = 18.1, 4.9 Hz, 1H), 2.18 (td, *J* = 12.4, 5.6 Hz, 1H), 2.08 (t, *J* = 3.6 Hz, 1H), 2.06 – 2.00 (m, 1H), 1.99 – 1.93 (m, 2H), 1.71 (q, *J* = 1.9 Hz, 3H), 1.62 (dd, *J* = 9.4, 5.7 Hz, 1H), 1.55 – 1.43 (m, 2H), 1.33 (s, 3H), 1.32 (d, *J* = 7.2 Hz, 3H), 1.15 (d, *J* = 6.7 Hz, 3H), 0.94 (s, 3H), 0.91 (s, 3H) ppm; **^{13}C NMR** (101 MHz, $CDCl_3$) δ 216.3, 209.5, 174.4, 132.1, 123.6, 64.19, 63.09, 61.34, 51.62, 49.04, 44.76, 44.22, 38.03, 37.83, 33.46, 32.10, 31.89, 27.58, 27.47, 26.42, 23.07, 23.03, 16.79, 13.59, 12.67 ppm; *major diastereoisomer;* $\Delta_{2,7}$-*isomer*: **^{1}H NMR** (400 MHz, $CDCl_3$) δ 4.82 (s, 1H), 4.59 (s, 1H), 4.32 – 4.24 (m, 1H), 4.10 (dd, *J* = 8.6, 4.3 Hz, 1H), 0.98 (s, 3H), 0.85 (s, 3H) ppm and further

signals could not be discerned; *mixture*: **IR** (neat) $\tilde{\nu}_{max}$ = 2931, 2875, 1727, 1713, 1458, 1382, 1324, 1259, 1162, 1123, 1103, 1068, 1021, 921, 846, 801 cm^{-1}; **HRMS** (ESI+) calcd. for $C_{25}H_{37}O_4^+$ $[M+H]^+$ 401.2686, found 401.2688; *minor diastereoisomer:* **TLC:** R_f = 0.23 (silica gel, hexanes/EtOAc; 80:20); $\Delta_{2,3}$-*isomer*: **^{1}H NMR** (400 MHz, $CDCl_3$) δ 5.47 (s, 1H), 4.16 – 4.04 (m, 2H), 2.77 (q, *J* = 7.1 Hz, 1H), 2.69 – 2.56 (m, 2H), 2.45 (dd, *J* = 18.2, 4.9 Hz, 1H), 2.18 (td, *J* = 12.3, 5.4 Hz, 1H), 2.07 (t, *J* = 3.6 Hz, 1H), 2.05 – 1.94 (m, 3H), 1.77 – 1.67 (m, 3H), 1.65 – 1.58 (m, 1H), 1.56 – 1.45 (m, 3H), 1.33 (s, 6H), 1.32 – 1.28 (m, 2H), 1.14 (d, *J* = 6.8 Hz, 3H), 0.94 (s, 3H), 0.91 (s, 3H) ppm; **^{13}C NMR** (101 MHz, $CDCl_3$) δ 216.2, 209.5, 174.6, 132.0, 123.8, 64.34, 63.06, 61.39, 51.78, 48.94, 44.70, 44.27, 38.02, 37.61, 33.46, 32.38, 31.89, 27.63, 27.41, 26.21, 23.00, 22.96, 16.77, 13.61, 12.63 ppm; **IR** (neat) $\tilde{\nu}_{max}$ = 2937, 1728, 1458, 1382, 1323, 1256, 1160, 1105, 1058, 1022, 846, 800 cm^{-1}; **HRMS** (ESI+) calcd. for $C_{25}H_{37}O_4^+$ $[M+H]^+$ 401.2686, found 401.2689.

1-((9*H*-Fluoren-9-yl)methyl) 2-((2,6,6-trimethylcyclohex-2-en-1-yl)methyl) (2*S*)-pyrrolidine-1,2-dicarboxylate (**216**), prepared from *N*-Fmoc-L-proline geranyl ester (70.6 mg, 149 µmol); produced as a 84:16 mixture of inseparable regioisomers ($\Delta_{2,3}$-**216** and $\Delta_{2,7}$-**216**) and a 52:48 mixture of diastereoisomers; colorless oil (41.5 mg, 87.6 µmol, 59%).

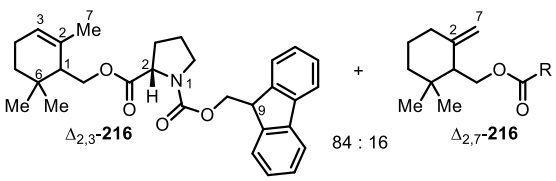

$\Delta_{2,3}$-**216** $\Delta_{2,7}$-**216**

TLC: R_f = 0.38 (silica gel, hexanes/EtOAc; 80:20); $\Delta_{2,3}$-**216**: **^{1}H NMR** (400 MHz, $CDCl_3$) δ 7.76 (dd, *J* = 7.5, 4.9 Hz, 2H), 7.65 – 7.52 (m, 2H), 7.40 (td, *J* = 7.5, 3.3 Hz, 2H), 7.31 (tdd, *J* = 7.5, 2.6, 1.2 Hz, 2H), 5.43 (br s, 1H), 4.45 – 4.23 (m, 4H), 4.23 – 4.01 (m, 2H), 3.65 (dtt, *J* = 10.1, 7.9, 5.2 Hz, 1H), 3.54 (dqd, *J* = 9.9, 7.1, 6.5, 2.9 Hz, 1H), 2.34 – 2.12 (m, 1H), 2.12 – 1.85 (m, 5H), 1.72 (d, *J* = 1.8 Hz, 1H), 1.66 (q, *J* = 2.0 Hz, 1H), 1.64 – 1.58 (m, 1H), 1.58 – 1.37 (m, 1H), 1.17 (dtd, *J* = 13.0, 9.6, 8.8, 6.6 Hz, 1H), 1.00 – 0.81 (m, 7H) ppm; **^{13}C NMR** (101 MHz, $CDCl_3$) δ 172.8, 172.7, 172.6, 155.0, 154.5, 144.3, 144.1, 143.9, 141.4, 132.2, 132.1, 131.8, 131.7, 127.8, 127.2, 127.2, 125.4, 125.3, 125.2, 123.7, 123.7, 123.5, 120.1, 67.89, 67.81, 67.59, 64.96, 64.68, 59.65, 59.59, 59.28, 49.03, 48.96, 48.91, 47.41, 47.15, 46.62, 32.35, 32.22, 31.86, 31.25, 31.19, 30.00, 29.93, 27.61, 27.50, 27.37, 27.29, 27.18, 27.06, 24.52, 23.58, 23.51, 23.03, 22.99 ppm; $\Delta_{2,7}$-**216**: **^{1}H NMR** (400 MHz, $CDCl_3$) δ 4.81 (dd, *J* = 12.4, 7.4 Hz, 1H), 4.65 – 4.54 (m, 1H) ppm, and further signals could not be discerned; *mixture*: **IR** (KBr) $\tilde{\nu}_{max}$ = 2957, 1740, 1704, 1451, 1419, 1350, 1176, 758 cm^{-1}; **HRMS** (ESI+) calcd. for $C_{30}H_{36}NO_4^+$ $[M+H]^+$ 474.2639, found 474.2639.

(2,6,6-Trimethylcyclohex-2-en-1-yl)methyl *N*6-((benzyloxy)carbonyl)-*N*2-(tert-butoxycarbonyl)-L-lysinate (**217**), prepared from *N*2-Boc-*N*6-Cbz-L-lysine geranyl ester (30.6 mg, 59.2 µmol); produced as a 88:12 mixture of inseparable regioisomers ($\Delta_{2,3}$-**217** and $\Delta_{2,7}$-**217**); colorless semisolid (23.6 mg, 45.6 µmol, 77%).

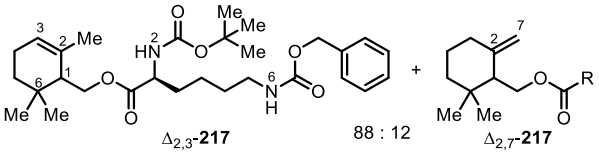

TLC: R_f = 0.18 (silica gel, hexanes/EtOAc; 80:20); $\Delta_{2,3}$-**217**: **^{1}H NMR** (400 MHz, $CDCl_3$) δ 7.38 – 7.29 (m, 4H), 7.33 – 7.29 (m, 1H), 5.46 (s, 1H), 5.09 (s, 2H), 5.08 – 5.00 (m, 1H), 4.81 (br s, 1H), 4.32 – 4.18 (m, 2H), 4.11 (ddd, *J* = 11.4, 7.5, 3.2 Hz, 1H), 3.18 (d, *J* = 7.4 Hz, 2H), 2.18 – 2.01 (m, 1H), 2.01 – 1.93 (m, 2H), 1.78 (br s, 2H), 1.71 (dd, *J* = 3.6, 1.8 Hz, 3H), 1.68 – 1.47 (m, 3H), 1.43 (s, 9H), 1.39 – 1.28 (m, 2H), 1.20 (dt, *J* = 13.7, 4.7 Hz, 1H), 0.93 (d, *J* = 2.6 Hz, 3H), 0.91 (s, 3H) ppm; **^{13}C NMR** (101 MHz, $CDCl_3$) δ 156.4, 136.6, 131.7, 128.5, 128.1, 128.1, 123.6, 123.5, 66.65, 65.02, 64.79, 53.26, 48.88, 48.82, 40.73, 32.37, 32.06, 31.99, 31.74, 29.40, 28.33, 27.36, 27.29, 27.19, 22.91, 22.88, 22.84, 22.37 ppm; $\Delta_{2,3}$-**217**: **^{1}H NMR** (400 MHz, $CDCl_3$) δ 4.65 (s, 1H), 4.63 (s, 1H), 4.58 (s, 1H), 4.56 (s, 1H) ppm and further signals could not be discerned; *mixture*: **IR** (neat) $\tilde{\nu}_{max}$ = 3342, 2932, 1712, 1524, 1250, 1168, 1023, 698 cm^{-1}; **HRMS** (ESI+) calcd. for $C_{29}H_{44}N_2O_6Na^+$ $[M+Na]^+$ 539.3091, found 539.3102.

2-(2,6,6-Trimethylcyclohex-2-en-1-yl)acetonitrile (**218**), prepared from geranyl nitrile (37.0 mg, 227 µmol); produced as a 55:32:13 mixture of regioisomers ($\Delta_{2,3}$-**218**, $\Delta_{1,2}$-**218**, and $\Delta_{2,7}$-**218**); yellow oil (33.3 mg, 204 µmol, 90%).

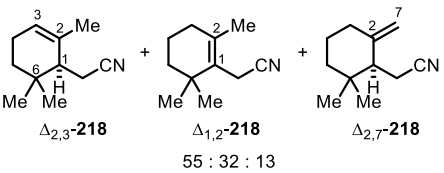

TLC: R_f = 0.33 (silica gel, hexanes/EtOAc; 95:5) [CAM]; $\Delta_{2,3}$-**218**: **^{1}H NMR** (500 MHz, $CDCl_3$) δ 5.50 (t, *J* = 3.3 Hz, 1H), 2.45 (dd, *J* = 17.3, 6.3 Hz, 1H), 2.37 (dd, *J* = 17.4, 4.6 Hz, 1H), 1.75 (q, *J* = 1.9 Hz, 3H), 1.01 (s, 3H), 0.93 (s, 3H) ppm and further signals could not be discerned. **^{13}C NMR** (75 MHz, $CDCl_3$) δ 132.4, 124.0, 120.2, 46.28, 32.36, 31.08, 27.82, 27.37, 27.01, 22.77, 17.78 ppm; $\Delta_{2,7}$-**218**: **^{1}H NMR** (500 MHz, $CDCl_3$) δ 4.95 (s, 1H), 4.74 (s, 1H), 2.55 (dd, *J* = 16.7, 4.3 Hz, 1H), 2.09 (dd, *J* = 7.8, 5.4 Hz, 1H), 0.99 (s, 3H), 0.80 (s, 3H) ppm and further signals could not be discerned; $\Delta_{1,2}$-**218**: **^{1}H NMR** (500 MHz, $CDCl_3$) δ 2.98 (s, 2H), 1.98 (t, *J* = 6.3 Hz, 2H), 1.70 (s, 3H), 1.04 (s, 6H) ppm and further signals could not be discerned.

The spectroscopic data are in accordance to those reported in the literature.[144]

Diethyl 2-((2,6,6-trimethylcyclohex-2-en-1-yl)methyl)malonate (**219**), prepared from diethyl 2-geranyl malonate (44.2 mg, 149 µmol); produced as a 44:23:33 mixture of inseparable regioisomers ($\Delta_{2,3}$-**219**, $\Delta_{2,7}$-**219**, and $\Delta_{1,2}$-**219**); colorless oil (38.0 mg, 128 µmol, 86%).

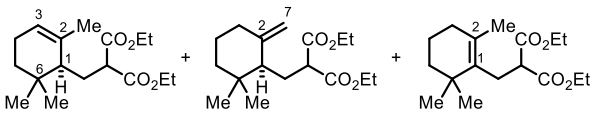

TLC: R_f = 0.32 (silica gel, hexanes/EtOAc; 90:10); $\Delta_{2,3}$-**219**: **^{1}H NMR** (400 MHz, $CDCl_3$) δ 5.30 (s, 1H), 4.23 – 4.13 (m, 4H), 3.52 (dd, *J* = 8.8, 6.6 Hz, 1H), 3.47 (t, *J* = 7.0 Hz, 1H), 1.68 (q, *J* = 1.7 Hz, 3H), 1.30 – 1.23 (m, 6H), 1.13 (dt, *J* = 13.6, 4.4 Hz, 1H), 0.93 (s, 3H), 0.87 (s, 3H) ppm and further signals could not be discerned; $\Delta_{2,7}$-**219**: **^{1}H NMR** (400 MHz, $CDCl_3$) δ 4.76 (s, 1H), 4.49 (s, 1H), 3.27 (dd, *J* = 11.2, 3.4 Hz, 1H), 2.12 (ddd, *J* = 14.1, 11.2, 3.1 Hz, 1H), 1.71 (dd, *J* = 12.2, 3.1 Hz, 1H), 0.86 (s, 3H), 0.82 (s, 3H) ppm and further signals could not be discerned; $\Delta_{1,2}$-**219**: **^{1}H NMR** (400 MHz, $CDCl_3$) δ 2.67 (d, *J* = 7.0 Hz, 2H), 1.50 (s, 3H), 0.92 (s, 6H) ppm and further signals could not be discerned; *mixture*: **^{13}C NMR** (75 MHz, $CDCl_3$) δ 170.3, 170.0, 169.9, 169.7, 148.1, 135.9, 134.1, 130.6, 121.2, 61.45, 61.42, 61.23, 52.89, 52.77, 51.66, 50.55, 46.80, 40.25, 34.94, 33.16, 32.91, 30.96, 30.35, 28.80, 28.40, 27.53, 27.30, 27.24, 26.21, 23.60, 23.48, 23.13, 20.58, 19.42, 14.29, 14.26, 14.23, 14.19 ppm.

The spectroscopic data are in accordance to those reported in the literature.[145]

2-((2,6,6-Trimethylcyclohex-2-en-1-yl)methyl)isoindoline-1,3-dione (**220**), prepared from *N*-geranyl phtalimide (18.5 mg, 65.4 µmol); produced as a 72:13:15 mixture of inseparable regioisomers ($\Delta_{2,3}$-**220**, $\Delta_{2,7}$-**220**, and $\Delta_{1,2}$-**220**); colorless oil (13.4 mg, 47.3 µmol, 72%).

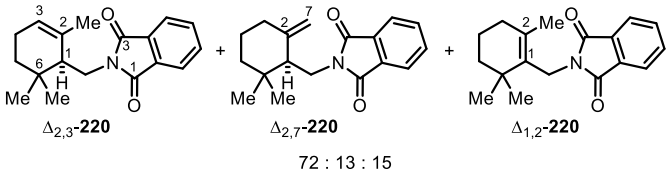

TLC: R_f = 0.37 (silica gel, hexanes/ EtOAc; 90:10); $\Delta_{2,3}$-**220**: **^{1}H NMR** (400 MHz, $CDCl_3$) δ 7.83 (dd, *J* = 5.4, 3.1 Hz, 2H), 7.70 (dd, *J* = 5.5, 3.0 Hz, 2H), 5.41 (s, 1H), 3.82 (dd, *J* = 14.0, 7.0 Hz, 1H), 3.54 (dd, *J* = 14.0, 5.9 Hz, 1H), 2.25 (t, *J* = 6.5 Hz, 1H), 2.10 – 1.96 (m, 2H), 1.72 (q, *J* = 1.9 Hz, 3H), 1.65 – 1.55 (m, 1H); 1.26 – 1.17 (m, 1H), 0.96 (s, 3H), 0.89 (s, 3H) ppm; **^{13}C NMR** (101 MHz, $CDCl_3$) δ 168.8, 134.0, 132.3, 123.3, 123.2, 122.8, 47.29, 40.21, 32.21, 30.40, 27.31, 26.96, 23.77, 23.20 ppm; $\Delta_{2,7}$-**220**: **^{1}H NMR** (400 MHz, $CDCl_3$) δ 4.59 (t, *J* = 2.2 Hz, 1H), 4.41 (t, *J* = 2.0 Hz, 1H), 4.00 (dd, *J* = 13.4, 12.2 Hz, 1H), 3.69 (dd, *J* = 13.4, 4.6 Hz, 1H) and further signals could not be discerned; $\Delta_{1,2}$-**220**: **^{1}H NMR** (400 MHz, $CDCl_3$) δ 4.39 (s, 2H), 1.81 (s, 3H), 1.04 (s, 3H) ppm and further signals could not be discerned; *mixture*: **IR** (neat) $\tilde{\nu}_{max}$ = 2916, 1771, 1713, 1436, 1398, 1353, 717 cm^{-1}; **HRMS** (ESI+) calcd. for $C_{18}H_{22}NO_2^+$ $[M+H]^+$ 284.1645, found 284.1646.

1,3,3-Trimethyl-2-oxabicyclo[2.2.2]octane (**162**), prepared from **161** (17.6 mg, 114 µmol); colorless liquid (13.5 mg, 87.5 µmol, 77%).

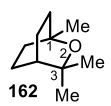

TLC: R_f = 0.63 (silica gel, hexanes/EtOAc; 95:5); **^{1}H NMR** (400 MHz, $CDCl_3$) δ 2.01 (tdd, *J* = 9.1, 3.8, 1.2 Hz, 2H), 1.73 – 1.57 (m, 2H), 1.56 – 1.43 (m, 4H), 1.39 (tq, *J* = 3.4, 1.2 Hz, 1H), 1.23 (s, 6H), 1.04 (s, 3H) ppm; **^{13}C NMR** (101 MHz, $CDCl_3$) δ 73.76, 69.92, 33.06, 31.63, 29.02, 27.71, 22.95 ppm.

The spectroscopic data are in accordance to those reported in the literature.[146]

2,2-Dimethyl-3,4-dihydro-2H-benzo[h]chromene-5,6-dione (**221**), prepared from lapachol (31.0 mg, 128 µmol); orange crystals (27.0 mg, 111 µmol, 87%).

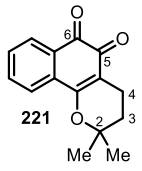

TLC: R_f = 0.20 (silica gel, hexanes/EtOAc; 80:20); **^{1}H NMR** (400 MHz, $CDCl_3$) δ 8.04 (dd, *J* = 7.6, 1.2 Hz, 1H), 7.80 (dd, *J* = 7.9, 1.2 Hz, 1H), 7.63 (td, *J* = 7.6, 1.4 Hz, 1H), 7.49 (td, *J* = 7.5, 1.2 Hz, 1H), 2.56 (t, *J* = 6.7 Hz, 2H), 1.85 (t, *J* = 6.7 Hz, 2H), 1.46 (s, 6H) ppm; **^{13}C NMR** (101 MHz, $CDCl_3$) δ 180.0, 178.7, 162.2, 134.9, 132.8, 130.8, 130.3, 128.7, 124.2, 112.9, 79.40, 31.74, 26.89 (2C), 16.29 ppm.

The spectroscopic data are in accordance to those reported in the literature.[147]

1,1,4a,10b-tetramethyl-1,2,3,4,4a,4b,5,6,10b,11,12,12a-dodecahydrochrysene (**225**), prepared from (*E*,*E*)-homofarnesyl benzene (35.2 mg, 119 µmol); colorless oil (24.3 mg, 82.1 µmol, 69%).

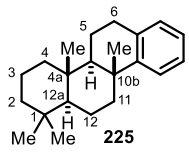

TLC: R_f = 0.56 (silica gel, *n*-hexane); **^{1}H NMR** (500 MHz, $CDCl_3$) δ 7.25 (d, *J* = 7.5 Hz, 1H), 7.12 (t, *J* = 7.5 Hz, 1H), 7.08 – 7.01 (m, 2H), 2.93 (ddd, *J* = 17.2, 6.6, 1.8 Hz, 1H), 2.86 – 2.78 (m, 1H), 2.39 (dd, *J* = 9.5, 3.2 Hz, 1H), 1.85-1.76 (m, 2H), 1.73 – 1.62 (m, 3H), 1.53 – 1.35 (m, 6H), 1.30 – 1.25 (m, 2H), 1.20 (s, 3H), 0.93 (s, 3H), 0.87 (s, 3H), 0.86 (s, 3H); **^{13}C NMR** (126 MHz, $CDCl_3$) δ 150.6, 135.3, 128.9, 125.8, 125.2, 124.7, 56.40, 55.30, 42.20, 40.71, 39.95, 38.29, 37.80, 33.48, 33.44, 31.02, 26.31, 21.60, 19.27, 18.76, 18.09, 16.44 ppm.

The spectroscopic data are in accordance to those reported in the literature.[59]

(2,5,5,8a-Tetramethyl-1,4,4a,5,6,7,8,8a-octahydronaphthalen-1-yl)methyl acetate (**226**), prepared from (*E*,*E*)-farnesyl acetate (39.4 mg, 149 µmol); produced as a 65:35 mixture of inseparable diastereoisomers at *C*1; clear oil (25.9 mg, 98.0 µmol, 66%).

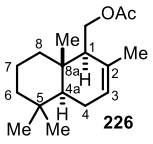

226

TLC: R_f = 0.61 (silica gel, hexanes/EtOAc; 90:10); *major diastereoisomer*: **^{1}H NMR** (300 MHz, $CDCl_3$) δ 5.52 – 5.42 (m, 1H), 4.24 (dd, *J* = 11.6, 3.3 Hz, 1H), 4.08 (dd, *J* = 11.7, 6.4 Hz, 1H), 2.03 (s, 3H), 2.05 – 1.82 (m, 4H), 1.67 (dt, *J* = 2.5, 1.4 Hz, 3H), 1.54 – 1.37 (m, 3H), 1.24 – 1.08 (m, 3H), 0.89 (s, 3H), 0.86 (s, 3H), 0.81 (s, 3H) ppm; *minor diastereoisomer*: **^{1}H NMR** (300 MHz, $CDCl_3$) δ 5.44 (br s, 1H) ppm and further signals could not be discerned; *mixture*: **^{13}C NMR** (101 MHz, $CDCl_3$) δ 171.3, 132.7, 123.8, 63.36, 53.52, 50.01, 42.23, 39.70, 36.10, 33.45, 33.11, 23.75, 22.08, 21.85, 21.40, 18.87, 14.62 ppm.

The spectroscopic data are in accordance to those reported in the literature.[148]

(2,5,5,8a-Tetramethyl-1,4,4a,5,6,7,8,8a-octahydronaphthalen-1-yl)methyl 3,5-dimethoxybenzoate (**227**), prepared from (*E*,*E*)-farnesyl 3,5-dimethoxybenzoate (48.2 mg, 125 µmol); produced as a 65:35 mixture of inseparable diastereoisomers at *C*1; clear oil (29.7 mg, 76.8 µmol, 62%).

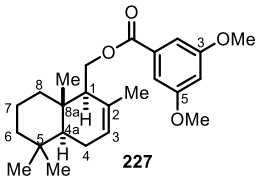

227

TLC: R_f = 0.61 (silica gel, hexanes/EtOAc; 90:10); *major diastereoisomer*: **^{1}H NMR** (400 MHz, $CDCl_3$) δ 7.17 (d, *J* = 2.3 Hz, 2H), 6.64 (t, *J* = 2.4 Hz, 1H), 5.56 – 5.53 (m, 1H), 4.55 (dd, *J* = 11.7, 3.4 Hz, 1H), 4.30 (dd, *J* = 11.7, 6.0 Hz, 1H), 3.82 (s, 6H), 2.18 (br s, 1H), 2.08 – 1.86 (m, 2H), 1.74 (s, 3H), 1.64 – 1.53 (m, 2H), 1.52 – 1.38 (m, 3H), 1.25 (q, *J* = 5.1 Hz, 1H), 1.17 (dd, *J* = 12.9, 3.9 Hz, 1H), 0.90 (s, 6H), 0.88 (s, 3H) ppm; *minor diastereoisomer*: **^{1}H NMR** (400 MHz, $CDCl_3$) δ 5.48 (t, *J* = 7.4 Hz, 1H), 1.00 (s, 3H) ppm and further signals could not be discerned; **^{13}C NMR** (75 MHz, $CDCl_3$) δ 166.5, 160. 8, 132.6, 132.5, 124.1, 107.3, 105.7, 63.85, 55.68, 53.77, 50.04, 42.23, 39.83, 36.21, 33.48, 33.13, 23.80, 22.12, 22.05, 18.90, 14.87; **IR** (KBr) $\tilde{\nu}_{max}$ = 2926, 1716, 1598, 1459, 1303, 1230, 1157, 1052, 759 cm^{-1}; **HRMS** (ESI+) calcd. for $C_{24}H_{35}O_4^+$ $[M+H]^+$ 387.2530, found 387.2537.

(±)-sclareolide (**23**), prepared from (*E*,*E*)-homofarnesoic acid (31.0 mg, 124 µmol); colorless solid (17.7 mg combined, 70.7 µmol, 57%); *minor 9-epi-sclareolide could not be separated from side products.*

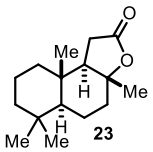

23

(±)-23: **TLC:** R_f = 0.44 (silica gel, hexanes/EtOAc; 80:20) [$KMnO_4$]; **^{1}H NMR** (300 MHz, $CDCl_3$) δ 2.41 (dd, *J* = 16.2, 14.7 Hz, 1H), 2.23 (ddd, *J* = 16.2, 6.5, 0.6 Hz, 1H), 2.08 (dt, *J* = 11.8, 3.3 Hz, 1H), 1.97 (dd, *J* = 14.7, 6.5 Hz, 1H), 1.88 (ddt, *J* = 14.0, 4.2, 2.9 Hz, 1H), 1.75 – 1.62 (m, 2H), 1.51 – 1.35 (m, 4H), 1.33 (d, *J* = 1.0 Hz, 3H), 1.19 (td, *J* = 13.6, 4.3 Hz, 1H), 1.04 (ddd, *J* = 13.8, 10.3, 3.3 Hz, 2H), 0.91 (s, 3H), 0.89 (s, 3H), 0.84 (s, 3H) ppm; **^{13}C NMR** (75 MHz, $CDCl_3$) δ 177.0, 86.52, 59.28, 56.82, 42.33, 39.67, 38.88, 36.22, 33.32, 33.28, 28.87, 21.72, 21.07, 20.71, 18.24, 15.22 ppm.

The spectroscopic data are in accordance to those reported in the literature.[149]

8. NXS, Morpholine and HFIP: The Ideal Combination for Biomimetic Haliranium-Induced Polyene Cyclizations[64]

— SUPPORTING INFORMATION —

NXS, Morpholine, and HFIP: The Ideal Combination for Biomimetic Haliranium-induced Polyene Cyclizations

Andreas M. Arnold,[a,b] Alexander Pöthig,[b] Markus Drees,[b] and Tanja Gulder[a,b*]

[a]*Biomimetic Catalysis, Department of Chemistry, Technical University of Munich, Lichtenbergstrasse 4, 85747 Garching, Germany*
[b]*Catalysis Research Center, Technical University of Munich, Ernst-Otto-Fischer-Straße 1, 85748 Garching, Germany*
*corresponding author: tanja.gulder@tum.de

Content

1. General Information

Solvents used in reactions were p.A. grade. Solvents for chromatography were technical grade and distilled prior to use. Anhydrous dichloromethane, diethylether and THF were obtained from a MBraun MB-SPS 800 solvent purification system. Other dry solvents were obtained from Fluka and Acros in the highest purity available and used without further purification. 1,1,1,3,3,3-Hexafluoroisopropanol (HFIP) was purchased from Fluorochem with a purity >99% and dried over activated 3Å molecular sieve for at least 48 h before use. *N*-Bromosuccinimide (NBS) was purchased from Carbolution Chemicals and recrystallized from water. *N*-Iodosuccinimide (NIS) was purchased from Carbolution Chemicals, 1,3-Dichloro-5,5-dimethyl hydanthoin (DCDMH) and BDSB (**17**) were purchased from Sigma-Aldrich, respectively, and used as received. Other reagents were purchased at the highest commercial quality and used without further purification. Yields refer to chromatographically and spectroscopically (^{1}H NMR) homogeneous materials, unless otherwise stated. Reactions were monitored by thin layer chromatography (TLC) carried out on Merck silica gel aluminium plates with F-254 indicator using UV light as the visualizing agent (UV), basic potassium permanganate solution ($KMnO_4$), ceric ammonium molybdate (CAN), and heat as developing agents. Silica gel Merck 60 (particle size 40 – 63 µm) was used for flash column chromatography. Solvent mixtures are understood as volume/volume. NMR spectra were recorded on Bruker AV300, Bruker AV400, Bruker AV500, or Bruker AV500-cryo spectrometers. The spectra were calibrated using residual undeuterated solvent as an internal reference ($CDCl_3$ @ 7.26 ppm, D_2O @ 4.79 ppm ^{1}H NMR, $CDCl_3$ @ 77.16 ppm ^{13}C NMR). The following abbreviations (or combinations thereof) were used to explain the multiplicities: s = singlet, d = doublet, dd = doublet of doublets, t = triplet, dt = doublet of triplets, q = quartet, p = pentet, quint = quintet (with 1:2:3:2:1 intensity), hept = heptet, m = multiplet, br = broad. In addition, the following abbreviations were used: EtOAc = ethyl acetate, MeCN = acetonitrile, DCM = dichloromethane, PFTB = perfluoro-*tert*-butanol, TFE = 1,1,1-trifluoroethanol, PFNP = 2,2,3,3,3-pentafluoro-1-propanol, TFA = trifluoroacetic acid, Oxone = potassium peroxymonosulfate triple salt, FA = formic acid, TLC = thin layer chromatography, rt = room temperature, sat. = saturated. Melting points were measured on a Büchi 510 and are not calibrated. IR spectra were recorded on a JASCO FT-IR-4100 (ATR) and are reported in terms of frequency of absorption (cm^{-1}). Mass spectra were conducted on a Finnigan MAT SSQ 7000 (MS-EI, 70 eV; CI, 100 eV), or a Thermo Scientific LTQ-FT ultra and ThermoFisher Scientific LTQ Orbitrap XL spectrometer (ESI HRMS).

2. Optimization of the Reaction Conditions

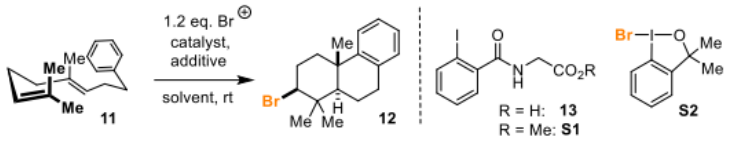

22.8 mg Homogeranyl benzene (**11**, 100 µmmol, 1.0 eq), 10.0 µmol additive (0.1 eq) and 10.0 µmol catalyst (0.1 eq) were mixed in 1.0 mL solvent. Then, 120 µmol electrophilic bromine source (1.2 eq) was added to the mixture at room temperature.

Table S1. Hypervalent Iodane catalyzed bromiranium-induced cyclizations of **11**.

Entry	Br^+ source	Solvent	Catalyst	Additive	Yield **12**[a]	d.r.[b]
1[c]	NBS	DCM	**13**	NH_4Cl_{solid}	<5%[d]	n.d.
2	NBS	DCM	**13**	NH_4Cl_{aq}	<5%[d]	n.d.
3	NBS	DCM	**S1**	NH_4Cl_{aq}	<5%[d]	n.d.
4	NBS	HFIP	**13**	–	33%	80:20
5[e]	KBr (3.0 eq)/oxone (1.1 eq.)	HFIP	**13**	–	<5%	n.d.
6	**S2**	HFIP	–	–	41%	77:23
7	NBS	HFIP	–	–	42%	79:21

[a]yield determined by ^{1}H-NMR spectroscopy using an internal standard. [b]determined from the ^{1}H-NMR spectrum of the crude mixture. [c]48 h reaction time. [d]complex product mixture. [e]1 drop of water was added to enhance solubility of KBr and oxone.

22.8 mg Homogeranyl benzene (**11**, 100 µmmol, 1.0 eq) was dissolved in 1.0 mL solvent. Then, 120 µmol electrophilic bromine source (1.2 eq) was added to the mixture at room temperature.

Table S2. Screening of various Br^+ sources and solvents.

Entry	Br^+ source	Solvent	Yield **12**[a]	d.r.[b]
1	NBS	HFIP	42%	79:21
2	**S3**	HFIP	27%	78:22
3	**S4**	HFIP	17%	77:23
4	**S5**	HFIP	21%	73:27
5	**S6**	HFIP	32%	79:21
6	**S7**	HFIP	39%	80:20
7	NBS	*i*PrOH	<5%[c]	n.d.
8	NBS	DCM	8%[c]	n.d.
9	NBS	MeCN	12%[d]	n.d.

[a]yield determined by ^{1}H-NMR spectroscopy using an internal standard. [b]determined from the ^{1}H-NMR spectrum of the crude mixture. [c]reaction stirred for 24 h. Mainly acyclic *i*PrO/Br addition product observed. [d]reaction stirred for 24 h. Monocyclic product observed as the main product.

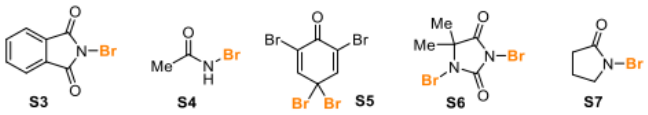

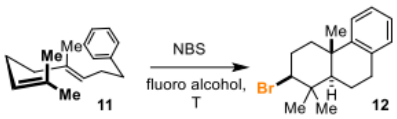

22.8 mg Homogeranyl benzene (**11**, 100 µmmol, 1.0 eq) was dissolved in 1.0 mL solvent. Then, 21.4 mg NBS (120 µmmol, 1.2 eq) was added to the mixture at the given temperature.

Table S3. Variation of fluorinated alcohols as solvent at different temperatures.

Entry	Solvent	T	Yield **12**[a]	d.r.[b]
1	HFIP	rt	42%	79:21
2	TFE	rt	18%	n.d.
3	TFE	–20 °C	<5%	n.d.
4	PFTB	0 °C	<5%	n.d.
5	PFNP	0 °C	17%	n.d.
6[c]	HFIP	0 °C	68%	79:21

[a]yield determined by ^{1}H-NMR spectroscopy using an internal standard. [b]determined from the ^{1}H-NMR spectrum of the crude mixture. [c]reaction was terminated after 1 minute.

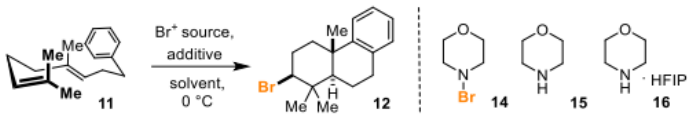

22.8 mg Homogeranyl benzene (**11**, 100 µmmol, 1.0 eq) and 140 µmol additive (1.4 eq) were mixed in 1.0 mL solvent. Then, 120 µmol of the electrophilic bromine source (1.2 eq) was added to the mixture at 0 °C.

Table S4. Screening of different *N*-bromo reagents at 0 °C.

Entry	Br^+ source	Solvent	Additive	Yield **12**[a]	d.r.[b]
1	NBS	HFIP	–	68%	79:21
2	**14**	HFIP	–	62%	>95:5
3	**14**	DCM	–	23%	>95:5
4	**14**	$MeNO_2$	–	27%	>95:5
5[c]	NBS	HFIP	**15**	72%	>95:5
6[d]	NBS	HFIP	**15**	78%	>95:5
7[d]	NBS	HFIP	**16**	78% (76%)[e]	>95:5
8[d]	NBS	HFIPMe	**15**	<5%	n.d.
9[d]	NBS	TFE	**15**	35%	>95:5
10[d]	NBS	PFTB	**15**	13%	>95:5

[a]yield determined by ^{1}H-NMR spectroscopy using an internal standard. [b]determined from the ^{1}H-NMR spectrum of the crude mixture. [c]additive was mixed with NBS for 1 min at 0 °C prior to the addition of **11**. [d]additive was mixed with NBS for 10 min at 0 °C prior to the addition of **11**. [e]isolated yield.

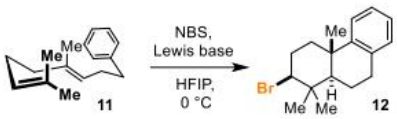

120 µmol bromine source (1.2 eq) and 140 µmol Lewis base (1.4 eq) were mixed in 1.0 mL HFIP. After 10 min, 22.8 mg homogeranyl benzene (**11**, 100 µmmol, 1.0 eq) was added to the mixture at 0 °C.

Table S5. Screening of different *N*-bromo reagents.

Entry	Additive	Conversion	Yield **12**[a]	d.r.[b]
1	Pyrrolidine	>95%	62%	91:9
2	Pyridine	71%	40%	78:22
3	Pyrrole	>95%	<5%	n.d
4	2,2,6,6-Tetramethylpiperidine	75%	42%	80:20
5	1,4-Diazabicyclo[2.2.2]octan (DABCO)	78%	37%	79:21
6	(*S*)-Proline	64%	33%	81:19
7	AcONa	>95%	50%	77:23
8	2,4,6-Trimethylaniline	>95%	<5%	n.d.
9	*N*,*O*-Dimethylhydroxylamine · HCl	>95%	7%	83:17
10	*n*-Butylamine	89%	51%	86:14
11	PPh_3	<5%	<5%	n.d.
12	Piperidine	>95%	63%	>95:5
13	*N*-Methylmorpholine	59%	45%	86:14
14	**15**	>95%	78%	>95:5
15	**16**	>95%	78%	>95:5
16	Morpholine HCl salt	>95%	35%	90:10
17	Morpholine TFA salt	>95%	40%	84:16

[a]yield determined by ^{1}H-NMR spectroscopy using an internal standard. [b]determined from the ^{1}H-NMR spectrum of the crude mixture.

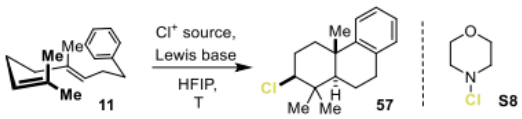

The electrophilic chlorine reagent and **16** were mixed in 1.0 mL HFIP at temperature T_1. After stirring for 1 h, 22.8 mg homogeranyl benzene (**11**, 100 µmol, 1.0 eq) were added at temperature T_2 and stirred for the time given.

Table S6. Screening of chlorination conditions.

Entry	Cl^+ source	**16** (eq)	T_1	T_2	t	Conversion	Yield[a]	d.r.[b]
1	DCDMH (0.60 eq)	0	–[c]	rt	5 min	>95%	16%	50:50
2	NCS (1.20 eq)	1.4	0 °C[d]	0 °C	30 min	81%	19%	56:44
3	**S8** (3.00 eq)	1.4	–[c]	0 °C	30 min	78%	22%	66:34
4	DCDMH (0.60 eq)	1.4	rt	rt	30 min	>95%	25%	65:35
5	DCDMH (0.65 eq)	1.4	rt	0 °C	1 h	>95%	39%	72:28
6	DCDMH (1.34 eq)	1.7	rt	0 °C	30 min	>95%	43% (32%)[e]	76:24

[a]yield determined by ^{1}H-NMR spectroscopy using an internal standard. [b]determined from the ^{1}H-NMR spectrum of the crude mixture. [c]Cl reagent was added directly to a solution of **11** in HFIP without **16** at temperature T_2. [d]NCS was stirred for 10 min at 0 °C with **16**. [e]isolated yield of the major isomer.

3. NMR Investigations on the in-situ Formation of NBM (14)

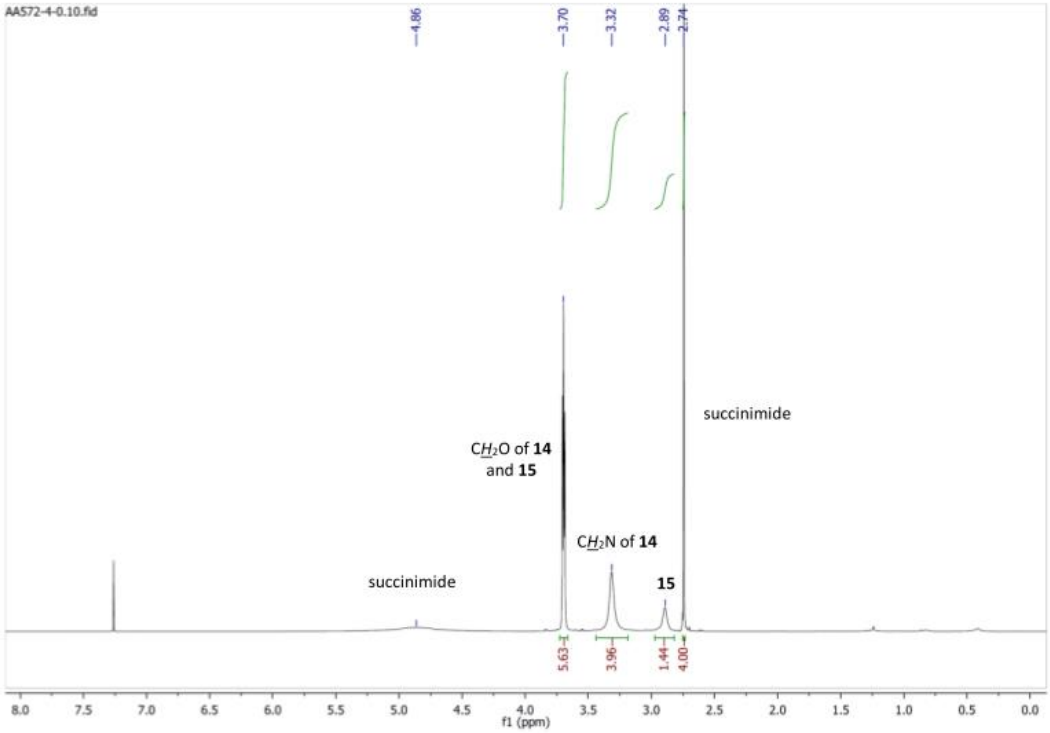

Figure S1. ^{1}H-NMR spectrum of 1.35 eq. morpholine (**15**) and 1.00 eq. NBS in $CDCl_3$.

4. NMR Investigations on the Interaction of HFIP with NBS

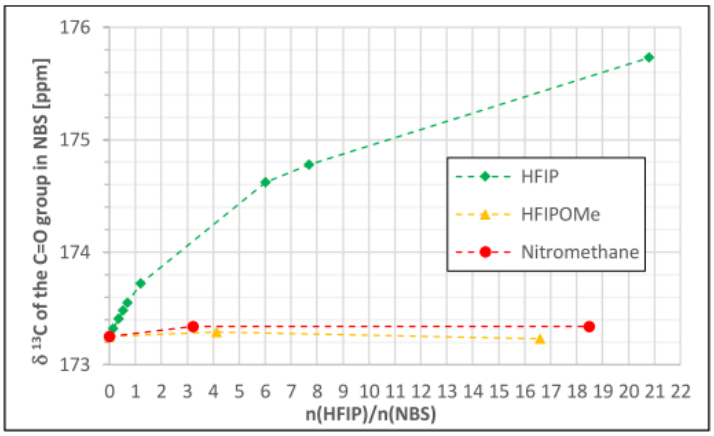

Figure S2. NMR titration curves of NBS with HFIP in $CDCl_3$ at 300 K.

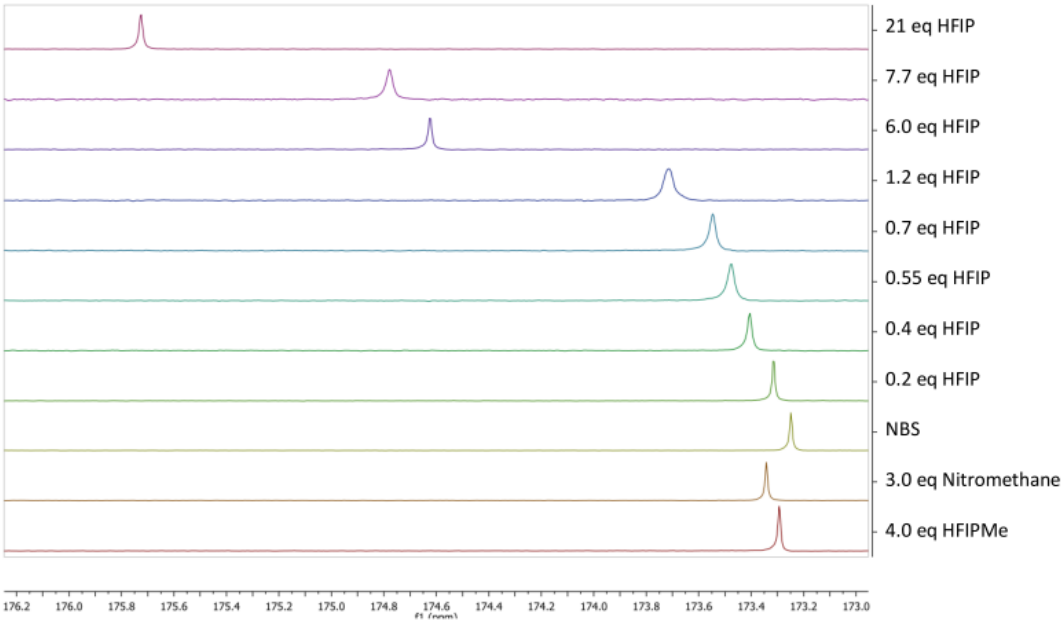

Figure S3. ^{13}C-shift of the NBS C=O group (0.1 M NBS in $CDCl_3$) upon addition of HFIP, nitromethane and HFIPMe, respectively, at 300 K, recorded with 125 MHz. The precise molar ratio of the mixtures was determined from the ^{1}H-NMR spectrum (500 MHz).

5. NMR Investigations on the Interaction of HFIP with NBM (14)

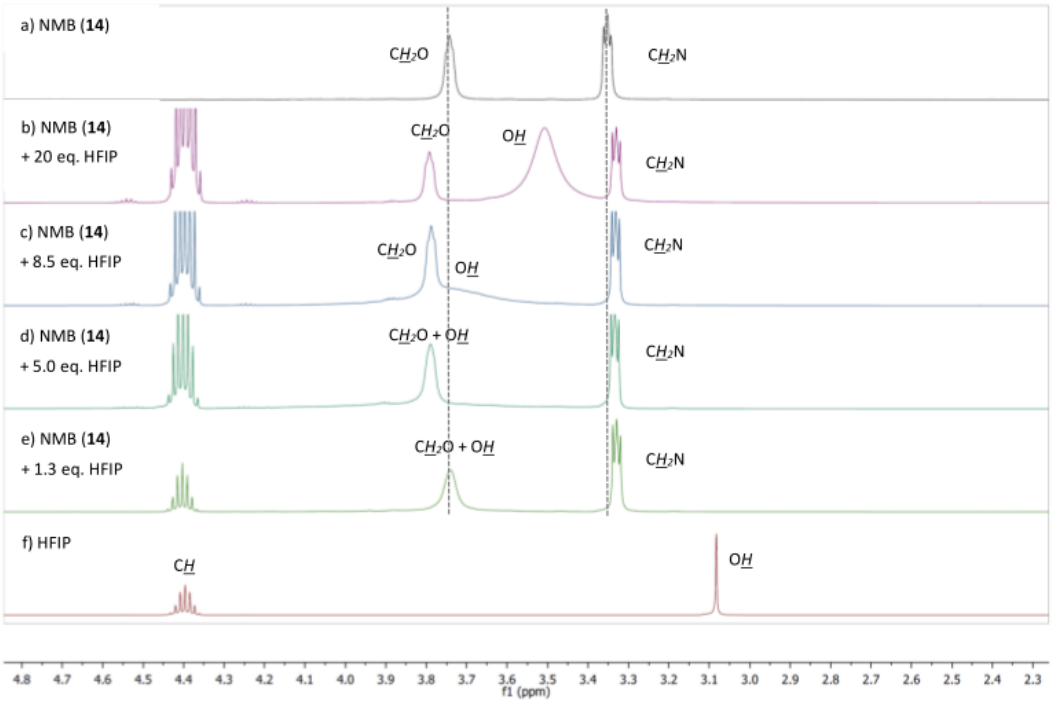

Figure S4. NMR study of 0.3 M *N*-bromo morpholine (**14**) mixtures with increasing amounts of HFIP in $CDCl_3$ (0.6 mL) at 300 K, recorded with 500 MHz. In entry d and e the signal of the HFIP-OH group overlapped with that of the CH_2O-moiety of **14**.

6. Determination of Halogenating Ability of *N*-Chloro Morpholine (S8)

In order to investigate the halogenating ability of *N*-chloro morpholine (**S8**) in comparison with other chlorinating agents,[1] 0.5 mL of a 0.1 M solution of collidine (**S9**, 50.0 µmol, 1.0 eq) were added to 50.0 µmol (1.0 eq) halogen source in abs. $CDCl_3$ in an NMR tube. A ^1H NMR spectrum was recoreded (Figure S5).

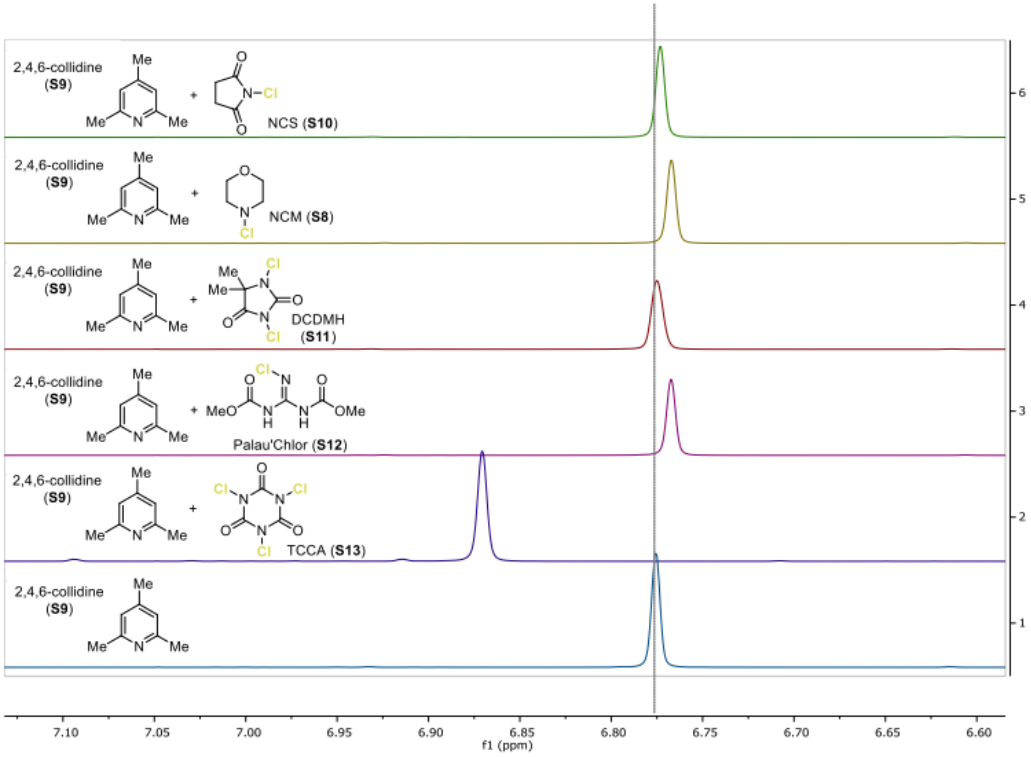

Figure S5. ^1H-NMR study of *N*-chloro reagents (0.1 M, 1.0 eq.) with 1.0 eq 2,4,6-collidine (**S9**) in $CDCl_3$.

In order to test the influence of the solvent HFIP on the chlorinating ability of **S8** compared to other common electrophilic halogenation reagents, increasing equivalents of HFIP were added to the NMR tube next, followed by subsequent 1H-NMR measurments. As standard, the same series of experiments has been conducted without adding any chloro reagent (Figure S6).

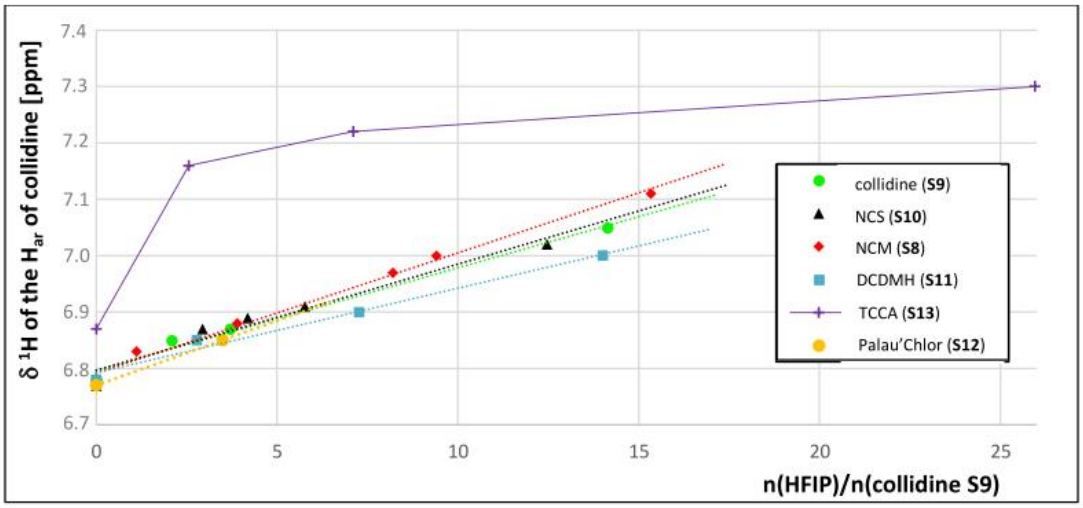

Figure S6. Titration of 1.0 eq chlorinating reagent **S8**, **S10** – **S13**, 1.0 eq collidine (**S9**) and increasing equivalents of HFIP.

In $CDCl_3$ the resonance of the aryl proton in collidine (**S9**) was significantly shifted to higher field upon addition of *N*-chloro morpholine (**S8**), indicating a halogen bonding interaction of **S8** and **S9** rather than a complete chlorenium ion transfer. In contrast, the collidine-aryl-H signal displayed a downfield shift in a mixture of HFIP/$CDCl_3$, which enhanced with increasing amounts of HFIP. This effect nicely corroborates the decisive impact of HFIP on the halogenating ability of **S8**. In HFIP, **S8** is more activated than other commonly used chlorenium sources and, as a consequence, it becomes more productive (selective) as observed in the described chloro cyclization.

7. General Procedures

7.1 Cyclization Procedure GP-A using NBS or NIS

119 mg Morpholine-HFIP salt (**16**, 280 µmol, 1.4 eq) were disolved in HFIP (2.0 mL) and the mixture cooled to 0 °C. 42.7 mg NBS (240 µmol, 1.2 eq) and 54.0 mg NIS (240 µmol, 1.2 eq), respectively, were added in one portion and the solution stirred for 10 minutes (NBS) or 5 min (NIS). Next, 200 µmol substrate (1.0 eq) were added to the solution and the mixture stirred for futher 20 min (NBS) or 10 min (NIS). The reaction was terminated by the addition of freshly prepared 10% aq. Na_2SO_3 solution (2.0 mL), the suspension stirred for 5 minutes, poured into water (20 mL) and extraced with EtOAc/*n*-hexane (1:1, 10 mL, 2×). The combined organic layers were washed with brine (20 mL), dried over $MgSO_4$, and filtered. The solvent was removed under reduced pressure, the d.r. determined by ^{1}H NMR from the crude sample (where applicable), and the combined crude product purified by column chromatography.

7.2 Cyclization Procedure GP-B using NBS or NIS

119 mg Morpholine-HFIP salt (**16**, 280 µmol, 1.4 eq) were disolved in HFIP (1.0 mL) and the mixture cooled to 0 °C. 42.7 mg NBS (240 µmol, 1.2 eq) and 54.0 mg NIS (240 µmol, 1.2 eq), respectively, were added in one portion and the solution stirred for 10 minutes (NBS) or 5 min (NIS). This solution was then added dropwise to a stirring emulsion of 200 µmol substrate (1.0 eq) in HFIP (1.0 mL) at 0 °C. After stirring for another 20 min (NBS) or 10 min (NIS) at 0 °C, the reaction was terminated by the addition of freshly prepared 10% aq. Na_2SO_3 solution (2.0 mL). The suspension was stirred for 5 minutes, poured into water (20 mL) and extraced with EtOAc/*n*-hexane (1:1, 10 mL, 2×). The combined organic layers were washed with brine (20 mL), dried over $MgSO_4$, and filtered. The solvent was removed under reduced pressure, the d.r. determined by ^{1}H NMR from the crude sample, and the combined crude product purified by column chromatography.

7.3 Cyclization Procedure GP-C using NBS or NIS

102 mg Morpholine-HFIP salt (**16**, 240 µmol, 1.2 eq) were disolved in HFIP (1.0 mL) and the mixture cooled to 0 °C. 33.8 mg NBS (190 µmol, 0.95 eq) and 42.8 mg NIS (190 µmol, 0.95 eq), respectively, were added in one portion and the solution stirred for 10 minutes (NBS) or 5 min (NIS). This solution was then added

dropwise to a stirring emulsion of 200 µmol substrate (1.0 eq) in HFIP (1.0 mL) at 0 °C. After stirring for another 20 min (NBS) or 10 min (NIS) at 0 °C, the reaction was terminated by the addition of freshly prepared 10% aq. Na_2SO_3 solution (2.0 mL). The suspension was stirred for 5 minutes, poured into water (20 mL) and extraced with EtOAc/*n*-hexane (1:1, 10 mL, 2×). The combined organic layers were washed with brine (20 mL), dried over $MgSO_4$, and filtered. The solvent was removed under reduced pressure, the d.r. determined by ^1H NMR from the crude sample, and the combined crude product purified by column chromatography.

7.4 Cyclization Procedure GP-D using NBS (10 mmol scale)

1.22 g Morpholine (**15**, 14.0 mmol, 1.4 eq) were placed in a 250 mL round bottom flask and dissolved in 70 mL abs. HFIP. The mixture was cooled to 0 °C and 2.14 g NBS (12.0 mmol, 1.2 eq.) were added in 3 portions over 30 seconds. After 10 minutes, 1.54 g geraniol (**34**, 10.0 mmol, 1.0 eq.) were added dropwise and the reaction mixture stirred for 30 minutes at 0 °C. The reaction was terminated by the addition of freshly prepared 10% aq. Na_2SO_3 solution (50 mL), the mixture stirred for 5 minutes, and the phases separated. The lower HFIP phase was withdrawn and recycled by destillation (62 mL recovered), and the residue diluted with EtOAc/*n*-hexane (1:1, 70 mL) and poured back into the separation funnel. The phases were separated, the aqueous phase extraced with EtOAc/*n*-hexane (2:1, 70 mL, ×2), the combined organic layers then washed with brine (70 mL), dried over $MgSO_4$, and filtered. The solvent was removed under reduced pressure and the crude product purified by column chromatography.

7.5 Cyclization Procedure GP-E using DCDMH

71.4 mg Morpholine-HFIP salt (**16**, 280 µmol, 1.4 eq) were disolved in HFIP (1.0 mL) at rt. 23.6 mg DCDMH (120 µmol, 0.6 eq) were added in one portion and the solution stirred for 1 h at rt. This solution was then added dropwise to a stirring emulsion of 200 µmol substrate (1.0 eq) in HFIP (1.0 mL) at 0 °C. After the addition the mixture was stirred for another 30 min. The reaction was terminated by the addition of freshly prepared 10% aq. Na_2SO_3 solution (2.0 mL), the inhomogeneous mixture stirred for 5 min., poured into water (20 mL) and extraced with EtOAc/*n*-hexane (1:1, 10 mL, 2×). The combined organic layers were washed with brine (20 mL), dried over $MgSO_4$, and filtered. The solvent was removed under reduced

pressure, the d.r. determined by ^{1}H NMR from the crude sample, and the combined crude product purified by column chromatography.

7.6 Cyclization Procedure (GP-F) using BDSB (17)

According to the literature procedure,[2] 54.9 mg BDSB (100 µmol, 1.0 eq) were dissolved in 0.5 mL abs. $MeNO_2$. The solution was added quickly to 100 µmol of the substrate (1.0 eq) dissolved in 1.5 mL abs. $MeNO_2$ at –25 °C. After stirring for 5 min, the reaction was stopped by the addition of freshly prepared 5% aq. $NaHCO_3$/5% aq. Na_2SO_3 solution (1:1, 5 mL), the mixture stirred for 15 min and then poured into water (5 mL). After extraction with DCM (5 mL, ×3), the combined organic layers were dried over $MgSO_4$. The solvent was removed under reduced pressure and the crude product subjected to NMR analysis.

7.7 Preparation of Morpholine-HFIP Salt (16)

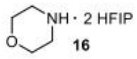

16

Morpholine-HFIP salt (**16**): 11.5 g abs. HFIP (7.2 mL, 68.2 mmol, 2.5 eq) were quickly added to 2.38 g neat morpholine (**15**, 27.3 mmol, 1.0 eq) in a round bottom flask under argon. A cristalline solid formed, which was, upon complete crystallization, suspended in abs. DCM (10 mL) and cooled to 0 °C for 10 minutes for further precipitation. The solid was then filtered, washed with cold DCM (10 mL) and dried for 1 h under vacuum at 40 °C to afford the product **16** as colorless crystals (6.57 g, 15.5 mmol, 57%); **m.p.** = 57 – 58 °C (DCM); **^{1}H NMR** (300 MHz, D_2O) δ 4.72 (dt, *J* = 13.2, 6.6 Hz, 2H, CH), 3.82 – 3.75 (m, 4H, CH_2), 3.02 – 2.96 (m, 4H, CH_2) ppm [Note: Due to signal overlap with the solvent, integration was performed for half the dt of HFIP resulting in an integral of 1.02]; **^{1}H NMR** (500 MHz, $CDCl_3$) δ 4.41 (br s, 1H, OH, NH), 4.34 (hept, *J* = 6.2 Hz, 1H, CH), 3.77 – 3.66 (m, 4H, CH_2), 2.94 – 2.82 (m, 4H, CH_2); **Anal. Calcd.** for $C_{10}H_{13}F_{12}NO_2$: C: 28.38; H: 3.10, N: 3.31. Found: C: 28.22; H: 3.09; N: 3.33.

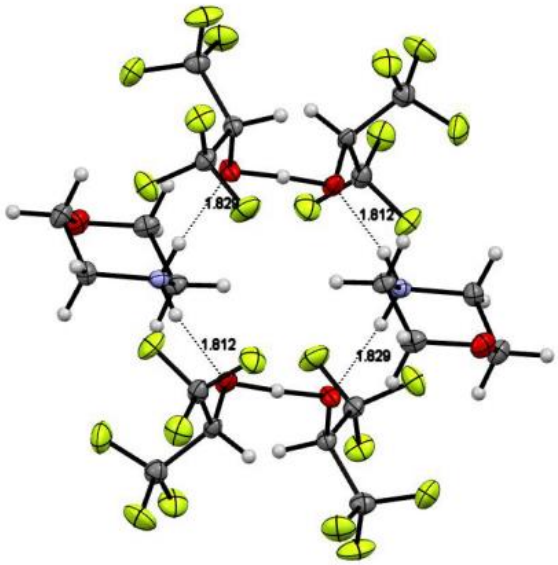

Figure S7. H-Bonding network with 4 molecules HFIP and 2 molecules morpholine in **16** (CCDC 1584440).

8. Physical and Spectroscopic Data of Bromocyclized Products

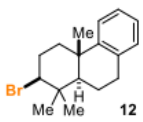

2-Bromo-1,1,4a-trimethyl-1,2,3,4,4a,9,10,10a-octahydrophenanthrene (**12**), prepared from **11** (43.4 mg, 190 µmol) by GP-A; colorless solid (44.4 mg, 144 µmol, 76%; d.r. >95:5); **TLC:** R_f = 0.32 (silica gel, *n*-hexane); **^{1}H NMR** (400 MHz, $CDCl_3$) δ 7.21 (d, *J* = 7.4 Hz, 1H), 7.16 – 7.05 (m, 3H), 4.06 (dd, *J* = 12.7, 4.2 Hz, 1H), 3.02 – 2.83 (m, 2H), 2.45 – 2.22 (m, 3H), 1.98 (dt, *J* = 12.1, 4.7 Hz, 1H), 1.89 – 1.76 (m, 1H), 1.65 – 1.54 (m, 1H), 1.48 (dd, *J* = 12.2, 2.2 Hz, 1H), 1.26 (s, 3H, CH_3), 1.17 (s, 3H, CH_3), 1.08 (s, 3H, CH_3) ppm; **^{13}C NMR** (101 MHz, $CDCl_3$) δ 148.8, 134.9, 129.2, 126.0, 125.7, 124.6, 69.01, 51.36, 40.17, 40.02, 38.02, 31.68, 30.92, 30.68, 25.04, 20.74, 18.40 ppm.

The spectroscopic data are in accordance to those reported in the literature.[2]

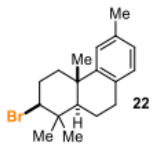

2-Bromo-1,1,4a,6-tetramethyl-1,2,3,4,4a,9,10,10a-octahydrophenanthrene (**22**), prepared from **18** (48.9 mg, 202 µmol) by GP A; colorless solid (46.7 mg, 145 µmol, 72%; d.r. >95:5); **TLC:** R_f = 0.29 (silica gel, *n*-hexane); **^{1}H NMR** (400 MHz, $CDCl_3$) δ 6.86 – 6.83 (m, 1H), 6.82 – 6.73 (m, 2H), 3.88 (dd, *J* = 12.6, 4.1 Hz, 1H), 2.71 (qdd, *J* = 18.1, 16.8, 9.2, 4.5 Hz, 2H), 2.23 – 2.14 (m, 2H), 2.13 (s, 3H, CH_3), 2.12 – 2.04 (m, 1H), 1.79 (ddt, *J* = 13.3, 7.0, 2.2 Hz, 1H), 1.63 (dtd, *J* = 13.3, 11.6, 6.7 Hz, 1H), 1.46 – 1.37 (m, 1H), 1.29 (dd, *J* = 12.0, 2.2 Hz, 1H), 1.08 (d, *J* = 0.8 Hz, 3H, CH_3), 1.00 (s, 3H, CH_3), 0.90 (s, 3H, CH_3) ppm; **^{13}C NMR** (75 MHz, $CDCl_3$) δ 148.7, 135.3, 131.7, 129.1, 126.6, 125.1, 69.15, 51.52, 40.23, 40.05, 37.98, 31.72, 30.72, 30.55, 25.01, 21.41, 20.83, 18.41 ppm.

The spectroscopic data are in accordance to those reported in the literature.[3]

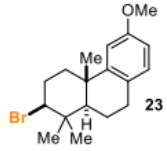

2-Bromo-6-methoxy-1,1,4a-trimethyl-1,2,3,4,4a,9,10,10a-octahydrophenanthrene (**23**), prepared from **19** (42.2 mg, 163 µmol) by GP-B; colorless solid (46.6 mg, 138 µmol, 85%; d.r. >95:5), **TLC:** R_f = 0.65 (silica gel, *n*-hexane/EtOAc; 9:1); **^{1}H NMR** (300 MHz, $CDCl_3$) δ 6.97 (dd, *J* = 8.3, 1.0 Hz, 1H), 6.74 (d, *J* = 2.6 Hz, 1H), 6.72 – 6.64 (m, 1H), 4.04 (dd, *J* = 12.3, 4.1 Hz, 1H), 3.77 (s, 3H), 2.96 – 2.71 (m, 2H), 2.44 – 2.19 (m, 3H), 1.95 (ddt, *J* = 13.4, 6.8, 2.3 Hz, 1H), 1.88 – 1.71 (m, 1H), 1.69 – 1.53 (m, 1H), 1.45 (dd, *J* = 11.9, 2.3 Hz, 1H), 1.25 (s, 3H, CH_3), 1.16

(s, 3H, CH_3), 1.06 (s, 3H, CH_3) ppm; **^{13}C NMR** (75 MHz, $CDCl_3$) δ 157.9, 150.1, 130.0, 127.1, 111.3, 110.3, 68.97, 55.41, 51.37, 40.18, 40.02, 38.21, 31.66, 30.69, 30.09, 24.93, 20.87, 18.42 ppm.

The spectroscopic data are in accordance to those reported in the literature.[2]

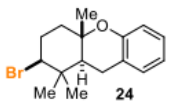

24

2-Bromo-1,1,4a-trimethyl-2,3,4,4a,9,9a-hexahydro-1H-xanthene (**24**), prepared from **20** (46.6 mg, 202 µmol) by GP-B; colorless solid (48.1 mg, 156 µmol, 77%; d.r. >95:5); **TLC:** R_f = 0.57 (silica gel, *n*-hexane/EtOAc; 19:1); **^{1}H NMR** (300 MHz, $CDCl_3$) δ 7.14 – 7.03 (m, 2H), 6.85 (td, *J* = 7.5, 1.3 Hz, 1H), 6.77 (dd, *J* = 8.0, 1.2 Hz, 1H), 4.06 (dd, *J* = 12.4, 4.2 Hz, 1H), 2.85 – 2.69 (m, 2H), 2.30 (dtd, *J* = 13.8, 4.3, 3.4 Hz, 1H), 2.24 – 2.10 (m, 1H), 2.02 (dt, *J* = 13.2, 3.5 Hz, 1H), 1.91 – 1.76 (m, 2H, CH), 1.25 (s, 3H, CH_3), 1.19 (s, 3H, CH_3), 1.05 (s, 3H, CH_3) ppm; **^{13}C NMR** (75 MHz, $CDCl_3$) δ 152.8, 129.5, 127.5, 121.8, 120.2, 117.2, 75.87, 66.13, 48.21, 40.85, 39.35, 31.66, 29.76, 24.72, 19.98, 17.06 ppm.

The spectroscopic data are in accordance to those reported in the literature.[4]

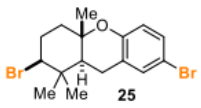

25

2,7-dibromo-1,1,4a-trimethyl-2,3,4,4a,9,9a-hexahydro-1H-xanthene (**25**), prepared from **20** (41.2 mg, 179 µmol) by GP-B but employing 70.1 mg NBS (394 µmol, 2.2 eq) and 197 mg morpholine HFIP salt (**16**, 465 µmol, 2.6 eq); colorless solid (61.2 mg, 158 µmol, 88%; d.r. >95:5); **TLC:** R_f = 0.78 (silica gel, *n*-hexane/EtOAc; 19:1); **^{1}H NMR** (300 MHz, $CDCl_3$) δ 7.21 – 7.13 (m, 2H), 6.67 – 6.60 (m, 1H), 4.03 (dd, *J* = 12.4, 4.1 Hz, 1H), 2.81 – 2.68 (m, 2H), 2.28 (dtd, *J* = 13.9, 4.2, 3.4 Hz, 1H), 2.20 – 2.08 (m, 1H), 1.99 (dt, *J* = 13.2, 3.5 Hz, 1H), 1.83 – 1.69 (m, 2H, CH), 1.22 (s, 3H, CH_3), 1.16 (s, 3H, CH_3), 1.02 (s, 3H, CH_3) ppm; **^{13}C NMR** (75 MHz, $CDCl_3$) δ 152.0, 132.2, 130.4, 124.1, 119.0, 112.2, 76.29, 65.69, 47.89, 40.70, 39.33, 31.58, 29.73, 24.61, 19.91, 17.03 ppm.

The spectroscopic data are in accordance to those reported in the literature.[4]

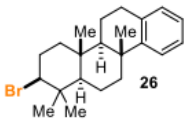

2-Bromo-1,1,4a,10b-tetramethyl-1,2,3,4,4a,4b,5,6,10b,11,12,12a-dodecahydrochrysene (**26**), prepared from **21** (33.6 mg, 113 µmol) by GP-A. After 20 min, the mixture was diluted with 2.00 mL *i*PrNO$_2$ and cooled to –25 °C. 75.1 µL ClSO$_3$H (1.13 mmol, 10.0 eq) was added and stirred for 40 min at that temperature before the reaction was terminated; colorless solid (17.0 mg, 45.2 µmol, 40%; d.r. >95:5); **TLC:** R_f = 0.27 (silica gel, *n*-hexane); **^{1}H NMR** (300 MHz, $CDCl_3$) δ 7.23 (dd, *J* = 7.7, 1.6 Hz, 1H), 7.16 – 6.98 (m, 3H), 4.01 (dd, *J* = 12.6, 4.5 Hz, 1H), 2.94 (ddd, *J* = 17.3, 6.6, 2.3 Hz, 1H), 2.81 (ddd, *J* = 17.4, 11.2, 7.2 Hz, 1H), 2.41 (dt, *J* = 12.6, 3.1 Hz, 1H), 2.26 (qd, *J* = 13.3, 3.9 Hz, 1H), 2.17 – 2.04 (m, 1H), 1.89 – 1.59 (m, 5H), 1.55 – 1.45 (m, 1H), 1.26 (dd, *J* = 11.7, 2.7 Hz, 1H), 1.20 (s, 3H, CH_3), 1.13 – 1.01 (m, 2H), 1.08 (s, 3H, CH_3), 0.99 (s, 3H, CH_3), 0.98 (s, 3H, CH_3) ppm; **^{13}C NMR** (75 MHz, $CDCl_3$) δ 149.9, 135.0, 129.0, 125.9, 125.4, 124.7, 69.96, 56.75, 55.17, 41.51, 40.72, 39.92, 37.98, 37.85, 31.10, 30.83, 30.62, 26.14, 20.73, 18.23 (2C), 16.41 ppm.

The spectroscopic data are in accordance to those reported in the literature.[2]

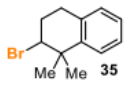

2-Bromo-1,1-dimethyl-1,2,3,4-tetrahydronaphthalene (**35**), prepared from **27** (30.0 mg, 187 µmol) by GP-A; colorless oil (37.1 mg, 155 µmol, 83%); **TLC:** R_f = 0.31 (silica gel, *n*-hexane); **^{1}H NMR** (300 MHz, $CDCl_3$) δ 7.36 (dd, *J* = 7.9, 1.5 Hz, 1H), 7.23 – 7.10 (m, 2H), 7.06 (ddq, *J* = 7.1, 1.5, 0.8 Hz, 1H), 4.44 (dd, *J* = 9.2, 3.4 Hz, 1H), 3.14 – 2.87 (m, 2H), 2.53 – 2.31 (m, 2H), 1.46 (s, 3H, CH_3), 1.45 (s, 3H, CH_3) ppm; **^{13}C NMR** (75 MHz, $CDCl_3$) δ 143.2, 133.8, 129.0, 126.9, 126.5, 126.2, 64.97 (CHBr), 39.78, 30.49, 30.11, 29.41, 28.88 ppm; **MS** (EI, 70 eV): *m/z* (%) =240/238 (17) $[M]^+$, 225/223 (26) $[M\text{-}Me]^+$, 159 (26) $[M\text{-}Br]^+$, 143 (100) $[M\text{-}Me\text{-}Br]^+$, 128 (51) $[M\text{-}2\times Me\text{-}Br]^+$, 91 (11) $[PhCH_2]^+$, 77 (9) $[Ph]^+$; **IR** (film) $\tilde{\nu}_{max}$ = 1489, 1387, 1364, 1207, 1161, 1043, 884, 790, 758, 733, 705 cm^{-1}; **HRMS** (EI) calcd. for $C_{12}H_{15}Br$ $[M]^+$ 238.0352, found 238.0315.

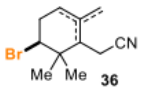

2-(5-Bromo-2,6,6-trimethylcyclohexen-1-yl)acetonitrile (**36**), prepared from **28** (33.0 mg, 202 µmol) by GP-C, isolated as an 12:53:35 mixture of inseparable elimination products (di-, tri- and tetrasubstituted alkenes); colorless oil (24.0 mg, 99.2 µmol, 52%); **TLC:** R_f = 0.34 (silica gel, *n*-hexane/EtOAc 9:1); **^{1}H NMR** (300 MHz, $CDCl_3$; *disubstituted isomer*) δ 5.07 (s, 1H), 4.81 (s, 1H), 1.22 (s, 3H), 0.89 (s, 3H) ppm (the other signals overlap with the signals of the other isomers); **^{1}H**

NMR (300 MHz, $CDCl_3$; *trisubstituted isomer*) δ 5.43 (br s, 1H), 4.16 – 4.10 (m, 1H), 2.73 (dd, *J* = 17.4, 5.0 Hz, 2H), 2.46 (dd, *J* = 17.4, 5.7 Hz, 1H), 1.82 (td, *J* = 2.0, 0.9 Hz, 3H), 1.18 (s, 3H), 1.05 (s, 3H) ppm; **^{1}H NMR** (300 MHz, $CDCl_3$; *tetrasubstituted isomer*) δ 4.24 – 4.18 (m, 1H), 3.15 – 2.95 (m, 2H), 1.74 (s, 3H), 1.27 (s, 3H), 1.19 (s, 3H) ppm; **^{13}C NMR** (75 MHz, $CDCl_3$; *trisubstituted isomer*) δ 132.7, 123.5, 120.0, 62.09, 46.88, 38.57, 34.84, 28.58, 21.79, 17.35, 16.90 ppm; **^{13}C NMR** (75 MHz, $CDCl_3$; *other isomers*) δ 133.2, 125.7, 118.6, 64.58, 63.82, 49.43, 40.33, 32.50, 31.74, 29.88, 28.50, 26.99, 24.28, 22.80, 19.99, 17.23, 14.27 ppm.

The spectroscopic data are in accordance to those reported in the literature.[2]

(3-Bromo-6-hydroxy-2,2,6-trimethylcyclohexyl)methyl acetate (**37**), prepared from **29** (40.4 mg, 206 µmol) by GP-C, a 82:18 mixture of separable diastereomers;

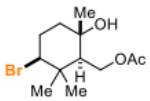

major-**37**

major diastereomer: colorless solid (31.5 mg, 107 µmol, 52%); **TLC:** R_f = 0.50 (silica gel, *n*-hexane/EtOAc; 1:1); **^{1}H NMR** (300 MHz, $CDCl_3$) δ 4.43 (dd, *J* = 11.9, 5.1 Hz, 1H), 4.32 (dd, *J* = 11.9, 5.0 Hz, 1H), 3.98 (dd, *J* = 12.4, 4.1 Hz, 1H), 2.50 (s, 1H), 2.19 (dq, *J* = 13.9, 4.0 Hz, 1H), 2.07 (s, 3H), 2.12 – 1.94 (m, 1H), 1.81 (dt, *J* = 13.4, 3.5 Hz, 1H), 1.72 (t, *J* = 5.2 Hz, 1H), 1.67 – 1.50 (m, 1H), 1.24 (s, 3H), 1.17 (s, 3H), 1.00 (s, 3H) ppm; **^{13}C NMR** (75 MHz, $CDCl_3$) δ 171.2, 71.90, 66.03, 63.59, 55.70, 43.12, 39.94, 32.15, 30.43, 23.95, 21.34, 17.82 ppm.

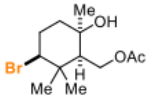

minor-**37**

minor diastereomer: colorless solid (6.1 mg, 20.8 µmol, 10%); **TLC:** R_f = 0.84 (silica gel, *n*-hexane/EtOAc; 1:1); **^{1}H NMR** (300 MHz, $CDCl_3$) δ 4.47 (dd, *J* = 12.3, 4.7 Hz, 1H), 4.35 (dd, *J* = 12.3, 2.9 Hz, 1H), 3.99 (dd, *J* = 12.8, 3.8 Hz, 1H), 2.43 (qd, *J* = 13.3, 4.0 Hz, 1H), 2.08 – 2.04 (m, 4H), 1.73 – 1.64 (m, 1H), 1.56 (td, *J* = 14.0, 4.1 Hz, 1H), 1.54 (br s, 1H), 1.41 (dd, *J* = 4.7, 2.9 Hz, 1H), 1.24 (s, 3H), 1.17 (s, 3H), 1.14 (s, 3H) ppm; **^{13}C NMR** (75 MHz, $CDCl_3$) δ 170.7, 71.84, 67.47, 63.44, 53.12, 42.24, 39.94, 30.67, 30.50, 29.97, 21.34, 17.89 ppm.

The spectroscopic data are in accordance to those reported in the literature.[2]

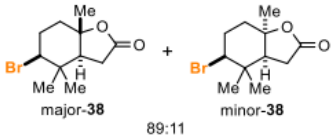

5-Bromo-4,4,7a-trimethylhexahydrobenzofuran-2(3H)-one (**38**), prepared from **30** (24.2 mg, 133 µmol) by GP-A; colorless solid (20.0 mg, 76.6 µmol, 58%; d.r. = 89:11); **TLC:** R_f = 0.39 (silica gel, *n*-hexane/EtOAc; 4:1); *major diastereomer*: **^{1}H NMR** (300 MHz, $CDCl_3$) δ 3.92 (dd, *J* = 12.4, 4.6 Hz, 1H, CHBr), 2.52 (dd, *J* = 16.3, 14.5 Hz, 1H), 2.45 – 2.28 (m, 2H), 2.13 – 1.95 (m, 3H), 1.86 – 1.73 (m, 1H), 1.37 (d, *J* = 0.8 Hz, 3H, CH_3), 1.07 (s, 3H, CH_3), 1.02 (s, 3H, CH_3) ppm; **^{13}C NMR** (75 MHz, $CDCl_3$) δ 175.5, 84.71, 62.90, 54.57, 38.66, 38.51, 32.44, 30.34, 30.11, 20.59, 17.18 ppm.

The spectroscopic data are in accordance to those reported in the literature.[2]

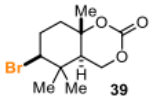

6-Bromo-5,5,8a-trimethylhexahydro-4H-benzo[d][1,3]dioxin-2-one (**39**), prepared from **31** (41.6 mg, 164 µmol) by GP-B and from **32** (48.2 mg, 189 µmol) by GP-A; colorless solid (25.7 mg, 92.7 µmol, 57%; d.r. >95:5 and 20.0 mg, 72.2 µmol, 38%; d.r. >95:5, respectively); **TLC:** R_f = 0.60 (silica gel, *n*-hexane/EtOAc; 1:1); **^{1}H NMR** (500 MHz, $CDCl_3$) δ 4.49 (dd, *J* = 10.8, 5.7 Hz, 1H), 4.42 (dd, *J* = 12.7, 10.8 Hz, 1H), 3.96 (dd, *J* = 12.5, 4.1 Hz, 1H), 2.30 (dtd, *J* = 13.9, 4.0, 3.0 Hz, 1H), 2.11 – 1.99 (m, 2H), 1.98 (dt, *J* = 13.2, 3.4 Hz, 1H), 1.81 – 1.72 (m, 1H), 1.52 (d, *J* = 1.0 Hz, 3H, CH_3), 1.15 (s, 3H, CH_3), 0.99 (s, 3H, CH_3) ppm; **^{13}C NMR** (126 MHz, $CDCl_3$) δ 148.5, 80.81, 67.72, 62.83, 47.23, 39.53, 38.11, 31.13, 29.31, 20.93, 17.35 ppm.

The spectroscopic data are in accordance to those reported in the literature.[2]

5-Bromo-4,4,7a-trimethyloctahydrobenzofuran (**40**), prepared from **33** (29.1 mg, 173 µmol) by GP-A; colorless oil (33.2 mg, 134 µmol, 78%; d.r. >95:5); **TLC:** R_f = 0.24 (silica gel, *n*-hexane/EtOAc; 19:1); **^{1}H NMR** (400 MHz, $CDCl_3$) δ 3.98 – 3.80 (m, 3H), 2.25 (dtd, *J* = 14.3, 4.4, 3.0 Hz, 1H), 2.06 (tdd, *J* = 14.1, 12.6, 4.0 Hz, 1H), 1.93 – 1.81 (m, 3H), 1.57 – 1.45 (m, 2H, CH), 1.13 (d, *J* = 0.9 Hz, 3H, CH_3), 1.08 (s, 3H, CH_3), 0.96 (s, 3H, CH_3) ppm; **^{13}C NMR** (101 MHz, $CDCl_3$) δ 79.02, 65.99, 65.13, 56.13, 39.43, 38.92, 32.98, 30.52, 24.97, 20.18, 17.16 ppm; **MS** (EI, 70 eV): *m/z* (%) = 233/231 (100/99) $[M\text{-}CH_3]^+$, 166 (3) $[M\text{-}HBr]^+$, 151 (29) $[M\text{-}CH_3\text{-}HBr]^+$, 107 (13) $[M\text{-}CH_3\text{-}HBr\text{-}CH_2CH_2O]^+$; **IR** (film) $\tilde{\nu}_{max}$

= 2960, 2873, 1456, 1378, 1153, 1068, 1009, 987, 925, 901, 783, 701 cm^{-1}; **HRMS** (ESI) calcd. for $C_{11}H_{20}BrO^+$ $[M+H]^+$ 247.0692, found 247.0694.

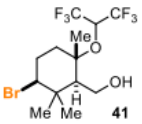

41

(3-Bromo-6-((1,1,1,3,3,3-hexafluoropropan-2-yl)oxy)-2,2,6-trimethylcyclohexyl) methanol (**41**), prepared from **34** (17.0 mg, 175 µmol and 1.54 g, 10.0 mmol) by GP-A and GP-D; colorless solid (45.3 mg, 113 µmol, 65%; d.r. >95:5 and 2.31 g, 5.75 mmol, 58%, d.r. >95:5, respectively); **m.p.** = 117 – 119 °C (EtOAc); **TLC:** R_f = 0.52 (silica gel, *n*-hexane/EtOAc; 4:1); **^{1}H NMR** (300 MHz, $CDCl_3$) δ 4.35 (hept, *J* = 5.7 Hz, 1H, $CH(CF_3)_2$), 4.05 – 3.95 (m, 1H, CHBr), 4.01 – 3.91 (m, 1H, CH_2O), 3.78 (d, *J* = 11.8 Hz, 1H, CH_2O), 2.27 (dq, *J* = 13.8, 3.9 Hz, 1H), 2.24 (br s, 1H, OH) 2.06 – 1.87 (m, 1H), 1.85 – 1.78 (m, 2H), 1.79 – 1.70 (m, 1H), 1.37 (s, 3H, CH_3), 1.28 (s, 3H, CH_3), 0.94 (s, 3H, CH_3) ppm; **^{13}C NMR** (126 MHz, $CDCl_3$) δ 121.4 (q, *J* = 287.0, 285.5 Hz, 2xCF_3), 85.60, 68.54 (hept, *J* = 32.6 Hz, $CH(CF_3)_2$), 64.62, 61.55, 58.45, 40.03, 38.61 (d, *J* = 2.4 Hz), 31.56, 30.59, 19.14 (t, *J* = 2.4 Hz), 18.43 ppm; **^{19}F NMR** (376 MHz, $CDCl_3$) δ -72.60 – -72.90 (m, 2x CF_3) ppm; **IR** (neat) $\tilde{\nu}_{max}$ = 3539, 1369, 1274, 1216, 1184, 1098, 1023, 906, 890, 686 cm^{-1}; **HRMS** (ESI) calcd. for $C_{13}H_{19}BrF_6O_2$ $[M+FA-H]^-$ 447.0434, found 447.0435.

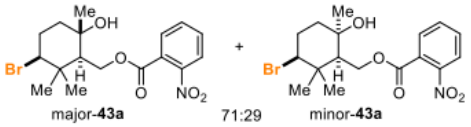

major-**43a** minor-**43a**

(3-Bromo-6-hydroxy-2,2,6-trimethylcyclohexyl)methyl 2-nitrobenzoate (**43a**), prepared from **42a** (41.7 mg, 137 µmol) by GP-A; colorless oil (33.2 mg, 82.9 µmol, 60 %; d.r. = 71:29); **TLC:** R_f = 0.56-0.59 (silica gel, *n*-hexane/EtOAc 1:1); **^{1}H NMR** (300 MHz, $CDCl_3$; *major diastereomer*) δ 8.01 – 7.87 (m, 1H), 7.80 – 7.52 (m, 3H), 4.77 (dd, *J* = 11.8, 4.3 Hz, 1H), 4.51 (dd, *J* = 11.8, 4.9 Hz, 1H), 3.99 (dd, *J* = 12.2, 4.3 Hz, 1H), 2.39 – 2.10 (m, 1H), 2.11 – 1.95 (m, 1H), 1.88 – 1.74 (m, 2H), 1.71 – 1.45 (m, 1H), 1.26 (s, 3H, CH_3), 1.19 (s, 3H, CH_3), 1.03 (s, 3H, CH_3) ppm; **^{1}H NMR** (300 MHz, $CDCl_3$; *minor diastereomer*) δ 7.85 (dd, *J* = 7.6, 1.6 Hz, 1H), 7.80 – 7.52 (m, 3H), 4.08 – 4.01 (m, 1H), 3.98 – 3.91 (m, 1H), 3.83 (dd, *J* = 11.7, 2.2 Hz, 1H), 3.03 (dt, *J* = 15.1, 3.4 Hz, 1H), 2.34 – 2.20 (m, 1H), 2.16 – 1.95 (m, 3H), 1.82 (s, 3H, CH_3), 1.32 (dd, *J* = 4.7, 2.2 Hz, 1H), 1.19 (s, 3H, CH_3), 0.81 (s, 3H, CH_3) ppm; **^{13}C NMR** (75 MHz, $CDCl_3$, *major* and *minor diastereomer*) δ 165.6, 164.5, 133.6, 133.2, 132.0, 131.3, 130.1, 129.9, 129.2, 127.7, 124.2, 124.1, 86.85, 71.84, 66.50, 65.69, 65.41, 60.74, 59.75, 55.83, 43.33, 40.04, 39.87, 36.52, 32.21, 30.41, 30.34, 29.91, 24.61, 23.69, 17.98 ppm; **IR** (film) $\tilde{\nu}_{max}$ = 3428, 1726, 1532, 1349, 1296, 1255, 1126, 1073, 911, 730 cm^{-1}; **HRMS** (ESI) calcd. for $C_{18}H_{23}BrNO_7$ $[M+FA-H]^-$ 444.0663, found 444.0665.

S22

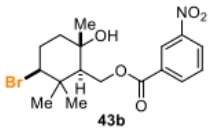

43b

(3-Bromo-6-hydroxy-2,2,6-trimethylcyclohexyl)methyl 3-nitrobenzoate (**43b**), prepared from **42b** (59.0 mg, 194 µmol) by GP-A; colorless solid (50.5 mg, 126 µmol, 65%; d.r. >95:5); **m.p.** = 117 – 118 °C (DCM); **TLC:** R_f = 0.58 (silica gel, *n*-hexane/EtOAc; 1:1); **^{1}H NMR** (300 MHz, $CDCl_3$) δ 8.82 (dd, *J* = 2.2, 1.6 Hz, 1H), 8.42 (ddd, *J* = 8.2, 2.4, 1.1 Hz, 1H), 8.33 (dt, *J* = 7.8, 1.4 Hz, 1H), 7.66 (t, *J* = 8.0 Hz, 1H), 4.84 (dd, *J* = 11.9, 3.4 Hz, 1H), 4.54 (dd, *J* = 11.9, 5.7 Hz, 1H), 4.02 (dd, *J* = 12.4, 4.1 Hz, 1H), 2.29 – 2.18 (m, 1H), 2.07 (tdd, *J* = 13.9, 11.6, 3.6 Hz, 1H), 1.91 – 1.81 (m, 2H), 1.63 (tdd, *J* = 13.4, 4.4, 1.1 Hz, 1H), 1.29 (d, *J* = 0.8 Hz, 3H), 1.25 (s, 3H), 1.09 (s, 3H) ppm; **^{13}C NMR** (75 MHz, $CDCl_3$) δ 164.7, 148.5, 135.3, 132.0, 129.9, 127.7, 124.7, 71.86, 65.53, 64.59, 56.18, 43.55, 40.18, 32.22, 30.65, 23.99, 18.02 ppm; **IR** (neat) $\tilde{\nu}_{max}$ = 3550 , 2969, 1723, 1533, 1350, 1296, 1260, 1140, 1072, 796, 718 cm^{-1}; **HRMS** (ESI) calcd. for $C_{18}H_{22}BrN_2O_9^-$ $[M+FA-H]^-$ 444.0663, found 444.0659.

3-Bromo-6-hydroxy-2,2,6-trimethylcyclohexyl)methyl 4-nitrobenzoate (**43c**), prepared from **42c** (60.0 mg, 198 µmol) by GP-A; produced as a 78:22 mixture of separable diastereomers;

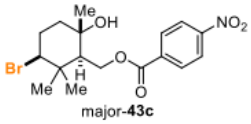

major-**43c**

major diastereomer: colorless solid (37.4 mg, 93.4 µmol, 47%); **m.p.** = 147 – 148 °C (EtOAc); **TLC:** R_f = 0.71 (silica gel, *c*-hexane/EtOAc; 1:1); **^{1}H NMR** (300 MHz, $CDCl_3$) δ 8.32 – 8.26 (m, 2H), 8.21 – 8.15 (m, 2H), 4.84 (dd, *J* = 11.9, 3.5 Hz, 1H), 4.53 (dd, *J* = 11.9, 5.7 Hz, 1H), 4.01 (dd, *J* = 12.4, 4.0 Hz, 1H, CHBr), 2.23 (dq, *J* = 13.7, 4.0 Hz, 1H), 2.04 (s, 1H, OH), 2.16 – 1.98 (m, 1H), 1.91 – 1.81 (m, 2H), 1.63 (td, *J* = 13.6, 4.5 Hz, 1H), 1.30 (s, 3H, CH_3), 1.25 (s, 3H, CH_3), 1.09 (s, 3H, CH_3) ppm; **^{13}C NMR** (75 MHz, $CDCl_3$) δ 164.9, 150.8, 135.5, 130.8 (2C), 123.8 (2C), 71.88, 65.50, 64.63, 56.14, 43.52, 40.16, 32.20, 30.67, 24.06, 18.01 ppm; **IR** (film) $\tilde{\nu}_{max}$ = 3554, 1719, 1515, 1343, 1292, 1109, 920, 720 cm^{-1}; **HRMS** (ESI) calcd. for $C_{18}H_{23}BrNO_7^-$ $[M+FA-H]^-$ 444.0663, found 444.0663.

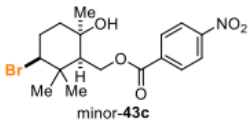

minor-**43c**

minor diastereomer: colorless solid (10.5 mg, 26.2 µmol, 13%); **m.p.** = 128 – 130 °C (EtOAc); **TLC:** R_f = 0.39 (silica gel, *c*-hexane/EtOAc; 4:1); **^{1}H NMR** (300 MHz, $CDCl_3$) δ 8.30 – 8.23 (m, 2H), 8.18 – 8.12 (m, 2H), 4.12 – 4.04 (m, 2H),

4.01 – 3.89 (m, 1H), 2.75 – 2.66 (m, 1H), 2.34 – 2.21 (m, 2H), 2.21 – 2.01 (m, 2H), 1.70 (s, 3H, CH_3), 1.31 (s, 3H, CH_3), 1.07 (s, 3H, CH_3); **^{13}C NMR** (75 MHz, $CDCl_3$) δ 163.5, 150.6, 137.2, 130.7 (2C), 123.7 (2C), 87.37, 65.00, 61.47, 56.93, 40.47, 38.32, 31.58, 30.67, 20.73, 18.93 ppm; **IR** (neat) $\tilde{\nu}_{max}$ = 3566, 1709, 1521, 1280, 1106, 1106, 875, 839, 719 cm^{-1}; **HRMS** (ESI) calcd. for $C_{18}H_{2379}BrNO_7$ $[M+FA-H]^-$ 444.0663, found 444.0663.

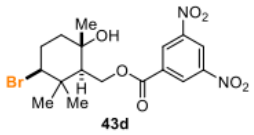

43d

(3-Bromo-6-hydroxy-2,2,6-trimethylcyclohexyl)methyl 3,5-dinitrobenzoate (**43d**), prepared from **42d** (69.6 mg, 195 µmol) by GP-A; colorless solid (44.5 mg, 100 µmol, 51%; d.r. >95:5); **m.p.** = 178 – 180 °C ($CHCl_3$); **TLC:** R_f = 0.61 (silica gel, *n*-hexane/EtOAc; 1:1); **^{1}H NMR** (300 MHz, $CDCl_3$) δ 9.23 (t, *J* = 2.2 Hz, 1H), 9.13 (d, *J* = 2.1 Hz, 2H), 4.91 (dd, *J* = 11.8, 3.4 Hz, 1H), 4.60 (dd, *J* = 11.8, 5.7 Hz, 1H), 4.03 (dd, *J* = 12.4, 4.1 Hz, 1H), 2.26 (dq, *J* = 14.0, 4.0 Hz, 1H), 2.17 – 2.01 (m, 1H), 1.95 – 1.82 (m, 2H), 1.70 (s, 1H), 1.62 (ddd, *J* = 13.4, 4.2, 1.0 Hz, 1H), 1.30 (s, 3H, CH_3), 1.25 (s, 3H, CH_3), 1.10 (s, 3H, CH_3) ppm; **^{13}C NMR** (75 MHz, $CDCl_3$) δ 162.7, 148.9 (2x C), 134.0, 129.5 (2x C), 122.6, 71.90, 65.46, 65.12, 56.02, 43.73, 40.17, 32.20, 30.65, 24.04, 18.08 ppm; **IR** (film) $\tilde{\nu}_{max}$ = 3555, 2934, 1717, 1515, 1341, 1280, 1104, 852, 720 cm^{-1}; **HRMS** (ESI) calcd. for $C_{18}H_{22}BrN_2O_9^-$ $[M+FA-H]^-$ 489.0514, found 489.0509.

(3-Bromo-6-hydroxy-2,2,6-trimethylcyclohexyl)methyl 3,5-difluorobenzoate (**43e**), prepared from **42e** (55.6 mg, 190 µmol) by GP-A; produced as a 71:29 mixture of separable diastereoisomes;

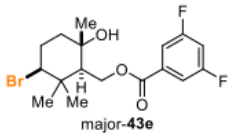

major-**43e**

major diastereomer: colorless solid (29.4 mg, 75.2 µmol, 40%); **m.p.** = 88 – 89 °C (DCM); **TLC:** R_f = 0.68 (silica gel, *n*-hexane/EtOAc; 1:1); **^{1}H NMR** (300 MHz, $CDCl_3$) δ 7.55 – 7.46 (m, 2H), 7.02 (tt, *J* = 8.5, 2.4 Hz, 1H), 4.79 (dd, *J* = 11.9, 3.6 Hz, 1H), 4.48 (dd, *J* = 11.9, 5.7 Hz, 1H), 4.00 (dd, *J* = 12.4, 4.1 Hz, 1H), 2.22 (dq, *J* = 13.9, 4.0 Hz, 1H), 2.15 (br s, 1H), 2.06 (tdd, *J* = 13.8, 12.4, 3.6 Hz, 1H), 1.88 – 1.79 (m, 2H), 1.61 (tdd, *J* = 13.4, 4.3, 1.1 Hz, 1H), 1.28 (d, *J* = 0.9 Hz, 3H, CH_3), 1.23 (s, 3H, CH_3), 1.07 (s, 3H, CH_3) ppm; **^{13}C NMR** (75 MHz, $CDCl_3$) δ 164.8 – 164.4 (m), 161.3 (d, *J* = 11.9 Hz, 2x C), 133.3 (t, *J* = 9.1 Hz), 113.0 – 112.5 (m), 108.8 (t, *J* = 25.2 Hz, 2x C), 71.84, 65.59, 64.46, 56.15, 43.47, 40.13, 32.20, 30.63, 23.99, 17.98 ppm; **^{19}F NMR** (376 MHz, $CDCl_3$) δ -108.19 (s) ppm; **IR** (neat) $\tilde{\nu}_{max}$ = 3491, 2961, 1703, 1595, 1442, 1329, 1236, 1123, 987, 974, 890, 862, 768, 661 cm^{-1}; **HRMS** (ESI) calcd. for $C_{18}H_{22}BrF_2O_5^-$ $[M+FA-H]^-$ 435.0624, found 435.0628.

Minor diastereomer: colorless solid [contained 16% of an impurity that could not be removed] (12.2 mg total, 10.5 mg of desired product alone, 26.8 µmol, 14%); **TLC:** R_f = 0.79 (silica gel, *n*-hexane/EtOAc; 1:1); **^{1}H NMR** (400 MHz, $CDCl_3$) δ 7.51 – 7.47 (m, 2H), 7.03 – 6.96 (m, 1H), 4.06 (ddd, *J* = 11.6, 5.7, 2.4 Hz, 2H), 3.94 (dt, *J* = 11.4, 5.0 Hz, 1H), 2.72 – 2.62 (m, 1H), 2.34 – 2.24 (m, 1H), 2.20 (t, *J* = 4.1 Hz, 1H), 2.15 – 1.96 (m, 2H), 1.67 (s, 3H, CH_3), 1.30 (s, 3H, CH_3), 1.06 (s, 3H, CH_3); **^{13}C NMR** (126 MHz, $CDCl_3$) δ 164.1 – 163.8 (m, 1C), 163.2 – 163.1 (m, 1C), 162.0 – 161.8 (m, 1C), 135.1 (t, *J* = 8.9 Hz, 1C), 112.8 – 112.5 (m, 1C), 108.7 – 108.1 (m, 2C), 87.06, 71.65, 67.08, 65.14, 61.44, 42.36, 40.42, 31.55, 31.02, 30.66, 30.04, 29.86, 20.68, 17.84 ppm; **^{19}F NMR** (376 MHz, $CDCl_3$) δ -108.5 (s, 2F) ppm; **IR** (film) $\tilde{\nu}_{max}$ = 3470, 1718, 1597, 1444, 1329, 1239, 1123, 989, 768 cm^{-1}; **HRMS** (ESI) calcd. for $C_{18}H_{22}BrF_2O_5^-$ $[M+FA-H]^-$ 435.0624, found 435.0628.

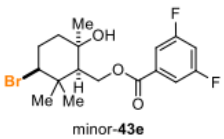

minor-**43e**

9. Physical and Spectroscopic Data of Iodocyclized Products

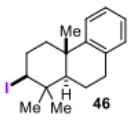

46

2-Iodo-1,1,4a-trimethyl-1,2,3,4,4a,9,10,10a-octahydrophenanthrene (**46**), prepared from **11** (26.6 mg, 117 µmol) by GP-A; colorless solid (32.1 mg, 90.6 µmol, 78%; d.r. >95:5); **TLC:** R_f = 0.37 (silica gel, *n*-hexane); **^{1}H NMR** (400 MHz, $CDCl_3$) δ 7.19 (dd, *J* = 7.7, 1.7 Hz, 1H), 7.13 (ddd, *J* = 7.7, 6.9, 1.9 Hz, 1H), 7.11 – 7.07 (m, 1H), 7.07 – 7.03 (m, 1H), 4.29 (dd, *J* = 12.9, 4.2 Hz, 1H), 2.90 (ddd, *J* = 10.6, 7.0, 1.8 Hz, 2H), 2.58 (qd, *J* = 13.4, 3.6 Hz, 1H), 2.46 (dq, *J* = 13.9, 3.9 Hz, 1H), 2.18 (dt, *J* = 13.3, 3.5 Hz, 1H), 2.05 – 1.95 (m, 1H), 1.83 (dddd, *J* = 13.2, 12.0, 10.5, 7.6 Hz, 1H), 1.64 – 1.54 (m, 2H), 1.26 (d, *J* = 0.7 Hz, 3H, CH_3), 1.14 (s, 3H, CH_3), 1.10 (s, 3H, CH_3) ppm; **^{13}C NMR** (101 MHz, $CDCl_3$) δ 148.9, 134.8, 129.2, 126.0, 125.7, 124.6, 53.59, 50.03, 41.97, 39.69, 38.32, 34.53, 33.22, 31.03, 25.04, 21.82, 21.32 ppm.

The spectroscopic data are in accordance to those reported in the literature.[5]

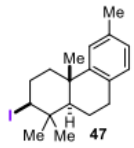

47

2-Iodo-1,1,4a,6-tetramethyl-1,2,3,4,4a,9,10,10a-octahydrophenanthrene (**47**), prepared from **18** (44.2 mg, 182 µmol) by GP-A; colorless crystals (59.9 mg, 163 µmol, 90%; d.r. >95:5); **TLC:** R_f = 0.34 (silica gel, *n*-hexane); **^{1}H NMR** (400 MHz, $CDCl_3$) δ 7.02 – 7.00 (m, $1H_r$), 6.98 – 6.91 (m, 2H), 4.29 (dd, *J* = 12.9, 4.2 Hz, 1H), 2.92 – 2.83 (m, 2H), 2.59 (qd, *J* = 13.4, 3.6 Hz, 1H), 2.47 (dq, *J* = 13.9, 3.9 Hz, 1H), 2.31 (s, 3H, CH_3), 2.18 (dt, *J* = 13.3, 3.5 Hz, 1H), 2.01 (ddt, *J* = 15.6, 5.5, 2.5 Hz, 1H), 1.88 – 1.76 (m, 1H), 1.66 – 1.51 (m, 2H), 1.27 (s, 3H, CH_3), 1.15 (s, 3H, CH_3), 1.11 (s, 3H, CH_3) ppm; **^{13}C NMR** (101 MHz, $CDCl_3$) δ 148.7, 135.3, 131.6, 129.1, 126.6, 125.1, 53.75, 50.16, 41.99, 39.69, 38.24, 34.56, 33.24, 30.65, 25.01, 21.89, 21.41, 21.33 ppm.

The spectroscopic data are in accordance to those reported in the literature.[3]

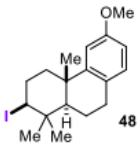

48

2-Iodo-6-methoxy-1,1,4a-trimethyl-1,2,3,4,4a,9,10,10a-octahydrophenanthrene (**48**), prepared from **19** (53.1 mg, 205 µmol) by GP-B; colorless solid (61.1 mg, 159 µmol, 77%; d.r. >95:5); **TLC:** R_f = 0.65 (silica gel, *n*-hexane/EtOAc; 9:1); **^{1}H NMR** (300 MHz, $CDCl_3$) δ 6.98 (dd, *J* = 8.3, 1.0 Hz, 1H), 6.74 (d, *J* = 2.6 Hz, 1H), 6.69 (dd, *J* = 8.3, 2.7 Hz, 1H), 4.28 (dd,

J = 12.7, 4.4 Hz, 1H), 3.78 (s, 3H), 2.89 – 2.78 (m, 2H), 2.57 (qd, *J* = 13.3, 3.6 Hz, 1H), 2.45 (dq, *J* = 13.9, 4.1 Hz, 1H), 2.13 (dt, *J* = 13.3, 3.5 Hz, 1H), 2.00 (ddq, *J* = 13.2, 5.6, 2.6 Hz, 1H), 1.81 (dddd, *J* = 13.2, 11.9, 10.7, 7.4 Hz, 1H), 1.58 (qd, *J* = 12.7, 12.0, 2.9 Hz, 2H), 1.26 (d, *J* = 0.8 Hz, 3H, CH_3), 1.14 (s, 3H, CH_3), 1.10 (s, 3H, CH_3) ppm; **^{13}C NMR** (75 MHz, $CDCl_3$) δ 157.9, 150.1, 130.0, 126.9, 111.2, 110.3, 55.38, 53.52, 50.00, 41.92, 39.65, 38.45, 34.48, 33.20, 30.19, 24.91, 21.92, 21.32 ppm.

The spectroscopic data are in accordance to those reported in the literature.[3]

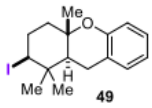

49

2-Iodo-1,1,4a-trimethyl-2,3,4,4a,9,9a-hexahydro-1H-xanthene (**49**), prepared from **20** (53.1 mg, 205 µmol) by GP-B; colorless solid (61.1 mg, 159 µmol, 78%; d.r. >95:5); **TLC:** R_f = 0.65 (silica gel, *n*-hexane/EtOAc; 9:1); **^{1}H NMR** (300 MHz, $CDCl_3$) δ 7.16 – 7.01 (m, 2H), 6.91 – 6.71 (m, 2H), 4.26 (dd, *J* = 12.7, 4.0 Hz, 1H), 2.91 – 2.69 (m, 2H), 2.47 (dtd, *J* = 14.0, 4.2, 3.4 Hz, 1H), 2.41 – 2.24 (m, 1H), 1.94 – 1.85 (m, 2H), 1.80 (ddd, *J* = 13.4, 4.4, 1.0 Hz, 1H), 1.25 (d, *J* = 0.9 Hz, 3H, CH_3), 1.15 (s, 3H, CH_3), 1.07 (s, 3H, CH_3) ppm; **^{13}C NMR** (75 MHz, $CDCl_3$) δ 152.7, 129.6, 127.5, 122.0, 120.1, 117.2, 76.07, 49.64, 46.75, 42.59, 39.05, 34.37, 32.28, 25.69, 19.97, 19.82 ppm.

The spectroscopic data are in accordance to those reported in the literature.[6]

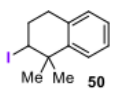

50

2-Iodo-1,1-dimethyl-1,2,3,4-tetrahydronaphthalene (**50**), prepared from **27** (23.1 mg, 144 µmol) by GP-A; colorless to beige oil (30.3 mg, 106 µmol, 74%); **TLC:** R_f = 0.51 (silica gel, *n*-hexane); **^{1}H NMR** (300 MHz, $CDCl_3$) δ 7.39 – 7.33 (m, 1H), 7.21 – 7.10 (m, 2H), 7.08 – 7.02 (m, 1H), 4.64 (dd, *J* = 8.0, 4.8 Hz, 1H), 2.96 (ddd, *J* = 7.4, 6.5, 1.0 Hz, 2H), 2.58 – 2.43 (m, 2H), 1.50 (s, 3H, CH_3), 1.48 (s, 3H, CH_3) ppm; **^{13}C NMR** (75 MHz, $CDCl_3$) δ 141.9, 133.9, 129.1, 127.2, 126.4, 126.2, 48.43, 39.36, 32.60, 32.37, 31.25 (2x C) ppm.; **MS** (EI, 70 eV): *m/z* (%) = 286 (1) $[M]^+$, 159 (100) $[M\text{-}I]^+$, 143 (19) $[M\text{-}Me\text{-}I]^+$, 128 (28) $[M\text{-}2\times Me\text{-}I]^+$, 91 (9) $[PhCH_2]^+$, 77 (4) $[Ph]^+$; **IR** (film) $\tilde{\nu}_{max}$ = 2967, 1489, 1446, 1218, 1194, 1143, 1042, 881, 757, 729 cm^{-1}; **HRMS** (EI) calcd. for $C_{12}H_{15}I^+$ $[M]^+$ 286.0213, found 286.0214.

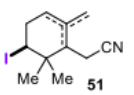

51

2-(5-Iodo-2,6,6-trimethylcyclohexen-1-yl)acetonitrile (**51**), prepared from **28** (32.6 mg, 200 µmol) by GP-C, isolated as an 51:40:9 mixture of inseparable elimination products (di-, tri- and tetrasubstituted alkene); colorless oil (42.9 mg, 148 µmol, 74%); **TLC:** R_f = 0.38 (silica gel, *n*-hexane/EtOAc 9:1); **^{1}H NMR** (300 MHz, $CDCl_3$; *disubstituted isomer*) δ 5.06 (t, *J* = 1.3 Hz, 1H), 4.78 (s, 1H), 1.22 – 1.21 (m, 3H), 0.88 (s, 3H, CH_3) ppm; **^{1}H NMR** (300 MHz, $CDCl_3$; *trisubstituted isomer*) δ 5.32 (s, 1H), 4.37 – 4.27 (m, 2H), 2.72 (dd, *J* = 17.1, 4.7 Hz, 2H), 2.47 (dd, *J* = 22.2, 5.2 Hz, 3H), 1.80 (dq, *J* = 2.7, 1.4 Hz, 3H), 1.18 (s, 3H, CH_3), 1.04 (s, 3H, CH_3); **^{1}H NMR** (300 MHz, $CDCl_3$; *tetrasubstituted isomer*) δ 4.41 (dd, *J* = 8.8, 4.8 Hz, 1H), 3.07 (q, *J* = 17.5 Hz, 4H), 1.74 (s, 3H, CH_3), 1.26 (s, 3H, CH_3), 1.23 (s, 3H, CH_3) ppm; **^{13}C NMR** (75 MHz, $CDCl_3$; *trisubstituted isomer*) δ 132.7, 125.2, 119.5, 46.92, 45.41, 37.72, 34.16, 28.08, 21.64, 18.09, 18.05 ppm; **^{13}C NMR** (75 MHz, $CDCl_3$; *other isomers*) δ 143.7, 110.6, 48.13, 47.80, 44.73, 41.27, 38.57, 38.11, 38.05, 31.90, 31.18, 27.63, 20.01, 18.27, 17.49, 16.38 ppm.

The spectroscopic data are in accordance to those reported in the literature.[5]

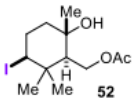

52

6-Hydroxy-3-iodo-2,2,6-trimethylcyclohexyl)methyl acetate (**52**), prepared from **29** (38.6 mg, 197 µmol) by GP-C, colorless solid (32.0 mg, 94.0 µmol, 50%, d.r. >95:5); **TLC:** R_f = 0.50 (silica gel, *n*-hexane/EtOAc 1:1); **^{1}H NMR** (300 MHz, $CDCl_3$) δ 4.45 (dd, *J* = 11.9, 4.8 Hz, 1H), 4.30 (dd, *J* = 11.9, 5.1 Hz, 1H), 4.16 (dd, *J* = 12.8, 4.0 Hz, 1H), 2.53 (s, 1H), 2.36 (dq, *J* = 14.1, 4.0 Hz, 1H), 2.19 (ddd, *J* = 27.2, 13.4, 4.0 Hz, 1H), 2.05 (s, 3H, CH_3), 1.76 (t, *J* = 4.9 Hz, 1H), 1.66 (dt, *J* = 13.3, 3.7 Hz, 1H), 1.56 (dddd, *J* = 14.3, 13.3, 4.2, 1.0 Hz, 1H), 1.22 (s, 3H, CH_3), 1.13 (s, 3H, CH_3), 1.02 (s, 3H, CH_3) ppm; **^{13}C NMR** (75 MHz, $CDCl_3$) δ 171.1, 72.04, 64.16, 54.37, 49.54, 44.98, 39.62, 34.92, 32.97, 23.84, 21.33, 20.54 ppm.

The spectroscopic data are in accordance to those reported in the literature.[5]

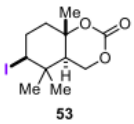

53

6-Iodo-5,5,8a-trimethylhexahydro-4H-benzo[d][1,3]dioxin-2-one (**53**), prepared from **31** (47.5 mg, 188 µmol) by GP-B and from **32** (50.6 mg, 199 µmol) by GP-A; colorless solid (43.6 mg, 135 µmol, 72%; d.r. >95:5 and 55.8 mg, 172 µmol, 87%; d.r. >95:5, respectively); **TLC:** R_f = 0.68 (silica gel, *n*-hexane/EtOAc; 1:1); **^{1}H NMR** (300 MHz, $CDCl_3$) δ 4.50 (dd, *J* = 10.8, 5.9 Hz, 1H),

4.40 (dd, *J* = 12.5, 10.8 Hz, 1H), 4.13 (dd, *J* = 12.8, 4.0 Hz, 1H, CHI), 2.46 (dtd, *J* = 14.4, 4.2, 3.3 Hz, 1H), 2.32 – 2.15 (m, 1H), 2.10 (dd, *J* = 12.5, 5.8 Hz, 1H), 1.90 – 1.69 (m, 2H), 1.51 (s, 3H, CH_3), 1.10 (s, 3H, CH_3), 1.00 (s, 3H, CH_3) ppm; **^{13}C NMR** (75 MHz, $CDCl_3$) δ 148.3, 80.97, 68.42, 45.64, 45.14, 41.17, 37.79, 33.78, 31.64, 20.88, 20.05 ppm.

The spectroscopic data are in accordance to those reported in the literature.[5]

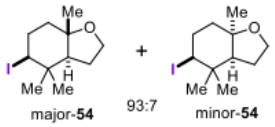

5-Iodo-4,4,7a-trimethyloctahydrobenzofuran (**54**), prepared from **33** (30.7 mg, 182 µmol) by GP-A; colorless oil (35.3 mg, 120 µmol, 66%; d.r. = 93:7); **TLC:** R_f = 0.21 (silica gel, *n*-hexane/EtOAc; 19:1); *major diastereomer:* **^{1}H NMR** (400 MHz, $CDCl_3$) δ 4.07 (dd, *J* = 12.9, 4.4 Hz, 1H), 3.94 – 3.78 (m, 2H), 2.40 (dtd, *J* = 14.3, 4.4, 3.0 Hz, 1H), 2.22 (dtd, *J* = 14.3, 13.2, 4.0 Hz, 1H), 2.00 – 1.81 (m, 2H), 1.72 (ddd, *J* = 12.4, 4.0, 3.0 Hz, 1H), 1.56 (dd, *J* = 12.7, 7.2 Hz, 1H), 1.49 (dddd, *J* = 13.4, 12.5, 4.4, 1.0 Hz, 1H), 1.12 (d, *J* = 0.9 Hz, 3H, CH_3), 1.03 (s, 3H, CH_3), 0.96 (s, 3H, CH_3) ppm; **^{13}C NMR** (101 MHz, $CDCl_3$) δ 79.08, 64.75, 54.45, 49.06, 41.07, 38.86, 35.64, 32.64, 25.88, 20.13, 19.79 ppm.

The spectroscopic data are in accordance to those reported in the literature.[7]

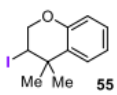

3-Iodo-4,4-dimethylchromane (**55**), prepared from prenylphenyl ether (36.1 mg, 222 µmol) by GP-B; slightly beige solid (38.2 mg, 133 µmol, 60%); **m.p.** = 47 – 48 °C ($CHCl_3$); **TLC:** R_f = 0.21 (silica gel, *n*-hexane); **^{1}H NMR** (400 MHz, $CDCl_3$) δ 7.29 (dt, *J* = 7.9, 1.6 Hz, 1H, H_{ar}), 7.13 (ddd, *J* = 8.2, 7.3, 1.6 Hz, 1H, H_{ar}), 6.92 (ddd, *J* = 7.8, 7.2, 1.3 Hz, 1H, H_{ar}), 6.79 (dd, *J* = 8.2, 1.3 Hz, 1H, H_{ar}), 4.56 (dd, *J* = 10.7, 3.6 Hz, 1H, CHI), 4.49 (dd, *J* = 11.2, 3.7 Hz, 1H), 4.39 (d, *J* = 11.3, 10.7 Hz, 1H), 1.47 (s, 3H, CH_3), 1.43 (s, 3H, CH_3); **^{13}C NMR** (101 MHz, $CDCl_3$) δ 152.3, 128.0, 127.6, 127.6, 121.3, 117.0, 69.11, 40.64, 36.34, 31.81, 29.57 ppm; **MS** (EI, 70 eV): *m/z* (%) = 286 (1) $[M]^+$, 159 (100) $[M\text{-}I]^+$, 143 (19) $[M\text{-}Me\text{-}I]^+$, 128 (28) $[M\text{-}2\times Me\text{-}I]^+$, 91 (9) $[PhCH_2]^+$, 77 (4) $[Ph]^+$; **IR** (film) $\tilde{\nu}_{max}$ = 2968, 1488, 1446, 1284, 1221, 1042, 1011, 797, 755, 722 cm^{-1}; **HRMS** (EI) calcd. for $C_{11}H_{13}IO^+$ $[M]^+$ 288.0006, found 287.9961.

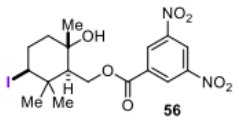

(3-Iodo-6-hydroxy-2,2,6-trimethylcyclohexyl)methyl 3,5-dinitrobenzoate (**56**), prepared from **42d** (68.4 mg, 196 µmol) by GP-A; faint yellow crystals (66.1 mg,

135 µmol, 69%; d.r. >95:5); **m.p.** = 122 – 123 °C (EtOAc, *n*-hexane); **TLC:** R_f = 0.70 (silica gel, *n*-hexane/EtOAc; 1:1); **^{1}H NMR** (300 MHz, $CDCl_3$) δ 9.22 (dt, *J* = 3.3, 2.1 Hz, 1H, H_{ar}), 9.11 (dd, *J* = 3.1, 2.0 Hz, 2H, H_{ar}), 4.93 (ddd, *J* = 11.8, 3.2, 1.6 Hz, 1H), 4.59 (ddd, *J* = 11.8, 5.8, 1.3 Hz, 1H), 4.21 (dd, *J* = 12.7, 4.0 Hz, 1H, CHI), 2.49 – 2.36 (m, 1H), 2.35 – 2.15 (m, 1H), 1.97 (dd, *J* = 5.8, 3.2 Hz, 1H), 1.81 (br s, 1H), 1.77 – 1.68 (m, 1H), 1.62 (td, *J* = 13.3, 4.4 Hz, 1H), 1.30 (s, 3H), 1.21 (s, 3H, CH_3), 1.11 (s, 3H, CH_3) ppm; **^{13}C NMR** (75 MHz, $CDCl_3$) δ 162.7, 148.8 (2x C), 134.0, 129.5 (2xC), 122.6, 72.07, 66.02, 54.66, 48.29, 45.55, 39.85, 34.94, 33.18, 23.90, 20.69 ppm; **IR** (neat) $\tilde{\nu}_{max}$ = 3574, 3100, 1723, 1541, 1344, 1269, 1164, 920, 719 cm^{-1}; **HRMS** (ESI) calcd. for $C_{18}H_{22}IN_2O_9^-$ $[M+FA-H]^-$ 537.0375, found 537.0373.

10. Physical and Spectroscopic Data of Chlorocyclized Products

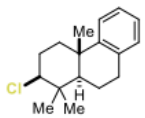

major-**57**

2-Chloro-1,1,4a-trimethyl-1,2,3,4,4a,9,10,10a-octahydrophenanthrene (**57**), prepared from **11** (33.2 mg, 146 µmol) by GP-E; produced as a 76:24 mixture of seperable diastereomes; *major diastereomer:* colorless solid (12.4 mg, 47.2 µmol, 32%); **TLC:** R_f = 0.38 (silica gel, *n*-hexane); **^{1}H NMR** (300 MHz, $CDCl_3$) δ 7.24 – 7.18 (m, 1H), 7.16 – 7.02 (m, 3H), 3.81 (dd, *J* = 11.5, 5.3 Hz, 1H), 2.36 (dt, *J* = 13.1, 3.6 Hz, 1H), 2.22 – 2.08 (m, 2H), 1.99 – 1.90 (m, 1H), 1.84 – 1.74 (m, 1H), 1.58 (d, *J* = 5.8 Hz, 3H), 1.42 (dd, *J* = 12.0, 2.4 Hz, 1H), 1.23 (d, *J* = 0.7 Hz, 3H, CH_3), 1.15 (s, 3H, CH_3), 1.02 (s, 3H, CH_3) ppm; **^{13}C NMR** (75 MHz, $CDCl_3$) δ 148.9, 134.9, 129.2, 126.0, 125.7, 124.6, 72.80, 51.42, 40.10, 38.87, 37.87, 30.84, 30.36, 29.37, 25.03, 20.06, 16.88 ppm.

The spectroscopic data are in accordance to those reported in the literature.[5]

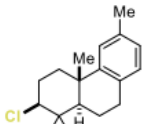

major-**58**

2-Chloro-1,1,4a,6-tetramethyl-1,2,3,4,4a,9,10,10a-octahydrophenanthrene (**58**), prepared from **18** (34.1 mg, 141 µmol) by GP-E; produced as a 76:24 mixture of seperable diastereoisomes; *major diastereomer:* colorless solid (11.8 mg, 42.6 µmol, 30%); **TLC:** R_f = 0.28 (silica gel, *n*-hexane); **^{1}H NMR** (500 MHz, $CDCl_3$) δ 7.15 – 6.95 (m, 2H), 6.92 (dd, *J* = 10.2, 8.5 Hz, 2H), 3.80 (dd, *J* = 12.2, 4.6 Hz, 1H), 2.96 – 2.89 (m, 1H), 2.83 (ddd, *J* = 17.5, 11.6, 7.2 Hz, 1H), 2.35 (dt, *J* = 13.3, 3.5 Hz, 1H), 2.29 (s, 3H, CH_3), 2.22 – 2.14 (m, 1H), 2.14 – 2.06 (m, 1H), 1.93 (ddt, *J* = 13.3, 7.3, 2.1 Hz, 1H), 1.78 (dtd, *J* = 13.3, 11.8, 6.6 Hz, 1H), 1.57 (td, *J* = 13.3, 3.9 Hz, 1H), 1.40 (dd, *J* = 12.1, 2.2 Hz, 1H), 1.23 (d, *J* = 0.8 Hz, 3H), 1.14 (s, 3H), 1.01 (s, 3H) ppm; **^{13}C NMR** (75 MHz, $CDCl_3$) δ 148.8, 135.3, 131.8, 129.1, 126.6, 125.1, 72.89, 51.58, 40.12, 38.93, 37.82, 30.47, 30.40, 29.40, 25.01, 21.42, 20.16, 16.89 ppm; **MS** (EI, 70 eV): *m/z* (%) = 278/276 (8/25) $[M]^+$, 263/261 (13/31) $[M\text{-}Me]^+$, 240 (33) $[M\text{-}HCl]^+$, 225 (100) $[M\text{-}Me\text{-}HCl]^+$, 210 (3) $[M\text{-}2Me\text{-}HCl]^+$, 77 (6) $[Ph]^+$; **IR** (film) $\tilde{\nu}_{max}$ = 2946, 1501, 1454, 1377, 1269, 1180, 970, 880, 870, 807, 767, 728 cm^{-1}; **HRMS** (EI) calcd. for $C_{18}H_{25}Cl^+$ $[M]^+$ 276.1639, found 276.1634.

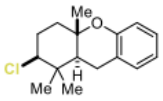

major-**59**

2-Chloro-1,1,4a-trimethyl-2,3,4,4a,9,9a-hexahydro-1H-xanthene (**59**), prepared from **20** (23.2 mg, 101 µmol) by GP-E; colorless oil (12.1 mg, 45.7 µmol, 45%; d.r. = 82:18); **TLC:** R_f = 0.53 (silica gel, *n*-hexane/EtOAC; 19:1); *major diastereomer*: **^{1}H NMR** (500 MHz, $CDCl_3$) δ 7.11 – 7.03 (m, 2H), 6.84 (td, *J* = 7.4, 1.2 Hz, 1H), 6.76 (dd, *J* = 8.1, 1.2 Hz, 1H), 3.85 (dd, *J* = 12.3, 4.0 Hz, 1H, CHCl), 2.85 – 2.67 (m, 2H), 2.19 – 2.08 (m, 1H), 2.08 – 2.00 (m, 1H), 1.99 – 1.91 (m, 1H), 1.79 – 1.74 (m, 2H), 1.24 (s, 3H, CH_3), 1.17 (s, 3H, CH_3), 0.99 (s, 3H, CH_3) ppm; **^{13}C NMR** (75 MHz, $CDCl_3$) δ 152.9, 129.7, 127.5, 121.8, 120.2, 117.2, 75.88, 70.86, 48.44, 39.66, 39.48, 30.50, 28.49, 24.14, 20.01, 15.63 ppm; **MS** (EI, 70 eV): *m/z* (%) = 266/264 (9/27) $[M]^+$, 228 (20) $[M\text{-}HCl]^+$, 159 (17) $[M\text{-}CH_2C_6H_4OH]^+$, 107 (100) $[CH_2C_6H_4OH]^+$, 91 (21) $[PhCH_2]^+$, 77 (21) $[Ph]^+$; **IR** (film) $\tilde{\nu}_{max}$ = 2927, 2357, 1584, 1488, 1455, 1239, 913, 754 cm^{-1}; **HRMS** (EI) calcd. for $C_{16}H_{21}ClO^+$ $[M]^+$ 264.1275, found 264.1256.

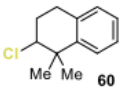

60

2-Chloro-1,1-dimethyl-1,2,3,4-tetrahydronaphthalene (**60**), prepared from **27** (26.0 mg, 162 µmol) by GP-E; colorless oil (16.0 mg, 82.2 µmol, 51%); **TLC:** R_f = 0.45 (silica gel, *n*-hexane); **^{1}H NMR** (300 MHz, $CDCl_3$) δ 7.35 (dd, *J* = 7.8, 1.6 Hz, 1H), 7.22 – 7.16 (m, 1H), 7.13 (td, *J* = 7.3, 1.6 Hz, 1H), 7.09 – 7.03 (m, 1H), 4.23 (dd, *J* = 9.2, 3.3 Hz, 1H), 3.05 (dt, *J* = 17.2, 6.0 Hz, 1H), 2.98 – 2.83 (m, 1H), 2.40 – 2.15 (m, 2H), 1.44 (s, 3H, CH_3), 1.40 (s, 3H, CH_3) ppm; **^{13}C NMR** (75 MHz, $CDCl_3$) δ 143.6, 133.9, 129.0, 126.9, 126.4, 126.1, 69.38, 39.97, 29.86, 28.99, 28.35, 27.01 ppm; **MS** (EI, 70 eV): *m/z* (%) = 196/194 (6/19) $[M]^+$, 181/179 (27/9) $[M\text{-}CH_3]^+$, 158 (19) $[M\text{-}HCl]^+$, 143 (100) $[M\text{-}Me\text{-}HCl]^+$, 128 (44) $[M\text{-}2Me\text{-}HCl]^+$; **IR** (film) $\tilde{\nu}_{max}$ = 1490, 1364, 1044, 890, 761 cm^{-1}; **HRMS** (EI) calcd. for $C_{12}H_{15}Cl$ $[M]^+$ 194.0857, found 194.0856.

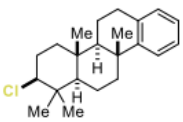

major-**61**

2-Chloro-1,1,4a,10b-tetramethyl-1,2,3,4,4a,4b,5,6,10b,11,12,12a-dodecahydrochrysene (**61**), prepared from **21** (53.4 mg, 180 µmol) by GP-E. After 30 min, the mixture was diluted with 2.00 mL *i*$PrNO_2$ and cooled to –25 °C. 120 µL $ClSO_3H$ (1.80 mmol, 10.0 eq) was added and stirred for 40 min at that temperature before the reaction was terminated; produced as a 85:15 mixture of separable diastereomes; *major diastereomer:* colorless semisolid (17.6 mg, 53.2 µmol, 30%); **TLC:** R_f = 0.24 (silica gel, *n*-hexane); **^{1}H NMR** (500 MHz, $CDCl_3$) δ 7.24 (d, *J* = 7.9 Hz, 1H), 7.12 (t, *J* = 7.5 Hz, 1H), 7.07 (td, *J* = 7.3, 1.3 Hz, 1H), 7.02 (d, *J* = 7.6 Hz, 1H), 3.75 (dd, *J* = 12.4, 4.5 Hz, 1H), 2.94 (ddd, *J* = 17.1, 6.6, 1.8 Hz, 1H), 2.82 (ddd, *J* = 17.5, 11.5, 7.3 Hz, 1H),

2.42 (dt, *J* = 12.7, 3.3 Hz, 1H), 2.06 (qd, *J* = 13.3, 3.8 Hz, 1H), 1.96 (dq, *J* = 13.7, 3.9 Hz, 1H), 1.89 (dt, *J* = 13.2, 3.7 Hz, 1H), 1.84 – 1.75 (m, 2H), 1.75 – 1.60 (m, 2H), 1.56 – 1.47 (m, 1H), 1.30 – 1.26 (m, 1H), 1.20 (s, 3H), 1.07 (s, 3H), 1.06 – 1.01 (m, 1H), 0.97 (s, 3H), 0.96 – 0.92 (m, 1H), 0.94 (s, 3H) ppm; **^{13}C NMR** (126 MHz, $CDCl_3$) δ 149.9, 135.0, 129.0, 125.9, 125.4, 124.7, 73.38, 56.81, 55.14, 40.66, 40.20, 39.96, 38.01, 37.65, 30.85, 29.72, 29.26, 26.17, 20.05, 18.21, 16.76, 16.42 ppm; **IR** (film) $\tilde{\nu}_{max}$ = 2944, 1451, 1379, 1175, 876, 760, 723 cm^{-1}; **HRMS** (EI) cald. for $C_{22}H_{31}Cl^+$ $[M]^+$ 330.2109, found 330.2100.

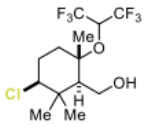

62

(3-Chloro-6-((1,1,1,3,3,3-hexafluoropropan-2-yl)oxy)-2,2,6-trimethylcyclohexyl) methanol (**62**), prepared from **34** (28.9 mg, 187 µmol) by GP-E; colorless crystalline solid (12.2 mg, 34.2 µmol, 18%, d.r. >95:5); **m.p.** = 100 – 101 °C (EtOAc); **TLC:** R_f = 0.63 (silica gel, *n*-hexane/EtOAc 4:1); **^{1}H NMR** (400 MHz, $CDCl_3$) δ 4.35 (hept, *J* = 5.7 Hz, 1H), 3.98 (ddd, *J* = 12.1, 6.3, 1.4 Hz, 1H), 3.83 – 3.73 (m, 2H), 2.22 (br d, *J* = 9.0 Hz, 1H), 2.18 – 2.10 (m, 1H), 1.89 – 1.69 (m, 4H), 1.38 (t, *J* = 1.1 Hz, 3H, CH_3), 1.28 (s, 3H, CH_3), 0.90 (s, 3H, CH_3) ppm; **^{13}C NMR** (126 MHz, $CDCl_3$) δ 124.8 – 118.1 (m, 2C), 85.64, 69.64, 68.57 (hept, *J* = 32.3 Hz) 61.13, 58.50, 40.13, 37.33, 30.38, 29.38, 19.18 (t, *J* = 2.6 Hz), 16.96 ppm; **^{19}F NMR** (376 MHz, $CDCl_3$) δ -72.61 – -72.88 (m, 2x CF_3) ppm; **IR** (film) $\tilde{\nu}_{max}$ = 3541, 2964, 1397, 1276, 1229, 1187, 1102, 909, 687 cm^{-1}; **HRMS** (ESI) calcd. for $C_{14}H_{20}ClF_6O_4^-$ $[M+FA-H]^-$ 401.0960, found 401.0957.

11. X-Ray Crystal Structure Analysis of Compound 16 (CCDC 1584440)

A suitable crystal of compound **16** was obtained by letting a clean sample stand for 1 week in a screw capped vial at ambient conditions. Crystals collected at the top of the vial via sublimation. A clear colourless fragment-like specimen of $C_{10}H_{13}F_{12}NO_3$, approximate dimensions 0.170 mm x 0.356 mm x 0.476 mm, was used for the X-ray crystallographic analysis. The X-ray intensity data were measured on a Bruker D8 Kappa-Apex II system equipped with a Triumph optic monochromator and a Mo fine-focus sealed tube (λ = 0.71073 Å).

A total of 2304 frames were collected. The total exposure time was 3.20 hours. The frames were integrated with the Bruker SAINT software package using a narrow-frame algorithm. The integration of the data using a monoclinic unit cell yielded a total of 16008 reflections to a maximum θ angle of 25.01° (0.84 Å resolution), of which 2795 were independent (average redundancy 5.727, completeness = 99.9%, R_{int} = 2.54%, R_{sig} = 1.63%) and 2561 (91.63%) were greater than $2\sigma(F^2)$. The final cell constants of a = 9.5076 (11) Å, b = 9.6913(11) Å, c = 9.7530(11) Å, α = 103.771(5)°, β = 91.642(5)°, γ = 113.628(4)° volume = 791.84(16) $Å^3$, are based upon the refinement of the XYZ-centroids of 92 reflections above 20 σ(I) with 10.67° < 2θ < 58.82°. The calculated minimum and maximum transmission coefficients (based on crystal size) are 0.9040 and 0.9640.

The final anisotropic full-matrix least-squares refinement on F^2 with 248 variables converged at R1 = 2.42%, for the observed data and wR2 = 6.30% for all data. The goodness-of-fit was 1.063. The largest peak in the final difference electron density synthesis was 0.270 $e^-/Å^3$ and the largest hole was -0.277 $e^-/Å^3$ with an RMS deviation of 0.039 $e^-/Å^3$. On the basis of the final model, the calculated density was 1.775 g/cm^3 and F(000), 424 e^-.

Table S7. Sample and crystal data for compound **16** (CCDC 1584440).

Chemical formula	$C_{10}H_{13}F_{12}NO_3$	
Formula weight	423.21	
Temperature	100(2) K	
Wavelength	0.71073 Å	
Crystal size	0.170 x 0.356 x 0.476 mm	
Crystal habit	clear colourless fragment	
Crystal system	triclinic	
Space group	P -1	
Unit cell dimensions	a = 9.5076(11) Å	α = 103.771(5)°
	b = 9.6913(11) Å	β = 91.642(5)°
	c = 9.7530(11) Å	γ = 113.628(4)°
Volume	791.84(16) $Å^3$	
Z	2	
Density (calculated)	1.775 g/cm^3	
Absorption coefficient	0.217 mm^{-1}	
F(000)	424	

Table S8. Data collection and structure refinement for compound **16** (CCDC 1584440).

Diffractometer	Bruker D8 Kappa-Apex II
Theta range for data collection	2.17 to 25.01°
Index ranges	$-11 \le h \le 11$, $-11 \le k \le 11$, $-11 \le l \le 11$
Reflections collected	16008
Independent reflections	2795 [R(int) = 0.0254]
Coverage of independent reflections	99.9%
Absorption correction	multi-Scan
Max. and min. transmission	0.9640 and 0.9040
Refinement method	Full-matrix least-squares on F^2
Refinement program	SHELXL-2014/7 (Sheldrick, 2014)
Function minimized	$\Sigma\, w(F_o^2 - F_c^2)^2$
Data / restraints / parameters	2795 / 0 / 248
Goodness-of-fit on F^2	1.063
Δ/σ_{max}	0.001
Final R indices	2561 data; $I>2\sigma(I)$ R1 = 0.0242, wR2 = 0.0613
	all data R1 = 0.0267, wR2 = 0.0630
Weighting scheme	$w=1/[\sigma^2(F_o^2)+(0.0304P)^2+0.2313P]$ where $P=(F_o^2+2F_c^2)/3$
Largest diff. peak and hole	0.270 and -0.277 eÅ^{-3}
R.M.S. deviation from mean	0.039 eÅ^{-3}

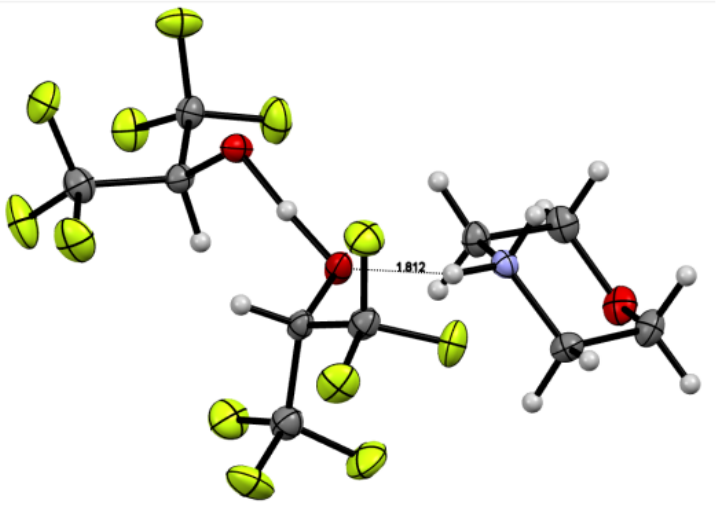

Figure S8. Crystal structre of **16** (CCDC 1584440).

12. X-Ray Crystal Structure Analysis of Compound 41 (CCDC 1571223)

A suitable crystal of compound **41** was grown by vapor-diffusion method using EtOAc/Et_2O. A clear colourless block-like specimen of $C_{13}H_{19}BrF_6O_2$, approximate dimensions 0.135 mm x 0.155 mm x 0.369 mm, was used for the X-ray crystallographic analysis. The X-ray intensity data were measured on a Bruker D8 Kappa-Apex II system equipped with a Triumph optic monochromator.

A total of 2917 frames were collected. The total exposure time was 16.21 hours. The frames were integrated with the Bruker SAINT software package using a narrow-frame algorithm. The integration of the data using a monoclinic unit cell yielded a total of 38407 reflections to a maximum θ angle of 25.02° (0.84 Å resolution), of which 2729 were independent (average redundancy 14.074, completeness = 100.0%, R_{int} = 3.71%, R_{sig} = 2.09%) and 2396 (87.80%) were greater than $2\sigma(F^2)$. The final cell constants of a = 7.071(2) Å, b = 21.450(8) Å, c = 10.258(3) Å, β = 95.885(15)°, volume = 1547.7(9) $Å^3$, are based upon the refinement of the XYZ-centroids of 99 reflections above 20 σ(I) with 6.622° < 2θ < 46.88°. Data were corrected for absorption effects using the Multi-Scan method (SADABS). The ratio of minimum to maximum apparent transmission was 0.828. The calculated minimum and maximum transmission coefficients (based on crystal size) are 0.4330 and 0.7100.

The final anisotropic full-matrix least-squares refinement on F^2 with 205 variables converged at R1 = 4.40%, for the observed data and wR2 = 11.85% for all data. The goodness-of-fit was 1.087. The largest peak in the final difference electron density synthesis was 1.389 $e^-/Å^3$ and the largest hole was -0.554 $e^-/Å^3$ with an RMS deviation of 0.105 $e^-/Å^3$. On the basis of the final model, the calculated density was 1.722 g/cm^3 and F(000), 808 e^-.

Table S9. Sample and crystal data for compound **41** (CCDC 1571223).

Chemical formula	$C_{13}H_{19}BrF_6O_2$	
Formula weight	401.19	
Temperature	100(2) K	
Wavelength	0.71073 Å	
Crystal size	0.135 x 0.155 x 0.369 mm	
Crystal habit	clear colourless block	
Crystal system	monoclinic	
Space group	P 1 21/n 1	
Unit cell dimensions	a = 7.071(2) Å	α = 90°
	b = 21.450(8) Å	β = 95.885(15)°
	c = 10.258(3) Å	γ = 90°
Volume	1547.7(9) $Å^3$	
Z	4	
Density (calculated)	1.722 g/cm^3	
Absorption coefficient	2.723 mm^{-1}	
F(000)	808	

Table S10. Data collection and structure refinement for compound **41** (CCDC 1571223).

Diffractometer	Bruker D8 Kappa-Apex II
Theta range for data collection	2.21 to 25.02°
Index ranges	$-8 \le h \le 8$, $-25 \le k \le 25$, $-12 \le l \le 12$
Reflections collected	38407
Independent reflections	2729 [R(int) = 0.0371]
Coverage of independent reflections	100.0%
Absorption correction	Multi-Scan
Max. and min. transmission	0.7100 and 0.4330
Refinement method	Full-matrix least-squares on F^2
Refinement program	SHELXL-2014/7 (Sheldrick, 2014)
Function minimized	$\Sigma\, w(F_o^2 - F_c^2)^2$
Data / restraints / parameters	2729 / 1 / 205
Goodness-of-fit on F^2	1.087
Δ/σ_{max}	0.001
Final R indices	2396 data; $I>2\sigma(I)$ R1 = 0.0440, wR2 = 0.1157
	all data R1 = 0.0495, wR2 = 0.1185
Weighting scheme	$w=1/[\sigma^2(F_o^2)+(0.0758P)^2+1.7780P]$ where $P=(F_o^2+2F_c^2)/3$
Largest diff. peak and hole	1.389 and -0.554 eÅ^{-3}
R.M.S. deviation from mean	0.105 eÅ^{-3}

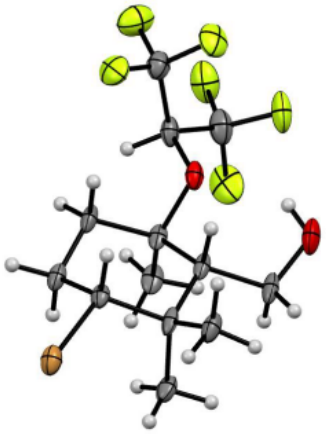

Figure S9. Crystal structure of **41** (CCDC 1571223).

13. X-ray Crystal Analysis of Compound 56 (CCDC 1584439)

A suitable crystal of compound **56** was grown by vapor-diffusion method using EtOAc/Et_2O. A clear colourless block-like specimen of $C_{17}H_{21}IN_2O_7$, approximate dimensions 0.063 mm x 0.138 mm x 0.158 mm, was used for the X-ray crystallographic analysis. The X-ray intensity data were measured on a Bruker D8 Venture TXS system equipped with a Helios optic monochromator and a Mo TXS rotating anode (λ = 0.71073 Å)

A total of 286 frames were collected. The total exposure time was 4.77 hours. The frames were integrated with the Bruker SAINT software package using a narrow-frame algorithm. The integration of the data using a monoclinic unit cell yielded a total of 33831 reflections to a maximum θ angle of 25.40° (0.83 Å resolution), of which 3593 were independent (average redundancy 9.416, completeness = 99.8%, R_{int} = 7.30%, R_{sig} = 3.21%) and 2572 (71.58%) were greater than $2\sigma(F^2)$. The final cell constants of a = 18.1478(7) Å, b = 6.6216(3) Å, c = 17.9704(7) Å, β = 114.684(2)°, volume = 1962.14(14) $Å^3$, are based upon the refinement of the XYZ-centroids of 246 reflections above 20 σ(I) with 4.880° < 2θ < 38.63°. Data were corrected for absorption effects using the Multi-Scan method (SADABS). The ratio of minimum to maximum apparent transmission was 0.848. The calculated minimum and maximum transmission coefficients (based on crystal size) are 0.7780 and 0.9020.

The final anisotropic full-matrix least-squares refinement on F^2 with 250 variables converged at R1 = 5.59%, for the observed data and wR2 = 13.48% for all data. The goodness-of-fit was 1.026. The largest peak in the final difference electron density synthesis was 0.971 $e^-/Å^3$ and the largest hole was -1.128 $e^-/Å^3$ with an RMS deviation of 0.087 $e^-/Å^3$. On the basis of the final model, the calculated density was 1.666 g/cm^3 and F(000), 984 e^-.

Table S11. Sample and crystal data for compound **56** (CCDC 1584439).

Chemical formula	$C_{17}H_{21}IN_2O_7$	
Formula weight	492.26	
Temperature	297(2) K	
Wavelength	0.71073 Å	
Crystal size	0.063 x 0.138 x 0.158 mm	
Crystal habit	clear colourless block	
Crystal system	monoclinic	
Space group	P 1 21/c 1	
Unit cell dimensions	a = 18.1478(7) Å	α = 90°
	b = 6.6216(3) Å	β = 114.684(2)°
	c = 17.9704(7) Å	γ = 90°
Volume	1962.14(14) $Å^3$	
Z	4	
Density (calculated)	1.666 g/cm^3	
Absorption coefficient	1.673 mm^{-1}	
F(000)	984	

Table S12. Data collection and structure refinement for compound **56** (CCDC 1571223).

Diffractometer	Bruker D8 Venture TXS	
Theta range for data collection	2.27 to 25.40°	
Index ranges	$-21 \le h \le 21$, $-7 \le k \le 7$, $-21 \le l \le 21$	
Reflections collected	33831	
Independent reflections	3593 [R(int) = 0.0730]	
Coverage of independent reflections	99.8%	
Absorption correction	Multi-Scan	
Max. and min. transmission	0.9020 and 0.7780	
Refinement method	Full-matrix least-squares on F^2	
Refinement program	SHELXL-2014/7 (Sheldrick, 2014)	
Function minimized	$\Sigma\, w(F_o^2 - F_c^2)^2$	
Data / restraints / parameters	3593 / 2 / 250	
Goodness-of-fit on F^2	1.026	
Δ/σ_{max}	0.001	
Final R indices	2572 data; $I>2\sigma(I)$	R1 = 0.0559, wR2 = 0.1195
	all data	R1 = 0.0849, wR2 = 0.1348
Weighting scheme	$w=1/[\sigma^2(F_o^2)+(0.0401)^2+8.9023P]$ where $P=(F_o^2+2F_c^2)/3$	
Largest diff. peak and hole	0.971 and -1.128 eÅ^{-3}	
R.M.S. deviation from mean	0.087 eÅ^{-3}	

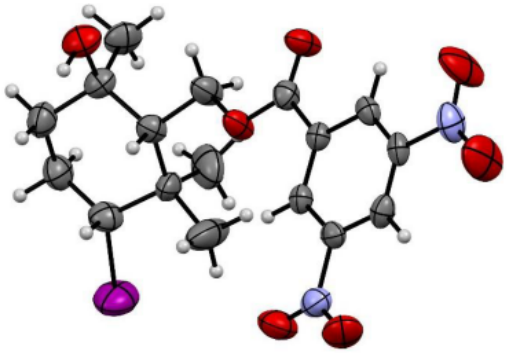

Figure S10. Crystal structure of **56** (CCDC 1584439).

14. Computational Details

All calculations have been performed with the software package Gaussian 09.E.03.[8] The level of theory consisted of the hybrid density functional B3LYP[9-12] and the basis set 6-311+G**.[13-14] All energy values reported are free energies (ΔG) taken from a frequency calculation after optimization of the relevant structure in gas-phase. The number of imaginary frequencies were used to determine an intermediate or ground state (NIMag=0) from a transition state (NImag=1). In the following section, you find all optimized structures with graphical representation and absolute energies.

a) Starting cationic compunds **44** and water

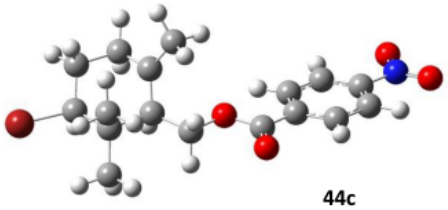

44c

Center Number	Atomic Number	Atomic Type	Coordinates (Angstroms) X	Y	Z
1	6	0	3.626896	-1.817024	0.477958
2	6	0	2.087219	-2.202168	0.510732
3	6	0	1.392593	-0.959303	0.845528
4	6	0	1.461368	0.111340	-0.147556
5	6	0	3.040472	0.628114	-0.130116
6	6	0	3.862927	-0.644529	-0.462992
7	1	0	1.816960	-2.546906	-0.491076
8	1	0	1.923950	-2.996662	1.238238
9	1	0	3.974125	-1.592196	1.487398
10	1	0	4.159528	-2.706801	0.140901
11	1	0	1.358500	-0.331392	-1.143372
12	1	0	3.652656	-0.940515	-1.491563
13	35	0	5.815766	-0.293348	-0.482838
14	6	0	3.408396	1.260670	1.219573
15	1	0	4.418089	1.668578	1.160990
16	1	0	2.741720	2.090233	1.460627
17	1	0	3.391417	0.557165	2.054898
18	6	0	3.175049	1.665925	-1.253087
19	1	0	2.827412	1.280445	-2.214810
20	1	0	2.635819	2.585849	-1.026175
21	1	0	4.230731	1.927058	-1.356384
22	6	0	0.781491	-0.798955	2.164956
23	1	0	1.240195	-1.438805	2.921220
24	1	0	0.687295	0.233396	2.498455
25	1	0	-0.251843	-1.172962	2.029717

26	6	0	0.442182	1.236115	0.005975
27	1	0	0.545991	1.793198	0.937837
28	1	0	0.530233	1.947419	-0.814162
29	8	0	-0.852959	0.609281	-0.045375
30	6	0	-1.912069	1.475800	0.114287
31	8	0	-1.735620	2.643762	0.343001
32	6	0	-3.231912	0.806972	-0.013052
33	6	0	-3.365075	-0.524696	-0.427383
34	6	0	-4.369338	1.567292	0.287716
35	6	0	-4.625787	-1.098138	-0.534221
36	1	0	-2.489167	-1.106138	-0.681052
37	6	0	-5.633560	1.000845	0.188279
38	1	0	-4.250971	2.597877	0.596787
39	6	0	-5.736603	-0.324302	-0.218820
40	1	0	-4.761835	-2.120977	-0.857166
41	1	0	-6.527941	1.563706	0.417558
42	7	0	-7.088295	-0.940784	-0.325714
43	8	0	-8.046025	-0.237101	-0.049218
44	8	0	-7.141911	-2.108774	-0.680432

HF= -3590.1601101 / NImag=0
Sum of electronic and thermal Enthalpies= -3589.780697
Sum of electronic and thermal Free Energies= -3589.860782

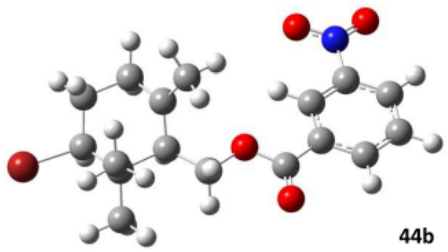

44b

Center Number	Atomic Number	Atomic Type	Coordinates (Angstroms) X	Y	Z
1	6	0	-3.163423	1.813690	0.376101
2	6	0	-1.599262	2.080639	0.394015
3	6	0	-1.000969	0.816376	0.822847
4	6	0	-1.156190	-0.316315	-0.090719
5	6	0	-2.766060	-0.706853	-0.042758
6	6	0	-3.487201	0.596251	-0.477429
7	1	0	-1.298644	2.329122	-0.627738
8	1	0	-1.375405	2.911548	1.062251
9	1	0	-3.529367	1.690458	1.396319
10	1	0	-3.625465	2.714250	-0.029444
11	1	0	-1.018656	0.046825	-1.114306
12	1	0	-3.252823	0.797179	-1.523622
13	35	0	-5.461428	0.393799	-0.486621
14	6	0	-3.181840	-1.201481	1.350260

15	1	0	-4.220702	-1.531659	1.319461
16	1	0	-2.581981	-2.059577	1.658328
17	1	0	-3.107658	-0.438957	2.128863
18	6	0	-2.980679	-1.816175	-1.081881
19	1	0	-2.604683	-1.534462	-2.068569
20	1	0	-2.511679	-2.753225	-0.780715
21	1	0	-4.052887	-2.004807	-1.170925
22	6	0	-0.399419	0.711395	2.151773
23	1	0	-0.829890	1.421651	2.861119
24	1	0	-0.354061	-0.299504	2.553027
25	1	0	0.648582	1.034380	1.999270
26	6	0	-0.218664	-1.499548	0.136135
27	1	0	-0.366894	-1.998505	1.095630
28	1	0	-0.345020	-2.245214	-0.647097
29	8	0	1.111341	-0.955471	0.072164
30	6	0	2.127144	-1.883644	0.052837
31	8	0	1.906734	-3.064026	0.119448
32	6	0	3.465421	-1.250197	-0.051340
33	6	0	4.597546	-2.076803	-0.045712
34	6	0	3.614444	0.133306	-0.154316
35	1	0	4.464908	-3.148708	0.032742
36	6	0	4.892496	0.661929	-0.242586
37	1	0	2.765539	0.798106	-0.174304
38	6	0	6.029285	-0.139634	-0.242405
39	1	0	7.007400	0.316322	-0.318053
40	7	0	5.035577	2.135755	-0.337183
41	8	0	4.009771	2.804840	-0.263675
42	8	0	6.159228	2.585915	-0.477176
43	6	0	5.869365	-1.520684	-0.142582
44	1	0	6.741763	-2.162048	-0.139766

HF= -3590.1648571 / NImag=0
Sum of electronic and thermal Enthalpies= -3589.785198
Sum of electronic and thermal Free Energies= -3589.864445

Water

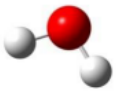

Center Number	Atomic Number	Atomic Type	Coordinates (Angstroms) X	Y	Z
1	8	0	-0.000000	0.000000	0.116996
2	1	0	-0.000000	0.764045	-0.467984
3	1	0	-0.000000	-0.764045	-0.467984

HF= / NImag=0
Sum of electronic and thermal Enthalpies= -76.433413
Sum of electronic and thermal Free Energies= -76.454836

b) Ester stabilized cations **S14**

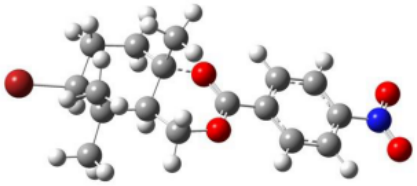

S14c

Center Number	Atomic Number	Atomic Type	Coordinates (Angstroms) X	Y	Z
1	6	0	-3.012617	1.713707	0.166622
2	6	0	-1.477050	1.837304	0.197858
3	6	0	-0.865133	0.581927	0.802703
4	6	0	-1.339475	-0.661305	0.031342
5	6	0	-2.899242	-0.881517	-0.024453
6	6	0	-3.457333	0.459895	-0.588703
7	1	0	-1.097409	1.960615	-0.820937
8	1	0	-1.177812	2.720371	0.767143
9	1	0	-3.423782	1.714010	1.178873
10	1	0	-3.422797	2.595482	-0.327252
11	1	0	-1.049145	-0.474710	-1.011292
12	1	0	-3.155955	0.542095	-1.634797
13	35	0	-5.441879	0.467962	-0.705044
14	6	0	-3.521055	-1.264141	1.332239
15	1	0	-4.560446	-1.556160	1.183585
16	1	0	-3.009489	-2.119791	1.780461
17	1	0	-3.522151	-0.451532	2.057657
18	6	0	-3.179750	-2.018334	-1.030070
19	1	0	-2.681631	-1.846446	-1.989132
20	1	0	-2.860044	-2.988955	-0.643373
21	1	0	-4.250763	-2.089159	-1.220597
22	6	0	-0.908923	0.567279	2.326480
23	1	0	-1.931202	0.691557	2.677888
24	1	0	-0.513843	-0.352629	2.760751
25	1	0	-0.323437	1.405202	2.709182
26	6	0	-0.539342	-1.866654	0.486221
27	1	0	-0.716141	-2.162776	1.518684
28	1	0	-0.652215	-2.729966	-0.163334
29	8	0	0.911955	-1.568272	0.406306
30	6	0	1.369190	-0.361203	0.356205
31	8	0	0.637528	0.684166	0.479561
32	6	0	2.802508	-0.191181	0.140884
33	6	0	3.619473	-1.319318	-0.049859
34	6	0	3.352998	1.102301	0.123336
35	6	0	4.980513	-1.154772	-0.259012
36	1	0	3.191695	-2.312579	-0.035359
37	6	0	4.713777	1.267635	-0.086189
38	1	0	2.720096	1.966735	0.271891
39	6	0	5.498998	0.135380	-0.273743
40	1	0	5.638521	-1.999435	-0.410685

41	1	0	5.171260	2.247296	-0.105713
42	7	0	6.966326	0.313230	-0.500966
43	8	0	7.391150	1.455706	-0.488547
44	8	0	7.622236	-0.698162	-0.681259

HF=-3590.1909292 / NImag=0
Sum of electronic and thermal Enthalpies= -3589.808349
Sum of electronic and thermal Free Energies= -3589.882918

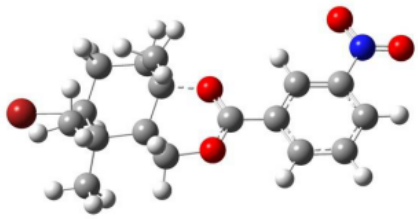

S14b

Center Number	Atomic Number	Atomic Type	Coordinates (Angstroms) X	Y	Z
1	6	0	2.600881	-1.735635	0.232173
2	6	0	1.061604	-1.672765	0.194591
3	6	0	0.583324	-0.336800	0.744554
4	6	0	1.235960	0.817930	-0.033839
5	6	0	2.812513	0.846891	-0.022371
6	6	0	3.226667	-0.566771	-0.530502
7	1	0	0.713922	-1.776191	-0.837713
8	1	0	0.632447	-2.497698	0.767776
9	1	0	2.963516	-1.755517	1.262547
10	1	0	2.922258	-2.674350	-0.220694
11	1	0	0.970705	0.636283	-1.083897
12	1	0	2.962135	-0.641318	-1.586992
13	35	0	5.199055	-0.817262	-0.556732
14	6	0	3.417468	1.188797	1.352549
15	1	0	4.488672	1.357105	1.243801
16	1	0	2.989287	2.107402	1.761887
17	1	0	3.295165	0.398910	2.092374
18	6	0	3.270911	1.913161	-1.039770
19	1	0	2.795133	1.775595	-2.015712
20	1	0	3.055823	2.925596	-0.689567
21	1	0	4.349609	1.848514	-1.183906
22	6	0	0.567733	-0.286938	2.268341
23	1	0	1.547321	-0.541813	2.667756
24	1	0	0.286084	0.689607	2.665950
25	1	0	-0.142485	-1.026676	2.642296
26	6	0	0.568508	2.124129	0.352940
27	1	0	0.739947	2.432026	1.382824
28	1	0	0.808872	2.945645	-0.315897
29	8	0	-0.905186	2.000389	0.222644
30	6	0	-1.502294	0.855123	0.191225
31	8	0	-0.905688	-0.266160	0.361530

32	6	0	-2.938910	0.847236	-0.054978
33	6	0	-3.624823	2.046203	-0.323500
34	6	0	-3.629529	-0.373071	-0.013618
35	1	0	-3.085492	2.983751	-0.353013
36	6	0	-4.992164	-0.360044	-0.243543
37	1	0	-3.129475	-1.308867	0.191868
38	6	0	-5.691161	0.813258	-0.511839
39	1	0	-6.758797	0.767836	-0.683907
40	7	0	-5.731684	-1.653142	-0.195497
41	8	0	-5.077517	-2.655675	0.045510
42	8	0	-6.931664	-1.611184	-0.399907
43	6	0	-4.994064	2.021013	-0.551156
44	1	0	-5.525069	2.941091	-0.759430

HF= HF=-3590.193267 / NImag=0
Sum of electronic and thermal Enthalpies= -3589.810605
Sum of electronic and thermal Free Energies= -3589.884348

c) Transition states **TS** and water adducts **45**

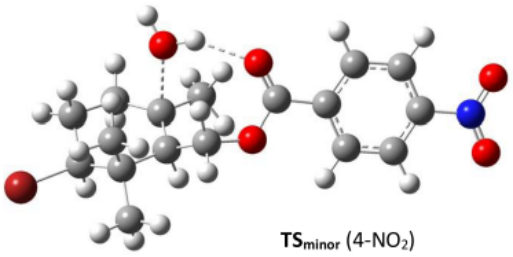

TS_{minor} (4-NO_2)

Center Number	Atomic Number	Atomic Type	Coordinates (Angstroms) X	Y	Z
1	6	0	5.893975	-0.360837	-0.099019
2	6	0	4.953741	-1.336998	-0.407247
3	6	0	3.614864	-1.076141	-0.145276
4	6	0	3.238012	0.152068	0.416913
5	6	0	4.208680	1.116632	0.723173
6	6	0	5.548498	0.862799	0.463618
7	6	0	1.826341	0.472138	0.724320
8	8	0	1.453407	1.495637	1.266683
9	7	0	7.331254	-0.638796	-0.383073
10	8	0	7.601712	-1.724409	-0.871395
11	8	0	0.958731	-0.490386	0.310346
12	6	0	-0.381692	-0.459357	0.830726
13	6	0	-1.488489	-0.263583	-0.242415
14	6	0	-1.417780	0.990541	-1.048014
15	6	0	-2.638547	1.645684	-1.540589
16	6	0	-3.953438	1.295921	-0.855897

17	6	0	-3.998667	-0.207820	-0.627331
18	6	0	-2.897975	-0.710924	0.345459
19	6	0	-0.153507	1.402282	-1.708770
20	8	0	-1.137668	2.537512	0.846856
21	6	0	-3.105789	-0.161806	1.772342
22	6	0	-2.924428	-2.254573	0.370566
23	35	0	-5.832934	-0.718241	-0.063487
24	8	0	8.132419	0.239759	-0.108744
25	1	0	-2.662710	1.313419	-2.599040
26	1	0	-2.451727	2.721337	-1.630131
27	1	0	-4.050992	1.833960	0.088433
28	1	0	-4.781060	1.611613	-1.491535
29	1	0	-1.244898	-0.990130	-1.046366
30	1	0	-3.894472	-0.729268	-1.582077
31	1	0	-4.121452	-0.378177	2.103195
32	1	0	-2.432900	-0.644452	2.483102
33	1	0	-2.941708	0.914489	1.835763
34	1	0	-2.841639	-2.674842	-0.636758
35	1	0	-2.122654	-2.673788	0.980748
36	1	0	-3.865046	-2.602611	0.796684
37	1	0	-0.463407	0.307143	1.593032
38	1	0	-0.532680	-1.435932	1.282100
39	1	0	2.867459	-1.825004	-0.368298
40	1	0	3.904941	2.055419	1.167754
41	1	0	5.277145	-2.274924	-0.837154
42	1	0	6.319297	1.586686	0.689595
43	1	0	0.516961	1.852474	-0.974226
44	1	0	0.369848	0.532150	-2.112698
45	1	0	-0.334097	2.134432	-2.495079
46	1	0	-1.455334	3.421354	1.063704
47	1	0	-0.236576	2.453585	1.207482

HF= -3666.6295511 / NImag=1 (-137.9295 cm^{-1})
Sum of electronic and thermal Enthalpies= -3666.223273
Sum of electronic and thermal Free Energies= -3666.305256

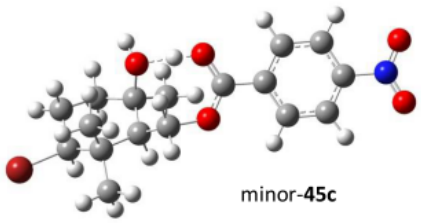

minor-**45c**

Center Number	Atomic Number	Atomic Type	Coordinates (Angstroms) X	Y	Z
1	6	0	-3.958717	1.517333	-0.290190
2	6	0	-2.706263	2.037924	-0.988638
3	6	0	-1.391266	1.353570	-0.590219
4	6	0	-1.509037	-0.195297	-0.407656
5	6	0	-2.894727	-0.778888	0.150930
6	6	0	-4.040443	0.018144	-0.527217

7	1	0	-2.828600	1.905906	-2.068236
8	1	0	-2.593060	3.119245	-0.842145
9	1	0	-3.953973	1.741017	0.779111
10	1	0	-4.833926	2.012921	-0.712488
11	1	0	-1.388096	-0.619515	-1.409347
12	1	0	-4.027743	-0.185130	-1.599965
13	35	0	-5.853601	-0.625275	-0.000263
14	6	0	-2.988616	-0.684715	1.690957
15	1	0	-3.998239	-0.938144	2.013962
16	1	0	-2.320534	-1.399220	2.176920
17	1	0	-2.754754	0.311320	2.070630
18	6	0	-2.997328	-2.257944	-0.280512
19	1	0	-2.984711	-2.358243	-1.369749
20	1	0	-2.190387	-2.871598	0.125476
21	1	0	-3.931939	-2.687306	0.079935
22	6	0	-0.410397	-0.785295	0.488167
23	1	0	-0.449012	-0.390489	1.499139
24	1	0	-0.499306	-1.865653	0.525782
25	8	0	0.987380	-0.618963	0.007815
26	6	0	1.795830	0.241111	0.546529
27	8	0	1.387088	1.235121	1.235551
28	6	0	3.223489	0.050077	0.331659
29	6	0	3.691570	-1.098221	-0.331681
30	6	0	4.124024	1.023949	0.799058
31	6	0	5.052841	-1.270182	-0.530834
32	1	0	2.994233	-1.846181	-0.683921
33	6	0	5.486029	0.851195	0.603931
34	1	0	3.755552	1.903277	1.310254
35	6	0	5.921133	-0.291448	-0.058701
36	1	0	5.448866	-2.140037	-1.036669
37	1	0	6.207621	1.578194	0.950571
38	7	0	7.389653	-0.476542	-0.273502
39	8	0	8.123459	0.399064	0.151458
40	8	0	7.737851	-1.488166	-0.857828
41	6	0	-0.334048	1.742141	-1.637076
42	1	0	0.663731	1.363994	-1.425133
43	1	0	-0.623460	1.352377	-2.614897
44	1	0	-0.273480	2.830505	-1.721438
45	8	0	-0.970284	1.877222	0.735350
46	1	0	-1.154939	2.824454	0.789968
47	1	0	0.376213	1.503778	1.096181

HF= -3666.6526602 / NImag=0
Sum of electronic and thermal Enthalpies= -3666.242911
Sum of electronic and thermal Free Energies= -3666.321177

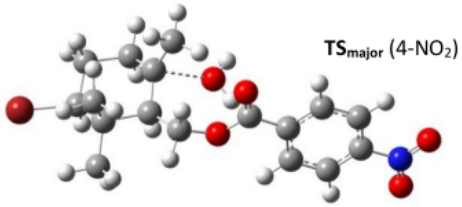

Center Number	Atomic Number	Atomic Type	Coordinates (Angstroms) X	Y	Z
1	6	0	3.008164	0.375503	0.678234
2	6	0	1.478686	0.062960	0.149411
3	6	0	1.522330	-1.142615	-0.704603
4	6	0	2.317964	-1.031603	-1.934725
5	6	0	3.805880	-0.787206	-1.491598
6	6	0	3.887013	0.440775	-0.599342
7	6	0	0.458876	0.055860	1.295371
8	8	0	-0.873532	0.244025	0.769111
9	6	0	-1.824255	-0.688499	1.081073
10	8	0	-1.557816	-1.741483	1.608975
11	6	0	1.060077	-2.457470	-0.252466
12	8	0	-0.571168	-0.533159	-2.121392
13	35	0	5.806009	0.745249	-0.181115
14	6	0	3.473641	-0.688803	1.682776
15	6	0	2.987536	1.757922	1.354385
16	6	0	-3.186760	-0.268516	0.661846
17	6	0	-3.463826	1.030400	0.211916
18	6	0	-4.756251	1.373205	-0.168038
19	6	0	-5.751046	0.405837	-0.088639
20	6	0	-5.505608	-0.885512	0.364719
21	6	0	-4.212377	-1.220057	0.743881
22	7	0	-7.135585	0.769291	-0.503921
23	8	0	-7.991748	-0.094376	-0.403629
24	8	0	-7.312606	1.904273	-0.918107
25	1	0	1.990425	-0.163192	-2.510417
26	1	0	2.251580	-1.924124	-2.555068
27	1	0	4.204829	-1.669521	-0.988068
28	1	0	4.390072	-0.645693	-2.401470
29	1	0	1.260527	0.911199	-0.507568
30	1	0	3.614154	1.331162	-1.167717
31	1	0	4.427827	-0.387539	2.115937
32	1	0	2.764808	-0.791263	2.506791
33	1	0	3.624091	-1.674492	1.237382
34	1	0	2.521137	2.516841	0.720770
35	1	0	2.477162	1.742622	2.317365
36	1	0	4.016806	2.066859	1.545677
37	1	0	1.820690	-2.810029	0.468732
38	1	0	0.132707	-2.421380	0.323507
39	1	0	1.007083	-3.184137	-1.060722
40	1	0	0.485531	-0.858066	1.884928
41	1	0	0.636178	0.903807	1.951995

42	1	0	-2.679002	1.774312	0.178724
43	1	0	-3.985874	-2.213552	1.108926
44	1	0	-5.003139	2.367731	-0.513405
45	1	0	-6.316275	-1.599305	0.416704
46	1	0	-0.972755	-0.934824	-2.901034
47	1	0	-1.275079	-0.033502	-1.690390

HF= -3666.6325721 / NImag=1 (-20.5178 cm^{-1})
Sum of electronic and thermal Enthalpies= -3666.226140
Sum of electronic and thermal Free Energies= -3666.310108

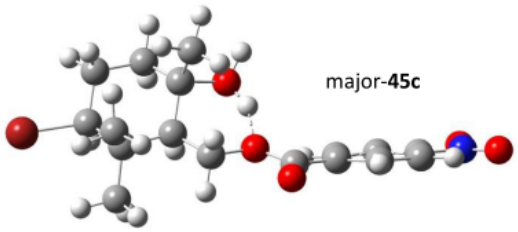

Center Number	Atomic Number	Atomic Type	Coordinates (Angstroms) X	Y	Z
1	6	0	-3.750999	1.660478	0.638172
2	6	0	-2.302801	2.172525	0.727548
3	6	0	-1.352402	1.019720	0.992750
4	6	0	-1.482102	-0.092786	-0.075523
5	6	0	-2.964333	-0.645211	-0.259218
6	6	0	-3.868501	0.606982	-0.458476
7	1	0	-2.029041	2.644789	-0.220088
8	1	0	-2.217228	2.929304	1.512591
9	1	0	-4.089732	1.261069	1.597244
10	1	0	-4.402763	2.504389	0.409508
11	1	0	-1.247887	0.398860	-1.027662
12	1	0	-3.627232	1.058657	-1.422585
13	35	0	-5.791051	0.139839	-0.664303
14	6	0	-3.432697	-1.527206	0.914932
15	1	0	-4.385597	-1.990908	0.660867
16	1	0	-2.725755	-2.335158	1.113815
17	1	0	-3.589691	-0.975086	1.841996
18	6	0	-2.994199	-1.491791	-1.550902
19	1	0	-2.563774	-0.953179	-2.400360
20	1	0	-2.461570	-2.437067	-1.434401
21	1	0	-4.025870	-1.738849	-1.801535
22	6	0	-1.253399	0.611876	2.451025
23	1	0	-2.216794	0.231488	2.789808
24	1	0	-0.510524	-0.166307	2.629711
25	1	0	-1.018536	1.477060	3.077894
26	6	0	-0.464625	-1.224875	0.103632
27	1	0	-0.550922	-1.744804	1.055392
28	1	0	-0.541243	-1.955988	-0.696443

29	8	0	0.878988	-0.632165	0.026099
30	6	0	1.952493	-1.511973	0.241811
31	8	0	1.748706	-2.642292	0.571323
32	6	0	3.269414	-0.867418	0.031245
33	6	0	3.423171	0.305409	-0.721707
34	6	0	4.388519	-1.498659	0.591068
35	6	0	4.686265	0.856006	-0.900420
36	1	0	2.571814	0.768414	-1.204407
37	6	0	5.652944	-0.948595	0.424314
38	1	0	4.257895	-2.414979	1.152592
39	6	0	5.775670	0.222111	-0.314853
40	1	0	4.840154	1.751451	-1.486855
41	1	0	6.533527	-1.409547	0.850604
42	7	0	7.129908	0.820359	-0.495377
43	8	0	8.068836	0.233624	0.015491
44	8	0	7.197191	1.856413	-1.137846
45	8	0	0.097250	1.631883	0.639384
46	1	0	0.458517	2.170753	1.362383
47	1	0	0.697390	0.829511	0.430186

HF= -3666.6411339 / NImag=0
Sum of electronic and thermal Enthalpies= -3666.231312
Sum of electronic and thermal Free Energies= -3666.311522

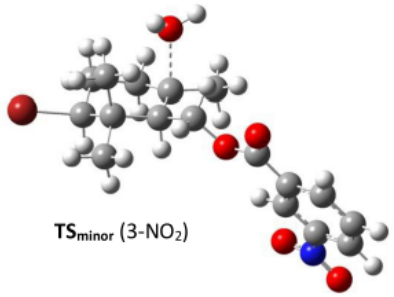

TS_{minor} (3-NO_2)

Center Number	Atomic Number	Atomic Type	Coordinates (Angstroms) X	Y	Z
1	6	0	-3.606620	1.159783	1.170085
2	6	0	-2.281116	1.407411	1.892779
3	6	0	-1.216404	0.397159	1.657460
4	6	0	-1.133829	-0.240056	0.302870
5	6	0	-2.483865	-0.467126	-0.497940
6	6	0	-3.363718	0.796743	-0.289342
7	1	0	-1.822429	2.340241	1.518771
8	1	0	-2.418631	1.567855	2.963543
9	1	0	-4.166167	0.373241	1.680231
10	1	0	-4.216486	2.061658	1.231379
11	1	0	-0.630399	0.588434	-0.234216
12	1	0	-2.894777	1.636780	-0.806050
13	35	0	-5.128259	0.652402	-1.192220
14	6	0	-3.207920	-1.758105	-0.057374

S56

15	1	0	-3.967113	-2.025434	-0.792152
16	1	0	-2.520837	-2.605379	0.010939
17	1	0	-3.743821	-1.646034	0.890129
18	6	0	-2.123768	-0.581573	-1.995677
19	1	0	-1.561792	0.291425	-2.340552
20	1	0	-1.534094	-1.472616	-2.214404
21	1	0	-3.034667	-0.646553	-2.590199
22	6	0	-0.148401	-1.418521	0.213599
23	1	0	-0.201185	-2.071884	1.087490
24	1	0	-0.352644	-2.033343	-0.659122
25	8	0	1.176541	-0.872709	0.102393
26	6	0	2.172765	-1.796411	-0.102330
27	8	0	1.944018	-2.978169	-0.135566
28	6	0	3.505998	-1.164152	-0.262312
29	6	0	3.671931	0.220466	-0.207210
30	6	0	4.615895	-1.994261	-0.472853
31	6	0	4.946013	0.744802	-0.358310
32	1	0	2.838710	0.888509	-0.055728
33	6	0	5.882855	-1.441082	-0.629053
34	1	0	4.469561	-3.066452	-0.514085
35	6	0	6.060214	-0.059847	-0.572485
36	1	0	7.035000	0.394386	-0.689682
37	7	0	5.112788	2.217587	-0.282638
38	8	0	6.228812	2.668963	-0.474027
39	8	0	4.114812	2.882782	-0.027581
40	6	0	0.007892	0.525108	2.496558
41	1	0	-0.235122	0.840596	3.511629
42	1	0	0.634735	-0.364183	2.498866
43	1	0	0.613029	1.323899	2.046440
44	8	0	-2.091544	-1.112190	2.825233
45	1	0	-1.544595	-1.501151	3.521556
46	1	0	-2.553157	-1.837935	2.381312
47	1	0	6.737781	-2.084685	-0.794346

HF= -3666.6305032 / NImag=1 (-116.1735 cm^{-1})
Sum of electronic and thermal Enthalpies= -3666.223806
Sum of electronic and thermal Free Energies= -3666.306644

minor-**45b**

Center Number	Atomic Number	Atomic Type	Coordinates (Angstroms) X	Y	Z
1	6	0	-3.685232	1.660138	-0.334485
2	6	0	-2.428014	1.974017	-1.142806
3	6	0	-1.182055	1.161182	-0.765108

4	6	0	-1.475953	-0.351402	-0.471707
5	6	0	-2.880197	-0.721721	0.210557
6	6	0	-3.966611	0.170726	-0.448275
7	1	0	-2.641578	1.773648	-2.197127
8	1	0	-2.168680	3.034991	-1.082939
9	1	0	-3.599146	1.959615	0.715350
10	1	0	-4.519793	2.232952	-0.740781
11	1	0	-1.484681	-0.846159	-1.447914
12	1	0	-4.056972	-0.102578	-1.501201
13	35	0	-5.801552	-0.199187	0.242812
14	6	0	-2.863951	-0.534075	1.744966
15	1	0	-3.869857	-0.671681	2.141192
16	1	0	-2.230617	-1.275215	2.236438
17	1	0	-2.527042	0.456392	2.062311
18	6	0	-3.192467	-2.200061	-0.110665
19	1	0	-3.254782	-2.366782	-1.189801
20	1	0	-2.445020	-2.884582	0.295731
21	1	0	-4.150954	-2.484687	0.323146
22	6	0	-0.392790	-1.020166	0.386248
23	1	0	-0.319199	-0.575617	1.374640
24	1	0	-0.597153	-2.080741	0.490625
25	8	0	0.979679	-1.034190	-0.181674
26	6	0	1.916084	-0.255829	0.270800
27	8	0	1.676124	0.809493	0.931513
28	6	0	3.293157	-0.630185	-0.008229
29	6	0	3.596658	-1.868442	-0.605545
30	6	0	4.319020	0.264252	0.336021
31	6	0	4.918504	-2.207818	-0.856783
32	1	0	2.799503	-2.552970	-0.863637
33	6	0	5.623641	-0.107857	0.073006
34	1	0	4.112245	1.221213	0.794643
35	6	0	5.945848	-1.326663	-0.517358
36	1	0	6.984721	-1.568632	-0.701293
37	7	0	6.719186	0.836169	0.434200
38	8	0	6.390441	1.897156	0.939855
39	8	0	7.858701	0.476209	0.196403
40	6	0	-0.157293	1.349515	-1.891977
41	1	0	0.807686	0.885136	-1.701532
42	1	0	-0.545985	0.915309	-2.814549
43	1	0	0.007998	2.415252	-2.059206
44	8	0	-0.561778	1.775038	0.430370
45	1	0	0.710533	1.208978	0.826494
46	1	0	-1.223319	2.060729	1.072223
47	1	0	5.156667	-3.159532	-1.314344

HF= -3666.6525511 / NImag=0
Sum of electronic and thermal Enthalpies= -3666.242936
Sum of electronic and thermal Free Energies= -3666.320996

S58

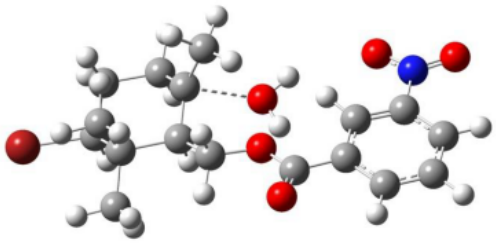

TS_{major} (3-NO_2)

Center Number	Atomic Number	Atomic Type	Coordinates (Angstroms) X	Y	Z
1	6	0	-5.990385	0.392731	-0.402090
2	6	0	-4.910573	-0.444351	-0.141690
3	6	0	-3.635999	0.047680	0.082060
4	6	0	-3.412585	1.420441	0.003730
5	6	0	-4.484455	2.284442	-0.255652
6	6	0	-5.762919	1.767892	-0.454141
7	6	0	-2.046014	1.977681	0.186446
8	8	0	-1.769281	3.134448	0.351599
9	7	0	-5.096044	-1.912822	-0.110253
10	8	0	-4.078230	-2.607378	-0.086234
11	8	0	-1.089602	0.987896	0.127948
12	6	0	0.265773	1.409217	0.378031
13	6	0	1.206827	0.277606	-0.045627
14	6	0	1.027047	-1.025551	0.635301
15	6	0	1.811547	-2.155935	0.111584
16	6	0	3.332491	-1.794401	0.203658
17	6	0	3.596909	-0.470847	-0.495401
18	6	0	2.784716	0.724973	0.068964
19	6	0	0.351832	-1.155540	1.933555
20	8	0	-0.893859	-1.836555	-0.807786
21	6	0	3.162797	1.075513	1.516593
22	6	0	2.978621	1.957802	-0.831333
23	35	0	5.557412	-0.147396	-0.444100
24	8	0	-6.232657	-2.343676	-0.120443
25	1	0	1.559537	-2.297961	-0.942429
26	1	0	1.603412	-3.081317	0.647416
27	1	0	3.655627	-1.761482	1.245747
28	1	0	3.884418	-2.602865	-0.276618
29	1	0	1.076956	0.088803	-1.117134
30	1	0	3.390964	-0.564151	-1.562789
31	1	0	4.197302	1.419317	1.545416
32	1	0	2.544600	1.887540	1.902862
33	1	0	3.086911	0.231783	2.206032
34	1	0	2.612003	1.783851	-1.846609
35	1	0	2.488667	2.844409	-0.428923
36	1	0	4.044762	2.182120	-0.893951
37	1	0	1.132169	-0.943786	2.688007
38	1	0	-0.446917	-0.435025	2.089113
39	1	0	0.011965	-2.174058	2.117819
40	1	0	0.366340	1.663463	1.434824
41	1	0	0.466582	2.308064	-0.199475

42	1	0	-2.841732	-0.635964	0.329676
43	1	0	-4.303788	3.351285	-0.304170
44	1	0	-6.974389	-0.027672	-0.562653
45	1	0	-1.591895	-2.495066	-0.676072
46	1	0	-1.356318	-1.044285	-1.107485
47	1	0	-6.589002	2.437609	-0.657931

HF= / NImag=1 (-57.9055 cm^{-1})
Sum of electronic and thermal Enthalpies= -3666.230203
Sum of electronic and thermal Free Energies= -3666.313463

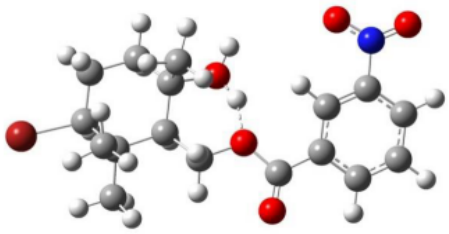

major-**45b**

Center Number	Atomic Number	Atomic Type	Coordinates (Angstroms) X	Y	Z
1	6	0	3.293314	-1.802818	-0.323880
2	6	0	1.821120	-2.101341	-0.655254
3	6	0	0.898095	-1.197856	0.143561
4	6	0	1.229162	0.300267	-0.068131
5	6	0	2.750293	0.674400	0.220917
6	6	0	3.604741	-0.335455	-0.598862
7	1	0	1.650328	-1.923228	-1.720751
8	1	0	1.594228	-3.152495	-0.454923
9	1	0	3.525962	-2.061793	0.711788
10	1	0	3.923872	-2.436863	-0.948138
11	1	0	1.098569	0.467496	-1.144142
12	1	0	3.462362	-0.126900	-1.660901
13	35	0	5.560524	-0.061151	-0.359240
14	6	0	3.109786	0.662720	1.719849
15	1	0	4.115911	1.060416	1.851363
16	1	0	2.438174	1.299770	2.298445
17	1	0	3.105545	-0.331752	2.167482
18	6	0	2.994054	2.097560	-0.329079
19	1	0	2.656706	2.196331	-1.365206
20	1	0	2.494752	2.860396	0.270553
21	1	0	4.060475	2.321545	-0.304338
22	6	0	0.613192	-1.678236	1.554353
23	1	0	1.538929	-1.686917	2.128990
24	1	0	-0.101077	-1.046267	2.083064
25	1	0	0.237684	-2.705374	1.543685
26	6	0	0.265820	1.256528	0.650280
27	1	0	0.334367	1.198497	1.735888
28	1	0	0.427204	2.284471	0.340615
29	8	0	-1.111757	0.895066	0.293278

30	6	0	-2.065374	1.921767	0.223864
31	8	0	-1.752452	3.067727	0.342338
32	6	0	-3.425955	1.388755	-0.023624
33	6	0	-3.726271	0.041212	0.168536
34	6	0	-4.429585	2.269091	-0.453597
35	6	0	-5.004715	-0.412231	-0.108314
36	1	0	-3.009315	-0.661511	0.561720
37	6	0	-5.712665	1.792761	-0.706569
38	1	0	-4.191541	3.317036	-0.587903
39	6	0	-6.014529	0.441163	-0.537596
40	1	0	-7.004304	0.049877	-0.733310
41	7	0	-5.271903	-1.860927	0.059522
42	8	0	-6.425312	-2.236569	-0.017276
43	8	0	-4.298650	-2.587730	0.253671
44	8	0	-0.507264	-1.324451	-0.629235
45	1	0	-0.984418	-2.147216	-0.423684
46	1	0	-1.044625	-0.505313	-0.353008
47	1	0	-6.484239	2.474510	-1.041482

HF= -3666.6459769 / NImag=0
Sum of electronic and thermal Enthalpies= -3666.235923
Sum of electronic and thermal Free Energies= -3666.316067

15. References

[1] Ashekar, K. D.; Marzijarani, N. S.; Jaganathan, A.; Holmes, D.; Jackson, J. E.; Borhan, B., *J. Am. Chem. Soc.* **2014**, *136*, 13355.

[2] Snyder, S. A.; Treitler, D. S., *Angew. Chem. Int. Ed.* **2009**, *48*, 7899.

[3] Sakakura, A.; Ukai, A.; Ishihara, K., *Nature* **2007**, *445*, 900.

[4] Samanta, R. C.; Yamamoto, H., *J. Am. Chem. Soc.* **2017**, *139*, 1460.

[5] Snyder, S. A.; Treitler, D. S.; Brucks, A. P., *J. Am. Chem. Soc.* **2010**, *132*, 14303.

[6] Barluenga, J.; Trincado, M.; Rubio, E.; González, J. M., *J. Am. Chem. Soc.* **2004**, *126*, 3416.

[7] Sakakura, A.; Shomi, G.; Ukai, A.; Ishihara, K., *Heterocycles* **2010**, *82*, 249.

[8] Gaussian 09, Revision **E.03**; Frisch, M. J.; Trucks, G. W.; Schlegel, H. B.; Scuseria, G. E.; Robb, M. A.; Cheeseman, J. R.; Scalmani, G.; Barone, V.; Petersson, G. A.; Nakatsuji, H.; Li, X.; Caricato, M.; Marenich, A. V.; Bloino, J.; Janesko, B. G.; Gomperts, R.; Mennucci, B.; Hratchian, H. P.; Ortiz, J. V.; Izmaylov, A. F.; Sonnenberg, J. L.; Williams-Young, D.; Ding, F.; Lipparini, F.; Egidi, F.; Goings, J.; Peng, B.; Petrone, A.; Henderson, T.; Ranasinghe, D.; Zakrzewski, V. G.; Gao, J.; Rega, N.; Zheng, G.; Liang, W.; Hada, M.; Ehara, M.; Toyota, K.; Fukuda, R.; Hasegawa, J.; Ishida, M.; Nakajima, T.; Honda, Y.; Kitao, O.; Nakai, H.; Vreven, T.; Throssell, K.; Montgomery, J. A., Jr.; Peralta, J. E.; Ogliaro, F.; Bearpark, M. J.; Heyd, J. J.; Brothers, E. N.; Kudin, K. N.; Staroverov, V. N.; Keith, T. A.; Kobayashi, R.; Normand, J.; Raghavachari, K.; Rendell, A. P.; Burant, J. C.; Iyengar, S. S.; Tomasi, J.; Cossi, M.; Millam, J. M.; Klene, M.; Adamo, C.; Cammi, R.; Ochterski, J. W.; Martin, R. L.; Morokuma, K.; Farkas, O.; Foresman, J. B.; Fox, D. J. Gaussian, Inc., Wallingford CT, 2016. Gaussian, Inc., Wallingford CT, **2016**.

[9] Becke, A.D., *J. Chem. Phys.* **1993**, *98*, 5648-5652.

[10] Lee, C.; Yang, W.; Parr, R. G., *Phys. Rev. B*, **1988**, *37*, 785-789.

[11] Vosko, S. H.; Wilk, L.; Nusair, M., *Can. J. Phys*. **1980**, *58*, 1200-1211.

[12] Stephens, P. J.; Devlin, F. J.; Chabalowski, C. F.; Frisch, M. J., *J. Phys. Chem.* **1994**, *98*, 11623-11627.

[13] Krishnan R.; Binkley, J. S.; Seeger, R.; Pople J. A., *J. Chem. Phys.* **1980**, *72*, 650-654.

[14] Curtiss, L. A.; McGrath, M. P.; Blandeau, J-P.; Davis, N. E.; Binning, R. C.; Radom Jr. L., *J. Chem. Phys.* **1995**, *103*, 6104-6113.

IV. Abbreviations

BDSB	bromo diethylsulfonium bromopentachloro antimonate(V)
BINOL	1,1’-bi-2-naphthol
CDSC	chloro diethylsulfonium hexachloroantimonate(V)
d.r.	diastereomeric ratio
DBDMH	1,3-dibromo-5,5-dimethylhydantoin
DCC	*N*,*N*’-dicyclohexycarbodiimide
DCE	1,2-dichloroethane
DMAPP	dimethylallypyrophosphate
DMF	*N*,*N*-dimethylformamide
ee	enantiomeric excess
et al.	et alii
G3P	glyceraldehyde-3-phosphate
GPP	geranylpyrophosphate
HFIP	1,1,1,3,3,3-hexafluoro-2-propanol
IDPI	imidodiphosphorimidate
IDSI	$(Et_2SI)_2Cl{\cdot}SbCl_6$
ÍL	ionic liquid
IPP	isoprenylpyrophosphate
IR	infrared spectroscopy
MEP	methyleritriol-4-phosphate
MVA	mevalonate
MVAPP	mevalonate pyrophosphate

NBS	*N*-bromosucinimide
NCS	*N*-chlorosucinimide
NIS	*N*-iodosucinimide
NMR	nuclear magnetic resonance spectroscopy
PFTB	perfluoro-*tert*-butanol
py	pyridine
quant.	quantitative
rac	racemic/racemate
rfx	reflux
SHC	squalene-hopene cyclase
TBDPS	*tert*-butyldiphenylsilyl
TFA	trifluoroacetic acid
THF	tetrahydrofuran
TLC	thin layer chromatography
tol	toluene

V. References

[1] a) A. Eschenmoser, L. Ruzicka, O. Jeger, D. Arigoni, *Helv. Chim. Acta* **1955**, *38*, 1890-1904; b) G. Stork, A. W. Burgstahler, *J. Am. Chem. Soc.* **1955**, *77*, 5068-5077.

[2] a) A. G. M. Barrett, T.-K. Ma, T. Mies, *Synthesis* **2019**, *51*, 67-82; b) A. C. A. D'Hollander, L. Peilleron, T. D. Grayfer, K. Cariou, *Synthesis* **2019**, *51*, 1753-1769.

[3] D. J. Reinert, G. Balliano, G. E. Schulz, *Chem. Biol.* **2004**, *11*, 121-126.

[4] K. Springob, T. M. Kutchan, in *Plant-derived Natural Products: Synthesis, Function, and Application* (Eds.: A. E. Osbourn, V. Lanzotti), Springer US, New York, NY, **2009**, pp. 3-50.

[5] a) H. Abozendadah, A. Bishop, S. Bittner, O. Lopez, C. Wiley, P. M. Flatt, *Consumer Chemistry: How Organic Chemistry Impacts Our Lives*, Western Oregon University, Available online: https://wou.edu/chemistry/courses/online-chemistry-textbooks/ch105-consumer-chemistry/, **2017**; b) K.-G. Fahlbusch, in *Ullmann's Encyclopedia of Industrial Chemistry (7th edition)*, Wiley, **2007**.

[6] P. Strathern, *Mendeleyev's Dream — The Quest For the Elements*, Berkley Books, New York, **2000**.

[7] Entry in the GoodScentsCompany Information Center: http://www.thegoodscentscompany.com/index.html, accessed on 19.01.2021, 14.24.

[8] B. Schäfer, *Chem. Unserer Zeit* **2011**, *45*, 374-388.

[9] https://de.wikipedia.org/wiki/Kiefern#/media/Datei:Raxalpe_-_junge_Zapfen_der_Latschenkiefer_-_Pinus_mugo.jpg, accessed on 28.09.2020, 16:46.

[10] https://de.wikipedia.org/wiki/Rosmarin#/media/Datei:Rosmarin2.jpg, accessed on 28.09.2020, 16:51.

[11] https://www.plantura.garden/gartentipps/obstratgeber/zitrusfruechte-besondere-arten-und-sorten-ueberblick-bilder, accessed on 01.10.2020, 14:25.

[12] https://www.derstandard.de/story/2000118879348/marihuana-im-wert-von-einer-million-euro-in-tirol-sichergestellt, accessed on 01.10.2020.

[13] https://www.baumschule-horstmann.de/shop/exec/product/77/6032/Edelrose-Grande-Amore.html, accessed on 01.10.2020, 14:51.

[14] https://allthatsinteresting.com/ambergris-whale-vomit, accessed on 01.10.2020, 14:27.

[15] Q. Zhang, L. Catti, L.-D. Syntrivanis, K. Tiefenbacher, *Nat. Prod. Rep.* **2019**, *36*, 1619-1627.

[16] Y. Kanda, H. Nakamura, S. Umemiya, R. K. Puthukanoori, V. R. Murthy Appala, G. K. Gaddamanugu, B. R. Paraselli, P. S. Baran, *J. Am. Chem. Soc.* **2020**, *142*, 10526-10533.

[17] R. R. Baadhe, N. K. Mekala, S. R. Palagiri, S. R. Parcha, *Appl. Biochem. Biotechnol.* **2012**, *167*, 1172-1182.

[18] D. W. Christianson, *Chem. Rev.* **2017**, *117*, 11570-11648.

[19] I. Ellouze, M. Abderrabba, N. Sabaou, F. Mathieu, A. Lebrihi, J. Bouajila, *F. Food Sci.* **2012**, *77*, T173-T180.

[20] E. Zlatic, A. Pichler, R. Vidrih, J. Hribar, V. Piližota, M. Kopjar, *Int. J. Food Prop.* **2018**, *20*, S3237-S3245.

[21] Z. Zebec, J. Wilkes, A. J. Jervis, N. S. Scrutton, E. Takano, R. Breitling, *Curr. Opin. Chem. Biol.* **2016**, *34*, 37-43.

[22] V. Zin, *La salud por medio de las plantas medicinales, 5th edition*, Ediciones Salesianas, Santiago de Chile, **1930**.

[23] B. J. Jansen, A. de Groot, *Nat. Prod. Rep.* **1991**, *8*, 309-318.

[24] G. Vediyappan, D. H. Hua, Patent *WO2013013178 (A1)*, USA, **2013**.

[25] a) M. Menger, D. Lentz, M. Christmann, *J. Org. Chem.* **2018**, *83*, 6793-6797; b) T. Kikuchi, K. Narita, K. Saijo, C. Ishioka, T. Katoh, *Eur. J. Org. Chem.* **2016**, 5659-5666; c) W. Zhang, H. Yao, J. Yu, Z. Zhang, R. Tong, *Angew. Chem. Int. Ed.* **2017**, *56*, 4787-4791; d) W. Cao, H. Deng, Y. Sun, B. Liu, S. Qin, *Chem. Eur. J.* **2018**, *24*, 9120-9129.

[26] S. A. Opiyo, L. O. A. Manguro, P. Okinda-Owuor, E. M. Ateka, P. Lemmen, *Phytochem. Letters* **2011**, *4*, 161-165.

[27] M. H. Foss, Y.-J. Eun, C. I. Grove, D. A. Pauw, N. A. Sorto, J. W. Rensvold, D. J. Pagliarini, J. T. Shaw, D. B. Weibel, *MedChemComm* **2013**, *4*, 112-119.

[28] T. Konoshima, M. Takasaki, H. Tokuda, K. Masuda, Y. Arai, K. Shiojima, H. Ageta, *Biol. Pharm. Bull.* **1996**, *19*, 962-965.

[29] M. Cortés, V. Delgado, C. Saitz, V. Armstrong, *Nat. Prod. Commun.* **2011**, *6*, doi: 10.1177/1934578x1100600408.

[30] M. Baunach, J. Franke, C. Hertweck, *Angew. Chem. Int. Ed.* **2015**, *54*, 2604-2626.

[31] S. Dettrakul, P. Kittakoop, M. Isaka, S. Nopichai, C. Suyarnsestakorn, M. Tanticharoen, Y. Thebtaranonth, *Bioorg. Med. Chem. Lett.* **2003**, *13*, 1253-1255.

[32] M. J. Durán-Peña, J. M. Botubol Ares, I. G. Collado, R. Hernández-Galán, *Nat. Prod. Rep.* **2014**, *31*, 940-952.

[33] R. Robinson, *J. Chem .Soc., Trans.* **1917**, *111*, 762-768.

[34] N. C. Ha, M. S. Kim, W. Lee, K. Y. Choi, B. H. Oh, *J. Biol. Chem.* **2000**, *275*, 41100-41106.

[35] R. A. Yoder, J. N. Johnston, *Chem. Rev.* **2005**, *105*, 4730-4756.

[36] L. Ruzicka, E. Capato, *Helv. Chim. Acta* **1925**, *8*, 259-274.

[37] L. Ruzicka, *Experientia* **1953**, *9*, 357-367.

[38] R. B. Woodward, K. Bloch, *J. Am. Chem. Soc.* **1953**, *75*, 2023-2024.

[39] E. Romann, A. J. Frey, P. A. Stadler, A. Eschenmoser, *Helv. Chim. Acta* **1957**, *40*, 1900-1917.

[40] P. A. Stadler, A. Eschenmoser, H. Schinz, G. Stork, *Helv. Chim. Acta* **1957**, *40*, 2191-2198.

[41] P. A. Stadler, A. Nechvatal, A. J. Frey, A. Eschenmoser., *Helv. Chim. Acta* **1957**, *40*, 1373-1409.

[42] K. U. Wendt, G. E. Schulz, E. J. Corey, D. R. Liu, *Angew. Chem. Int. Ed.* **2000**, *39*, 2812-2833.

[43] K. D. Ashtekar, N. S. Marzijarani, A. Jaganathan, D. Holmes, J. E. Jackson, B. Borhan, *J. Am. Chem. Soc.* **2014**, *136*, 13355-13362.

[44] R. R. Naredla, D. A. Klumpp, *Chem. Rev.* **2013**, *113*, 6905-6948.

[45] G. Stork, H. Conroy, *J. Am. Chem. Soc.* **1951**, *73*, 4748-4751.

[46] T. Kawanobe, K. Kogami, M. Matsui, *Agric. Biol. Chem.* **1986**, *50*, 1475-1480.

[47] a) R. L. Snowden, J. C. Eichenberger, S. M. Linder, P. Sonnay, C. Vial, K. H. Schulte-Elte, *J. Org. Chem.* **1992**, *57*, 955-960; b) R. L. Snowden, J.-C. Eichenberger, W. Giersch, W. Thommen, K. H. Schulte-Elte, *Helv. Chim. Acta* **1993**, *76*, 1608-1618; c) R. L. Snowden, S. Linder, *Helv. Chim. Acta* **2005**, *88*, 3055-3068; d) R. L. Snowden, *Chem. Biodiversity* **2008**, *5*, 958-969.

[48] a) T. Kato, S. Kumazawa, Y. Kitahara, *Synthesis* **1972**, *1972*, 573-574; b) R. E. Ireland, C. A. Lipinski, C. J. Kowalski, J. W. Tilley, D. M. Walba, *J. Am. Chem. Soc.* **1974**, *96*, 3333-3335; c) C. G. M. Janssen, E. F. Godefroi, *J. Org. Chem.* **1984**, *49*, 3600-3603; d) V. Rosales, J. L. Zambrano, M. Demuth, *J. Org. Chem.* **2002**, *67*, 1167-1170; e) Y.-J. Zhao, S.-S. Chng, T.-P. Loh, *J. Am. Chem. Soc.* **2007**, *129*, 492-493.

[49] a) A. Saito, H. Matsushita, H. Kaneko, *Agric. Biol. Chem.* **1986**, *50*, 771-772; b) M. Tada, S. Nishiiri, Y. Zhixiang, Y. Imai, S. Tajima, N. Okazaki, Y. Kitano, K. Chiba, *J. Chem. Soc. Perkin 1* **2000**, 2657-2664; c) M. Graham, R. W. Baker, C. S. P. McErlean, *Eur. J. Org. Chem.* **2017**, *2017*, 908-913.

[50] T.-H. Chou, B.-H. Yu, R.-J. Chein, *Chem. Commun.* **2019**, *55*, 13522-13525.

[51] a) S. W. Youn, S. J. Pastine, D. Sames, *Org. Lett.* **2004**, *6*, 581-584; b) K. Xie, S. Wang, P. Li, X. Li, Z. Yang, X. An, C.-C. Guo, Z. Tan, *Tetrahedron Lett.* **2010**, *51*, 4466-4469; c) S.-C. Lin, R.-J. Chein, *J. Org. Chem.* **2017**, *82*, 1575-1583.

[52] K. Surendra, W. Qiu, E. J. Corey, *J. Am. Chem. Soc.* **2011**, *133*, 9724-9726.

[53] R. A. Shenvi, K. K. Wan, in *Applications of Domino Transformations in Organic Synthesis 1*, 2016 ed. (Eds.: S. A. Snyder, E. Schaumann), Georg Thieme Verlag, Stuttgart, **2016**.

[54] K. Ishihara, H. Ishibashi, H. Yamamoto, *J. Am. Chem. Soc.* **2002**, *124*, 3647-3655.

[55] Z. Yang, H. Li, L. Zhang, M. T. Zhang, J. P. Cheng, S. Luo, *Chemistry* **2015**, *21*, 14723-14727.

[56] a) Q.-Y. Meng, J.-J. Zhong, Q. Liu, X.-W. Gao, H.-H. Zhang, T. Lei, Z.-J. Li, K. Feng, B. Chen, C.-H. Tung, L.-Z. Wu, *J. Am. Chem. Soc.* **2013**, *135*, 19052-19055; b) Q. Liu, Y.-N. Li, H.-H. Zhang, B. Chen, C.-H. Tung, L.-Z. Wu, *Chem. Eur. J.* **2012**, *18*, 620-627.

[57] a) U. Hoffmann, Y. Gao, B. Pandey, S. Klinge, K. D. Warzecha, C. Krueger, H. D. Roth, M. Demuth, *J. Am. Chem. Soc.* **1993**, *115*, 10358-10359; b) C. Heinemann, M. Demuth, *J. Am. Chem. Soc.* **1997**, *119*, 1129-1130; c) X. Xing, M. Demuth, *Synlett* **1999**, *1999*, 987-990.

[58] K. Ishihara, S. Nakamura, H. Yamamoto, *J. Am. Chem. Soc.* **1999**, *121*, 4906-4907.

[59] K. Surendra, E. J. Corey, *J. Am. Chem. Soc.* **2012**, *134*, 11992-11994.

[60] A. Crusco, C. Bordoni, A. Chakroborty, K. C. L. Whatley, H. Whiteland, A. D. Westwell, K. F. Hoffmann, *Eur. J. Med. Chem.* **2018**, *152*, 87-100.

[61] L. Fan, C. Han, X. Li, J. Yao, Z. Wang, C. Yao, W. Chen, T. Wang, J. Zhao, *Angew. Chem. Int. Ed.* **2018**, *57*, 2115-2119.

[62] I. Čorić, B. List, *Nature* **2012**, *483*, 315-319.

[63] a) B. Mitschke, M. Turberg, B. List, *Chem* **2020**; b) N. Tsuji, J. L. Kennemur, T. Buyck, S. Lee, S. Prévost, P. S. J. Kaib, D. Bykov, C. Farès, B. List, *Science* **2018**, *359*, 1501.

[64] A. M. Arnold, A. Pöthig, M. Drees, T. Gulder, *J. Am. Chem. Soc.* **2018**, *140*, 4344-4353.

[65] E. E. van Tamelen, E. J. Hessler, *Chem. Commun.* **1966**, 411-413.

[66] a) C. N. Ungarean, E. H. Southgate, D. Sarlah, *Org. Biomol. Chem.* **2016**, *14*, 5454-5467; b) C. N. Ungarean, E. H. Southgate, D. Sarlah, *Org. Biomol. Chem.* **2016**, *14*, 5454-5467.

[67] T. R. Hoye, M. J. Kurth, *J. Org. Chem.* **1978**, *43*, 3693-3697.

[68] S. Fujiwara, K. Takeda, T. Uyehara, T. Kato, *Chem. Lett.* **1986**, *15*, 1763-1766.

[69] T. Kato, I. Ichinose, *J. Chem. Soc. Perkin Trans. I* **1980**, 1051-1056.

[70] C. Ascheberg, J. Bock, F. Buß, C. Mück-Lichtenfeld, C. G. Daniliuc, K. Bergander, F. Dielmann, U. Hennecke, *Chem. Eur. J.* **2017**, *23*, 11578-11586.

[71] T. D. Grayfer, P. Retailleau, R. H. Dodd, J. Dubois, K. Cariou, *Org. Lett.* **2017**, *19*, 4766-4769.

[72] A. Sakakura, A. Ukai, K. Ishihara, *Nature* **2007**, *445*, 900-903.

[73] J. Barluenga, M. Trincado, E. Rubio, J. M. González, *J. Am. Chem. Soc.* **2004**, *126*, 3416-3417.

[74] S. A. Snyder, Z.-Y. Tang, R. Gupta, *J. Am. Chem. Soc.* **2009**, *131*, 5744-5745.

[75] S. A. Snyder, D. S. Treitler, A. P. Brucks, *J. Am. Chem. Soc.* **2010**, *132*, 14303-14314.

[76] S. A. Snyder, D. S. Treitler, *Angew. Chem. Int. Ed.* **2009**, *48*, 7899-7903.

[77] a) Y. Sawamura, H. Nakatsuji, A. Sakakura, K. Ishihara, *Chem. Sci.* **2013**, *4*, 4181-4186; b) Y. Sawamura, H. Nakatsuji, M. Akakura, A. Sakakura, K. Ishihara, *Chirality* **2014**, *26*, 356-360.

[78] R. C. Samanta, H. Yamamoto, *J. Am. Chem. Soc.* **2017**, *139*, 1460-1463.

[79] S. A. Snyder, D. S. Treitler, A. Schall, *Tetrahedron* **2010**, *66*, 4796-4804.

[80] D. C. Braddock, J. S. Marklew, K. M. Foote, A. J. P. White, *Chirality* **2013**, *25*, 692-700.

[81] A. J. Burckle, V. H. Vasilev, N. Z. Burns, *Angew. Chem. Int. Ed.* **2016**, *55*, 11476-11479.

[82] M. L. Landry, G. M. McKenna, N. Z. Burns, *J. Am. Chem. Soc.* **2019**, *141*, 2867-2871.

[83] a) D. X. Hu, G. M. Shibuya, N. Z. Burns, *J. Am. Chem. Soc.* **2013**, *135*, 12960-12963; b) D. X. Hu, F. J. Seidl, C. Bucher, N. Z. Burns, *J. Am. Chem. Soc.* **2015**, *137*, 3795-3798.

[84] a) C. Wagner, M. El Omari, G. M. König, *J. Nat. Prod.* **2009**, *72*, 540-553; b) G. W. Gribble, *Mar. Drugs* **2015**, *13*, 4044-4136.

[85] a) G. A. Olah, J. M. Bollinger, *J. Am. Chem. Soc.* **1967**, *89*, 4744-4752; b) G. A. Olah, J. M. Bollinger, *J. Am. Chem. Soc.* **1968**, *90*, 947-953; c) G. A. Olah, J. M. Bollinger, J. Brinich, *J. Am. Chem. Soc.* **1968**, *90*, 2587-2594; d) S. E. Denmark, W. E. Kuester, M. T. Burk, *Angew. Chem. Int. Ed.* **2012**, *51*, 10938-10953.

[86] S. E. Denmark, M. T. Burk, A. J. Hoover, *J. Am. Chem. Soc.* **2010**, *132*, 1232-1233.

[87] R. S. Brown, R. W. Nagorski, A. J. Bennet, R. E. D. McClung, G. H. M. Aarts, M. Klobukowski, R. McDonald, B. D. Santarsiero, *J. Am. Chem. Soc.* **1994**, *116*, 2448-2456.

[88] W. M. Hart-Cooper, K. N. Clary, F. D. Toste, R. G. Bergman, K. N. Raymond, *J. Am. Chem. Soc.* **2012**, *134*, 17873-17876.

[89] Q. Zhang, K. Tiefenbacher, *Nature Chem.* **2015**, *7*, 197-202.

[90] T. M. Brauer, Q. Zhang, K. Tiefenbacher, *Angew. Chem. Int. Ed.* **2016**, *55*, 7698-7701.

[91] a) Q. Zhang, L. Catti, J. Pleiss, K. Tiefenbacher, *J. Am. Chem. Soc.* **2017**, *139*, 11482-11492; b) K. Tiefenbacher, L. Catti, Q. Zhang, *Synthesis* **2015**, *48*, 313-328.

[92] a) A. Berkessel, M. R. M. Andreae, *Tetrahedron Lett.* **2001**, *42*, 2293-2295; b) A. Berkessel, J. A. Adrio, *Adv. Synth. Catal.* **2004**, *346*, 275-280.

[93] I. A. Shuklov, N. V. Dubrovina, A. Börner, *Synthesis* **2007**, *2007*, 2925-2943.

[94] W. Reeve, C. M. Erikson, P. F. Aluotto, *Can. J. Chem.* **1979**, *57*, 2747-2754.

[95] A. Berkessel, J. A. Adrio, D. Hüttenhain, J. M. Neudörfl, *J. Am. Chem. Soc.* **2006**, *128*, 8421-8426.

[96] I. Colomer, A. E. R. Chamberlain, M. B. Haughey, T. J. Donohoe, *Nat. Rev. Chem.* **2017**, *1*, 0088.

[97] O. Hollóczki, A. Berkessel, J. Mars, M. Mezger, A. Wiebe, S. R. Waldvogel, B. Kirchner, *ACS Catal.* **2017**, *7*, 1846-1852.

[98] a) A. Di Salvo, M. David, B. Crousse, D. Bonnet-Delpon, *Adv. Synth. Catal.* **2006**, *348*, 118-124; b) B. T. Kelley, J. C. Walters, S. E. Wengryniuk, *Org. Lett.* **2016**, *18*, 1896-1899.

[99] J. P. Pezacki, D. Shukla, J. Lusztyk, J. Warkentin, *J. Am. Chem. Soc.* **1999**, *121*, 6589-6598.

[100] V. Pozhydaiev, M. Power, V. Gandon, J. Moran, D. Leboeuf, *Chem. Commun.* **2020**, *56*, 11548-11564.

[101] S. J. Brenek, S. Caron, E. Chisowa, M. P. Delude, M. T. Drexler, M. D. Ewing, R. E. Handfield, N. D. Ide, D. V. Nadkarni, J. D. Nelson, M. Olivier, H. H. Perfect, J. E. Phillips, J. J. Teixeira, R. M. Weekly, J. P. Zelina, *Org. Process Res. Dev.* **2012**, *16*, 1348-1359.

[102] T. W. Bentley, G. E. Carter, *J. Org. Chem.* **2002**, *48*, 579-584.

[103] a) T. D. Grayfer, P. Retailleau, R. H. Dodd, J. Dubois, K. Cariou, *Org. Lett.* **2017**, *19*, 4766-4769; b) R. C. Samanta, H. Yamamoto, *J. Am. Chem. Soc.* **2017**, *139*, 1460-1463.

[104] a) D. C. Fabry, M. Stodulski, S. Hoerner, T. Gulder, *Chem. Eur. J.* **2012**, *18*, 10834-10838; b) M. Stodulski, A. Goetzinger, S. V. Kohlhepp, T. Gulder, *Chem. Commun.* **2014**, *50*, 3435-3438; c) A. Ulmer, M. Stodulski, S. V. Kohlhepp, C. Patzelt, A. Pöthig, W. Bettray, T. Gulder, *Chem. Eur. J.* **2015**, *21*, 1444-1448; d) C. Patzelt, A. Pöthig, T. Gulder, *Org. Lett.* **2016**, *18*, 3466-3469; e) A. Ulmer, C. Brunner, A. M. Arnold, A. Pöthig, T. Gulder, *Chem. Eur. J.* **2016**, *22*, 3660-3664; f) C. Brunner, A. Andries-Ulmer, G. M. Kiefl, T. Gulder, *Eur. J. Org. Chem.* **2018**, *2018*, 2615-2621; g) A. Andries-Ulmer, C. Brunner, J. Rehbein, T. Gulder, *J. Am. Chem. Soc.* **2018**, *140*, 13034-13041; h) M. Stodulski, S. V. Kohlhepp, G. Raabe, T. Gulder, *Eur. J. Org. Chem.* **2016**, *2016*, 2170-2176.

[105] a) A. Berkessel, J. A. Adrio, *J. Am. Chem. Soc.* **2006**, *128*, 13412-13420; b) I. Colomer, C. Batchelor-McAuley, B. Odell, T. J. Donohoe, R. G. Compton, *J. Am. Chem. Soc.* **2016**, *138*, 8855-8861; c) Y. Zhu, I. Colomer, A. L. Thompson, T. J. Donohoe, *J. Am. Chem. Soc.* **2019**, *141*, 6489-6493; d) Z. Li, B. Yu, *Chemistry* **2019**; e) S. K. Sinha, T. Bhattacharya, D. Maiti, *React. Chem. Eng.* **2019**, *4*, 244-253; f) J. M. Ramos-Villaseñor, E. Rodríguez-Cárdenas, C. E. Barrera Díaz, B. A. Frontana-Uribe, *J. Electrochem. Soc.* **2020**, *167*; g) Z. Zhu, C. M. Glinkerman, D. L. Boger, *J. Am. Chem. Soc.* **2020**, *142*, 20778-20787; h) C. Wei, Y. He, J. Wang, X. Ye, L. Wojtas, X. Shi, *Org. Lett.* **2020**, *22*, 5462-5465; i) F. Z. Zhang, Y. Tian, G. X. Li, J. Qu, *J. Org. Chem.* **2015**, *80*, 1107-1115; j) Y. Tian, X. Xu, L. Zhang, J. Qu, *Org. Lett.* **2016**, *18*, 268-271.

[106] A. M. Arnold, Master's thesis, Technical University Munich (Munich), **2015**.

[107] S. A. Snyder, D. A. Treitler, A. P. Brucks, *Aldrichim. Acta* **2011**, 27-42.

[108] K. Kumazawa, K. Ishihara, H. Yamamoto, *Org. Lett.* **2004**, *6*, 2551-2554.

[109] Entry in product catalogue of Sigma-Aldrich for hexafluoroacetone sesquihydrate, https://www.sigmaaldrich.com, accessed on 05.02.2021, 14:34.

[110] Evan's pKa Table: http://ccc.chem.pitt.edu/wipf/MechOMs/evans_pKa_table.pdf and references therein, accessed on 19.01.2021, 22:11.

[111] J. P. Guthrie, *Can. J. Chem.* **1978**, *56*, 2342-2354.

[112] K. Jones, C. DeAmicis, in *Encyclopedia of Reagents for Organic Synthesis*, **2009**, pp. 1-9.

[113] C. Yang, X.-S. Xue, J.-L. Jin, X. Li, J.-P. Cheng, *J. Org. Chem.* **2013**, *78*, 7076-7085.

[114] H. H. Jaffé, G. O. Doak, *J. Am. Chem. Soc.* **1955**, *77*, 4441-4444.

[115] T. N. Sudakova, V. V. Krasnoshchekov, *Zh. Neorg. Khim.* **1978**, *23*, 1506.

[116] A. Trummal, L. Lipping, I. Kaljurand, I. A. Koppel, I. Leito, *J. Phys. Chem. A* **2016**, *120*, 3663-3669.

[117] Z. Tao, K. A. Robb, K. Zhao, S. E. Denmark, *J. Am. Chem. Soc.* **2018**, *140*, 3569-3573.

[118] a) I. Krossing, I. Raabe, *Angew. Chem. Int. Ed.* **2004**, *43*, 2066-2090; b) A. Martens, P. Weis, M. C. Krummer, M. Kreuzer, A. Meierhöfer, S. C. Meier, J. Bohnenberger, H. Scherer, I. Riddlestone, I. Krossing, *Chem. Sci.* **2018**, *9*, 7058-7068.

[119] a) S. Decato, T. Bemis, E. Madsen, S. Mecozzi, *Polym. Chem.* **2014**, *5*, 6461-6471; b) C. Lu, J.-H. Kim, D. D. DesMarteau, *J. Fluorine Chem.* **2010**, *131*, 17-20.

[120] R. Filler, R. M. Schure, *J. Org. Chem.* **1967**, *32*, 1217-1219.

[121] N. J. Matuska, R. N. Bose, *Res. Chem. Intermed.* **1997**, *23*, 109-119.

[122] a) U. Mayer, V. Gutmann, W. Gerger, *Monatsh. Chemie* **1975**, *106*, 1235-1257; b) M. A. Beckett, G. C. Strickland, J. R. Holland, K. Sukumar Varma, *Polymer* **1996**, *37*, 4629-4631.

[123] Y. Chen, Y.-F. Zhao, Y.-W. Yin, X.-Q. Yang, *Phosphorus Sulfur* **1991**, *61*, 31-39.

[124] M. A. Beckett, D. S. Brassington, S. J. Coles, M. B. Hursthouse, *Inorg. Chem. Commun.* **2000**, *3*, 530-533.

[125] W.-Y. Tsang, J. P. Richard, *J. Am. Chem. Soc.* **2007**, *129*, 10330-10331.

[126] Personal communication with Dr. Maik Icker, Leipzig University, October 2020.

[127] a) J. Stonehouse, P. Adell, J. Keeler, A. J. Shaka, *J. Am. Chem. Soc.* **1994**, *116*, 6037-6038; b) M. J. Thrippleton, J. Keeler, *Angew. Chem. Int. Ed.* **2003**, *42*, 3938-3941.

[128] P. G. M. Wuts, in *Greene's Protective Groups in Organic Synthesis* (Ed.: P. G. M. Wuts), Wiley, Weinheim, **2014**, pp. 17-471.

[129] A. P. J. Brunskill, H. W. Thompson, R. A. Lalancette, *Acta Cryst. C* **1999**, *55*, 566-568.

[130] M. Delarmelina, C. D. Nicoletti, M. C. de Moraes, D. O. Futuro, M. Bühl, F. de C. da Silva, V. F. Ferreira, J. W. de M. Carneiro, *ChemPlusChem* **2019**, *84*, 52-61.

[131] D. Seebach, H. A. Oei, *Angew. Chem.* **1975**, *87*, 629-630.

[132] C. Reichardt, *Solvents and Solvent Effects in Organic Chemistry*, Wiley-VCH, Weinheim, **2003**.

[133] B. Pégot, G. Vo-Thanh, D. Gori, A. Loupy, *Tetrahedron Lett.* **2004**, *45*, 6425-6428.

[134] R. Gausepohl, P. Buskens, J. Kleinen, A. Bruckmann, C. W. Lehmann, J. Klankermayer, W. Leitner, *Angew. Chem. Int. Ed.* **2006**, *45*, 3689-3692.

[135] https://arctomsci.com/652-21-1-428911, accessed on 01.02.2021, 00:19.

[136] D. Enders, O. Meyer, G. Raabe, J. Runsink, *Synthesis* **1994**, *1994*, 66-72.

[137] S. A. Babu, K. K. Krishnan, S. M. Ujwaldev, G. Anilkumar, *Asian J. Org. Chem.* **2018**, *7*, 1033-1053.

[138] J. R. Wolstenhulme, V. Gouverneur, *Acc. Chem. Res.* **2014**, *47*, 3560-3570.

[139] V. P. Glazunov, S. E. Odinokov, *Spectrochim. Acta A* **1982**, *38*, 399-408.

[140] A. Sakakura, M. Sakuma, K. Ishihara, *Org. Lett.* **2011**, *13*, 3130-3133.

[141] P. M. Imamura, G. M. P. Santiago, *Synth. Commun.* **1997**, *27*, 2479-2485.

[142] K. B. Upar, S. J. Mishra, S. P. Nalawade, S. A. Singh, R. P. Khandare, S. V. Bhat, *Tetrahedron Asymmetry* **2009**, *20*, 1637-1640.

[143] C. Tsangarakis, M. Stratakis, *Adv. Synth. Catal.* **2005**, *347*, 1280-1284.

[144] A. Fernandez Mateos, A. M. Lopez Barba, *J. Org. Chem.* **1995**, *60*, 3580-3585.

[145] A. Fernández Mateos, G. Pascual Coca, J. J. Pérez Alonso, R. R. González, C. T. Hernández, *Tetrahedron Lett.* **1995**, *36*, 621-624.

[146] R. J. Abraham, M. A. Warne, L. Griffiths, *J. Chem. Soc. Perkin 2* **1998**, 1751-1758.

[147] T. B. Gontijo, R. P. de Freitas, G. F. de Lima, L. C. D. de Rezende, L. F. Pedrosa, T. L. Silva, M. O. F. Goulart, B. C. Cavalcanti, C. Pessoa, M. P. Bruno, J. R. Corrêa, F. S. Emery, E. N. da Silva Júnior, *Chem. Commun.* **2016**, *52*, 13281-13284.

[148] I. Hayakawa, T. Nakamura, O. Ohno, K. Suenaga, H. Kigoshi, *Org. Biomol. Chem.* **2015**, *13*, 9969-9976.

[149] G. Laudadio, S. Govaerts, Y. Wang, D. Ravelli, H. F. Koolman, M. Fagnoni, S. W. Djuric, T. Noël, *Angew. Chem. Int. Ed.* **2018**, *57*, 4078-4082.

VI. Appendix

1. Letter of Approval from the American Chemical Society (II.1)

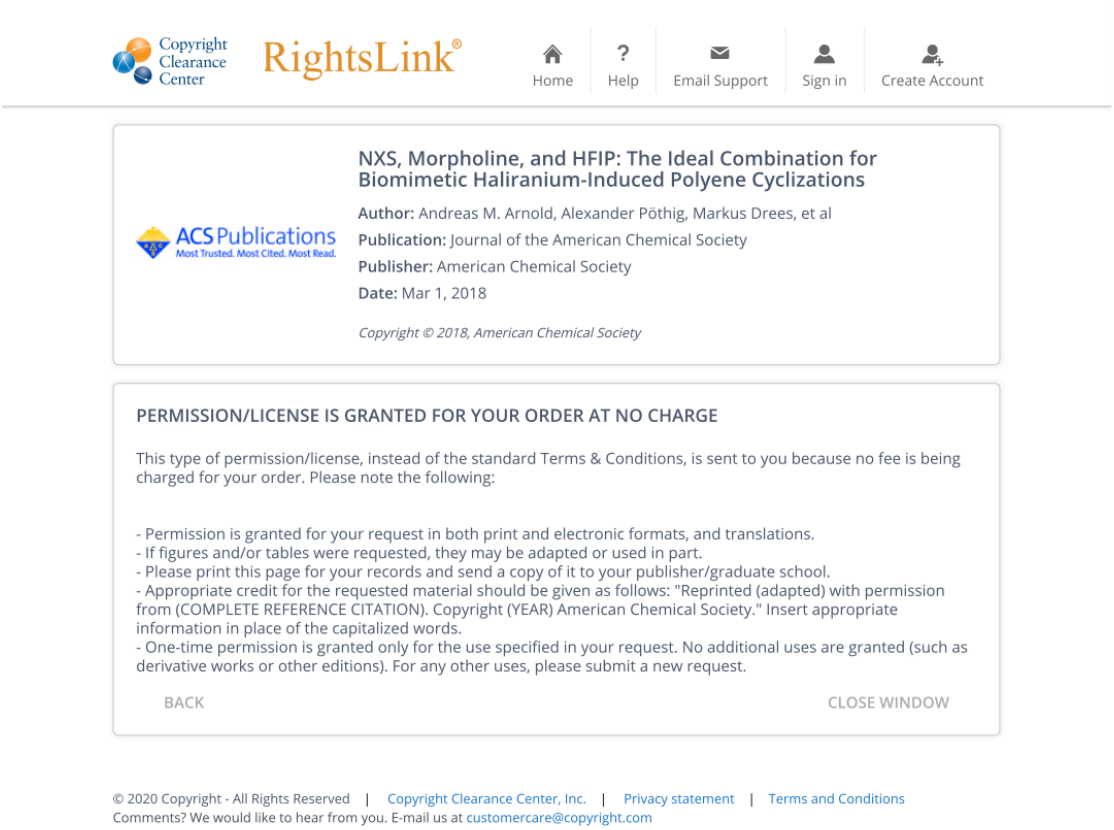

Copyright Clearance Center RightsLink®

Home | Help | Email Support | Sign in | Create Account

ACS Publications
Most Trusted. Most Cited. Most Read.

NXS, Morpholine, and HFIP: The Ideal Combination for Biomimetic Haliranium-Induced Polyene Cyclizations

Author: Andreas M. Arnold, Alexander Pöthig, Markus Drees, et al
Publication: Journal of the American Chemical Society
Publisher: American Chemical Society
Date: Mar 1, 2018

Copyright © 2018, American Chemical Society

PERMISSION/LICENSE IS GRANTED FOR YOUR ORDER AT NO CHARGE

This type of permission/license, instead of the standard Terms & Conditions, is sent to you because no fee is being charged for your order. Please note the following:

- Permission is granted for your request in both print and electronic formats, and translations.
- If figures and/or tables were requested, they may be adapted or used in part.
- Please print this page for your records and send a copy of it to your publisher/graduate school.
- Appropriate credit for the requested material should be given as follows: "Reprinted (adapted) with permission from (COMPLETE REFERENCE CITATION). Copyright (YEAR) American Chemical Society." Insert appropriate information in place of the capitalized words.
- One-time permission is granted only for the use specified in your request. No additional uses are granted (such as derivative works or other editions). For any other uses, please submit a new request.

BACK CLOSE WINDOW

2. Letter of Approval from Elsevier (Figure 2)

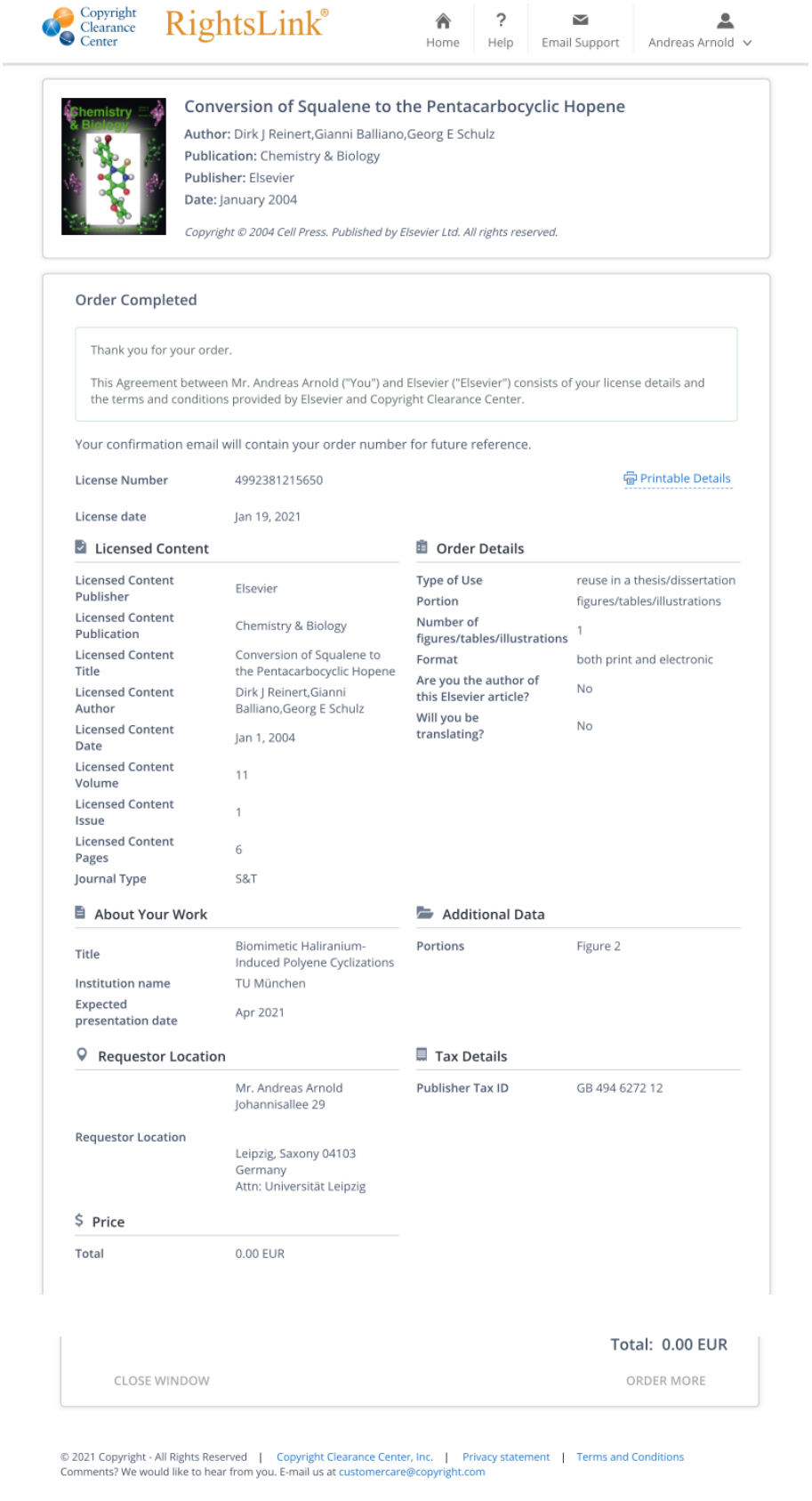

Copyright Clearance Center RightsLink®

Home | Help | Email Support | Andreas Arnold

Conversion of Squalene to the Pentacarbocyclic Hopene

Author: Dirk J Reinert,Gianni Balliano,Georg E Schulz
Publication: Chemistry & Biology
Publisher: Elsevier
Date: January 2004

Copyright © 2004 Cell Press. Published by Elsevier Ltd. All rights reserved.

Order Completed

Thank you for your order.

This Agreement between Mr. Andreas Arnold ("You") and Elsevier ("Elsevier") consists of your license details and the terms and conditions provided by Elsevier and Copyright Clearance Center.

Your confirmation email will contain your order number for future reference.

Printable Details

License Number	4992381215650
License date	Jan 19, 2021

Licensed Content

Licensed Content Publisher	Elsevier
Licensed Content Publication	Chemistry & Biology
Licensed Content Title	Conversion of Squalene to the Pentacarbocyclic Hopene
Licensed Content Author	Dirk J Reinert,Gianni Balliano,Georg E Schulz
Licensed Content Date	Jan 1, 2004
Licensed Content Volume	11
Licensed Content Issue	1
Licensed Content Pages	6
Journal Type	S&T

Order Details

Type of Use	reuse in a thesis/dissertation
Portion	figures/tables/illustrations
Number of figures/tables/illustrations	1
Format	both print and electronic
Are you the author of this Elsevier article?	No
Will you be translating?	No

About Your Work

Title	Biomimetic Haliranium-Induced Polyene Cyclizations
Institution name	TU München
Expected presentation date	Apr 2021

Additional Data

Portions	Figure 2

Requestor Location

Requestor Location	Mr. Andreas Arnold Johannisallee 29 Leipzig, Saxony 04103 Germany Attn: Universität Leipzig

Tax Details

Publisher Tax ID	GB 494 6272 12

Price

Total	0.00 EUR

Total: 0.00 EUR

CLOSE WINDOW ORDER MORE

3. Letter of Approval from Elsevier (Scheme 8)

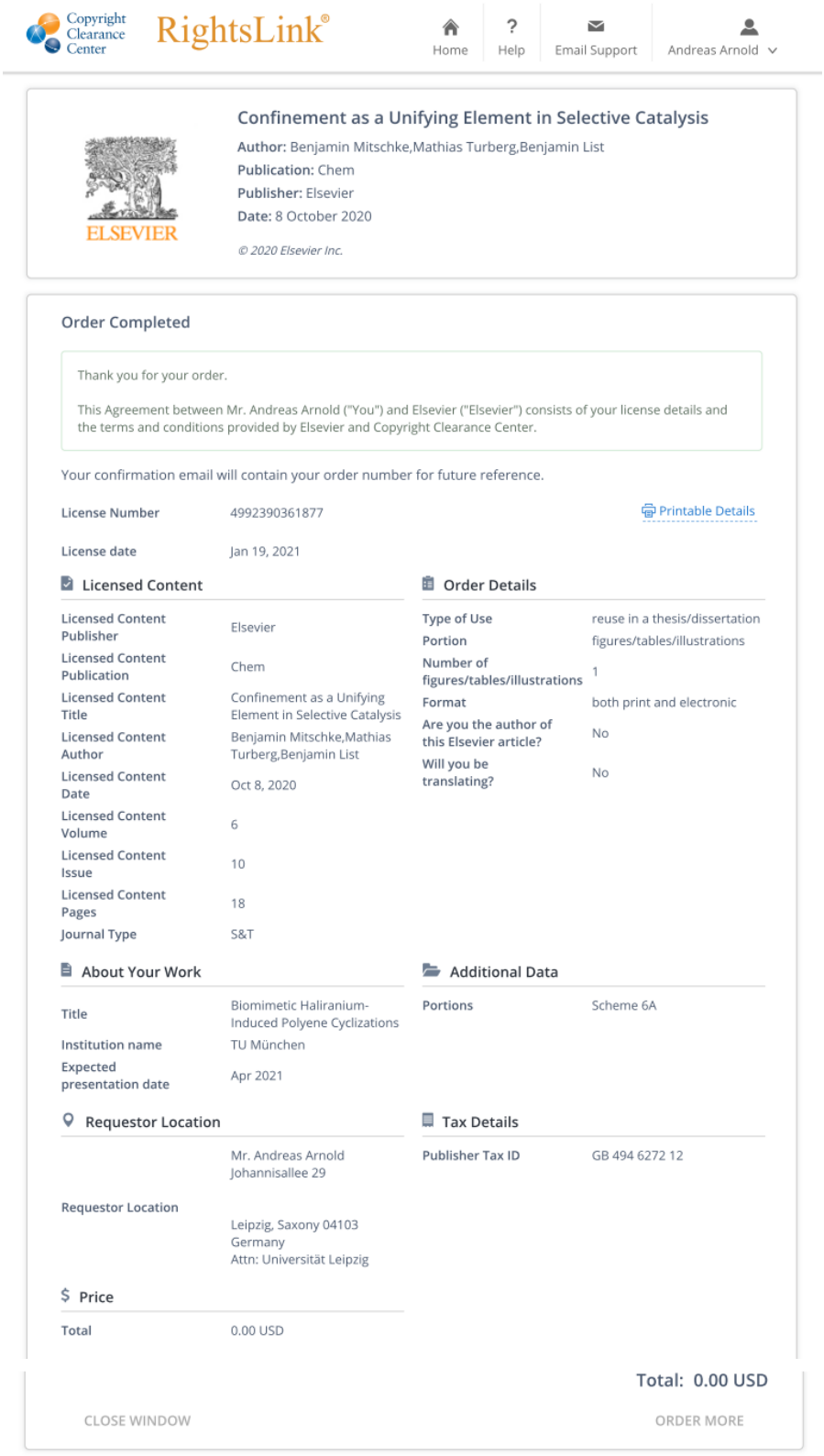

Copyright Clearance Center RightsLink®

Home | Help | Email Support | Andreas Arnold

Confinement as a Unifying Element in Selective Catalysis

Author: Benjamin Mitschke,Mathias Turberg,Benjamin List
Publication: Chem
Publisher: Elsevier
Date: 8 October 2020

© 2020 Elsevier Inc.

Order Completed

Thank you for your order.

This Agreement between Mr. Andreas Arnold ("You") and Elsevier ("Elsevier") consists of your license details and the terms and conditions provided by Elsevier and Copyright Clearance Center.

Your confirmation email will contain your order number for future reference.

Printable Details

License Number	4992390361877
License date	Jan 19, 2021

Licensed Content

Licensed Content Publisher	Elsevier
Licensed Content Publication	Chem
Licensed Content Title	Confinement as a Unifying Element in Selective Catalysis
Licensed Content Author	Benjamin Mitschke,Mathias Turberg,Benjamin List
Licensed Content Date	Oct 8, 2020
Licensed Content Volume	6
Licensed Content Issue	10
Licensed Content Pages	18
Journal Type	S&T

Order Details

Type of Use	reuse in a thesis/dissertation
Portion	figures/tables/illustrations
Number of figures/tables/illustrations	1
Format	both print and electronic
Are you the author of this Elsevier article?	No
Will you be translating?	No

About Your Work

Title	Biomimetic Haliranium-Induced Polyene Cyclizations
Institution name	TU München
Expected presentation date	Apr 2021

Additional Data

Portions	Scheme 6A

Requestor Location

	Mr. Andreas Arnold Johannisallee 29
Requestor Location	Leipzig, Saxony 04103 Germany Attn: Universität Leipzig

Tax Details

Publisher Tax ID	GB 494 6272 12

Price

Total	0.00 USD

Total: 0.00 USD

CLOSE WINDOW ORDER MORE

4. Letter of Approval from Springer Nature (Scheme 19)

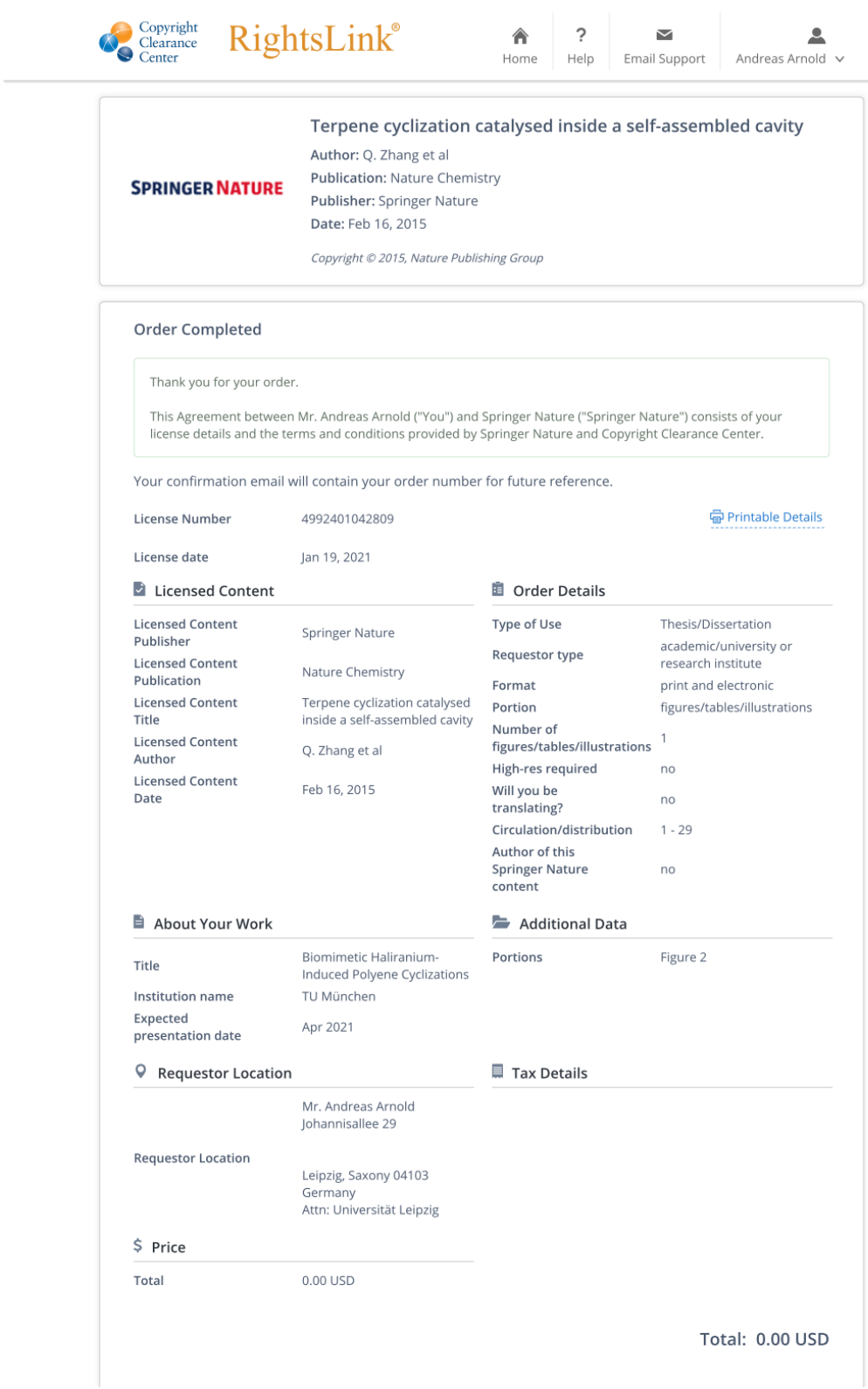

Copyright Clearance Center RightsLink®

Home | Help | Email Support | Andreas Arnold

SPRINGER NATURE

Terpene cyclization catalysed inside a self-assembled cavity

Author: Q. Zhang et al
Publication: Nature Chemistry
Publisher: Springer Nature
Date: Feb 16, 2015

Copyright © 2015, Nature Publishing Group

Order Completed

Thank you for your order.

This Agreement between Mr. Andreas Arnold ("You") and Springer Nature ("Springer Nature") consists of your license details and the terms and conditions provided by Springer Nature and Copyright Clearance Center.

Your confirmation email will contain your order number for future reference.

License Number	4992401042809
License date	Jan 19, 2021

Printable Details

Licensed Content

Licensed Content Publisher	Springer Nature
Licensed Content Publication	Nature Chemistry
Licensed Content Title	Terpene cyclization catalysed inside a self-assembled cavity
Licensed Content Author	Q. Zhang et al
Licensed Content Date	Feb 16, 2015

Order Details

Type of Use	Thesis/Dissertation
Requestor type	academic/university or research institute
Format	print and electronic
Portion	figures/tables/illustrations
Number of figures/tables/illustrations	1
High-res required	no
Will you be translating?	no
Circulation/distribution	1 - 29
Author of this Springer Nature content	no

About Your Work

Title	Biomimetic Haliranium-Induced Polyene Cyclizations
Institution name	TU München
Expected presentation date	Apr 2021

Additional Data

Portions	Figure 2

Requestor Location

Requestor Location	Mr. Andreas Arnold Johannisallee 29 Leipzig, Saxony 04103 Germany Attn: Universität Leipzig

Tax Details

Price

Total	0.00 USD

Total: 0.00 USD

5. Letter of Approval from the American Chemical Society (Figure 7)

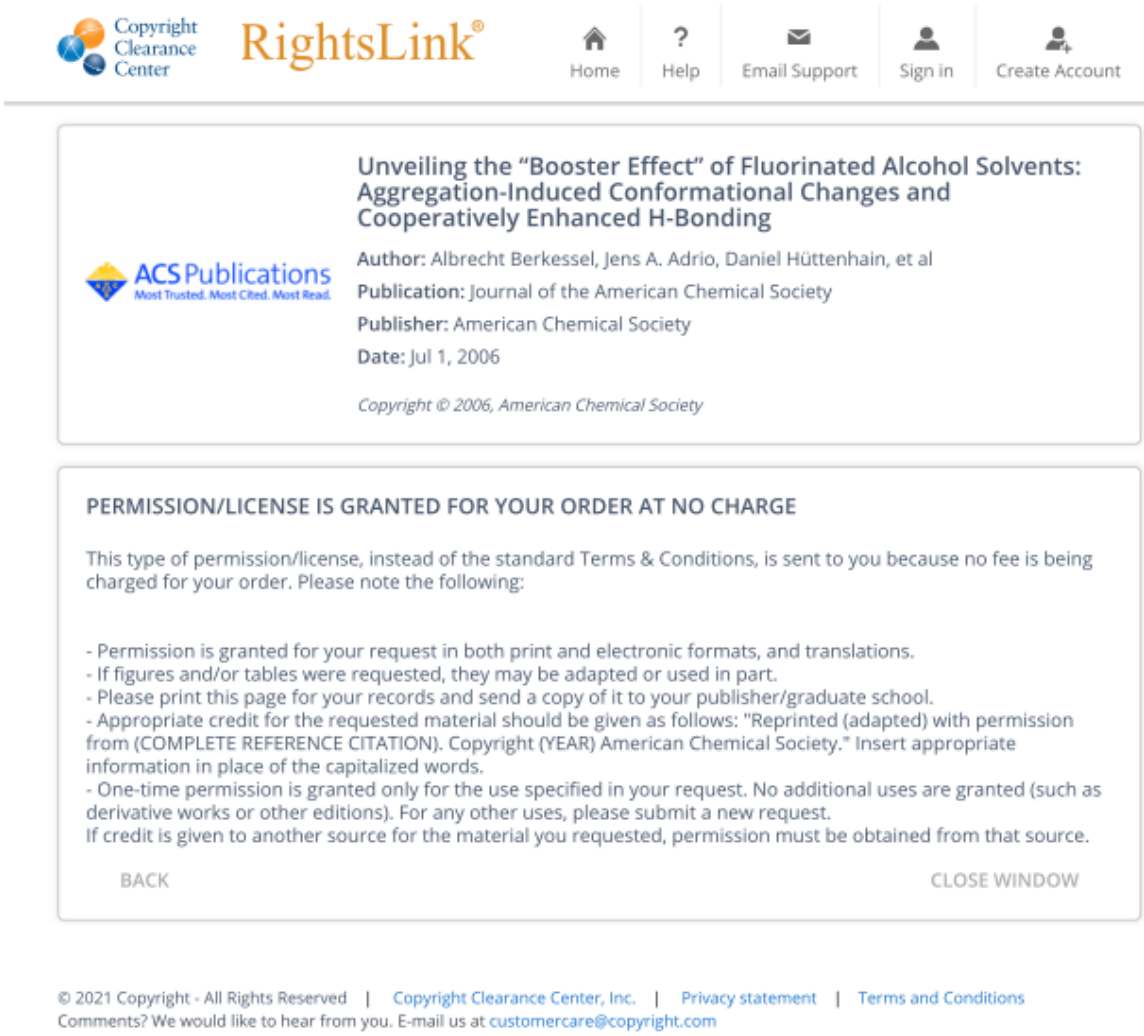

Copyright Clearance Center RightsLink®

Home | Help | Email Support | Sign in | Create Account

Unveiling the "Booster Effect" of Fluorinated Alcohol Solvents: Aggregation-Induced Conformational Changes and Cooperatively Enhanced H-Bonding

ACS Publications
Most Trusted. Most Cited. Most Read.

Author: Albrecht Berkessel, Jens A. Adrio, Daniel Hüttenhain, et al
Publication: Journal of the American Chemical Society
Publisher: American Chemical Society
Date: Jul 1, 2006

Copyright © 2006, American Chemical Society

PERMISSION/LICENSE IS GRANTED FOR YOUR ORDER AT NO CHARGE

This type of permission/license, instead of the standard Terms & Conditions, is sent to you because no fee is being charged for your order. Please note the following:

- Permission is granted for your request in both print and electronic formats, and translations.
- If figures and/or tables were requested, they may be adapted or used in part.
- Please print this page for your records and send a copy of it to your publisher/graduate school.
- Appropriate credit for the requested material should be given as follows: "Reprinted (adapted) with permission from (COMPLETE REFERENCE CITATION). Copyright (YEAR) American Chemical Society." Insert appropriate information in place of the capitalized words.
- One-time permission is granted only for the use specified in your request. No additional uses are granted (such as derivative works or other editions). For any other uses, please submit a new request.

If credit is given to another source for the material you requested, permission must be obtained from that source.

BACK CLOSE WINDOW

© 2021 Copyright - All Rights Reserved | Copyright Clearance Center, Inc. | Privacy statement | Terms and Conditions
Comments? We would like to hear from you. E-mail us at customercare@copyright.com

6. Declaration

Die experimentellen Arbeiten zur vorliegenden Dissertation wurden von mir, Andreas Michael Arnold, selbständig im Zeitraum von Februar 2015 bis Dezember 2019 an der Fakultät für Chemie, Arbeitskreis für Biomimetische Katalyse der Technischen Universität München sowie von Januar 2020 bis Februar 2021 an der Fakultät für Chemie und Mineralogie, Professur für Biomimetische Katalyse der Universität Leipzig durchgeführt.

Die vorliegende Dissertation mit dem Titel „Biomimetic Proton- and Halonium-Induced Cyclization Reactions" habe ich selbständig verfasst und mich außer den angegebenen Quellen keiner weiteren Hilfsmittel bedient.

_____

Andreas M. Arnold